Modelling and Performance Assessment of OFDM Communication Systems in the Presence of Non-linearities

Miguel Raul Dias Rodrigues

A thesis submitted for the degree of Doctor of Philosophy

October 2002

Department of Electronic and Electrical Engineering
University College London

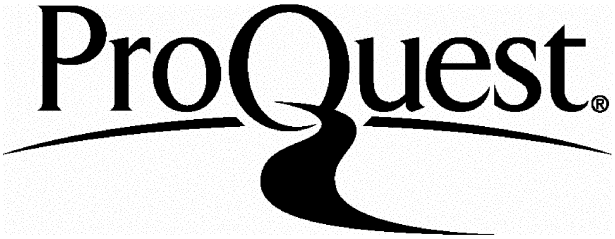

To my fiancée Eduarda

Acknowledgements

First and foremost I wish to express my sincere gratitude to my supervisors, Professor John O'Reilly and Dr. Izzat Darwazeh. I would like to thank Professor John O'Reilly for having introduced me to this field and for the guidance and support during the course of this research. I would like to thank Dr. Izzat Darwazeh for the valuable advice and discussions in the final year of this research and for his continuous friendship.

I am grateful once again to Dr. Izzat Darwazeh, Professor Pedro Guedes de Oliveira and Professor Artur Pimenta Alves whose support enabled me to undertake my postgraduate studies. I am also grateful to the Foundation for Science and Technology of the Portuguese Government for the financial support through the PRAXIS XXI research programme.

I would like to acknowledge fruitful discussions with Dr. Henrique Salgado, Dr. Jorge Castro and Joe Attard as well as research collaborations with Nishita Hathi and Dimitrios Karampatsis. I would also like to thank all the present and past members of the Telecommunications Research Group who have provided a pleasant working environment.

I am also indebted to my family and friends for their constant support and encouragement. Particularly, I here recognise the dedication of my parents which has been essential in all my endeavours.

Last, but certainly not least, I thank wholeheartedly my fiancée Eduarda for her immense love, understanding, help and for much having contributed to my happiness throughout "our" many years.

Abstract

This thesis is concerned with the development of analytic techniques to assess the impact of non-linearities on the performance of orthogonal frequency division multiplexing (OFDM) signals in fibre-radio based wireless networks.

Volterra series are used to model both the frequency independent and the frequency dependent behaviour exhibited by fibre-radio system non-linearities.

Expressions to determine the power density spectrum (PDS) of non-linearly distorted OFDM signals are derived and validated by comparing analytic to simulation results. Such expressions relate the PDS of the distorted signal to the harmonic power density spectra (HPDS) of the non-distorted signal and the transfer functions of the non-linearity.

Expressions to determine the error probability of non-linearly distorted OFDM signals in additive white Gaussian noise (AWGN) are also derived and validated by comparing analytic to simulation results. Such expressions relate the error probability of the OFDM signal to the error probabilities of the OFDM sub-channels, each of which is given as the expectation with respect to the intermodulation distortion (IMD) random variable (RV) of the error probability in AWGN conditioned by a given value of the IMD RV. To calculate the error probability expectations, an investigation of appropriate approximations/estimations for the IMD distribution based on a limited number of moments of the IMD RV is carried out.

Finally, the analytic techniques are applied to two different intensity modulation/direct detection (IM/DD) fibre-radio systems. One of the systems is based on the direct modulation of a laser source and exhibits frequency dependent non-linear behaviour. The other system is based on the external modulation of a laser source and exhibits frequency independent non-linear behaviour. Merits and demerits of the techniques are discussed by comparing analytic to simulation results.

Overall, this thesis provides a range of analytical tools to assess the performance of fibre-radio based wireless networks employing OFDM signalling as well as further insight into the behaviour of non-linearly distorted OFDM signals.

Contents

List of Figures

List of Tables

List of Abbreviations

A/D	Analogue-to-Digital Converter
ACF	Auto-Correlation Function
ADSL	Asymmetric Digital Subscriber Line
AP	Access Point
ATM	Asynchronous Transfer Mode
AWGN	Additive White Gaussian Noise
BER	Bit Error Rate
BPSK	Binary Phase Shift Keying
BS	Base Station
CC	Central Controller
CCF	Cross-Correlation Function
CDF	Cumulative Distribution Function
CDMA	Code Division Multiple Access
CLT	Central Limit Theorem
COFDM	Coded Orthogonal Frequency Division Multiplexing
CPDS	Cross-Power Density Spectrum
CS	Control Station
D/A	Digital-to-Analogue Converter
DAB	Digital Audio Broadcasting
DFT	Discrete Fourier Transform
DMT	Discrete Multi-Tone
DSP	Digital Signal Processing
DVB	Digital Video Broadcasting
FEXT	Far-End Crosstalk
FFT	Fast Fourier Transform

FOFDM	Fast Orthogonal Frequency Division Multiplexing
HACF	Harmonic Auto-Correlation Function
HD	Harmonic Distortion
HDSL	High-Bit-Rate Digital Subscriber Line
HF	High Frequency
HPA	High Power Amplifier
HPDS	Harmonic Power Density Spectrum
ICI	Inter-Carrier Interference
IDFT	Inverse Discrete Fourier Transform
IFFT	Inverse Fast Fourier Transform
IM/DD	Intensity Modulation/Direct Detection
IMD	Intermodulation Distortion
IMP	Intermodulation Product
IP	Internet Protocol
ISI	Inter-Symbol Interference
LAN	Local Area Network
LD	Laser Diode
M-ASK	M-ary Amplitude Shift Keying
M-DPSK	M-ary Differential Phase Shift Keying
M-PSK	M-ary Phase Shift Keying
M-QAM	M-ary Quadrature Amplitude Modulation
MEM	Maximum Entropy Method
MMSE	Minimum Mean Square Error
MREM	Minimum Relative Entropy Method
MS	Mobile Station
MT	Mobile Terminal
MZM	Mach-Zehnder Modulator
NEXT	Near-End Crosstalk
OBO	Output Back-Off
OFDM	Orthogonal Frequency Division Multiplexing
P/S	Parallel-to-Serial Converter
PAPR	Peak-to-Average Power Ratio
PDF	Probability Density Function

PDS	Power Density Spectrum
QoS	Quality of Service
QPSK	Quadrature Phase Shift Keying
RF	Radio Frequency
RV	Random Variable
Rx	Receiver
S/P	Serial-to-Parallel Converter
SCM	Sub-Carrier Multiplexing
SDR	Signal-to-Distortion Ratio
SFN	Single Frequency Network
SIR	Signal-to-Interference Ratio
SNR	Signal-to-Noise Ratio
Tx	Transmitter
UMTS	Universal Mobile Telecommunication System
VHDSL	Very High-Speed Digital Subscriber Line
ZF	Zero Forcing

Chapter 1

Introduction

Recent advances in wireless networking have made use of orthogonal frequency division multiplexing (OFDM) techniques to allow for high data rate transmission in multi-path fading channels [1,2]. Besides handling frequency selective fading without requiring complex time domain equalisation techniques, OFDM also uses the available bandwidth efficiently and allows for efficient digital signal processing (DSP) based transceiver implementations. OFDM has been adopted in a variety of wireless applications including digital audio broadcasting (DAB) [3], digital video broadcasting (DVB) [4] and indoor wireless local area networks (LAN) [5-7].

Concurrently, recent advances in wireless networking have also made use of fibre-radio techniques to allow for high capacity and cost effective wireless network deployment [8-12]. In a conventional wireless network, the radio frequency (RF) data signal to and from a mobile station (MS) is conveyed between control stations (CS) and base stations (BS) in baseband format and the BSs perform all the required radio interface operations. In a fibre-radio based wireless network, on the other hand, the RF data signal to be transmitted to an MS is imposed onto an optical carrier at the CS and delivered over optical fibre to the BS, which then retrieves the RF modulation using standard optical technology, amplifies it and radiates it. Similarly, the RF data signal received from an MS is imposed onto an optical carrier at the BS and delivered over optical fibre to the CS. Transmission of the actual RF signal between CSs and BSs offers cost effective wireless network deployment because not only the air interface equipment is concentrated at the CSs and hence shared among a number of BSs but also a BS is less complex consisting only of an optical transceiver, a filter, an amplifier and an antenna. Fibre-radio techniques are particularly attractive in

wireless systems with micro- or pico-cell architectures for which lowering complexity and cost are of utmost importance.

Clearly, the integration of OFDM techniques with fibre-radio techniques opens up the possibility of cost effective high data rate wireless networks. However, the performance of fibre-radio based wireless networks employing OFDM signalling can be significantly impaired due to the effects of non-linearities associated with the optical infrastructure on the multi-carrier nature of the OFDM signals. A potential deployment of fibre-radio based wireless networks employing OFDM signalling therefore calls for powerful, yet tractable, analytic techniques to provide a first-order approximation to the degradation induced by fibre-radio system non-linearities on the performance of the OFDM signals before recoursing to time consuming simulations or costly experimentation.

The development of analytic techniques to assess the impact of non-linearities on the performance of OFDM signals has been a subject of extensive research [13-25]. However, the fact that such techniques focused on the performance of OFDM signals distorted by clipping devices and high power amplifiers (HPA), which exhibit frequency independent non-linear behaviour, generally renders them inappropriate to determine the performance of OFDM signals distorted by fibre-radio system elements, which normally exhibit frequency dependent non-linear behaviour. Accordingly, new developments in the area of modelling and analysis of OFDM communication systems in the presence of non-linearities are required.

This thesis is concerned with the development of analytic techniques to investigate the impact of fibre-radio system non-linearities on the performance of OFDM signals. The details of the thesis organisation and the thesis contributions are given in the following sections.

1.1 Thesis organisation

Following this introductory chapter, a general overview of OFDM is presented in chapter 2. The oscillator based implementation and the fast Fourier transform (FFT) based implementation of an OFDM transceiver, and the role of the guard time, the cyclic prefix and windowing are reviewed. Drawbacks of OFDM are also reviewed. Particularly, emphasis is given to the effects of synchronisation errors and non-linear distortion on OFDM. Subsequently, the major elements of an OFDM communication system are

described, including coders/decoders and interleavers/deinterleavers, mappers/demappers, channel estimators and synchronisers. Examples of OFDM applications are also outlined. These include the asymmetric digital subscriber line (ADSL), digital broadcasting systems (DAB and DVB) and indoor wireless LANs. Chapter 2 concludes with a discussion of other OFDM initiatives. Particularly, a fast orthogonal frequency division multiplexing (FOFDM) scheme with twice the bandwidth efficiency of conventional OFDM schemes, which was recently proposed by the author, is introduced.

Chapters 3, 4 and 5 consider the development of analytic tools to investigate the impact of fibre-radio system non-linearities on the performance of OFDM signals. These include techniques to evaluate the power density spectrum (PDS) and the error probability of non-linearly distorted OFDM signals.

In chapter 3, an analytic technique to determine the impact of non-linearities on the PDS of OFDM signals is developed. Initially, the Volterra series representation of a non-linearity is introduced because such representation is the basis for the development of the PDS technique so that both frequency independent and frequency dependent non-linear behaviour can be accounted for. Subsequently, expressions are derived to determine the PDS of non-linearly distorted OFDM signals. The PDS of the non-linearity output is given in terms of the harmonic power density spectra (HPDS) of the non-linearity input and the transfer functions of the non-linearity. Finally, analytic and simulation results are compared that validate the derived expressions.

In chapter 4, an analytic technique to determine the impact of non-linearities on the error probability of OFDM signals is developed. Initially, the equivalent baseband Volterra series representation of a bandpass non-linearity is introduced because such representation is the basis for the development of the error probability technique to accommodate both frequency independent and frequency dependent non-linear behaviour. Subsequently, expressions are derived to determine the error probability of non-linearly distorted OFDM/binary phase shift keying (BPSK) and OFDM/quadrature phase shift keying (QPSK) signals in additive white Gaussian noise (AWGN). The overall error probability of an OFDM signal is given as the average of the error probability in all OFDM sub-channels. In turn, the error probability in each OFDM sub-channel is given as the statistical expectation with respect to the intermodulation distortion (IMD) random variable (RV) of the error probability in AWGN conditioned by a given value of the IMD RV. Expressions are also derived to determine the moments of the IMD RV in each OFDM sub-channel.

Finally, it is shown that the moment computation procedure is extremely time-consuming and hence, to compute the error probability expectations, one cannot rely on series expansion methods or Gauss quadrature rules because these moment based methods typically require a large number of moments, but rather on alternative approximations/estimations for the IMD distribution which require a limited number of moments.

In chapter 5, various approximation/estimation methods for the IMD distribution and the error probability of non-linearly distorted OFDM signals are investigated. Initially, the properties of the IMD RV are analysed, as a means to select appropriate approximations/estimations. The relative performance of a number of approximation/estimation methods are then examined by comparing analytic to simulation results. Methods considered include Gaussian, Laplace, generalised Gaussian and Pearson approximations and maximum entropy and minimum relative entropy estimations.

In chapter 6, we consider the application of the analytic techniques developed in chapters 3, 4 and 5 to two particular intensity modulation/direct detection (IM/DD) fibre-radio systems. One of the systems is based on the direct modulation of a laser source and it exhibits frequency dependent non-linear behaviour. The other system is based on the external modulation of a laser source and it exhibits frequency independent non-linear behaviour. In this chapter, merits and demerits of the analytic techniques are discussed by comparing analytic to simulation results.

Chapter 7 concludes this thesis, summarising the main contributions and suggesting areas for future research.

The thesis includes two appendices. Appendix A introduces the FOFDM scheme. Appendix B lists skewness and kurtosis values of the IMD RV.

1.2 Contributions

The primary goal of this research work was to develop powerful, yet tractable, analytic techniques to investigate the impact of fibre-radio system non-linearities on the performance of OFDM signals. Volterra series techniques were used to model both the frequency independent and frequency dependent non-linear behaviour typical of fibre-radio system non-linearities. As performance metrics we have considered the PDS and the error probability. The main contributions of this research work are summarised below:

- Development of an analytic technique to evaluate the PDS of non-linearly distorted OFDM signals. This technique is based on the Volterra series representation of a non-linearity and accounts for up to third-order non-linear distortion components. The developed expressions, which are applicable to a cyclo-stationary zero-mean Gaussian stochastic process, are in fact an extension of the familiar Bedrosian-Rice expressions, which are applicable to a stationary zero-mean Gaussian stochastic process.

- Development of an analytic technique to evaluate the error probability of non-linearly distorted OFDM/BPSK and OFDM/QPSK signals in AWGN. This technique is based on the equivalent baseband Volterra series representation of a bandpass non-linearity and accounts for up to third-order non-linear distortion components.

- Investigation of the relative performance of a range of approximation/estimation methods for the IMD distribution and the error probability of non-linearly distorted OFDM/BPSK and OFDM/QPSK signals. These methods include Gaussian, Laplace, generalised Gaussian and Pearson approximations and maximum entropy and minimum relative entropy estimations.

- Through the detailed analysis of the IMD of non-linearly distorted OFDM signals we have concluded that such IMD is characterised by heavy tails and hence the generally accepted assumption of Gaussian distributed IMD is not always valid.

- Through the detailed analysis of the error probability of non-linearly distorted OFDM signals we have concluded that the error probability performance of different OFDM sub-channels is not equal.

- From the IMD and the error probability studies we have concluded that in the presence of non-linear distortion and AWGN, contrary to implicit assumptions, OFDM signals with a high number of sub-channels exhibiting a correspondingly high peak-to-average power ratio (PAPR) may outperform (in terms of error rate) OFDM signals with a low number of sub-channels exhibiting a correspondingly low PAPR.

- Verification of the developed techniques by application to two different IM/DD fibre-radio systems. One of the systems is based on the direct modulation of a laser source and it exhibits frequency dependent non-linear behaviour. The other system is based on the external modulation of a laser source and it exhibits frequency independent non-linear behaviour. Merits and demerits of the developed techniques were identified by comparing analytic to simulation results.

- Development of an FOFDM scheme with twice the bandwidth efficiency of conventional OFDM schemes.

- Development of "software tools" implemented in MATLAB and SIMILINK for the analysis and simulation of the PDS, the IMD and the error probability of non-linearly distorted OFDM signals.

These contributions have led to the following publications:

1. M. R. D. Rodrigues and J. J. O'Reilly, "Assessment of the performance of radio-over-fibre based wireless networks employing OFDM signalling," Proceedings of the London Communications Symposium 1999, pp. 47-50, July 1999. (London, U.K.)

2. M. R. D. Rodrigues and J. J. O'Reilly, "Error probability assessment of radio-over-fibre based wireless networks employing OFDM signalling," Proceedings of the London Communications Symposium 2000, pp. 95-99, September 2000. (London, U.K.)

3. M. R. D. Rodrigues and J. J. O'Reilly, "An analytic technique to determine the impact of non-linearities on the PDS of OFDM signals in RoF based wireless networks," Proceedings of the International Symposium on Information Theory and Its Applications, vol. 2, pp. 769-773, November 2000. (Honolulu, Hawaii, U.S.A.)

4. M. R. D. Rodrigues and J. J. O'Reilly, "An analytic technique to assess the impact of frequency dependent non-linearities on the error probability of OFDM/M-PSK and OFDM/M-QAM signals," Proceedings of the 35th Annual Conference on Information Sciences and Systems, vol. 2, pp. 748-752, March 2001. (Baltimore, Maryland, U.S.A.)

5. M. R. D. Rodrigues and J. J. O'Reilly, "An analytic technique to assess the impact of non-linearities on the error probability of OFDM signals in RoF based wireless networks," Proceedings of the IEEE International Symposium on Information Theory 2001, p. 316, June 2001. (Washington, D.C., U.S.A.)

6. M. R. D. Rodrigues and J. J. O'Reilly, "On the distribution of the intermodulation distortion in OFDM communication systems," Proceedings of the London Communications Symposium 2001, pp. 87-90, September 2001. (London, U.K.)

7. M. R. D. Rodrigues, I. Darwazeh and J. J. O'Reilly, "On the distribution of the intermodulation distortion and the error probability of non-linearly distorted OFDM signals," Proceedings of the 36th Annual Conference on Information Sciences and Systems, pp. 636-641, March 2002. (Princeton, New Jersey, U.S.A.)

8. N. Hathi, M. R. D. Rodrigues, I. Darwazeh and J. J. O'Reilly, "Performance assessment of MC-CDMA and MC-DS-CDMA in the presence of high power amplifier non-linearities," Proceedings of the IEEE Vehicular Technology Conference, vol. 3, pp. 1467-1471, May 2002. (Birmingham, Alabama, U.S.A.)

9. M. R. D. Rodrigues and I. Darwazeh, "Fast OFDM: A proposal for doubling the data rate of OFDM schemes," Proceedings of the International Conference on Telecommunications, vol. 3, pp. 484-487, June 2002. (Beijing, China) (invited paper)

10. M. R. D. Rodrigues and J. J. O'Reilly, "Statistical characterisation of the response of a Volterra non-linearity to a cyclo-stationary zero-mean Gaussian stochastic process," Proceedings of the IEEE International Symposium on Information Theory, p. 8, June/July 2002. (Lausanne, Switzerland)

11. M. R. D. Rodrigues and I. Darwazeh, "On the behaviour of non-linearly distorted OFDM signals," Proceedings of the London Communications Symposium 2002, pp. 113-116, September 2002. (London, U.K.)

12. D. Karampatsis, M. R. D. Rodrigues and I. Darwazeh, "Implications of linear phase dispersion on OFDM and Fast-OFDM systems," Proceedings of the London Communications Symposium 2002, pp. 117-120, September 2002. (London, U.K.)

13. N. Hathi, M. R. D. Rodrigues, I. Darwazeh and J. J. O'Reilly, "Analysis of the influence of Walsh-Hadamard code allocation strategies on the performance of multi-carrier CDMA systems in the presence of HPA non-linearities," accepted for presentation at the IEEE International Symposium on Personal, Indoor and Mobile Radio Communications, Lisbon, Portugal, September 2002.

14. M. R. D. Rodrigues, I. Darwazeh and J. J. O'Reilly, "Assessment of the impact of optical non-linearities on the performance of OFDM signals in optical fibre supported wireless networks," accepted for presentation at the International Symposium on Information Theory and Its Applications, Xi'an, China, October 2002.

15. M. R. D. Rodrigues, I. Darwazeh and J. J. O'Reilly, "Volterra series assessment of non-linearly distorted OFDM signals: Power density spectrum evaluation," accepted for presentation at the 2nd IMA Conference on Mathematics in Communications, Lancaster, U.K., December 2002.

16. M. R. D. Rodrigues, I. Darwazeh and J. J. O'Reilly, "Volterra series assessment of non-linearly distorted OFDM signals: Error probability evaluation," accepted for presentation at the 2nd IMA Conference on Mathematics in Communications, Lancaster, U.K., December 2002.

Chapter 2

OFDM overview

2.1 Introduction

In recent years, the wired and the wireless industry have shown great interest in OFDM signalling schemes. Indeed, such signalling schemes have been adopted in a variety of applications such as ADSL, DAB, DVB and indoor wireless LANs. This growing interest was due to the realisation that OFDM is an efficient scheme to convey information in a frequency selective fading channel without requiring complex time-domain equalisation techniques. Moreover, OFDM uses the bandwidth efficiently and can be efficiently generated/detected using DSP techniques.

In this chapter, we present the principal ideas behind OFDM that will be used throughout this thesis. Section 2.2 introduces the OFDM principle where concepts such as the oscillator based implementation and the FFT based implementation of an OFDM transceiver, the guard time and the cyclic prefix and windowing are outlined. Section 2.3 discusses the drawbacks of OFDM. Particularly, OFDM vulnerability to synchronisation errors and non-linear distortion are emphasised. The elements of an OFDM communication system and applications of OFDM are presented in section 2.4 and section 2.5, respectively. In section 2.4, we introduce mapping/demapping techniques, coding/decoding and interleaving/deinterleaving techniques, and synchronisation and channel estimation operations. In section 2.5, we discuss the use of OFDM in ADSL, digital broadcasting systems (DAB and DVB) and indoor wireless LANs. Finally, in section 2.6 we review a number of OFDM initiatives that have been proposed throughout the

years. Particularly, we consider an FOFDM scheme with twice the bandwidth efficiency of conventional OFDM schemes.

2.2 Principles of OFDM

In a single-carrier modulation scheme data is transmitted sequentially on a single-carrier. In a multi-carrier modulation scheme, on the other hand, a high-rate data stream is partitioned into several low-rate data sub-streams which modulate a set of sub-carriers. Accordingly, the signalling interval of a multi-carrier system is much larger than that of an equivalent single-carrier system so that the time dispersive effects of a multi-path fading channel can be efficiently combated without requiring complex time-domain equalisation techniques.

Multi-carrier modulation schemes initially relied on conventional frequency division multiplexing (FDM) technology to transmit information on multiple carriers. At the transmitter, the spectra of different sub-carriers were assigned to non-overlapping frequency slots and, at the receiver, the individual sub-channels were retrieved using filters. Orthogonal multi-carrier modulation schemes or OFDM schemes were later proposed where the spectra of different sub-carriers were assigned to overlapping frequency slots and individual sub-channels were retrieved thanks to orthogonal properties that eliminated the crosstalk between the individual sub-channels. Orthogonal multi-carrier schemes yielded a more efficient utilisation of the available bandwidth when compared to conventional multi-carrier schemes.

Research on OFDM can be traced back to the 1950s. In the 1950s/1960s, the OFDM technique was used in several high frequency (HF) military communication systems such as KINEPLEX [26,27], ANDEFT [28] and KATHRYN [29-31]. In the 1980s, OFDM was studied for high-speed modems [32-34], digital mobile communications [35] and high density recording. In the 1990s, OFDM was studied for high-bit-rate digital subscriber lines (HDSL) [36], ADSL [37], very high-speed digital subscriber line (VHDSL) [37], DAB [38,39] and DVB [40]. This research has resulted in the implementation of OFDM systems in ADSL [41], DAB [3], DVB [4] and indoor wireless LANs [5-7]. The principles of OFDM are described in the following sections.

2.2.1 Oscillator based implementation

The structure of an oscillator based baseband OFDM transmitter and receiver is shown in Figure 2.1. At the transmitter, N consecutive complex data symbols modulate N complex orthogonal sub-carriers which are then added and transmitted. The frequency separation between adjacent sub-carriers is equal to the inverse of the signalling interval T, which is the minimum frequency separation required to achieve orthogonality between two complex sub-carriers over a signalling interval of length T [42-45]. For this frequency separation there is considerable overlapping between the spectra of the different sub-carriers but the information can still be reliably recovered. An OFDM symbol is then given by

$$x(t) = \frac{1}{\sqrt{T}} \sum_{n=0}^{N-1} X_n e^{j\frac{2\pi nt}{T}}, \quad 0 < t < T \tag{2.1}$$

where X_n is the complex modulation symbol conveyed on sub-channel n or by sub-carrier n. At the receiver, the nth complex modulation symbol is recovered by multiplying the OFDM symbol by the complex conjugate of the nth sub-carrier and by integrating over the signalling interval. The nth complex modulation symbol is then given by

$$X_n = \frac{1}{\sqrt{T}} \int_0^T x(t) e^{-j\frac{2\pi nt}{T}} dt \tag{2.2}$$

In a typical system, up- and down-conversion blocks would be present at the transmitter and the receiver, respectively, to transform the baseband signal to a bandpass signal and vice-versa.

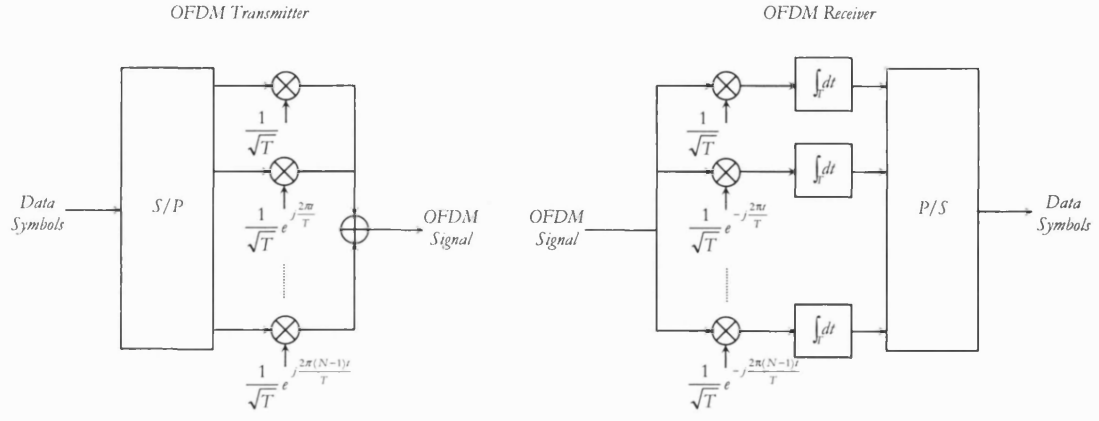

Figure 2.1: Structure of an oscillator based baseband OFDM transmitter and receiver.

The operation of an OFDM receiver can be viewed from two different perspectives. From one view point, the receiver correlates the set of modulated complex sub-carriers in the incoming OFDM symbol with a local version of each complex sub-carrier (see (2.2)). Orthogonality implies that the correlation between any two different complex sub-carriers is zero but when the complex sub-carriers have the same frequency. Therefore, the correlation operation yields the information conveyed in each sub-channel without any inter-carrier interference (ICI). From another view point, the receiver evaluates the Fourier transform of an OFDM symbol at frequencies n/T, $n = 0,\ldots,N-1$ (see (2.2)). The spectrum of an OFDM symbol is given by

$$X(f) = \int_{-\infty}^{\infty} x(t) e^{-j2\pi ft}\, dt = \sqrt{T} \sum_{n=0}^{N-1} X_n \operatorname{sinc}\left[(f - n/T)T\right] e^{-j\pi(f-n/T)T} \tag{2.3}$$

where

$$\operatorname{sinc}(x) = \frac{\sin(\pi x)}{\pi x} \tag{2.4}$$

i.e., the spectrum of an OFDM symbol consists of a series of $\operatorname{sinc}(\cdot)$ functions where the maximum of each $\operatorname{sinc}(\cdot)$ function corresponds to the zero-crossings of all the other $\operatorname{sinc}(\cdot)$ functions (see Figure 2.2). Essentially, the spectrum of an OFDM symbol fulfils Nyquist's criterion for an inter-symbol interference (ISI) free pulse shape, where in the OFDM case the pulse shape is present in the frequency domain and not in the time domain. Therefore, the Fourier transformation operation yields the information conveyed in each sub-channel without any ICI.

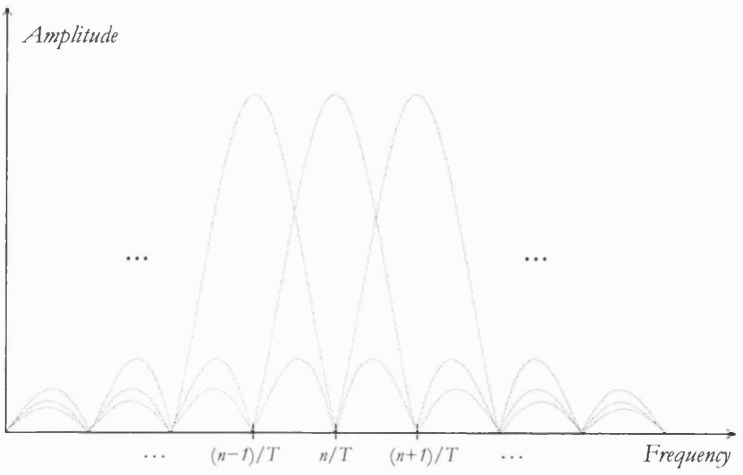

Figure 2.2: Amplitude spectrum of an OFDM symbol.

2.2.2 FFT based implementation

An oscillator based OFDM transceiver comprises a bank of oscillators both at the transmitter and the receiver and hence it is highly complex. However, Weinstein and Ebert have shown that OFDM generation and detection can be achieved by employing an inverse discrete Fourier transform (IDFT) and a discrete Fourier transform (DFT) at the transmitter and the receiver, respectively [46]. Specifically, the scaled samples $x_k = \sqrt{T/N}\, x(kT/N),\ k = 0,\ldots,N-1$, of an OFDM symbol can be generated by taking the IDFT of the complex modulation symbols to be conveyed in each sub-channel, i.e.,

$$x_k = \frac{1}{\sqrt{N}} \sum_{n=0}^{N-1} X_n e^{j\frac{2\pi kn}{N}},\quad k = 0,\ldots,N-1 \tag{2.5}$$

and the complex modulation symbols conveyed in each sub-channel can be detected by taking the DFT of the scaled samples $x_k = \sqrt{T/N}\, x(kT/N),\ k = 0,\ldots,N-1$, of an OFDM symbol, i.e.,

$$X_n = \frac{1}{\sqrt{N}} \sum_{k=0}^{N-1} x_k e^{-j\frac{2\pi kn}{N}},\quad n = 0,\ldots,N-1 \tag{2.6}$$

This major breakthrough shows that efficient implementations of an OFDM transmitter and receiver can be built around the inverse fast Fourier transform (IFFT) and the FFT, respectively. The structure of an FFT based baseband OFDM transmitter and receiver is shown in Figure 2.3. At the transmitter, a digital-to-analogue converter (D/A) converts the digital OFDM signal to an analogue format and, at the receiver, an analogue-to-digital converter (A/D) converts the analogue OFDM signal to a digital format. In a typical system, up- and down-conversion blocks would be present at the transmitter and the receiver, respectively, to transform the baseband signal to a bandpass signal and vice-versa.

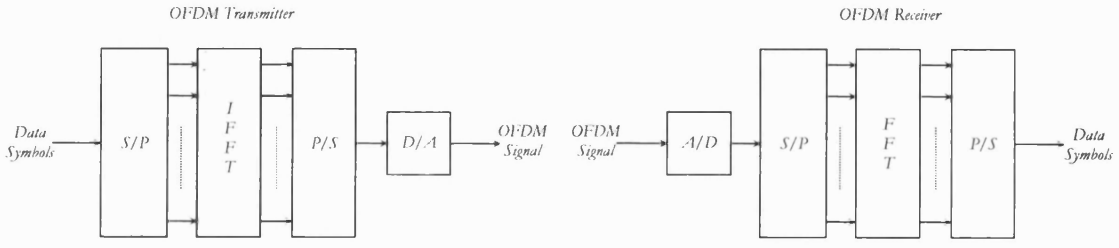

Figure 2.3: Structure of an FFT based baseband OFDM transmitter and receiver.

In practice, N samples per OFDM symbol do not provide the required oversampling to yield the continuous-time signal from the discrete-time signal. Note that both the OFDM symbol bandwidth and the IFFT output sample rate are equal to N/T, i.e., the OFDM symbol is sampled at the Nyquist rate[1]. Thus, from the spectrum of a non-oversampled IFFT output a filter with a realistic passband-to-stopband transition region cannot be used to recover the continuous-time OFDM symbol from its samples (see Figure 2.4). To provide for the required oversampling a technique known as zero-padding is often employed. Essentially, $N' > N$ point IFFTs/FFTs are used at the transmitter/receiver to generate/detect a N sub-channel OFDM symbol. Upon OFDM generation the last $N' - N$ IFFT input values are set to zero and upon OFDM detection the last $N' - N$ FFT output values are discarded. Thus, from the spectrum of an oversampled IFFT output a filter with a realistic passband-to-stopband transition region can be used to recover the continuous-time OFDM symbol from its samples (see Figure 2.5).

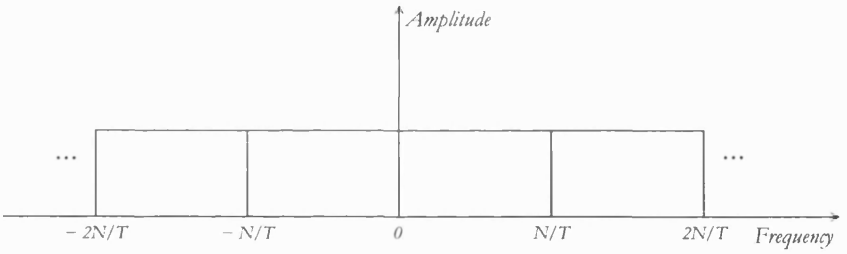

Figure 2.4: Amplitude spectrum (in the limit for an infinite number of OFDM sub-channels) of a non-oversampled IFFT output.

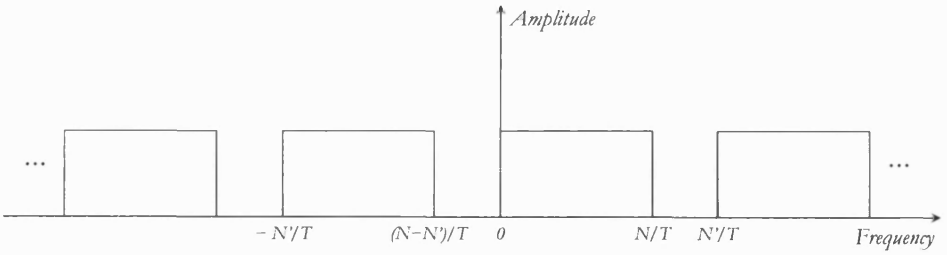

Figure 2.5: Amplitude spectrum (in the limit for an infinite number of OFDM sub-channels) of an oversampled IFFT output.

[1] Strictly speaking, the OFDM symbol bandwidth tends to N/T when N tends to infinity.

2.2.3 Guard time and cyclic prefix

By transmitting information on N sub-carriers then the symbol duration of an OFDM signal is N times longer than the symbol duration of an equivalent single-carrier signal. Accordingly, ISI effects introduced by linear time dispersive channels are minimised. To eliminate ISI completely a guard time is inserted with a duration longer than the duration of the impulse response of the channel [46]. Moreover, to eliminate ICI the guard time is cyclically extended [47,48]. Note that in the presence of linear time dispersive channels an appropriate guard time avoids ISI but not ICI, unless it is cyclically extended.

Cyclic extension of an OFDM symbol is shown in Figure 2.6. At the transmitter, the last "T_{CP}" samples of the IFFT output are inserted at the start of the OFDM symbol. At the receiver, the first "T_{CP}" samples of the OFDM symbol are discarded. Note that now T denotes the duration of the cyclically extended OFDM symbol and T_{CP} denotes the duration of the cyclic prefix. Note also that now the duration of the useful part of an OFDM symbol is equal to $T - T_{CP}$ and hence the sub-carrier spacing is equal to $1/(T - T_{CP})$.

To appreciate the basic operation of the cyclic prefix let us consider a two-path channel. In this case, the received OFDM signal consists of two replicas of the transmitted OFDM signal possibly attenuated and delayed with respect to one another. With an ordinary guard time, whose duration is larger than the two-path channel relative delay, then over the FFT "integration time" the sum of any two multipath components corresponding to a particular OFDM sub-carrier does not yield a sine wave (see Figure 2.7). Hence, ICI occurs at the output of the receiver's FFT. With a cyclically extended guard time, whose duration is larger than the two-path channel relative delay, then over the FFT "integration time" the sum of any two multipath components corresponding to a particular OFDM sub-carrier yields an attenuated/phase rotated version of the same sub-carrier (see Figure 2.8). Hence, ICI does not occur at the output of the receiver's FFT and each data symbol is received only with a random amplitude/phase rotation. Specifically, the amplitude/phase rotation of the nth complex data symbol corresponds to the amplitude/phase of the frequency response of the two-path channel evaluated at the nth sub-carrier frequency. Generally, if the duration of the cyclic prefix is longer than the duration of the impulse response of a linear time dispersive channel then, from the receiver's point of view, the channel's linear convolution is equivalent to a circular convolution. Therefore, the FFT output $Y_n, n = 0,\ldots,N-1$, and the IFFT input $X_n, n = 0,\ldots,N-1$, are related by [47,48]

$$Y_n = H_n X_n \tag{2.7}$$

where H_n is the frequency response of the channel evaluated at the nth sub-carrier frequency.

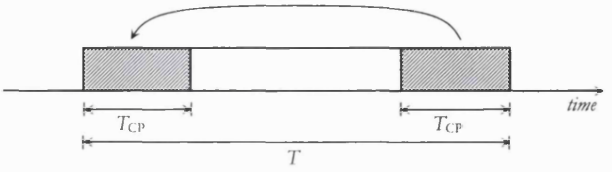

Figure 2.6: Cyclic extension of an OFDM symbol.

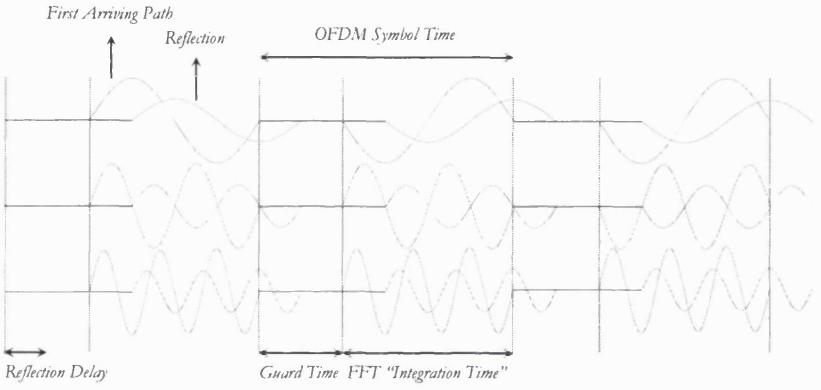

Figure 2.7: Transmission of an OFDM signal with an ordinary guard time over a two-path channel. For simplicity three BPSK modulated sine waves are shown separately.

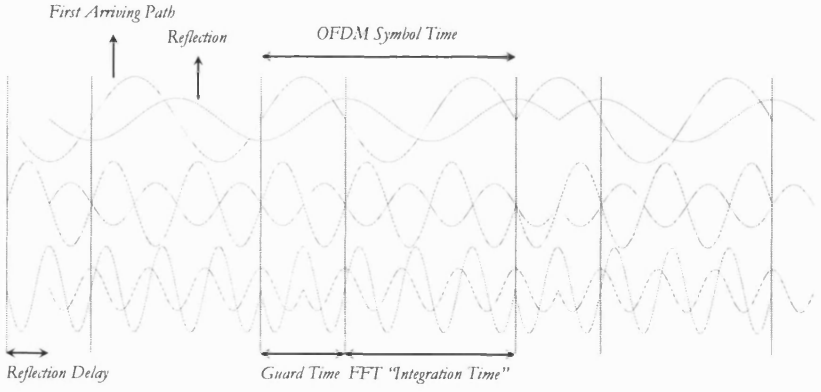

Figure 2.8: Transmission of an OFDM signal with a cyclically extended guard time over a two-path channel. For simplicity three BPSK modulated sine waves are shown separately.

Insertion of an appropriate cyclically extended guard time eliminates ISI and ICI in a linear time dispersive channel but it also introduces a loss in the signal-to-noise ratio (SNR) and an increase in the bandwidth. The SNR loss is given by

$$SNR_{loss}\,(\mathrm{dB}) = 10\log\frac{T}{T - T_{CP}} \tag{2.8}$$

and the bandwidth expansion factor is given by

$$\text{bandwidth expansion factor} = \frac{T}{T - T_{CP}} \tag{2.9}$$

2.2.4 Windowing

For an infinite number of sub-channels, the OFDM spectrum exhibits the ideal brick-wall characteristic. For a finite number of sub-channels, the OFDM spectrum exhibits a relatively slow decay, according to a $\mathrm{sinc}(\cdot)$ function. Such a spectral characteristic will therefore cause high interference to users of adjacent frequency bands.

"Non-contained" spectra are associated with sharp phase transitions in the signal's symbol boundaries. "Contained" spectra, on the other hand, are associated with smooth phase transitions in the signal's symbol boundaries. Accordingly, in OFDM a raised cosine window is often used to allow the amplitude of an OFDM symbol to go smoothly to zero at the symbol boundaries [44-46]. The raised cosine window is given by [44-46]

$$w(t) = \begin{cases} \sin^2(\pi t/2\beta T), & t \in [0, \beta T] \\ 1, & t \in [\beta T, T] \\ \cos^2(\pi(t-T)/2\beta T), & t \in [T, (1+\beta)T] \\ 0, & \text{elsewhere} \end{cases} \tag{2.10}$$

where β is the raised cosine window rolloff factor and T is the OFDM symbol duration.

The time structure of a windowed OFDM signal is shown in Figure 2.9. At the transmitter, the last "T_{CP}" samples of the IFFT output are inserted at the start of the OFDM symbol and the first "βT" samples of the IFFT output are inserted at the end of the OFDM symbol. Subsequently, the OFDM symbol is multiplied by the raised cosine window. Finally, consecutive OFDM symbols are delayed with respect to one another by T so that there is an overlap region of βT. At the receiver, the first "T_{CP}" samples and the last "βT" samples of the OFDM symbol are discarded.

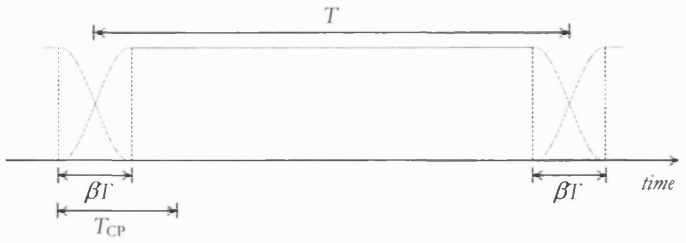

Figure 2.9: Time structure of a windowed OFDM signal.

We shall now evaluate the PDS of an OFDM signal with raised cosine windowing. We start by determining its mean value and its auto-correlation function (ACF) and only then we determine its PDS. We write the OFDM signal as

$$x(t) = \mathrm{Re}\left\{\tilde{x}(t)e^{j2\pi f_c t}\right\} \tag{2.11}$$

where $\tilde{x}(t)$ is its complex envelope and f_c is the frequency of its first sub-carrier, and we write the complex envelope of the OFDM signal as

$$\tilde{x}(t) = \sum_{k=-\infty}^{\infty}\sum_{n=0}^{N-1} X_{k,n} g_n(t - kT) \tag{2.12}$$

$$g_n(t) = \begin{cases} \sin^2(\pi t/2\beta T)e^{j\frac{2\pi n(t-T_{CP})}{T-T_{CP}}}, & t \in [0, \beta T] \\ e^{j\frac{2\pi n(t-T_{CP})}{T-T_{CP}}}, & t \in [\beta T, T] \\ \cos^2(\pi(t-T)/2\beta T)e^{j\frac{2\pi n(t-T_{CP})}{T-T_{CP}}}, & t \in [T, (1+\beta)T] \\ 0, & \text{elsewhere} \end{cases} \tag{2.13}$$

where $X_{k,n}$ denotes the complex modulation symbol conveyed in time slot k and sub-channel n, N is the number of OFDM sub-channels, T is the OFDM symbol duration, T_{CP} is the OFDM cyclic prefix duration and β is the raised cosine window rolloff factor.

The mean value of the OFDM signal, $E[x(t)]$, is related to the mean value of its complex envelope, $E[\tilde{x}(t)]$, as follows[2]

$$E[x(t)] = \mathrm{Re}\left\{E[\tilde{x}(t)]e^{j2\pi f_c t}\right\} \tag{2.14}$$

where

$$E[\tilde{x}(t)] = \sum_{k=-\infty}^{\infty}\sum_{n=0}^{N-1} E[X_{k,n}] g_n(t - kT) \tag{2.15}$$

[2] Throughout this thesis, $E[\cdot]$ denotes the expectation operator.

By assuming that the mean value of the complex modulation symbols is zero, i.e., $E[X_{k,n}]=0$, then

$$E[\tilde{x}(t)]=0 \tag{2.16}$$

The ACF of the OFDM signal, $\phi_{xx}(t+\tau,t)$, is related to the ACF of its complex envelope, $\phi_{\tilde{x}\tilde{x}}(t+\tau,t)$, as follows[3]

$$\phi_{xx}(t+\tau,t)=\mathrm{Re}\left\{\phi_{\tilde{x}\tilde{x}}(t+\tau,t)e^{j2\pi f_c\tau}\right\} \tag{2.17}$$

where

$$\phi_{\tilde{x}\tilde{x}}(t+\tau,t)=\frac{1}{2}E[\tilde{x}(t+\tau)\tilde{x}^*(t)]=\sum_{k_1=-\infty}^{\infty}\sum_{n_1=0}^{N-1}\sum_{k_2=-\infty}^{\infty}\sum_{n_2=0}^{N-1}\frac{1}{2}E[X_{k_1,n_1}X^*_{k_2,n_2}]g_{n_1}(t+\tau-k_1T)g^*_{n_2}(t-k_2T) \tag{2.18}$$

By assuming that the complex modulation symbols conveyed in different time slots and different sub-channels are independent then

$$\frac{1}{2}E[X_{k_1n_1}X^*_{k_2n_2}]=\begin{cases}0, & k_1\neq k_2 \text{ or } n_1\neq n_2\\ \sigma_n^2, & k_1=k_2=k \text{ and } n_1=n_2=n\end{cases} \tag{2.19}$$

and

$$\phi_{\tilde{x}\tilde{x}}(t+\tau,t)=\sum_{k=-\infty}^{\infty}\sum_{n=0}^{N-1}\sigma_n^2 g_n(t+\tau-kT)g_n^*(t-kT) \tag{2.20}$$

Note that since the mean value and the ACF of the complex envelope of the OFDM signal are periodic in time with period T, i.e.,

$$m_{\tilde{x}}(t+kT)=m_{\tilde{x}}(t)=0 \tag{2.21}$$

$$\phi_{\tilde{x}\tilde{x}}(t+kT+\tau,t+kT)=\phi_{\tilde{x}\tilde{x}}(t+\tau,t) \tag{2.22}$$

then the mean value and the ACF of the OFDM signal are also periodic in time with the same period T, i.e.,

---

[3] Strictly speaking, this expression is valid if and only if $E[\tilde{x}(t+\tau)\tilde{x}(t)]=0$ [43]. To circumvent this difficulty, we may alternatively write the OFDM signal as $x(t)=\mathrm{Re}\left\{\tilde{x}(t)e^{j(2\pi f_c t+\Phi)}\right\}$, where $\tilde{x}(t)$ is its complex envelope, f_c is the frequency of its first sub-carrier and Φ is a random angle uniformly distributed over 2π radians.

$$m_x(t+kT) = m_x(t) = 0 \tag{2.23}$$

$$\phi_{xx}(t+kT+\tau, t+kT) = \phi_{xx}(t+\tau, t) \tag{2.24}$$

Accordingly, an OFDM signal is a cyclo-stationary stochastic process (at least in the wide-sense) and hence we determine its average PDS by Fourier transforming its average ACF [49-51]. The average ACF of the OFDM signal, $\bar{\phi}_{xx}(\tau)$, is given by

$$\bar{\phi}_{xx}(\tau) = \frac{1}{T}\int_T \phi_{xx}(t+\tau, t)dt \tag{2.25}$$

and by substituting (2.17) into (2.25) then

$$\bar{\phi}_{xx}(\tau) = \frac{1}{2}\bar{\phi}_{\tilde{x}\tilde{x}}(\tau)e^{j2\pi f_c\tau} + \frac{1}{2}\bar{\phi}^*_{\tilde{x}\tilde{x}}(\tau)e^{-j2\pi f_c\tau} \tag{2.26}$$

where $\bar{\phi}_{\tilde{x}\tilde{x}}(\tau)$ is the average ACF of the complex envelope of the OFDM signal, i.e.,

$$\bar{\phi}_{\tilde{x}\tilde{x}}(\tau) = \frac{1}{T}\int_T \phi_{\tilde{x}\tilde{x}}(t+\tau, t)dt \tag{2.27}$$

This average ACF can be found by using (2.20) in (2.27) and carrying out the integration. Thus,

$$\bar{\phi}_{\tilde{x}\tilde{x}}(\tau) = \frac{1}{T}\sum_{n=0}^{N-1}\sigma_n^2\phi_{g_ng_n}(\tau) \tag{2.28}$$

where $\phi_{g_ng_n}(\tau) = g_n(\tau) * g_n^*(-\tau)$ is the ACF of $g_n(t)$.

The average PDS of the OFDM signal, $\bar{\Phi}_{xx}(f)$, is given by

$$\bar{\Phi}_{xx}(f) = \int_{-\infty}^{\infty}\bar{\phi}_{xx}(\tau)e^{-j2\pi f\tau}d\tau \tag{2.29}$$

and by substituting (2.26) into (2.29) then

$$\bar{\Phi}_{xx}(f) = \frac{1}{2}\left[\bar{\Phi}_{\tilde{x}\tilde{x}}(f-f_c) + \bar{\Phi}^*_{\tilde{x}\tilde{x}}(-f-f_c)\right] \tag{2.30}$$

where $\bar{\Phi}_{\tilde{x}\tilde{x}}(f)$ is the average PDS of the complex envelope of the OFDM signal, i.e.,

$$\bar{\Phi}_{\tilde{x}\tilde{x}}(f) = \int_{-\infty}^{\infty}\bar{\phi}_{\tilde{x}\tilde{x}}(\tau)e^{-j2\pi f\tau}d\tau \tag{2.31}$$

This average PDS can be found by using (2.28) in (2.31) and carrying out the integration. Thus,

$$\overline{\Phi}_{\tilde{x}\tilde{x}}(f)=\frac{1}{T}\sum_{n=0}^{N-1}\sigma_n^2\Phi_{g_ng_n}(f) \tag{2.32}$$

where $\Phi_{g_ng_n}(f)=|G_n(f)|^2$ is the energy density spectrum of $g_n(t)$ and $G_n(f)$ is the spectrum of $g_n(t)$. The energy density spectrum for $g_n(t)$ is given by

$$\Phi_{g_ng_n}(f)=\frac{\cos^2\left[\pi\beta T\left(f-\frac{n}{T-T_{CP}}\right)\right]}{\left[1-\left[2\beta T\left(f-\frac{n}{T-T_{CP}}\right)\right]^2\right]^2}T^2\mathrm{sinc}^2\left[\left(f-\frac{n}{T-T_{CP}}\right)T\right] \tag{2.33}$$

Figure 2.10 shows the PDS of an OFDM signal with raised cosine windowing for $\beta = 0, 0.025, 0.05$ and 0.1. Note that both the horizontal axis and the vertical axis have been normalised in this figure. The horizontal axis has been normalised to the centre frequency f_{centre} and the 3dB bandwidth B_{3dB} of the OFDM signal given by

$$f_{centre} = f_c + \frac{N/2-1/2}{T-T_{CP}} \tag{2.34}$$

$$B_{3dB} = \frac{N}{T-T_{CP}} \tag{2.35}$$

The vertical axis has been normalised to the maximum value in the PDS. A raised cosine window significantly improves the spectral characteristics of an OFDM signal but it also diminishes the delay spread tolerance of the same signal by βT.

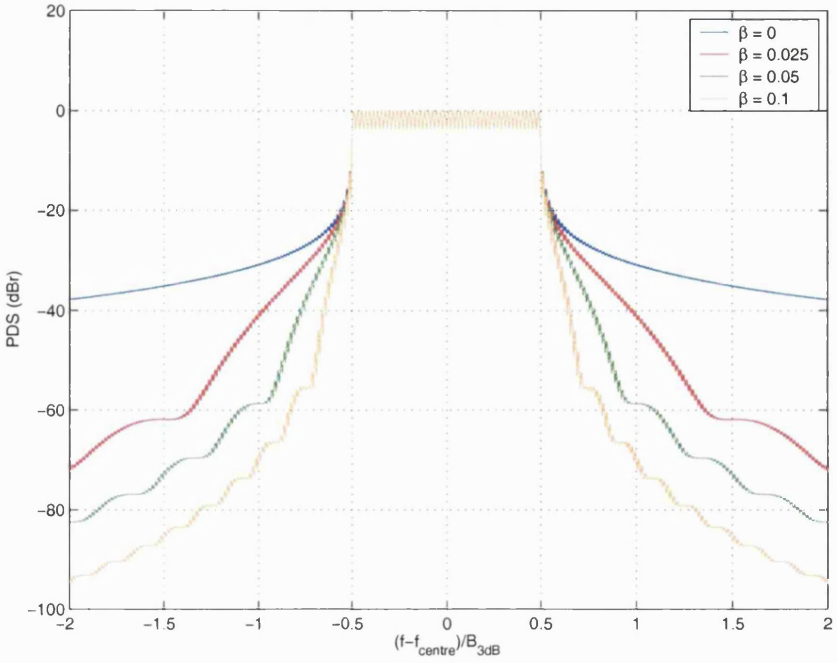

Figure 2.10: PDS of OFDM/BPSK signals with $f_c = 1 GHz$, $N = 48$, $T = 4000\ ns$, $T_{CP} = 800\ ns$ and $\beta = 0, 0.025, 0.05$ and 0.1.

2.3 Drawbacks of OFDM

The main advantage of OFDM is its capability to handle the time dispersive effects of a multi-path fading channel. Long symbol durations allow for relatively long cyclic prefix durations to eliminate ISI and ICI with minimal SNR loss. Van Nee and Prasad have shown that for a given delay spread, the implementation complexity of an OFDM system is significantly lower than that of an equivalent single-carrier system with a time-domain equaliser [45]. However, OFDM systems also exhibit other advantages when compared to single-carrier systems. Specifically, OFDM can be used in conjunction with bit loading techniques to improve the capacity of a highly frequency selective channel and it can also be used to deploy single frequency networks (SFN) to improve the spectrum efficiency of broadcasting systems. Bit loading techniques and SFNs are discussed in section 2.5.1 and section 2.5.2, respectively.

The two main disadvantages of OFDM are its vulnerability to synchronisation errors, such as symbol timing offsets and carrier frequency offsets, and to non-linear distortion.

The effects of synchronisation errors and non-linear distortion in OFDM systems are discussed in section 2.3.1 and section 2.3.2, respectively.

2.3.1 Synchronisation errors

In this section, we highlight the effects of symbol timing and carrier frequency offsets in OFDM systems [44,45,52-54]. Carrier frequency offsets originate from frequency differences in the local oscillators at the transmitter and the receiver used to convert the baseband signal to a bandpass signal and vice versa. Symbol timing offsets originate due to an uncertainty to establish the OFDM symbol boundaries.

Carrier frequency offsets induce a frequency domain shift in the spectrum of the received OFDM signal. If the frequency offset is an integer multiple of the sub-carrier spacing of $1/(T-T_{CP})$ then the sub-carriers are still orthogonal but the nth received symbol does not correspond to the nth transmitted symbol and hence a very high bit error rate (BER) occurs. If, however, the frequency offset is not an integer multiple of the sub-carrier spacing of $1/(T-T_{CP})$ then a reduction of the power of the desired received symbol and ICI from other sub-carriers occur. These effects occur for at the sampling frequencies not only is the peak value of the desired $\mathrm{sinc}(\cdot)$ function not obtained but also values of other $\mathrm{sinc}(\cdot)$ functions are obtained. Essentially, such a frequency offset destroys the orthogonality between the sub-carriers for these will not anymore contain different integer numbers of cycles within the FFT "integration time". The amount of ICI for the sub-carriers in the centre of the frequency band is approximately twice as large as that for the sub-carriers on the edge of the frequency band because at a certain frequency distance more interferers affect the former than the later. Frequency offsets therefore induce degradation in the BER. Figure 2.11 shows the effects of a frequency error of Δf.

OFDM is more robust to timing offsets or FFT window time misalignments rather than to frequency offsets because the symbol timing offset may vary over an interval equal to the cyclically extended guard time without causing any ISI or ICI. When a timing misalignment extends over the OFDM symbol boundaries then ISI and ICI occur. When, however, a timing misalignment does not extend over the OFDM symbol boundaries then no ISI or ICI occur and it is as if each sub-carrier was only phase offset. The relation between the phase offset φ_n of the nth complex sub-carrier and the timing offset τ is given by

$$\varphi_n = 2\pi f_n \tau \tag{2.36}$$

where f_n is the frequency of the nth complex sub-carrier. For an OFDM system with N sub-carriers and a sub-carrier spacing of $1/(T - T_{CP})$, a timing delay of one sampling interval of $(T - T_{CP})/N$ causes a significant phase shift of $2\pi(1 - 1/N)$ between the first and the last sub-carriers. These phase shifts add to any phase shifts already present due to a linear time dispersive channel and need to be estimated to perform coherent detection, as explained later.

Figure 2.12 shows the earliest and latest possible timing offsets that do not yield any ISI or ICI. Generally, we may distinguish between two types of timing offsets or FFT window time misalignments, negative time shifts and positive time shifts. An OFDM symbol with a cyclic prefix only allows for negative time shifts if both ISI and ICI are to be avoided. An OFDM symbol with both a cyclic prefix and a cyclic postfix allows for both negative and positive time shifts. It is important to note, however, that any window misalignment will compromise the delay spread tolerance of the OFDM signal.

Other sources of problems in OFDM systems include oscillator phase noise stemming from inaccuracies in the transmitter and receiver oscillators [52,53,55-59] and sampling frequency errors [60,61]. These effects also introduce ICI in the received OFDM signal.

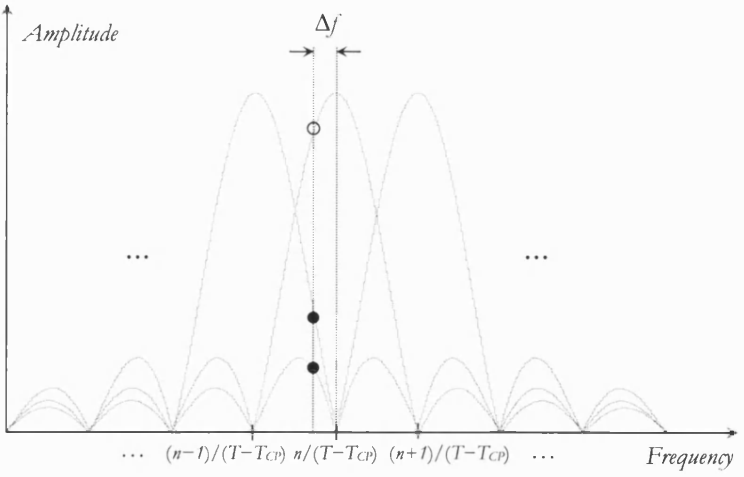

Figure 2.11: Effects of a frequency error of Δf : reduction of the power of the desired received symbol (○) and ICI from other sub-carriers (●).

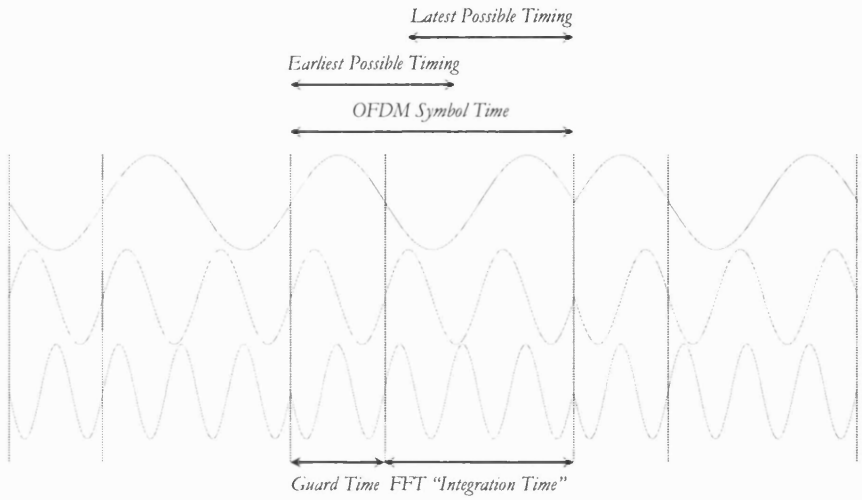

Figure 2.12: Earliest and latest possible timing offsets that do not yield any ISI or ICI. For simplicity three BPSK modulated sine waves are shown separately.

2.3.2 Non-linear distortion

In this section, we highlight the effects of non-linear distortion in OFDM systems. Since an OFDM signal generally consists of a large sum of independently modulated sub-carriers then it may exhibit large signal excursions and a large PAPR. Accordingly, an OFDM signal is very vulnerable to non-linear distortion caused by any non-linear element in the OFDM communication system such as HPAs.

The effect of a non-linearity on an OFDM signal can be appreciated from two different perspectives. From one view point, the large signal excursions occasionally reach the non-linear region of any non-linear element in the system and hence the non-linearity output is a distorted replica of the non-linearity input. From another view point, any non-linear element in the system introduces severe harmonic distortion (HD) and IMD due to the multi-carrier nature of an OFDM signal. For example, the response of a third-order or cubic non-linearity to a sum of sine waves with frequencies f_i, i=1,…,N, corresponds to a sum of sine waves consisting of the original sine waves with frequencies f_i, i=1,…,N, harmonics with frequencies $3f_i$, i=1,…,N,, and intermodulation products (IMP) of the type $f_i+f_j\pm f_k$ and $2f_i\pm f_j$, where i, j and k are integers that distinguish the different input frequencies. Generally, the response of an nth-order non-linearity to a signal consisting of a sum of sine waves corresponds to a signal also consisting of a sum of sine waves with frequencies corresponding to every possible combination of sums and/or differences of n input frequencies. These newly generated frequencies can fall in-band or out-of-band. Frequencies that fall in-band are associated with signal error probability degradation and

frequencies that fall out-of-band are associated with signal spectral spreading. Note that the two perspectives discussed above are related as the large signal excursions are the consequence of the multi-carrier nature of the OFDM signal.

Some of these considerations are illustrated in Figure 2.13 and Figure 2.14. Figure 2.13 shows the amplitude spectrum of the response of a non-linearity exhibiting up to third-order non-linear behaviour to a 3 sub-channel OFDM signal with sub-carrier frequencies f_1, f_2 and f_3. From this figure we observe that for narrowband systems frequencies resulting from even-order non-linear behaviour can in general be filtered out as they fall out-of-band whereas frequencies resulting from odd-order non-linear behaviour cannot as they may fall in-band. Third-order IMPs of the type $f_i+f_j-f_k$ and $2f_i-f_j$ are the most problematic. The number of IMPs of type $f_i+f_j-f_k$ and $2f_i-f_j$ falling in sub-channel n for an OFDM signal with N sub-channels are given respectively by [62]

$$_{n}IM_{11\bar{1}}^{N} = \frac{n}{2}(N-n+1)+\frac{1}{4}\left[(N-3)^2-5-\frac{1}{2}\left(1-(-1)^N\right)(-1)^{N+n}\right] \tag{2.37}$$

$$_{n}IM_{2\bar{1}}^{N} = \frac{1}{2}\left[N-2-\frac{1}{2}\left(1-(-1)^N\right)(-1)^n\right] \tag{2.38}$$

Figure 2.14 shows the total number of third-order IMPs as a function of sub-channel number for OFDM signals with different numbers of sub-channels. From this figure we observe that for the sub-channels on the edge of the band the number of IMPs is the lowest and for the sub-channels in the centre of the band the number of IMPs is the highest. It is therefore expected that the sub-channels located on the edge experience less degradation than the sub-channels located in the centre (see chapter 5 and chapter 6).

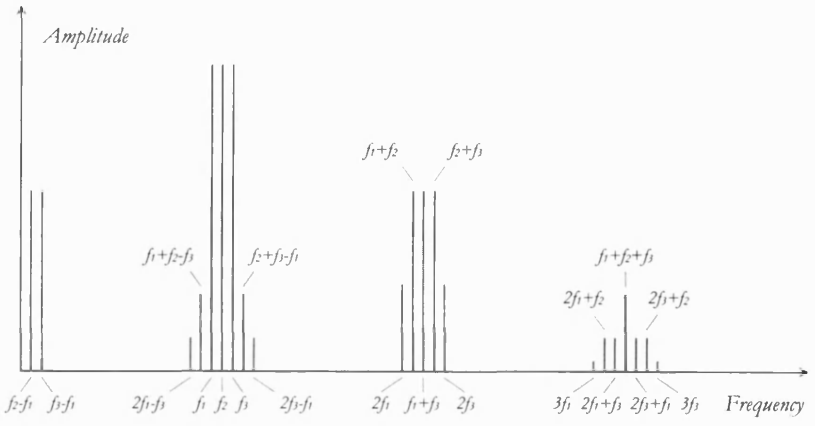

Figure 2.13: Amplitude spectrum of the response of a non-linearity exhibiting up to third-order non-linear behaviour to a 3 sub-channel OFDM signal with sub-carrier frequencies f_1, f_2 and f_3. For simplicity the amplitude spectrum for unmodulated OFDM sub-carriers is shown.

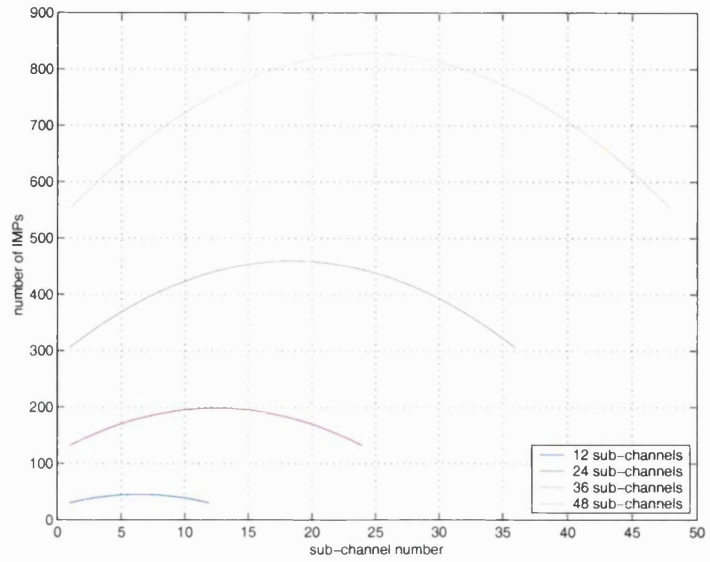

Figure 2.14: Total number of third-order IMPs as a function of sub-channel number for OFDM signals with different numbers of sub-channels.

Recently, considerable attention has been devoted to the performance assessment and performance improvement of non-linearly distorted OFDM signals. To assess the performance of a non-linearly distorted OFDM signal its PDS and its error probability have often been determined either by analysis [13-25], simulation [63,64], or hybrid analytical-simulation procedures [65,66]. PAPR reduction techniques such as clipping and peak windowing [67-69], peak cancellation [70], selective mapping and partial transmit sequences [71-76] and PAPR reduction codes [77-81] have been proposed to improve the performance of non-linearly distorted OFDM signals. For example, PAPR reduction codes introduce a set of redundant symbols into the set of data symbols in order to eliminate combinations that produce high peaks. Moreover, pre-distortion techniques have also been proposed to improve the performance of non-linearly distorted OFDM signals [82-84]. Pre-distortion relies on the prior distortion of an OFDM signal such that the effect of non-linearly distorting the distorted OFDM signal yields the original OFDM signal.

2.4 Elements of OFDM communication systems

Figure 2.15 depicts the principal elements of an OFDM communication system. In section 2.2, we have introduced the role of the IFFT and the FFT, the cyclic extension and the window. In this section, we consider other elements of an OFDM communication system such as encoders/decoders, interleavers/deinterleavers and mappers/demappers. Moreover, channel estimation and synchronisation operations are also considered.

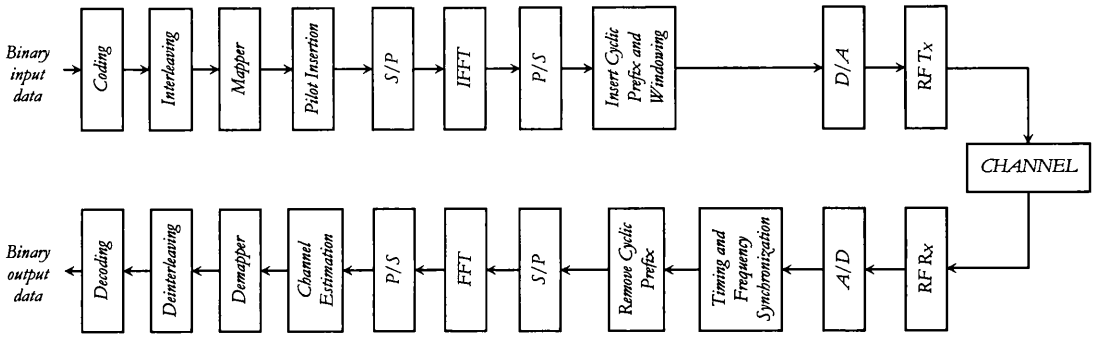

Figure 2.15: Principal elements of an OFDM communication system.

2.4.1 Coding/decoding and interleaving/deinterleaving blocks

We have shown in section 2.2.3 that the nth complex received symbol is an attenuated and phase shifted version of the nth complex transmitted symbol, where the attenuation and phase shift are given by the frequency response of the channel evaluated at the nth sub-carrier frequency (see (2.7)). Generally, the complex data symbol received in time slot k and sub-channel n, $R_{k,n}$, and the complex data symbol transmitted in time slot k and sub-channel n, $S_{k,n}$, are related by

$$R_{k,n} = H_{k,n}S_{k,n} + N_{k,n} \tag{2.39}$$

where $H_{k,n}$ is the channel frequency response in time slot k and sub-channel n and $N_{k,n}$ is a complex Gaussian RV. If the channel is a multi-path fading channel with many propagation paths between the transmitter and the receiver and without any line-of-sight propagation path then the amplitude of the transfer factors $H_{k,n}$ is Rayleigh distributed. Accordingly, some sub-carriers will be amplified resulting in high SNR based decisions at the receiver whereas other sub-carriers will be attenuated resulting in low SNR based decisions at the receiver. In the presence of Rayleigh fading, the error rate decreases only inversely with the SNR whereas, in the absence of Rayleigh fading, the error rate decreases exponentially with the SNR [42].

In OFDM channel coding is used so that the correctly received data of the relatively strong sub-carriers corrects the erroneously received data of the relatively weak sub-carriers. A number of channel coding schemes have been proposed for OFDM applications including block codes [44,45], convolutional codes [44,45,85], concatenated codes [38,39,44,45] and turbo codes [44,45,86]. Moreover, trellis-coded modulation has also been proposed for OFDM applications [40,44,45].

Occasional deep fades in the frequency response of the channel cause some groups of sub-carriers to be less reliable than other groups and hence cause bit errors to occur in bursts rather than independently. Since channel coding schemes are normally designed to deal with independent errors and not with error bursts then interleaving techniques are used to guarantee independence by effecting randomly scattered errors. At the transmitter, after encoding, the bits are permuted in such a way that adjacent bits are separated by several bits. At the receiver, before decoding, the reverse permutation is performed. Block or convolution interleavers can be used to accomplish this task [44,45]. For example, block interleavers write the bits in a matrix column by column and read the bits out from the matrix row by row.

Coding and interleaving techniques are therefore exploited to provide a link between independently fading time slots and sub-channels so that the information conveyed by well received sub-carriers corrects the information conveyed by fading sub-carriers. Note that the amount of separation in time and frequency that the interleaver ought to introduce is dictated by the coherence time and the coherence bandwidth of the channel[4]. Particularly, to guarantee for independently fading time slots and sub-channels the amount of separation in time has to be higher than the coherence time of the channel and the amount of separation in frequency has to be higher than the coherence bandwidth of the channel.

---

[4] The coherence bandwidth is a statistical measure of the range of frequencies over which the channel frequency response is essentially flat, or, in other words, the range of frequencies over which any two different frequency components conveyed over the channel have a strong potential for amplitude correlation. The coherence time is a statistical measure of the time duration over which the channel impulse response is essentially invariant, or, in other words, the time duration over which any two delayed versions of the same signal conveyed over the channel have a strong potential for amplitude correlation. The coherence time corresponds to the inverse of the Doppler spread introduced by the channel and the coherence bandwidth corresponds to the inverse of the delay spread introduced by the channel [42].

2.4.2 Mapping/demapping blocks

At the transmitter, after encoding and interleaving, the bits to be conveyed in the kth OFDM time slot and the nth OFDM sub-channel are mapped to a convenient modulation symbol, $S_{k,n}$. At the receiver, before de-interleaving and decoding, the received modulation symbols, $R_{k,n}$, are demapped yielding the bits conveyed in the kth OFDM time slot and the nth OFDM sub-channel[5].

The mapping between the bits to be conveyed in each OFDM time slot and sub-channel and the complex modulation symbols, $S_{k,n}$, can be carried out with or without differential encoding. With no differential encoding, the data bits are directly mapped to the complex modulation symbols, $S_{k,n}$. Examples of this modulation technique include M-ary phase shift keying (M-PSK) or M-ary quadrature amplitude modulation (M-QAM), where groups of $\log_2 M$ bits are mapped to a particular point in an M-PSK or an M-QAM signal constellation. Figure 2.16 illustrates Gray coded 16-PSK and 16-QAM signal constellations, where binary digit words assigned to adjacent symbol states differ by one binary digit only.

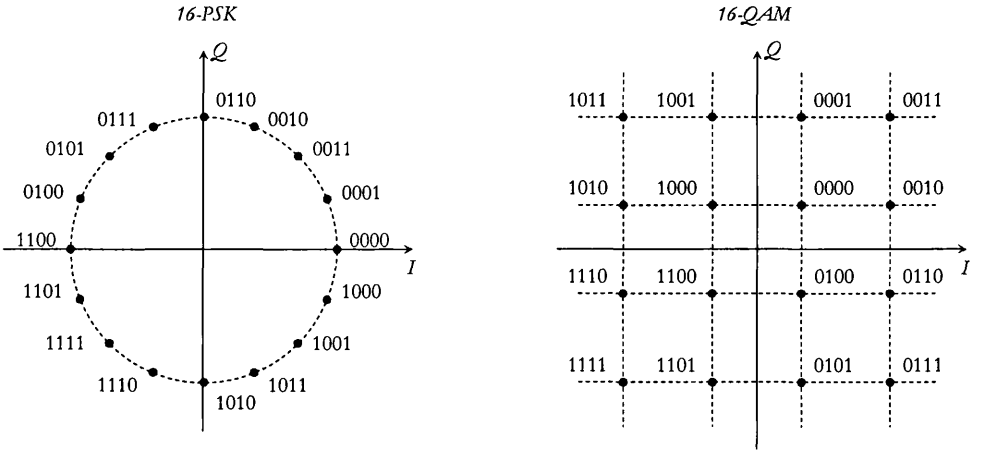

Figure 2.16: Gray coded 16-PSK and 16-QAM signal constellations.

[5] For hard decision based decoding, the demapper indeed yields the bits from the modulation symbols. However, for soft decision based decoding, the demapper yields a measure of the analogue error caused by the noise for each possible modulation symbol. The performance in noise for soft decision decoding is higher than that for hard decision decoding [42,85]. However, the complexity of soft decision decoders is also higher than that of hard decision decoders [42,85]. In this section, we shall only consider hard decision decoding.

With differential encoding, the data bits are not directly mapped to the complex modulation symbols, $S_{k,n}$, but rather to the quotient, $B_{k,n}$, of two successive complex modulation symbols, either in the time direction or in the frequency direction. If performed in the time direction then

$$S_{k,n} = S_{k-1,n} B_{k,n} \tag{2.40}$$

and to initialise this differential encoding process each sub-carrier of the first OFDM symbol conveys a known/reference value. If performed in the frequency direction then

$$S_{k,n} = S_{k,n-1} B_{k,n} \tag{2.41}$$

and to initialise this differential encoding process the first sub-carrier of each OFDM symbol conveys a known/reference value. Examples of this modulation technique include M-ary differential phase shift keying (M-DPSK), where $B_{k,n} \in \left\{ e^{j2\pi m/M} ; m = 0,\ldots,M-1 \right\}$.

Coherent detection or differential detection is employed at the receiver depending on the mapping scheme. For mappings without differential encoding then coherent detection is used at the receiver, whereby the decision is based on the quotient $D_{k,n}$ given by

$$D_{k,n} = \frac{R_{k,n}}{\hat{H}_{k,n}} \approx S_{k,n} + \frac{N_{k,n}}{\hat{H}_{k,n}} \tag{2.42}$$

where $\hat{H}_{k,n}$ is an estimate of the channel transfer factor $H_{k,n}$[6]. Such an estimate is important to identify the amplitude and phase references of the constellation in each OFDM sub-carrier so that the complex data symbols can be demodulated correctly. The principal advantage of OFDM follows from this simple equalisation operation. Essentially, by transmitting on multiple narrowband sub-channels the overall frequency selective channel is transformed into a collection of flat fading channels whose only effect is to introduce a random attenuation/phase shift in each OFDM sub-carrier. Accordingly, an OFDM channel equaliser corresponds to a bank of complex multipliers.

---

[6] Multiplication of the received symbols by $1/\hat{H}_{k,n}$ corresponds to an equalisation operation based on the zero-forcing (ZF) criterion. A ZF criterion aims at minimising the ISI regardless of the noise power. An equalisation operation based on the minimum mean square error (MMSE) criterion would correspond to a multiplication of the received symbols by $\hat{H}^*_{k,n}/(|\hat{H}_{k,n}|^2+\sigma^2_n/\sigma^2_s)$, where σ^2_s is the variance of the data symbols and σ^2_n is the variance of the noise. An MMSE criterion aims at minimising the combined effects of ISI and noise and hence the performance of an MMSE equaliser is higher than that of a ZF equaliser, especially for channels with spectral nulls [42].

For mappings with differential encoding then differential detection is used at the receiver. If differential encoding has been performed in the time direction then differential detection is achieved by comparing the information on the same sub-carrier in consecutive OFDM symbols and the decision is based on the quotient

$$D_{k,n} = \frac{R_{k,n}}{R_{k-1,n}} = \frac{S_{k-1,n}B_{k,n}H_{k,n} + N_{k,n}}{S_{k-1,n}H_{k-1,n} + N_{k-1,n}} \tag{2.43}$$

If differential encoding has been performed in the frequency direction then differential detection is achieved by comparing the information on consecutive sub-carriers in the same OFDM symbol and the decision is based on the quotient

$$D_{k,n} = \frac{R_{k,n}}{R_{k,n-1}} = \frac{S_{k,n-1}B_{k,n}H_{k,n} + N_{k,n}}{S_{k,n-1}H_{k,n-1} + N_{k,n-1}} \tag{2.44}$$

Note that, in the absence of noise, the symbol containing the information is recovered provided that the channel transfer factors $H_{k,n}$ and $H_{k-1,n}$ or $H_{k,n}$ and $H_{k,n-1}$ are identical. Therefore, encoding in the time direction requires that the signalling interval is smaller than the coherence time of the channel so that $H_{k,n} \approx H_{k-1,n}$ whereas encoding in the frequency direction requires that the sub-carrier spacing is smaller than the coherence bandwidth of the channel so that $H_{k,n} \approx H_{k,n-1}$.

Differential schemes, when compared to non-differential schemes, are very robust to residual phase offsets caused by a symbol timing offset or a non-perfect phase lock between the transmitter up-converter oscillator and the receiver down-converter oscillator. Moreover, differential schemes allow simpler receiver implementations because no channel estimation is necessary. However, in the presence of noise, differential detection exhibits up to 3 dB degradation in the SNR when compared to ideal coherent detection [42].

2.4.3 Channel estimation operations

We have shown in section 2.4.2 that whilst for differential detection no channel estimate is necessary, for coherent detection a channel estimate is necessary. Such an estimate is important to identify the amplitude and phase references of the constellation in each sub-carrier so that the complex data symbols can be demodulated correctly.

Channel estimation in OFDM systems involves the insertion of known symbols or a pilot structure into the OFDM signal that yield point estimates of the channel frequency response and an interpolation operation that yields the remaining points of the channel

frequency response from the point estimates. These two operations are interconnected since the performance of the estimator depends on how pilot information is transmitted [44,45].

A typical pilot structure to track channel variations in time and in frequency is shown in Figure 2.17. Since the channel can be viewed as a two-dimensional signal (in time and in frequency) sampled at the pilot positions then the two-dimensional sampling theorem imposes limits on the density of pilots to obtain an accurate representation of the channel. Essentially, the coherence time of the channel dictates the minimum separation of the pilots in the time direction and the coherence bandwidth of the channel dictates the minimum separation of the pilots in the frequency direction. On the one hand, the higher the density of pilot symbols the better the accuracy. On the other hand, the higher the density of pilot symbols the higher the loss in SNR and/or data rate [44,45].

One-dimensional and two-dimensional estimators have been proposed to extract the remaining points of the channel frequency response from the point estimates. One-dimensional estimators perform first a one-dimensional interpolation in the frequency direction for all symbols containing pilots and then a one-dimensional interpolation in the time direction to estimate the remaining channel values [87]. Two-dimensional estimators perform a two-dimensional interpolation based on all the pilot values [88,89]. Note that the complexity of one-dimensional estimators is lower than that of two-dimensional estimators but the former are less accurate than the later [44,45].

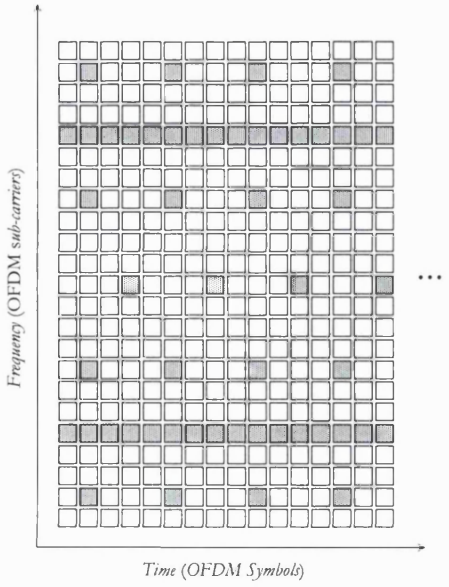

Figure 2.17: Typical pilot structure (marked grey) to track channel variations in time and in frequency.

2.4.4 Synchronisation operations

We have shown in section 2.3.1 that perfect symbol timing and carrier frequency synchronisation between the OFDM transmitter and the OFDM receiver is required to eliminate ISI and ICI. Synchronisation in OFDM systems is performed before demodulation and involves two phases: acquisition and tracking. In the acquisition phase, the frequency and timing errors are coarsely estimated and corrected. Then, in the tracking phase, only small short-term deviations are estimated and corrected. A number of techniques based on the transmission of special OFDM training symbols and on the cyclic prefix have been proposed to perform symbol timing and carrier frequency synchronisation [90-98]. Synchronisation techniques based on the cyclic prefix rely on the computation of the correlation of the received OFDM signal with a delayed version of the same received OFDM signal (the duration of the delay is equal to the duration of the useful OFDM symbol) over an interval equal to the cyclic prefix interval. Synchronisation techniques based on the transmission of special OFDM training symbols rely on the computation of the correlation of the received OFDM signal with the known OFDM training symbols. In both cases, the peaks of the correlation function yield the timing information and the phase of the peaks of the correlation function yield the frequency information [45].

2.5 Examples of OFDM communication systems

Hitherto, OFDM has been proposed for a variety of applications including ADSL, DAB, DVB and indoor wireless LANs. In this section, we discuss the use of OFDM in such applications.

2.5.1 ADSL

OFDM under the acronym of discrete multi-tone (DMT) has been adopted for ADSL [41]. ADSL is a scheme for digital high speed communication in the telephone access network or the subscriber line, where the bit rate offered in the downstream direction (to the subscriber) is larger than the bit rate offered in the upstream direction (to the central office). For example, in the USA the ADSL standard supports downstream bit rates from 1.54 to 6.1 Mbit/s and upstream bit rates from 9.6 to 192 kbit/s. ADSL is

suitable for applications like video on demand, games, virtual shopping and internet surfing.

Copper wire pairs are the dominating medium type in telephone access networks or subscriber lines. Impairments in this environment include the "highly spectrally shaped" frequency response of a typical copper wire pair and various noise sources. The attenuation transfer function of a typical copper wire pair is given by

$$A(f) = e^{dk\sqrt{f}} \tag{2.45}$$

where d is the length of the wire pair and k is a constant of the wire pair. Noise sources include crosstalk from other copper wire pairs in the same cable, RF noise from nearby transmitters and impulse noise from relays, switches and electrical machines. AWGN is not generally a limiting factor in subscriber lines for short cables but for long cables. Two different forms of crosstalk exist, near-end crosstalk (NEXT) and far-end crosstalk (FEXT). NEXT occurs at the central office when the weak upstream signal is disturbed by strong downstream signals (see Figure 2.18). FEXT is crosstalk from one transmitted signal to another in the same direction and appears both at the central office and the subscriber (see Figure 2.19).

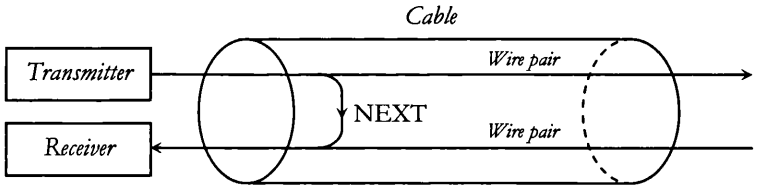

Figure 2.18: NEXT.

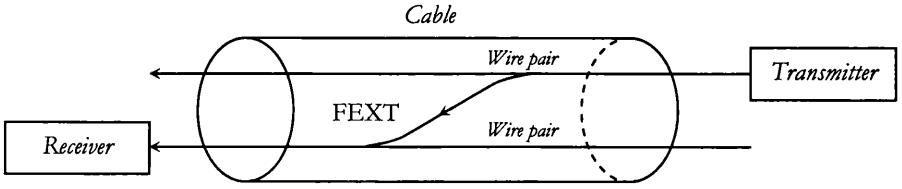

Figure 2.19: FEXT.

OFDM in conjunction with bit loading techniques has been selected for ADSL for it efficiently combats the adverse effects in the telephone access network or the subscriber line. Bit loading is a scheme whereby higher-order constellations are assigned to high SNR sub-channels and lower-order constellations are assigned to low SNR sub-channels. Essentially, OFDM in conjunction with bit loading techniques offers a practical solution to achieve transmission rates close to the capacity of a "highly frequency shaped" linear channel [99]. Shannon derived the "water pouring" or "water filling" theorem, which formalises the concept of allocating higher power to lower SNR sub-channels and lower power to higher SNR sub-channels to achieve the capacity of a "highly frequency shaped" linear channel [100][7].

2.5.2 Digital broadcasting systems

OFDM systems have been proposed to assist the migration from old analogue broadcasting systems to new digital broadcasting systems. For example, in Europe OFDM has been adopted for DAB [3] and terrestrial DVB [4].

OFDM in conjunction with powerful coding and interleaving techniques, i.e., coded orthogonal frequency division multiplexing (COFDM), has been selected for digital broadcasting systems due to its capability to combat multi-path propagation and narrowband interference and due to its capability to allow for the implementation of SFNs.

Narrowband interference originates from the coexistence of analogue and digital broadcasting systems. Narrowband interference can be combated efficiently using spectrum shaping techniques. Essentially, sub-carriers experiencing high signal-to-interference ratios (SIR) are transmitted whereas sub-carriers experiencing low SIRs are not transmitted.

The structure of an SFN is shown in Figure 2.20. In a conventional broadcasting network, geographically adjacent transmitters transmit the same signal/program on distinct frequencies. In a single frequency broadcasting network, on the other hand, several geographically dispersed transmitters transmit the same signal/program synchronously on

[7] Recently, OFDM in conjunction with bit loading techniques or adaptive OFDM modulation has also been introduced in wireless systems [101]. Application of these techniques in the wireless environment is more complex than in the wired environment for in the first case the channel varies with time whereas in the second case it does not significantly.

the same frequency. A receiver therefore observes several replicas of the same signal possibly attenuated and delayed with respect to one another. Provided that an efficient means is available to combat the dispersion in time observed by the receiver then an SFN can greatly enhance the spectrum and power efficiency of a broadcasting system. Spectrum efficiency is improved because only a single frequency instead of multiple frequencies is used to cover an entire region or country. Power efficiency is improved because the coverage area served for example by two transmitters operating simultaneously is greater than the sum of the coverage areas for each of the two transmitters operating independently [86]. Essentially, the phenomena occurring in an SFN is analogous to the phenomena occurring in a multi-path fading channel and hence it can be combated efficiently with COFDM.

2.5.3 Indoor wireless LANs

Growing interest in high speed wireless packet switched services such as wireless Internet access and wireless multimedia, on the one hand, and advances in integrated personal computers and communication devices, on the other hand, has resurrected a high interest in wireless LANs. Recently, OFDM has been selected as the basis for the physical layer of a number of packet based indoor wireless LAN standards such as the HIPERLAN2 [5] and the IEEE 802.11a [6] for the 5 GHz band, and the IEEE 802.11g [7] for the 2.4 GHz band, after projects like the European Magic WAND demonstrated the viability of OFDM for this type of application [102].

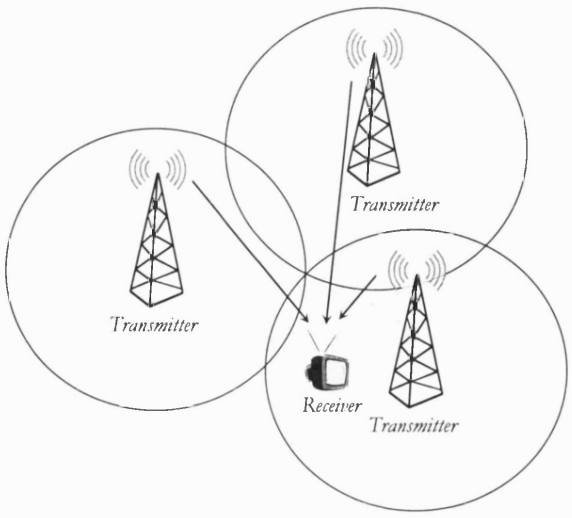

Figure 2.20: Structure of an SFN.

For example, HIPERLAN2 is a standard to interconnect portable devices to broadband networks based on Internet protocol (IP), asynchronous transfer mode (ATM), or other technologies and universal mobile telecommunication system (UMTS) networks. It offers data rates ranging from 6 Mbit/s to 54 Mbit/s and quality of service (QoS) support and mobility support within the area of service. The topology of a typical HIPERLAN2 network is shown in Figure 2.21. In the centralised mode, HIPERLAN2 is operated as an access network via a fixed access point (AP) and the mobile terminals (MT) communicate with APs over an air interface. In the direct mode, HIPERLAN2 is operated as an adhoc network without relying on a cellular network infrastructure and MTs communicate directly with each other. In this case, a central controller (CC), which is dynamically selected among the portable devices, provides the same QoS support as the fixed APs.

Table 2.1 shows the main OFDM parameters of the HIPERLAN2 standard. The key parameter that largely determined the majority of the other parameters was the cyclic prefix duration. To provide for robustness against delay spreads up to several hundreds of nano seconds, which are typical of indoor environments and large factory buildings, the OFDM cyclic prefix duration was set to 800 ns. And, to limit the SNR loss to 1 dB the OFDM symbol duration was set to 4000 ns. A total of 52 sub-carriers are used, 48 are data carriers and 4 are pilot carriers. The sub-carrier spacing, which corresponds to the inverse of the OFDM symbol duration minus the OFDM cyclic prefix duration, is equal to 312.5 kHz. And, the overall signal bandwidth, which is equal to the total number of sub-carriers times the sub-carrier spacing, is equal to 16.25 MHz. Table 2.2 shows the different combinations of modulation and forward error correction to obtain the different data rates ranging from 6 Mbit/s to 54 Mbit/s. Modulation schemes used are BPSK, QPSK, 16-QAM and 64-QAM. Forward error correction uses the industrial standard convolutional code with rate 1/2, constraint length 7 and generator polynomials (133,171) octal. Higher coding rates of 9/16 and 3/4 are obtained by puncturing the rate 1/2 code.

In Europe two frequency bands have been defined for HIPERLAN2 transmissions. In the lower frequency band from 5.150 GHz to 5.350 GHz, the first OFDM channel is centred around 5.180 GHz and the last one is centred around 5.320 GHz. In the upper frequency band from 5.470 GHz to 5.725 GHz, the first OFDM channel is centred around 5.500 GHz and the last one is centred around 5.700 GHz. Consecutive OFDM channels are spaced 20 MHz apart.

Table 2.1: Main OFDM parameters of the HIPERLAN2 standard.

Number of data sub-carriers	48
Number of pilot sub-carriers	4
OFDM symbol duration	4000 ns
OFDM cyclic prefix duration	800 ns
Sub-carrier spacing	312.5 kHz
3 dB bandwidth	16.56 MHz

Table 2.2: Different combinations of modulation and forward error correction to obtain data rates ranging from 6 Mbit/s to 54 Mbit/s.

Modulation	Coding Rate	Data Rate (Mbit/s)
BPSK	1/2	6
BPSK	3/4	9
QPSK	1/2	12
QPSK	3/4	18
16-QAM	9/16	27
16-QAM	3/4	36
64-QAM	3/4	54

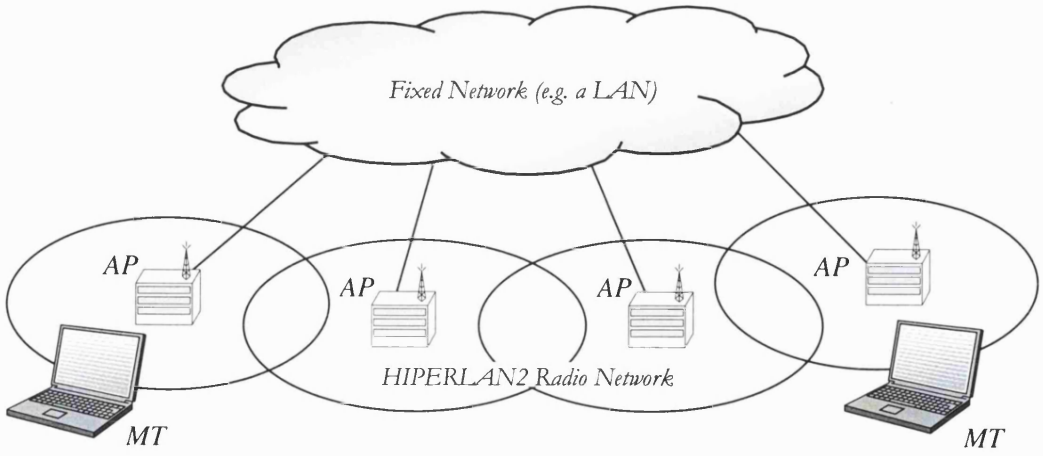

Figure 2.21: Topology of a HIPERLAN2 network.

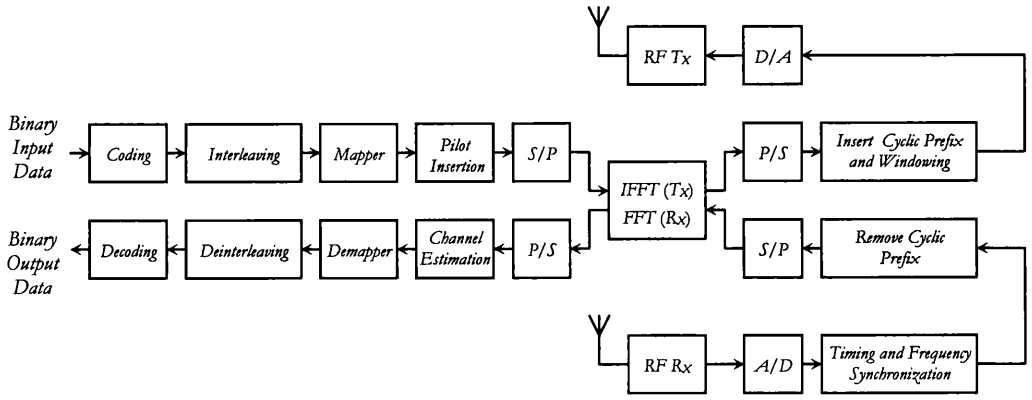

Figure 2.22: Structure of the OFDM transceiver.

The structure of the OFDM transceiver is shown in Figure 2.22. In the transmitter path, the binary data is encoded using a convolutional encoder, interleaved and then mapped to QAM values. Four pilot values are added to 48 data values which are modulated onto 52 sub-carriers using a 64-size IFFT. Subsequently, a cyclic prefix and windowing are applied to the IFFT output. Finally, the digital signal is converted to an analogue signal, up-converted to the 5 GHz band, amplified and radiated. In the receiver path, the reverse operations are performed. Moreover, in the receiver path, additional training tasks such as start-of-packet detection, automatic gain control, symbol timing and frequency offset estimation, and channel frequency response estimation are also performed by using special training symbols in the preamble of each OFDM packet and the pilot symbols.

2.6 Other OFDM initiatives

Throughout this chapter, we have considered an OFDM scheme where N orthogonal sub-carriers are modulated by N complex data symbols. However, other OFDM initiatives have been proposed in the literature

Chang and Saltzberg have introduced an OFDM scheme with bounded spectrum. In this scheme, a set of sub-carriers spaced in frequency by $1/T$ (T is the useful symbol duration) are modulated by a set of data symbols using staggered or offset QAM such that adjacent sub-carriers are staggered or offset oppositely [103-105]. The data is filtered by a square-root Nyquist filter with a roll-off factor between 0 and 1. Figure 2.23 shows the bandpass transmitter and receiver of such a scheme.

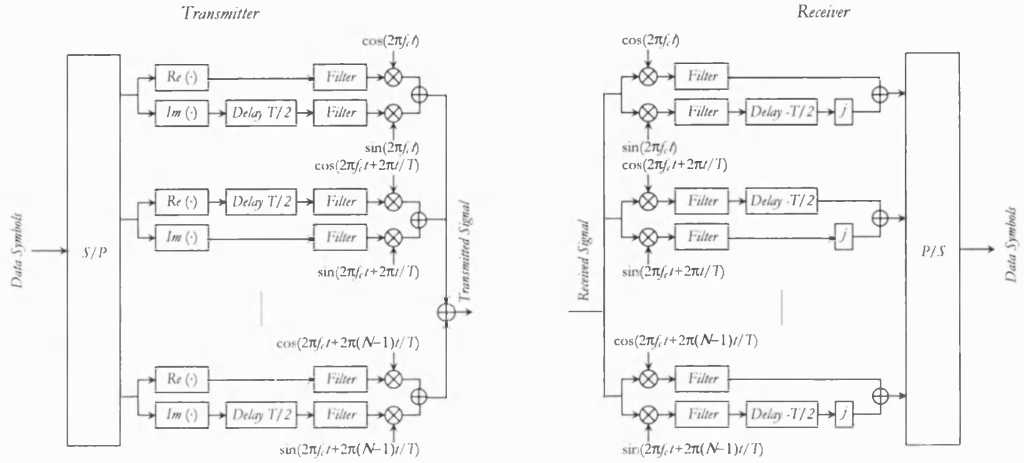

Figure 2.23: Bandpass transmitter and receiver of the OFDM scheme proposed by Chang and Saltzberg [103-105].

Recently, Rodrigues and Darwazeh have introduced an FOFDM scheme with a higher bandwidth efficiency [106]. In this scheme, a set of sub-carriers spaced in frequency by $1/2T$ are modulated by a set of data symbols. Figure 2.24 shows the baseband transmitter and receiver of such a scheme. The bandwidth efficiency of FOFDM is twice the bandwidth efficiency of OFDM because in FOFDM a $1/2T$ inter-carrier frequency spacing is used whereas in OFDM the inter-carrier frequency spacing is $1/T$. However, whilst each OFDM sub-carrier can be modulated by complex modulation symbols drawn from any M-PSK or any M-QAM signal constellation, each FOFDM sub-carrier can only be modulated by real modulation symbols drawn from a BPSK or an M-ary amplitude shift keying (M-ASK) signal constellation otherwise severe ICI results upon demodulation.

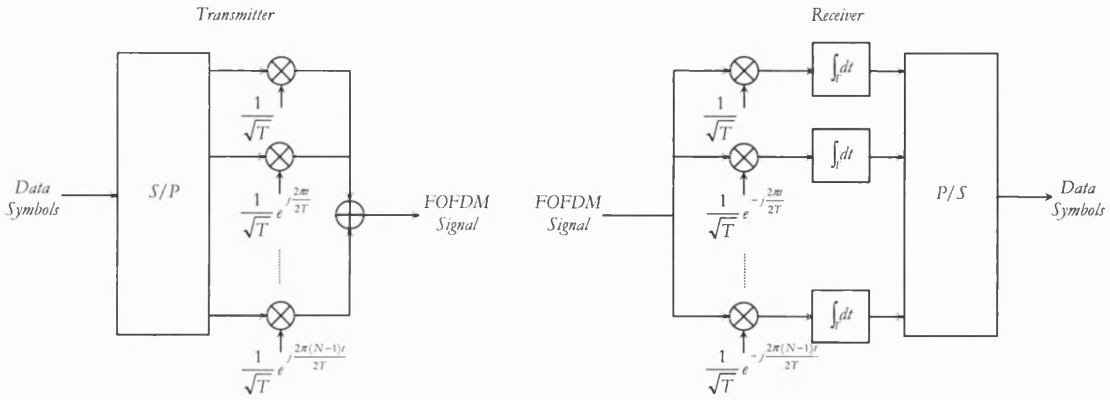

Figure 2.24: Baseband transmitter and receiver of the FOFDM scheme proposed by Rodrigues and Darwazeh [106].

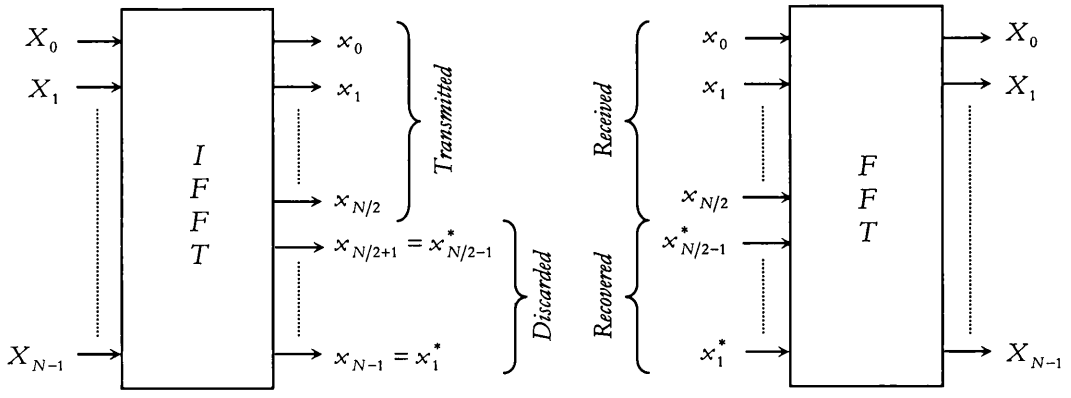

Figure 2.25: Principles of the FOFDM scheme proposed by Oh and Lim [107].

Oh and Lim have proposed an alternative FOFDM scheme in the context of multi-carrier code division multiple access (CDMA) systems [107]. Essentially, Oh and Lim have observed that if the IFFT input values X_n, $n = 0,\ldots,N-1$ are binary and hence real then the output IFFT values x_k, $k = 0,\ldots,N-1$ are such that $x_{N-k} = x_k^*$. Accordingly, instead of transmitting the N samples only the first $N/2+1$ samples are transmitted because the receiver can always recover the remaining values from the received values (see Figure 2.25). In the limit, the number of samples to be transmitted decreases by a factor of 2 and hence the bandwidth also decreases by a factor of 2.

FOFDM has been introduced by the author after completion of the research work contained in this thesis and hence it will not be considered further. Appendix A includes the paper written by the author which introduces the basics of FOFDM and its advantages and disadvantages.

2.7 Summary

In this chapter, we have presented the principal ideas behind OFDM that will be used throughout this thesis. The chapter began with a discussion of the basic OFDM principle where concepts such as the oscillator based implementation and the FFT based implementation of an OFDM transceiver, the guard time and the cyclic prefix and windowing were reviewed. The drawbacks of OFDM were then reviewed. Particularly, we have introduced the effects of synchronisation errors and non-linear distortion on an OFDM signal. Subsequently, the elements of an OFDM communication system including

mapping/demapping blocks, coding/decoding and interleaving/deinterleaving blocks, and synchronisation and channel estimation operations were described. Examples of OFDM communication systems including ADSL, digital broadcasting systems (DAB and DVB) and indoor wireless LANs were then described. Finally, the chapter ended with a discussion of other OFDM initiatives. Particularly, we have introduced an FOFDM scheme with twice the bandwidth efficiency of conventional OFDM schemes.

In the following chapters, we concentrate on the development of analytic techniques to assess the impact of fibre-radio system non-linearities on the performance of OFDM signals. These analytic techniques aim at capturing the two main effects of a non-linearity on an OFDM signal, which are signal spectral spreading due to IMD frequency components falling out-of-band and error probability degradation due to IMD frequency components falling in-band. Specifically, we concentrate on the impact of the non-linearities on OFDM/BPSK and OFDM/QPSK signals, i.e., OFDM signals with either BPSK or QPSK modulation in each sub-carrier. Coding/decoding and interleaving/deinterleaving operations are not considered. Moreover, the effect of non-perfect channel estimation and synchronisation operations or any form of interaction between these effects and non-linear effects are not considered either. Accordingly, with these simplifications we will be able to clearly define the effects of a non-linearity on an OFDM signal.

Chapter 3

Impact of non-linearities on the PDS of OFDM signals

3.1 Introduction

In the previous chapter, we have argued that any non-linear element in an OFDM communication system will introduce HD and IMD due to the multi-carrier nature of the OFDM signals. We have also argued that IMD frequency components falling out-of-band will induce signal spectral spreading whereas IMD frequency components falling in-band will induce signal error probability degradation. In this chapter, we develop an analytic technique to determine the impact of non-linearities on the PDS of OFDM signals, which enables us to evaluate the spectral spreading of OFDM signals. We note that aspects of the research presented in this chapter have been presented in papers published in the open literature [108-110].

The development of analytic techniques to determine the PDS of non-linearly distorted OFDM signals has been a subject of extensive research [13-25]. Yet, since these developments have focused on techniques for assessing the impact on the PDS of OFDM signals of clipping devices and HPAs, which exhibit frequency independent non-linear behaviour, then they cannot be carried over directly to determine the impact of fibre-radio system elements, which normally exhibit frequency dependent non-linear behaviour. In this chapter, in order to accommodate frequency dependent behaviour we use a Volterra series to model the non-linearities encountered in the OFDM system. An introduction to the

Volterra series representation of non-linearities is the subject of section 3.2. The development of the analytical method itself and then its application to simple non-linearities are considered in section 3.3 and section 3.4, respectively. Finally, section 3.5 summarises the main contributions of this chapter.

3.2 Volterra series representation of non-linearities

The Volterra series representation of non-linear systems can be seen as a generalisation of the convolution integral representation of linear systems [111,112]. This representation relates the response $y(t)$ of a non-linearity to the excitation $x(t)$ as follows

$$y(t) = \sum_{n=1}^{\infty} y_n(t) \tag{3.1}$$

$$y_n(t) = \int_{-\infty}^{\infty} \cdots \int_{-\infty}^{\infty} h_n(\tau_1, \ldots, \tau_n) x(t-\tau_1) \cdots x(t-\tau_n) d\tau_1 \cdots d\tau_n \tag{3.2}$$

where $h_n(\tau_1, \ldots, \tau_n)$ is the nth-order kernel or the nth-order impulse response of the non-linearity. Note that in this series expansion the first term corresponds to the familiar convolution integral and takes into account the linear contribution of the non-linearity; the second term corresponds to a two-dimensional convolution of $x(t)$ and the second-order kernel $h_2(\tau_1, \tau_2)$ and is of a quadratic nature; the third term corresponds to a three-dimensional convolution of $x(t)$ and the third-order kernel $h_3(\tau_1, \tau_2, \tau_3)$ and is of a cubic nature; etc. The Volterra series representation of a non-linearity can also be seen as a generalisation of the power series representation of an instantaneous non-linearity and hence it accommodates both frequency dependent and frequency independent non-linear behaviour. Frequency dependence implies that the output depends on the past values of the input whereas frequency independence implies that the output only depends on the current value of the input. For a frequency independent non-linearity the kernels consist of Dirac delta impulses, i.e., $h_n(\tau_1, \ldots, \tau_n) = c_n \delta(\tau_1) \cdots \delta(\tau_n)$, whereas for a frequency dependent non-linearity the kernels have some support, i.e., $h_n(\tau_1, \ldots, \tau_n)$ is non-zero for

$\tau_1 \in [0, \tau_{1_{max}}], \ldots, \tau_n \in [0, \tau_{n_{max}}]$, where the lower limits defining the support of the nth-order kernels guarantee that the non-linearity is causal. Figure 3.1 shows the equivalent block diagram for the Volterra series representation of a non-linear system.

The n-dimensional Fourier transform of the nth-order kernel yields the nth-order transfer function of the system

$$H_n(f_1,\ldots,f_n) = \int_{-\infty}^{\infty}\cdots\int_{-\infty}^{\infty} h_n(\tau_1,\ldots,\tau_n) e^{-j2\pi(f_1\tau_1+\cdots+f_n\tau_n)} d\tau_1 \cdots d\tau_n \tag{3.3}$$

Conversely, the n-dimensional inverse Fourier transform of the nth-order transfer function yields the nth-order kernel of the system

$$h_n(\tau_1,\ldots,\tau_n) = \int_{-\infty}^{\infty}\cdots\int_{-\infty}^{\infty} H_n(f_1,\ldots,f_n) e^{j2\pi(f_1\tau_1+\cdots+f_n\tau_n)} df_1 \cdots df_n \tag{3.4}$$

The response of the nth-order contribution of a non-linearity to a sum of m complex exponentials with frequencies f_k, where $k = 1,2,\ldots,m$, corresponds to the sum of m^n complex exponentials with frequencies $f_{k_1} + f_{k_2} + \cdots + f_{k_n}$, where $k_1, k_2, \ldots, k_n = 1,2,\ldots,m$. The nth-order transfer function $H_n(f_{k_1}, f_{k_2}, \ldots, f_{k_n})$ then gives the amplitude and phase of the complex exponential with frequency $f_{k_1} + f_{k_2} + \cdots + f_{k_n}$. Constant transfer functions $H_n(f_1,\ldots,f_n) = c_n$, corresponding to the n-dimensional Fourier transform of kernels $h_n(\tau_1,\ldots,\tau_n) = c_n\delta(\tau_1)\cdots\delta(\tau_n)$, indicate frequency independent behaviour. Non-constant transfer functions, corresponding to the n-dimensional Fourier transform of other kernels, indicate frequency dependent behaviour.

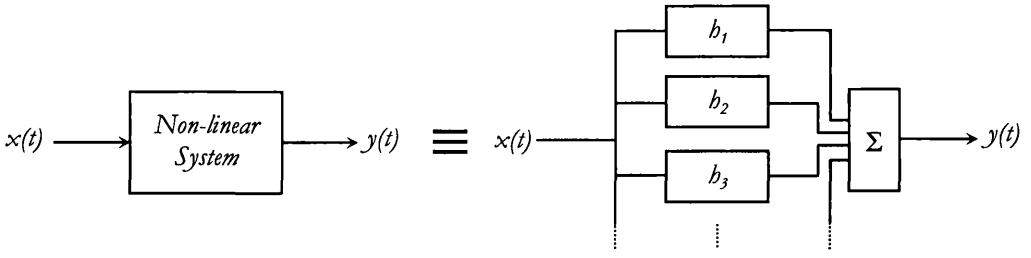

Figure 3.1: Equivalent block diagram for the Volterra series representation of a non-linear system.

Note that the transfer functions of a non-linearity exhibit Hermitian symmetry because the kernels of a non-linearity are real, i.e.,

$$H_n^*(f_1,\ldots,f_n) = H_n(-f_1,\ldots,-f_n) \tag{3.5}$$

The spectrum of the response $Y(f)$ of the non-linearity is related to the spectrum of the excitation $X(f)$ as follows

$$Y(f) = \sum_{n=1}^{\infty} Y_n(f) \tag{3.6}$$

$$Y_n(f) = \int_{-\infty}^{\infty}\cdots\int_{-\infty}^{\infty} H_n(f_1,\ldots,f_n)X(f_1)\cdots X(f_n)\delta(f-f_1-\cdots-f_n)df_1\cdots df_n \tag{3.7}$$

where $\delta(\cdot)$ is the Dirac delta function. This relation was determined by taking the Fourier transform of (3.1) and (3.2). Again, the familiar linear contribution and higher-order contributions of the non-linearity are recognisable in the previous equations.

Finally, we observe that since the nth-order contribution of the non-linearity in (3.2) or (3.7) does not depend on the order of the arguments in $h_n(\tau_1,\ldots,\tau_n)$ or $H_n(f_1,\ldots,f_n)$, respectively, then all kernels or transfer functions that differ only by a permutation of their arguments are equivalent in representing the non-linearity. Hereafter, we assume without loss of generality that the kernels and the transfer functions are symmetric functions of their arguments, i.e., that the order of the arguments can be interchanged in $h_n(\tau_1,\ldots,\tau_n)$ and $H_n(f_1,\ldots,f_n)$. Note that symmetric kernels $h_n'(\tau_1,\ldots,\tau_n)$ and symmetric transfer functions $H_n'(f_1,\ldots,f_n)$ can always be obtained from non-symmetric kernels $h_n(\tau_1,\ldots,\tau_n)$ and non-symmetric transfer functions $H_n(f_1,\ldots,f_n)$ as follows [111,112]

$$h_n'(\tau_1,\ldots,\tau_n) = \frac{1}{n!}\sum_{\substack{\text{all permutations}\\ \text{of } \tau_1,\ldots,\tau_n}} h_n(\tau_1,\ldots,\tau_n) \tag{3.8}$$

and

$$H_n'(f_1,\ldots,f_n) = \frac{1}{n!}\sum_{\substack{\text{all permutations}\\ \text{of } f_1,\ldots,f_n}} H_n(f_1,\ldots,f_n) \tag{3.9}$$

The Volterra series has been used extensively to model and analyse non-linear devices, such as amplifiers [113-117] or laser diodes (LD) [118-120], and non-linear communication systems, such as digital communication systems [121-128] or optical fibre communication systems [129-133]. The Volterra series is mostly useful for mild non-linearities when the number of kernels or transfer functions required to model the non-linearities is small and hence the number of terms in (3.1) or (3.6) is also small. In this thesis, we use a Volterra series to model and analyse non-linear OFDM communication systems, which can be represented by three kernels or three transfer functions.

3.2.1 Finding the kernels/transfer functions of a non-linearity

To represent a non-linearity by a Volterra series its kernels and its transfer functions have to be known. In this section, we describe an analytical method, the harmonic input method, to determine the transfer functions and hence the kernels of a non-linearity from the equations that define the behaviour of the same non-linearity [117,121].

The harmonic input method relies on the fact that a harmonic input results in a harmonic output, or, in other words, an input that consists of a sum of complex exponentials results in an output that also consists of a sum of complex exponentials. Thus, if the input signal is given by

$$x(t)=\sum_{k=1}^{n} e^{j2\pi f_k t} \tag{3.10}$$

where the frequencies $f_k, k=1,\ldots,n$, are linearly independent, i.e., the ratio of all possible pairs of frequencies is not a rational number, then the output signal is given by

$$\begin{aligned} y(t) &= \sum_{i=1}^{\infty} \int_{-\infty}^{\infty} \cdots \int_{-\infty}^{\infty} h_i(\tau_1,\ldots,\tau_i)\left[\sum_{k=1}^{n} e^{j2\pi f_k(t-\tau_1)}\right]\cdots\left[\sum_{k=1}^{n} e^{j2\pi f_k(t-\tau_i)}\right] d\tau_1\cdots d\tau_i \\ &= \sum_{i=1}^{\infty}\sum_{k_1=1}^{n}\cdots\sum_{k_i=1}^{n}\left[\int_{-\infty}^{\infty}\cdots\int_{-\infty}^{\infty} h_i(\tau_1,\ldots,\tau_i) e^{-j2\pi\left(f_{k_1}\tau_1+\cdots+f_{k_i}\tau_i\right)} d\tau_1\cdots d\tau_i\right] e^{j2\pi\left(f_{k_1}+\cdots+f_{k_i}\right)t} \\ &= \sum_{i=1}^{\infty}\sum_{k_1=1}^{n}\cdots\sum_{k_i=1}^{n} H_i\left(f_{k_1},\ldots,f_{k_i}\right) e^{j2\pi\left(f_{k_1}+\cdots+f_{k_i}\right)t} \end{aligned} \tag{3.11}$$

The (symmetric) nth-order transfer function is therefore obtained from the coefficient of $n!e^{j2\pi(f_1+f_2+\cdots+f_n)t}$. This result follows by realising that the response of the non-linearity to the sum of n complex exponentials, whose frequencies $f_k, k=1,\ldots,n$, are linearly independent, contains exactly $n!$ terms with frequencies $f_1+f_2+\cdots f_n$, where each term corresponds to a permutation of $f_1,f_2,\ldots,f_n$ in the argument of $H_n(f_1,\ldots,f_n)$. Moreover, this result suggests a recursive method for evaluating the transfer functions from the equations that define the behaviour of a non-linearity. Firstly, the system is probed by a single complex exponential and the first-order transfer function $H_1(f_1)$ is determined; secondly, the system is probed by the sum of two complex exponentials and the second-order transfer function $H_2(f_1,f_2)$ is determined; etc. This procedure continues with one additional complex exponential being added to the input at each step. Obviously, the (symmetric) nth-order kernel is obtained by taking the n-dimensional inverse Fourier transform of the (symmetric) nth-order transfer function.

As an example, we determine the transfer functions and the kernels of a frequency independent and a frequency dependent non-linearity, which will be used later in the chapter. The frequency independent non-linearity is shown in Figure 3.2, where $f(\cdot)$ represents a memoryless device whose characteristics can be expanded in a power series

$$f(z)=\sum_{i=1}^{\infty}c_i z^i \tag{3.12}$$

so that the input-output relationship can be written as

$$y(t)=\sum_{i=1}^{\infty}c_i[x(t)]^i \tag{3.13}$$

The transfer functions and hence the kernels of this non-linearity can be determined by following the procedure outlined above.

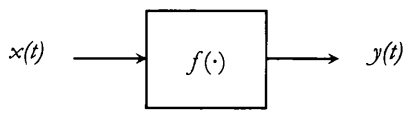

Figure 3.2: Frequency independent non-linearity model.

The response of the frequency independent non-linearity to a sum of n complex exponentials, whose frequencies are assumed to be linearly independent, is

$$\begin{aligned} y(t) &= \sum_{i=1}^{\infty} c_i \left[\sum_{k=1}^{n} e^{j2\pi f_k t} \right]^i \\ &= \sum_{i=1}^{\infty} \sum_{k_1=1}^{n} \cdots \sum_{k_i=1}^{n} c_i e^{j2\pi (f_{k_1} + \cdots + f_{k_i}) t} \end{aligned} \tag{3.14}$$

and the nth-order transfer function follows by identifying the coefficient of $n! e^{j2\pi(f_1+f_2+\cdots+f_n)t}$ in (3.14), i.e.,

$$H_n(f_1, f_2, \ldots, f_n) = c_n \tag{3.15}$$

Finally, the nth-order kernel of the frequency independent non-linearity is obtained by taking the n-dimensional inverse Fourier transform of its nth-order transfer function. Thus,

$$h_n(\tau_1, \tau_2, \ldots, \tau_n) = c_n \delta(\tau_1)\delta(\tau_2)\cdots\delta(\tau_n) \tag{3.16}$$

The results in (3.15) and (3.16) are not surprising as we had already commented on the nature of the transfer functions and the kernels for a frequency independent non-linearity.

The frequency dependent non-linearity is shown in Figure 3.3, where $H'(f)$ and $H''(f)$ are frequency responses of linear systems and $f(\cdot)$ again represents a memoryless device whose characteristics can be expanded in a power series

$$f(z) = \sum_{i=1}^{\infty} c_i z^i \tag{3.17}$$

so that the input-output relationship can be written as

$$y(t) = \sum_{i=1}^{\infty} c_i \int_{-\infty}^{\infty} h''(\lambda_1) \left[\int_{-\infty}^{\infty} h'(\lambda_2) x(t - \lambda_1 - \lambda_2) d\lambda_2 \right]^i d\lambda_1 \tag{3.18}$$

where $h'(t)$ and $h''(t)$ are the impulse responses of the linear systems.

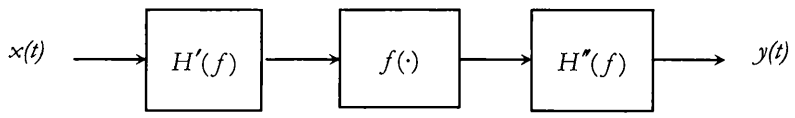

Figure 3.3: Frequency dependent non-linearity model.

By following the procedure outlined above the transfer functions and hence the kernels of this non-linearity can be determined. The response of the frequency dependent non-linearity to a sum of n complex exponentials, whose frequencies are assumed to be linearly independent, is

$$\begin{aligned} y(t) &= \sum_{i=1}^{\infty} c_i \int_{-\infty}^{\infty} h''(\lambda_1) \left[\int_{-\infty}^{\infty} h'(\lambda_2) \left[\sum_{k=1}^{n} e^{j2\pi f_k (t-\lambda_1-\lambda_2)} \right] d\lambda_2 \right]^i d\lambda_1 \\ &= \sum_{i=1}^{\infty} \sum_{k_1=1}^{n} \cdots \sum_{k_i=1}^{n} c_i H''(f_{k_1} + \cdots + f_{k_i}) H'(f_{k_1}) \cdots H'(f_{k_i}) e^{j2\pi (f_{k_1} + \cdots + f_{k_i})t} \end{aligned} \tag{3.19}$$

and by identifying the coefficient of $n! e^{j2\pi(f_1+f_2+\cdots+f_n)t}$ in (3.19) the nth-order transfer function follows, i.e.,

$$H_n(f_1, f_2, \ldots, f_n) = c_n H''(f_1 + f_2 + \cdots + f_n) H'(f_1) H'(f_2) \cdots H'(f_n) \tag{3.20}$$

Finally, the nth-order kernel of the frequency dependent non-linearity is obtained by taking the n-dimensional inverse Fourier transform of its nth-order transfer function. Thus,

$$h_n(\tau_1, \tau_2, \ldots, \tau_n) = c_n \int_{-\infty}^{\infty} h''(\lambda) h'(\tau_1 - \lambda) h'(\tau_2 - \lambda) \cdots h'(\tau_n - \lambda) d\lambda \tag{3.21}$$

3.3 Analytic technique

In this section, we develop an analytic technique to determine the PDS of OFDM signals distorted by frequency independent and frequency dependent non-linearities by deriving all the necessary mathematical relations and expressions. This development will be carried out with respect to the model shown in Figure 3.4. In this figure, $x(t)$ is the non-distorted OFDM signal, $y(t)$ is the non-linearly distorted OFDM signal and the non-linearity is represented by its kernels $h_n(\tau_1, \ldots, \tau_n), n = 1,2,3,\ldots$, or by its transfer functions $H_n(f_1, \ldots, f_n), n = 1,2,3,\ldots$, which are assumed to be symmetric.

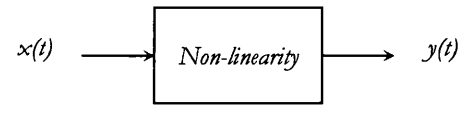

Figure 3.4: Model used to investigate the impact of non-linearities on the PDS of OFDM signals.

To develop this technique we take into consideration the statistical properties of non-distorted OFDM signals. We consider an OFDM signal to be a zero-mean Gaussian stochastic process, which implies that samples of the process are zero-mean Gaussian RVs [13-25]. We also consider an OFDM signal to be a cyclo-stationary stochastic process, which implies that the mean value and the ACF of the process are periodic in time with some period T (see chapter 2). The first consideration is consistent with assumptions of previous researchers that have developed analytic techniques to determine the PDS of OFDM signals distorted by frequency independent non-linearities while the second consideration is not because such researchers have implicitly assumed that an OFDM signal is a stationary rather than a cyclo-stationary stochastic process [13-25]. With such assumptions previous researchers treated the analysis of the PDS of non-linearly distorted OFDM signals by using classical results relative to the analysis of the PDS of non-linearly distorted Gaussian noise [13-25]. Therefore, the technique developed here differs from previous techniques in two fundamental points: first, it accommodates both frequency independent and frequency dependent non-linear behaviour; and second, it accommodates the true (cyclo-stationary) statistical properties of non-distorted OFDM signals.

In the following sections, we first obtain the mean value and the ACF of the output signal and then, by realising that the output signal is also a cyclo-stationary stochastic process, we obtain the output average PDS by Fourier transforming the output average ACF. Expressions are derived strictly for non-linearities which exhibit up to third-order non-linear behaviour. Higher-order behaviour is not considered because up to third-order behaviour often serves as a good approximation to a broad range of non-linearities encountered in practice and expressions for non-linearities of order greater than three are difficult to obtain and apply. To derive these expressions the calculation of the expectation of the product of a number of zero-mean Gaussian RVs is of fundamental importance. The calculation of these expectations is achieved by referring to the following theorem [111,134]:

Theorem 1: The expectation of the product of an odd number of zero-mean jointly Gaussian RVs, $\xi_1, \xi_2, \ldots, \xi_n$, is zero irrespective of their mutual correlation, i.e.,

$$E[\xi_1 \xi_2 \cdots \xi_n] = 0, \quad \text{n is odd} \tag{3.22}$$

The expectation of the product of an even number of zero-mean jointly Gaussian RVs, $\xi_1,\xi_2,\ldots,\xi_n$, is equal to the summation over all distinct ways of partitioning the RVs into products of expectations of pairs irrespective of their mutual correlation, i.e.,

$$E[\xi_1\xi_2\cdots\xi_n]=\sum\prod E[\xi_i\xi_j] \quad \text{n is even} \tag{3.23}$$

where the symbol $\sum\prod$ stands for the summation over all distinct ways of partitioning the RVs into products of expectations of pairs.

Note that two partitions of the n RVs, where n is even, are distinct if one cannot be obtained from the other by a reordering of the RVs within the pairs and/or by a reordering of the pairs themselves [111,134]. Note also that the number of distinct ways N of partitioning the n RVs, where n is even, into products of expectations of pairs is [111,134]

$$N=\frac{n!}{(n/2)!2^{(n/2)}} \tag{3.24}$$

3.3.1 Mean value

The output mean value is given by

$$m_y(t)=E[y(t)] \tag{3.25}$$

Noting that the response of the non-linearity is expressed as a Volterra series and that the expectation of a sum of elements is equal to the sum of the expectations of the elements then the output mean value is also given by

$$m_y(t)=E\left[\sum_{n=1}^{\infty}y_n(t)\right]=\sum_{n=1}^{\infty}E[y_n(t)]=\sum_{n=1}^{\infty}m_{y_n}(t) \tag{3.26}$$

where $m_{y_n}(t)$ is the mean value of the nth-order contribution of the non-linearity. An expression for this mean value is obtained by making use of the n-dimensional integral that yields $y_n(t)$ and then by interchanging the expectation and integral operations as follows

$$m_{y_n}(t)=\int_{-\infty}^{\infty}\cdots\int_{-\infty}^{\infty}h_n(\tau_1,\ldots,\tau_n)E[x(t-\tau_1)\cdots x(t-\tau_n)]d\tau_1\cdots d\tau_n \tag{3.27}$$

A simpler expression for the mean value of the nth-order contribution of the non-linearity is obtained by invoking theorem 1 as the expectation operator in (3.27) comprises the product of a number of zero-mean Gaussian RVs corresponding to samples of the OFDM process. Accordingly, if n is odd then $m_{y_n}(t)$ is zero since the expectation of the product of an odd number of zero-mean Gaussian RVs is zero. Conversely, if n is even then the expectation in (3.27) is broken into a sum of products of expectations of pairs so that in this case $m_{y_n}(t)$ is given in terms of the nth-order kernel of the non-linearity and the ACF of the input OFDM signal, $\phi_{xx}(t+\tau,t)$. Additionally, further simplification is achieved by making use of the fact that some of the terms that result from applying theorem 1 to simplify the expectation operator are identical by virtue of the symmetry of the kernels.

We have derived expressions that yield the mean value of the response of a non-linearity exhibiting up to third-order non-linear behaviour to an OFDM signal by following the procedure outlined above. From our derivation, the output mean value is given by

$$m_y(t) = \sum_{n=1}^{3} m_{y_n}(t) \tag{3.28}$$

where

$$m_{y_1}(t) = 0 \tag{3.29}$$

$$m_{y_2}(t) = \int_{-\infty}^{\infty}\int_{-\infty}^{\infty} h_2(\tau_1,\tau_2)\phi_{xx}(t-\tau_1,t-\tau_2)d\tau_1 d\tau_2 \tag{3.30}$$

and

$$m_{y_3}(t) = 0 \tag{3.31}$$

Finally, we observe that since $m_{y_n}(t)$ is either zero or determined only by the time-independent nth-order kernel and the input OFDM signal ACF, which is periodic in time with some period T, then the output mean value $m_y(t)$ is also periodic in time with period T.

3.3.2 ACF

The output ACF is given by

$$\phi_{yy}(t+\tau,t) = E\left[y(t+\tau)\,y(t)\right] \tag{3.32}$$

Noting again that the response of the non-linearity is expressed as a Volterra series and that the expectation of a sum of elements is equal to the sum of the expectations of the elements then the output ACF is also given by

$$\phi_{yy}(t+\tau,t)=E\left[\sum_{m=1}^{\infty}\sum_{n=1}^{\infty}y_m(t+\tau)y_n(t)\right]=\sum_{m=1}^{\infty}\sum_{n=1}^{\infty}E[y_m(t+\tau)y_n(t)]=\sum_{m=1}^{\infty}\sum_{n=1}^{\infty}\phi_{y_my_n}(t+\tau,t) \quad (3.33)$$

where $\phi_{y_my_n}(t+\tau,t)$ is the cross-correlation function (CCF) between the mth-order and the nth-order contributions of the non-linearity. An expression for this CCF is obtained by transforming the m-dimensional and the n-dimensional integrals that yield $y_m(t+\tau)$ and $y_n(t)$, respectively, into a single (m+n)-dimensional integral and then by interchanging the expectation and integral operations as follows

$$\begin{aligned}\phi_{y_my_n}(t+\tau,t)=&\int_{-\infty}^{\infty}\cdots\int_{-\infty}^{\infty}h_m(\tau_1,\ldots,\tau_m)h_n(\tau_{m+1},\ldots,\tau_{m+n})\\&E[x(t+\tau-\tau_1)\cdots x(t+\tau-\tau_m)x(t-\tau_{m+1})\cdots x(t-\tau_{m+n})]d\tau_1\cdots d\tau_{m+n}\end{aligned} \quad (3.34)$$

The simplification of (3.34) follows the simplification of (3.27) as the expectation operator in (3.34) also comprises the product of a number of zero-mean Gaussian RVs corresponding to samples of the OFDM process. Accordingly, if m+n is odd then $\phi_{y_my_n}(t+\tau,t)$ is zero since the expectation of the product of an odd number of zero-mean Gaussian RVs is zero. Conversely, if m+n is even then the expectation in (3.34) is broken into a sum of products of expectations of pairs so that in this case $\phi_{y_my_n}(t+\tau,t)$ is given in terms of the mth-order and the nth-order kernels of the non-linearity and the ACF of the input OFDM signal, $\phi_{xx}(t+\tau,t)$. Additionally, once again further simplification is achieved by making use of the fact that some of the terms that result from applying theorem 1 to simplify the expectation operator are identical by virtue of the symmetry of the kernels.

By following the procedure outlined above we have derived expressions that yield the ACF of the response of a non-linearity exhibiting up to third-order non-linear behaviour to an OFDM signal. From our derivation, the output ACF is given by

$$\phi_{yy}(t+\tau,t)=\sum_{m=1}^{3}\sum_{n=1}^{3}\phi_{y_my_n}(t+\tau,t) \quad (3.35)$$

where

$$\phi_{y_1y_1}(t+\tau,t)=\int_{-\infty}^{\infty}\int_{-\infty}^{\infty}h_1(\tau_1)h_1(\tau_2)\phi_{xx}(t+\tau-\tau_1,t-\tau_2)d\tau_1 d\tau_2 \tag{3.36}$$

$$\phi_{y_1y_3}(t+\tau,t)=3\int_{-\infty}^{\infty}\cdots\int_{-\infty}^{\infty}h_1(\tau_1)h_3(\tau_2,\tau_3,\tau_4)\phi_{xx}(t+\tau-\tau_1,t-\tau_2)\phi_{xx}(t-\tau_3,t-\tau_4)d\tau_1\cdots d\tau_4 \tag{3.37}$$

$$\begin{aligned}\phi_{y_2y_2}(t+\tau,t)=&\int_{-\infty}^{\infty}\cdots\int_{-\infty}^{\infty}h_2(\tau_1,\tau_2)h_2(\tau_3,\tau_4)\phi_{xx}(t+\tau-\tau_1,t+\tau-\tau_2)\phi_{xx}(t-\tau_3,t-\tau_4)d\tau_1\cdots d\tau_4\\&+2\int_{-\infty}^{\infty}\cdots\int_{-\infty}^{\infty}h_2(\tau_1,\tau_2)h_2(\tau_3,\tau_4)\phi_{xx}(t+\tau-\tau_1,t-\tau_3)\phi_{xx}(t+\tau-\tau_2,t-\tau_4)d\tau_1\cdots d\tau_4\end{aligned} \tag{3.38}$$

$$\phi_{y_3y_1}(t+\tau,t)=3\int_{-\infty}^{\infty}\cdots\int_{-\infty}^{\infty}h_3(\tau_1,\tau_2,\tau_3)h_1(\tau_4)\phi_{xx}(t+\tau-\tau_1,t+\tau-\tau_2)\phi_{xx}(t+\tau-\tau_3,t-\tau_4)d\tau_1\cdots d\tau_4 \tag{3.39}$$

$$\begin{aligned}\phi_{y_3y_3}(t+\tau,t)=&9\int_{-\infty}^{\infty}\cdots\int_{-\infty}^{\infty}h_3(\tau_1,\tau_2,\tau_3)h_3(\tau_4,\tau_5,\tau_6)\\&\phi_{xx}(t+\tau-\tau_1,t+\tau-\tau_2)\phi_{xx}(t+\tau-\tau_3,t-\tau_4)\phi_{xx}(t-\tau_5,t-\tau_6)d\tau_1\cdots d\tau_6\\&+6\int_{-\infty}^{\infty}\cdots\int_{-\infty}^{\infty}h_3(\tau_1,\tau_2,\tau_3)h_3(\tau_4,\tau_5,\tau_6)\\&\phi_{xx}(t+\tau-\tau_1,t-\tau_4)\phi_{xx}(t+\tau-\tau_2,t-\tau_5)\phi_{xx}(t+\tau-\tau_3,t-\tau_6)d\tau_1\cdots d\tau_6\end{aligned} \tag{3.40}$$

and

$$\phi_{y_1y_2}(t+\tau,t)=\phi_{y_2y_1}(t+\tau,t)=\phi_{y_2y_3}(t+\tau,t)=\phi_{y_3y_2}(t+\tau,t)=0 \tag{3.41}$$

Finally, we observe that since $\phi_{y_my_n}(t+\tau,t)$ is either zero or depends only on the time-independent mth-order and nth-order kernels and the input OFDM signal ACF, which is periodic in time with some period T, then the output ACF $\phi_{yy}(t+\tau,t)$ is also periodic in time with period T.

3.3.3 PDS

In sections 3.3.1 and 3.3.2 we have observed that both the output mean value and the output ACF are periodic in time with some period T, i.e., the output signal is a cyclo-stationary stochastic process (at least in the wide-sense) [49-51]. Thus, we determine the output average PDS by Fourier transforming the output average ACF [49-51]. The output average ACF is given by

$$\bar{\phi}_{yy}(\tau)=\frac{1}{T}\int_{T}\phi_{yy}(t+\tau,t)dt \tag{3.42}$$

and by substituting (3.33) into (3.42) and by noting that the integration of a sum of elements is equal to the sum of the integrations of each individual element then

$$\bar{\phi}_{yy}(\tau)=\frac{1}{T}\int_{T}\left[\sum_{m=1}^{\infty}\sum_{n=1}^{\infty}\phi_{y_m y_n}(t+\tau,t)\right]dt=\sum_{m=1}^{\infty}\sum_{n=1}^{\infty}\frac{1}{T}\int_{T}\phi_{y_m y_n}(t+\tau,t)dt=\sum_{m=1}^{\infty}\sum_{n=1}^{\infty}\bar{\phi}_{y_m y_n}(\tau) \tag{3.43}$$

where $\bar{\phi}_{y_m y_n}(\tau)$ is the average CCF between the mth-order and the nth-order contributions of the non-linearity.

For the non-linearity under consideration it follows that the output average ACF is given as

$$\bar{\phi}_{yy}(\tau)=\sum_{m=1}^{3}\sum_{n=1}^{3}\bar{\phi}_{y_m y_n}(\tau) \tag{3.44}$$

where

$$\bar{\phi}_{y_1 y_1}(\tau)=\int_{-\infty}^{\infty}\int_{-\infty}^{\infty}h_1(\tau_1)h_2(\tau_2)\bar{\phi}_{xx_0}(\tau+\tau_2-\tau_1)d\tau_1 d\tau_2=\int_{-\infty}^{\infty}\int_{-\infty}^{\infty}h_1(\tau_1)h_2(\tau_2)\bar{\phi}_{xx}(\tau+\tau_2-\tau_1)d\tau_1 d\tau_2 \tag{3.45}$$

$$\bar{\phi}_{y_1 y_3}(\tau)=\sum_{\substack{n_1=-\infty\\ n_1+n_2=0}}^{\infty}\sum_{n_2=-\infty}^{\infty}3\int_{-\infty}^{\infty}\cdots\int_{-\infty}^{\infty}h_1(\tau_1)h_3(\tau_2,\tau_3,\tau_4)\bar{\phi}_{xx_{n_1}}(\tau+\tau_2-\tau_1)e^{-j\frac{2\pi n_1\tau_2}{T}}\bar{\phi}_{xx_{n_2}}(\tau_4-\tau_3)e^{-j\frac{2\pi n_2\tau_4}{T}}d\tau_1\cdots d\tau_4 \tag{3.46}$$

$$\begin{aligned}\bar{\phi}_{y_2 y_2}(\tau)=&\sum_{\substack{n_1=-\infty\\ n_1+n_2=0}}^{\infty}\sum_{n_2=-\infty}^{\infty}\int_{-\infty}^{\infty}\cdots\int_{-\infty}^{\infty}h_2(\tau_1,\tau_2)h_2(\tau_3,\tau_4)\bar{\phi}_{xx_{n_1}}(\tau_2-\tau_1)e^{j\frac{2\pi n_1(\tau-\tau_2)}{T}}\bar{\phi}_{xx_{n_2}}(\tau_4-\tau_3)e^{-j\frac{2\pi n_2\tau_4}{T}}d\tau_1\cdots d\tau_4\\ &+\sum_{\substack{n_1=-\infty\\ n_1+n_2=0}}^{\infty}\sum_{n_2=-\infty}^{\infty}2\int_{-\infty}^{\infty}\cdots\int_{-\infty}^{\infty}h_2(\tau_1,\tau_2)h_2(\tau_3,\tau_4)\bar{\phi}_{xx_{n_1}}(\tau+\tau_3-\tau_1)e^{-j\frac{2\pi n_1\tau_3}{T}}\bar{\phi}_{xx_{n_2}}(\tau+\tau_4-\tau_2)e^{-j\frac{2\pi n_2\tau_4}{T}}d\tau_1\cdots d\tau_4\end{aligned} \tag{3.47}$$

$$\bar{\phi}_{y_3 y_1}(\tau)=\sum_{\substack{n_1=-\infty\\ n_1+n_2=0}}^{\infty}\sum_{n_2=-\infty}^{\infty}3\int_{-\infty}^{\infty}\cdots\int_{-\infty}^{\infty}h_3(\tau_1,\tau_2,\tau_3)h_1(\tau_4)\bar{\phi}_{xx_{n_1}}(\tau_2-\tau_1)e^{j\frac{2\pi n_1(\tau-\tau_2)}{T}}\bar{\phi}_{xx_{n_2}}(\tau+\tau_4-\tau_3)e^{-j\frac{2\pi n_2\tau_4}{T}}d\tau_1\cdots d\tau_4 \tag{3.48}$$

$$\bar{\phi}_{y_3y_3}(\tau)=\sum_{\substack{n_1=-\infty\\ n_1+n_2+n_3=0}}^{\infty}\sum_{n_2=-\infty}^{\infty}\sum_{n_3=-\infty}^{\infty}9\int_{-\infty}^{\infty}\cdots\int_{-\infty}^{\infty}h_3(\tau_1,\tau_2,\tau_3)h_3(\tau_4,\tau_5,\tau_6)$$
$$\bar{\phi}_{xx_{n_1}}(\tau_2-\tau_1)e^{j\frac{2\pi n_1(\tau-\tau_2)}{T}}\bar{\phi}_{xx_{n_2}}(\tau+\tau_4-\tau_3)e^{-j\frac{2\pi n_2\tau_4}{T}}\bar{\phi}_{xx_{n_3}}(\tau_6-\tau_5)e^{-j\frac{2\pi n_3\tau_6}{T}}d\tau_1\ldots d\tau_6 \quad (3.49)$$
$$\sum_{\substack{n_1=-\infty\\ n_1+n_2+n_3=0}}^{\infty}\sum_{n_2=-\infty}^{\infty}\sum_{n_3=-\infty}^{\infty}6\int_{-\infty}^{\infty}\cdots\int_{-\infty}^{\infty}h_3(\tau_1,\tau_2,\tau_3)h_3(\tau_4,\tau_5,\tau_6)$$
$$\bar{\phi}_{xx_{n_1}}(\tau+\tau_4-\tau_1)e^{-j\frac{2\pi n_1\tau_4}{T}}\bar{\phi}_{xx_{n_2}}(\tau+\tau_5-\tau_2)e^{-j\frac{2\pi n_2\tau_5}{T}}\bar{\phi}_{xx_{n_3}}(\tau+\tau_6-\tau_3)e^{-j\frac{2\pi n_3\tau_6}{T}}d\tau_1\ldots d\tau_6$$

and

$$\bar{\phi}_{y_1y_2}(\tau)=\bar{\phi}_{y_2y_1}(\tau)=\bar{\phi}_{y_2y_3}(\tau)=\bar{\phi}_{y_3y_2}(\tau)=0 \quad (3.50)$$

Expressions (3.45), (3.46), (3.47), (3.48), (3.49) and (3.50) were obtained by averaging (3.36), (3.37), (3.38), (3.39), (3.40) and (3.41), respectively, after expanding the periodic ACFs of the input OFDM signal in a complex Fourier series. Note that the complex Fourier series expansion of the ACF of the input OFDM signal is given by

$$\phi_{xx}(t+\tau,t)=\sum_{n=-\infty}^{\infty}\bar{\phi}_{xx_n}(\tau)e^{j\frac{2\pi nt}{T}} \quad (3.51)$$

where the nth coefficient in this complex Fourier series expansion, also known as the nth harmonic auto-correlation function (HACF), is given by

$$\bar{\phi}_{xx_n}(\tau)=\frac{1}{T}\int_{T}\phi_{xx}(t+\tau,t)e^{-j\frac{2\pi nt}{T}}dt \quad (3.52)$$

Note also that in (3.45) we have used the fact that $\bar{\phi}_{xx_0}(\tau)=\bar{\phi}_{xx}(\tau)$, i.e., the 0th HACF corresponds to the average ACF.

The output average PDS is given by

$$\bar{\Phi}_{yy}(f)=\int_{-\infty}^{\infty}\bar{\phi}_{yy}(\tau)e^{-j2\pi f\tau}d\tau \quad (3.53)$$

and by substituting (3.43) into (3.53) and by noting that the Fourier transform of a sum of elements is equal to the sum of the Fourier transforms of each individual element then

$$\bar{\Phi}_{yy}(f)=\int_{-\infty}^{\infty}\left[\sum_{m=1}^{\infty}\sum_{n=1}^{\infty}\bar{\phi}_{y_my_n}(\tau)\right]e^{-j2\pi f\tau}d\tau=\sum_{m=1}^{\infty}\sum_{n=1}^{\infty}\int_{-\infty}^{\infty}\bar{\phi}_{y_my_n}(\tau)e^{-j2\pi f\tau}d\tau=\sum_{m=1}^{\infty}\sum_{n=1}^{\infty}\bar{\Phi}_{y_my_n}(f) \quad (3.54)$$

where $\overline{\Phi}_{y_m y_n}(f)$ is the average cross-power density spectrum (CPDS) between the mth-order and the nth-order contributions of the non-linearity.

For the non-linearity under consideration it follows that the output average PDS is given as

$$\overline{\Phi}_{yy}(f)=\sum_{m=1}^{3}\sum_{n=1}^{3}\overline{\Phi}_{y_m y_n}(f) \tag{3.55}$$

where

$$\overline{\Phi}_{y_1 y_1}(f)=\overline{\Phi}_{xx_0}(f)H_1(f)H_1(-f)=\overline{\Phi}_{xx}(f)H_1(f)H_1(-f) \tag{3.56}$$

$$\overline{\Phi}_{y_1 y_3}(f)=\sum_{\substack{n_1=-\infty \\ n_1+n_2=0}}^{\infty}\sum_{n_2=-\infty}^{\infty}3\int_{-\infty}^{\infty}\overline{\Phi}_{xx_{n_1}}(f)\overline{\Phi}_{xx_{n_2}}(f_1)H_1(f)H_3(-f+n_1/T,f_1,-f_1+n_2/T)df_1 \tag{3.57}$$

$$\begin{aligned}\overline{\Phi}_{y_2 y_2}(f)=&\sum_{\substack{n_1=-\infty \\ n_1+n_2=0}}^{\infty}\sum_{n_2=-\infty}^{\infty}\int_{-\infty}^{\infty}\int_{-\infty}^{\infty}\overline{\Phi}_{xx_{n_1}}(f_1)\overline{\Phi}_{xx_{n_2}}(f_2)H_2(f_1,-f_1+n_1/T)H_2(f_2,-f_2+n_2/T)df_1df_2\,\delta(f-n_1/T)\\&+\sum_{\substack{n_1=-\infty \\ n_1+n_2=0}}^{\infty}\sum_{n_2=-\infty}^{\infty}2\int_{-\infty}^{\infty}\overline{\Phi}_{xx_{n_1}}(f_1)\overline{\Phi}_{xx_{n_2}}(f-f_1)H_2(f_1,f-f_1)H_2(-f_1+n_1/T,-f+f_1+n_2/T)df_1\end{aligned} \tag{3.58}$$

$$\overline{\Phi}_{y_3 y_1}(f)=\sum_{\substack{n_1=-\infty \\ n_1+n_2=0}}^{\infty}\sum_{n_2=-\infty}^{\infty}3\int_{-\infty}^{\infty}\overline{\Phi}_{xx_{n_1}}(-f)\overline{\Phi}_{xx_{n_2}}(f_1)H_1(-f)H_3(f+n_1/T,f_1,-f_1+n_2/T)df_1 \tag{3.59}$$

$$\begin{aligned}\overline{\Phi}_{y_3 y_3}(f)=&\sum_{\substack{n_1=-\infty \\ n_1+n_2+n_3=0}}^{\infty}\sum_{n_2=-\infty}^{\infty}\sum_{n_3=-\infty}^{\infty}9\int_{-\infty}^{\infty}\int_{-\infty}^{\infty}\overline{\Phi}_{xx_{n_1}}(f_1)\overline{\Phi}_{xx_{n_2}}(f-n_1/T)\overline{\Phi}_{xx_{n_3}}(f_2)\\&H_3(f_1,-f_1+n_1/T,f-n_1/T)H_3(-f-n_3/T,f_2,-f_2+n_3/T)df_1df_2\\&+\sum_{\substack{n_1=-\infty \\ n_1+n_2+n_3=0}}^{\infty}\sum_{n_2=-\infty}^{\infty}\sum_{n_3=-\infty}^{\infty}6\int_{-\infty}^{\infty}\int_{-\infty}^{\infty}\overline{\Phi}_{xx_{n_1}}(f_1)\overline{\Phi}_{xx_{n_2}}(f_2)\overline{\Phi}_{xx_{n_3}}(f-f_1-f_2)\\&H_3(f_1,f_2,f-f_1-f_2)H_3(-f+n_1/T,-f_2+n_2/T,-f+f_1+f_2+n_3/T)df_1df_2\end{aligned} \tag{3.60}$$

and

$$\overline{\Phi}_{y_1 y_2}(f)=\overline{\Phi}_{y_2 y_1}(f)=\overline{\Phi}_{y_2 y_3}(f)=\overline{\Phi}_{y_3 y_2}(f)=0 \tag{3.61}$$

Expressions (3.56), (3.57), (3.58), (3.59), (3.60) and (3.61) were obtained by taking the Fourier transform of (3.45), (3.46), (3.47), (3.48), (3.49) and (3.50), respectively. Moreover, in (3.56), (3.57), (3.58), (3.59) and (3.60) the nth HPDS of the input signal $\overline{\Phi}_{xx_n}(f)$ corresponds to the Fourier transform of the nth HACF of the input signal $\overline{\phi}_{xx_n}(\tau)$, in (3.56) we have used the fact that $\overline{\Phi}_{xx_0}(f) = \overline{\Phi}_{xx}(f)$, i.e., the 0th HPDS corresponds to the average PDS, and in (3.58) $\delta(\cdot)$ denotes the Dirac delta function.

Finally, it is interesting to observe that our expressions can be seen as a series embedded in a series. One of the series yields the various contributions of the non-linearity whereas the other series yields the contributions of the HPDSs of the input signal to the PDS of the output signal. It is also interesting to observe that our expressions reduce to the familiar Bedrosian-Rice expressions when the input signal is not cyclo-stationary but stationary. Note that our expressions give the PDS of the response of a Volterra non-linearity to a zero-mean Gaussian cyclo-stationary process whereas the Bedrosian-Rice expressions give the PDS of the response of such a non-linearity to a zero-mean Gaussian stationary process [121].

3.4 Analytic and simulation results

In this section, we investigate the application of the PDS expressions to specific OFDM/BPSK signals distorted by specific non-linearities. We write the OFDM signals as

$$x(t) = \mathrm{Re}\left\{\tilde{x}(t)e^{j2\pi f_c t}\right\} \tag{3.62}$$

where $\tilde{x}(t)$ is its complex envelope and f_c is the frequency of its first sub-carrier, and we write the complex envelope of the OFDM signals as

$$\tilde{x}(t) = \sum_{k=-\infty}^{\infty}\sum_{n=0}^{N-1} X_{k,n} g_n(t-kT) \tag{3.63}$$

$$g_n(t) = \begin{cases} e^{j\frac{2\pi n(t-T_{CP})}{T-T_{CP}}}, & t \in [0,T] \\ 0, & t \notin [0,T] \end{cases} \tag{3.64}$$

where $X_{k,n}$ denotes the complex modulation symbol conveyed in time slot k and sub-channel n, N is the number of OFDM sub-channels, T is the OFDM symbol duration and T_{CP} is the OFDM cyclic prefix duration. We assume that the mean value of the complex modulation symbols is zero and we also assume that the complex modulation symbols conveyed in different time slots and different sub-channels are independent[8]. We consider OFDM signals with rectangular windowing and not OFDM signals with raised cosine windowing in order to facilitate the evaluation of the HACFs and the HPDSs of the signal.

We have found in chapter 2 that the mean value of the OFDM signal, $E[x(t)]$, is related to the mean value of its complex envelope, $E[\tilde{x}(t)]$, as follows

$$E[x(t)] = \mathrm{Re}\left\{E[\tilde{x}(t)]e^{j2\pi f_c t}\right\} \tag{3.65}$$

where

$$E[\tilde{x}(t)] = \sum_{k=-\infty}^{\infty}\sum_{n=0}^{N-1} E[X_{k,n}]g_n(t-kT) \tag{3.66}$$

We have also found in chapter 2 that the ACF of the OFDM signal, $\phi_{xx}(t+\tau,t)$, is related to the ACF of its complex envelope, $\phi_{\tilde{x}\tilde{x}}(t+\tau,t)$, as follows

$$\phi_{xx}(t+\tau,t) = \mathrm{Re}\left\{\phi_{\tilde{x}\tilde{x}}(t+\tau,t)e^{j2\pi f_c \tau}\right\} \tag{3.67}$$

where

$$\phi_{\tilde{x}\tilde{x}}(t+\tau,t) = \sum_{k=-\infty}^{\infty}\sum_{n=0}^{N-1}\frac{1}{2}E\left[|X_{k,n}|^2\right]g_n(t+\tau-kT)g_n^*(t-kT) = \sum_{k=-\infty}^{\infty}\sum_{n=0}^{N-1}\sigma_n^2 g_n(t+\tau-kT)g_n^*(t-kT) \tag{3.68}$$

Note that since the mean value and the ACF of the complex envelope of the OFDM signal are periodic in time with period T, i.e.,

$$m_{\tilde{x}}(t+kT) = m_{\tilde{x}}(t) = 0 \tag{3.69}$$

$$\phi_{\tilde{x}\tilde{x}}(t+kT+\tau,t+kT) = \phi_{\tilde{x}\tilde{x}}(t+\tau,t) \tag{3.70}$$

[8] The zero-mean condition is satisfied provided that the modulation symbols take any value belonging to an M-PSK or an M-QAM signal constellation with equal probability. Independence is satisfied in a variety of situations including COFDM systems provided that an interleaver is employed. Independence would not be satisfied in situations where PAPR reduction codes are employed.

then the mean value and the ACF of the OFDM signal are also periodic in time with the same period T, i.e.,

$$m_x(t+kT) = m_x(t) = 0 \tag{3.71}$$

$$\phi_{xx}(t+kT+\tau, t+kT) = \phi_{xx}(t+\tau, t) \tag{3.72}$$

Note also that the central limit theorem (CLT) ensures that the distribution for the samples at a particular time instant of different realisations of an OFDM signal approach a (zero-mean) Gaussian distribution when N is large (see Figure 3.5). Consequently, an OFDM signal is indeed a cyclo-stationary (zero-mean) Gaussian stochastic process.

The lth HACF of the OFDM signal, $\bar{\phi}_{xx_l}(\tau)$, corresponds to the lth coefficient in the complex Fourier series expansion of its ACF, $\phi_{xx}(t+\tau, t)$, i.e.,

$$\bar{\phi}_{xx_l}(\tau) = \frac{1}{T}\int_T \phi_{xx}(t+\tau, t) e^{-j\frac{2\pi l t}{T}} dt \tag{3.73}$$

and by substituting (3.67) into (3.73) then

$$\bar{\phi}_{xx_l}(\tau) = \frac{1}{2}\bar{\phi}_{\tilde{x}\tilde{x}_l}(\tau) e^{j2\pi f_c \tau} + \frac{1}{2}\bar{\phi}^*_{\tilde{x}\tilde{x}_{-l}}(\tau) e^{-j2\pi f_c \tau} \tag{3.74}$$

where $\bar{\phi}_{\tilde{x}\tilde{x}_l}(\tau)$ is the lth HACF of the complex envelope of the OFDM signal, i.e.,

$$\bar{\phi}_{\tilde{x}\tilde{x}_l}(\tau) = \frac{1}{T}\int_T \phi_{\tilde{x}\tilde{x}}(t+\tau, t) e^{-j\frac{2\pi l t}{T}} dt \tag{3.75}$$

This HACF can be found by using (3.68) in (3.75) and carrying out the integration. Thus,

$$\bar{\phi}_{\tilde{x}\tilde{x}_l}(\tau) = \begin{cases} \sum_{n=0}^{N-1} \sigma_n^2 \frac{T-|\tau|}{T} \operatorname{sinc}\left[\frac{l(T-|\tau|)}{T}\right] e^{-j\frac{\pi l(T-\tau)}{T}} e^{j\frac{2\pi n \tau}{T-T_{CP}}}, & |\tau| \le T \\ 0, & |\tau| > T \end{cases} \tag{3.76}$$

The lth HPDS of the OFDM signal, $\bar{\Phi}_{xx_l}(f)$, corresponds to the Fourier transform of its lth HACF, $\bar{\phi}_{xx_l}(\tau)$, i.e.,

$$\bar{\Phi}_{xx_l}(f) = \int_{-\infty}^{\infty} \bar{\phi}_{xx_l}(\tau) e^{-j2\pi f \tau} d\tau \tag{3.77}$$

and by substituting (3.74) into (3.77) then

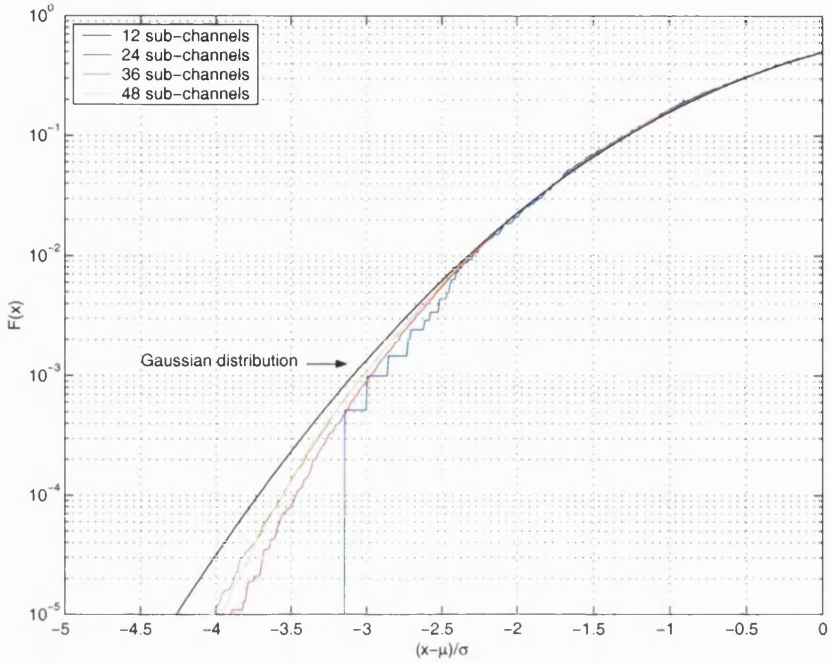

Figure 3.5: Cumulative distribution function (CDF), *F(x)*, for the samples at a particular time instant of different realisations of OFDM/BPSK signals with $f_c = 1GHz$, $T = 4000\,ns$, $T_{CP} = 800\,ns$ and $N = 12, 24, 36$ and 48. The x-axis is normalised to the mean μ and standard deviation σ of the distributions.

$$\overline{\Phi}_{xx_l}(f) = \frac{1}{2}\left[\overline{\Phi}_{\widetilde{x}\widetilde{x}_l}(f - f_c) + \overline{\Phi}^*_{\widetilde{x}\widetilde{x}_{-l}}(-f - f_c)\right] \tag{3.78}$$

where $\overline{\Phi}_{\widetilde{x}\widetilde{x}_l}(f)$ is the lth HPDS of the complex envelope of the OFDM signal, i.e.,

$$\overline{\Phi}_{\widetilde{x}\widetilde{x}_l}(f) = \int_{-\infty}^{\infty} \overline{\phi}_{\widetilde{x}\widetilde{x}_l}(\tau) e^{-j2\pi f\tau} d\tau \tag{3.79}$$

This HPDS can be found by using (3.76) in (3.79) and carrying out the integration. Thus,

$$\overline{\Phi}_{\widetilde{x}\widetilde{x}_l}(f) = \begin{cases} \sum_{n=0}^{N-1} \frac{\sigma_n^2 T}{\pi l}\left[\sin\left[\pi\left(f - \frac{n}{T - T_{CP}} - \frac{l}{T}\right)T\right]\operatorname{sinc}\left[\left(f - \frac{n}{T - T_{CP}} - \frac{l}{T}\right)T\right] - \right. \\ \left. \sin\left[\pi\left(f - \frac{n}{T - T_{CP}}\right)T\right]\operatorname{sinc}\left[\left(f - \frac{n}{T - T_{CP}}\right)T\right]\right], & l \neq 0 \\ \sum_{n=0}^{N-1} \sigma_n^2 T \operatorname{sinc}^2\left[\left(f - \frac{n}{T - T_{CP}}\right)T\right], & l = 0 \end{cases} \tag{3.80}$$

We have obtained the PDS of the response of both a simple frequency independent and a simple frequency dependent non-linearity, which exhibit up to third-order non-linear behaviour, to the OFDM signals. The frequency independent non-linearity is modelled as in Figure 3.2 where the characteristic of the memoryless device $f(\cdot)$ is given by

$$f(z) = c_1 z + c_2 z^2 + c_3 z^3 \tag{3.81}$$

with $c_1 = 1$, $c_2 = 0$ and $c_3 = -0.25$[9]. The transfer functions for this non-linearity can be obtained from (3.15) by noting that $c_1 = 1$, $c_2 = 0$, $c_3 = -0.25$ and $c_n = 0$ for $n > 3$.

The frequency dependent non-linearity is modelled as in Figure 3.3 where the characteristic of the memoryless device $f(\cdot)$ is also given by

$$f(z) = c_1 z + c_2 z^2 + c_3 z^3 \tag{3.82}$$

with $c_1 = 1$, $c_2 = 0$ and $c_3 = -0.25$, and $H'(f)$ and $H''(f)$ are frequency responses of two bandpass first-order Butterworth filters

$$H'(f) = H''(f) = \frac{1}{1 + j\frac{f_0}{B}\left(\frac{f}{f_0} - \frac{f_0}{f}\right)} \tag{3.83}$$

where f_0 is the centre frequency and B is the 3 dB bandwidth of the bandpass filters. The centre frequency and the 3 dB bandwidth of the bandpass filters were set to be equal to the centre frequency and the 3 dB bandwidth of the OFDM signals, respectively. The transfer functions for this non-linearity can be obtained from (3.20) by noting that $c_1 = 1$, $c_2 = 0$, $c_3 = -0.25$ and $c_n = 0$ for $n > 3$, and $H'(f)$ and $H''(f)$ are given in (3.83).

We have obtained the PDS of the response of these non-linearities to the OFDM signals for a 3 dB output back-off (OBO) given by

$$OBO = 10 \log_{10} \frac{P_{OUT_{max}}}{\langle P_{OUT} \rangle} \tag{3.84}$$

where $P_{OUT_{max}}$ and $\langle P_{OUT} \rangle$ are the maximum power and the average power at the output of the non-linearity under consideration, respectively. The output average power is

[9] Although a ratio $c_1/c_3 = -4$ is typical for non-linear elements encountered in communication systems (e.g., HPAs) [135], the analysis presented hereafter is independent of the actual value of the ratio.

determined by integrating the output average PDS. The output maximum power is determined by taking the input signal to be a sine wave with frequency f_0 (f_0 corresponds to the centre frequency of the bandpass first-order Butterworth filters) and each non-linearity to be followed by a zonal filter whose purpose is to eliminate all the harmonics but the fundamental frequency without introducing any distortion in the band of interest. Thus, if the input signal is given by

$$x(t) = A\cos(2\pi f_0 t + \phi) \tag{3.85}$$

then the output signal is given by

$$y(t) = \left(c_1 A + 0.75 c_3 A^3\right)\cos(2\pi f_0 t + \phi) \tag{3.86}$$

In this case, the power in the output signal is

$$P_{OUT} = \frac{\left(c_1 A + 0.75 c_3 A^3\right)^2}{2} \tag{3.87}$$

and, by using differentiation techniques, the maximum possible power in the output signal is

$$P_{OUT_{\max}} = -\frac{16}{162}\frac{c_1^3}{c_3} \tag{3.88}$$

Note that there is a maximum output power if and only if the values of c_1 and c_3 have opposite signs. The OBO was set by varying the power in the constellations of each OFDM sub-channel until a specified value, as given by (3.84), was achieved.

Analytic results were obtained in MATLAB by inserting the appropriate transfer functions and HPDSs of the input OFDM signal into the PDS expressions and by carrying out the integrations numerically.

Simulation results were obtained in MATLAB as follows: Initially, an OFDM signal was generated given a set of randomly generated BPSK symbols; subsequently, the OFDM signal was distorted by the non-linearity; finally, the PDS of the non-linearly distorted OFDM signal was estimated using the periodogram or direct method [136]. The simulation

sampling frequency was chosen so that the highest frequency component in the non-linearly distorted OFDM signal could be accounted for[10].

The aim of our investigation is to evaluate the consequences of inserting higher-order HPDSs of the input OFDM signal into the mathematical expressions and the consequences for the accuracy of the (zero-mean) Gaussian approximation for the distribution of the samples at a particular time instant of different realisations of an OFDM signal. To examine the effect of inserting higher-order HPDSs into the mathematical expressions we have considered a 48 sub-channel OFDM/BPSK signal for which the Gaussian approximation is accurate (see Figure 3.5). The other parameters of the OFDM signal are as follows: $f_c = 1\,GHz$, $T = 4\,\mu s$ and $T_{CP} = 0.8\,\mu s$. Figure 3.6 and Figure 3.7 compare the PDSs of the response of the frequency independent non-linearity to the OFDM signal obtained by analysis and simulation. In the first figure the analytical PDS was determined by considering only the average PDS of the input OFDM signal and in the second figure the analytical PDS was determined by considering the HPDSs, $\overline{\Phi}_{xx_n}(f)$, of the input OFDM signal for $n = -3,\ldots,3$. Observation of the figures reveals that by incorporating higher-order HPDSs into the mathematical expressions then analysis approaches simulation. Similar trends are also observed for the case of the frequency dependent non-linearity, as shown in Figure 3.8 and Figure 3.9. Again, in the first figure analysis was carried out by considering only the average PDS of the input OFDM signal while in the second figure analysis was carried out by considering the HPDSs, $\overline{\Phi}_{xx_n}(f)$, of the input OFDM signal for $n = -3,\ldots,3$.

To examine the effect of the accuracy of the Gaussian approximation we have considered a 12 sub-channel OFDM/BPSK signal for which the Gaussian approximation is not so accurate (see Figure 3.5). The other parameters of the OFDM signal are as follows: $f_c = 1\,GHz$, $T = 4\,\mu s$ and $T_{CP} = 0.8\,\mu s$. Figure 3.10 and Figure 3.11 still show that analysis perfectly agrees with simulation if a sufficient number of HPDSs of the input OFDM signal are inserted into the mathematical expressions. These figures refer to the cases of frequency independent and frequency dependent non-linearity, respectively.

[10] Note that we have used MATLAB to obtain both analytic and simulation PDS results. Analytic results were determined by using MATLAB as a calculator, where we have effectively implemented and solved all the mathematical relations and expressions. Simulation results were determined by using MATLAB as a simulator, where we have implemented all the underlying processes unfolding in time.

However, if only the average PDS of the input OFDM signal is inserted into the mathematical expressions then analysis does not perfectly agree with simulation as shown in Figure 3.12 and Figure 3.13. Again, these figures refer to the frequency independent and the frequency dependent non-linearity cases, respectively. Evidently, we would not expect analysis to match simulation for OFDM signals with fewer sub-channels but since OFDM signals with fewer sub-channels are not common then we can conclude that the PDS expressions are applicable to most cases encountered in practice provided that the sub-channels are modulated independently so that the Gaussian approximation is valid.

It is important to mention that although the non-linearities that we have considered produce spectral components around the fundamental frequency and the third harmonic we have only shown the spectra around the fundamental frequency in the previous figures. In fact, the spectral components around the harmonics can often be filtered out and hence do not need to be considered. It is also important to mention that both the horizontal axis and the vertical axis have been normalised in the previous figures. The horizontal axis has been normalised to the centre frequency and the 3 dB bandwidth of the OFDM signal, given by (2.34) and (2.35) respectively. The vertical axis has been normalised to the maximum value of the output PDS.

Finally, we observe that by inserting only the average PDS of an OFDM signal into the mathematical expressions then relatively good agreement is already observed between analysis and simulation (see Figure 3.6, Figure 3.8, Figure 3.12 and Figure 3.13). In fact, the powers calculated from the approximate PDS and the exact PDS in a selected frequency band whose normalised limits are -1 and -0.5 are nearly identical (see Table 3.1). Cases A and B correspond to the 48 sub-channel OFDM signal distorted by the frequency independent and the frequency dependent non-linearity, respectively. Cases C and D correspond to the 12 sub-channel OFDM signal distorted by the frequency independent and the frequency dependent non-linearity, respectively. We note that with this simplification our expressions, which apply to a zero-mean Gaussian cyclo-stationary process, reduce to the familiar Bedrosian-Rice expressions, which apply to a zero-mean Gaussian stationary process [121]. We also note that this simplification explains why previous researchers that have developed analytic techniques to determine the PDS of non-linearly distorted OFDM signals, based only on considering an OFDM signal to be a stationary and not a cyclo-stationary stochastic process, have observed good agreement between analysis and simulation [13-25].

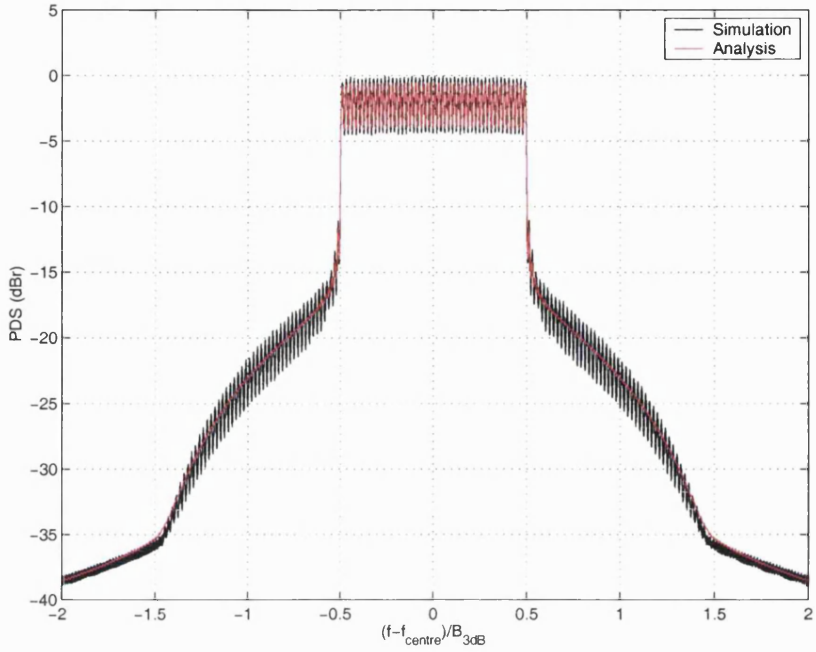

Figure 3.6: PDS of the response of the frequency independent non-linearity to a 48 sub-channel OFDM/BPSK signal. Analytic results were obtained by considering only the average PDS of the input OFDM signal.

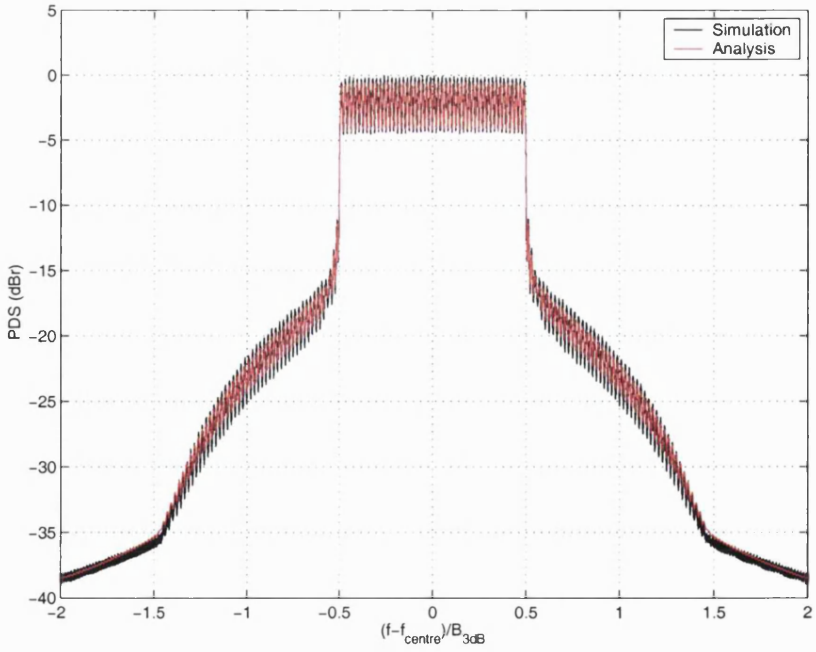

Figure 3.7: PDS of the response of the frequency independent non-linearity to a 48 sub-channel OFDM/BPSK signal. Analytic results were obtained by considering the HPDSs $\overline{\Phi}_{xx_n}(f)$ of the input OFDM signal for $n=-3,\ldots,3$.

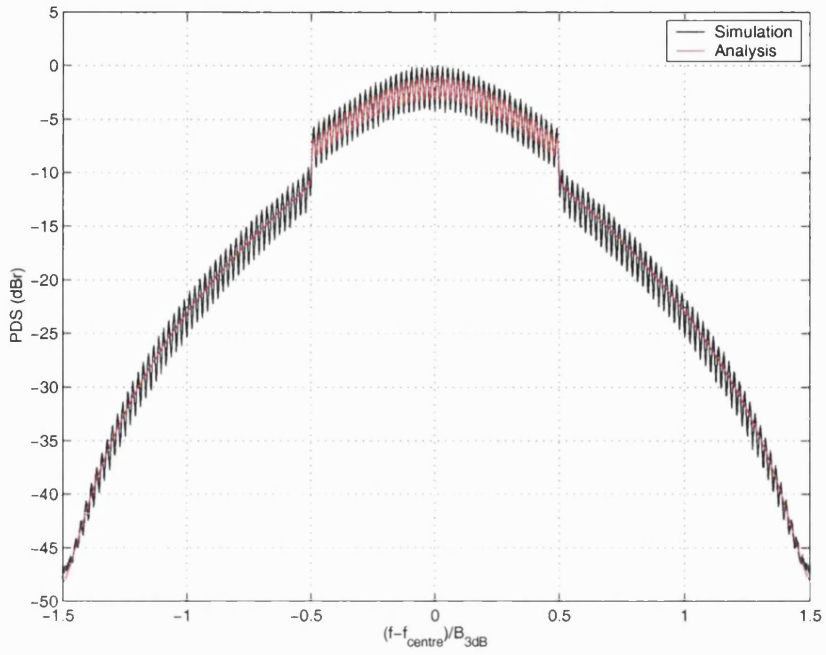

Figure 3.8: PDS of the response of the frequency dependent non-linearity to a 48 sub-channel OFDM/BPSK signal. Analytic results were obtained by considering only the average PDS of the input OFDM signal.

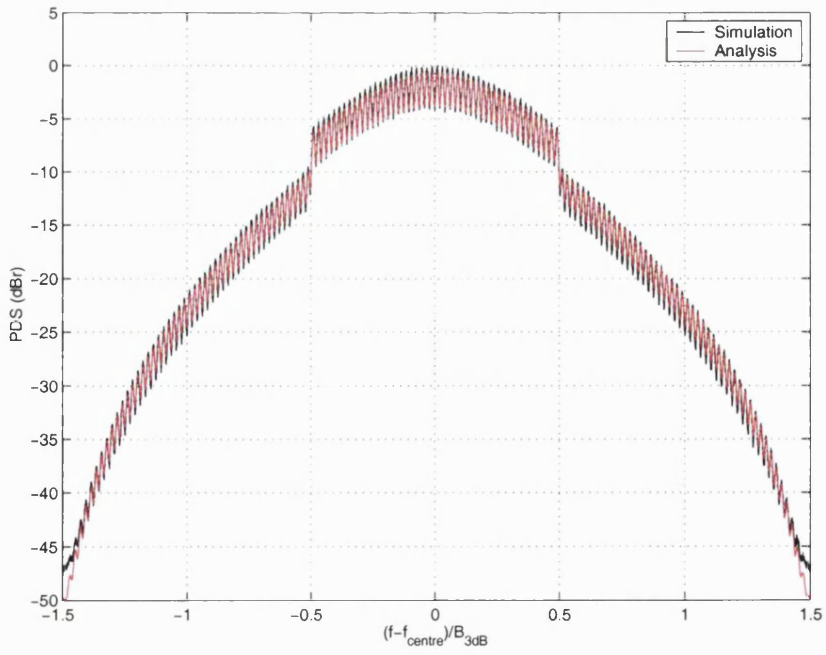

Figure 3.9: PDS of the response of the frequency dependent non-linearity to a 48 sub-channel OFDM/BPSK signal. Analytic results were obtained by considering the HPDSs $\overline{\Phi}_{xx_n}(f)$ of the input OFDM signal for $n=-3,\ldots,3$.

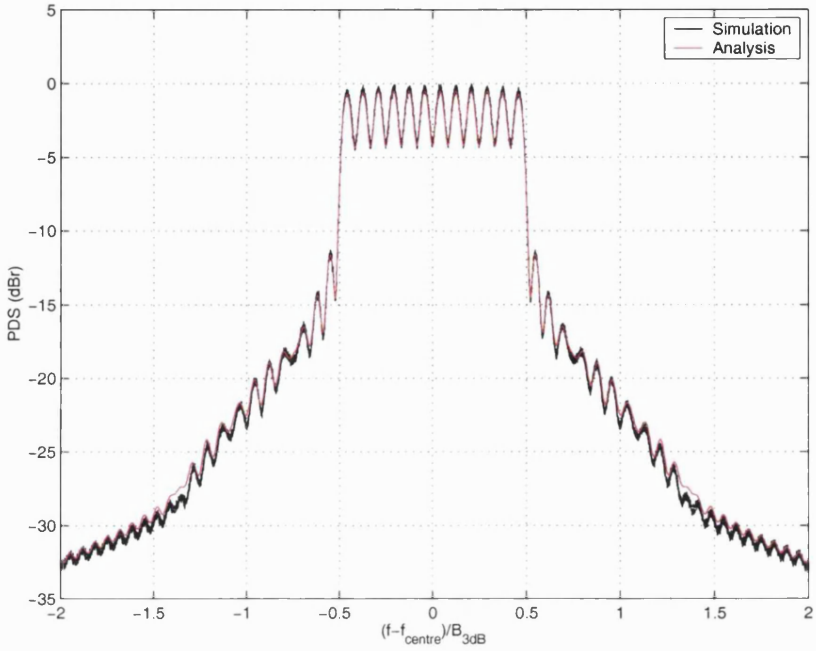

Figure 3.10: PDS of the response of the frequency independent non-linearity to a 12 sub-channel OFDM/BPSK signal. Analytic results were obtained by considering the HPDSs $\overline{\Phi}_{xx_n}(f)$ of the input OFDM signal for $n=-3,\ldots,3$.

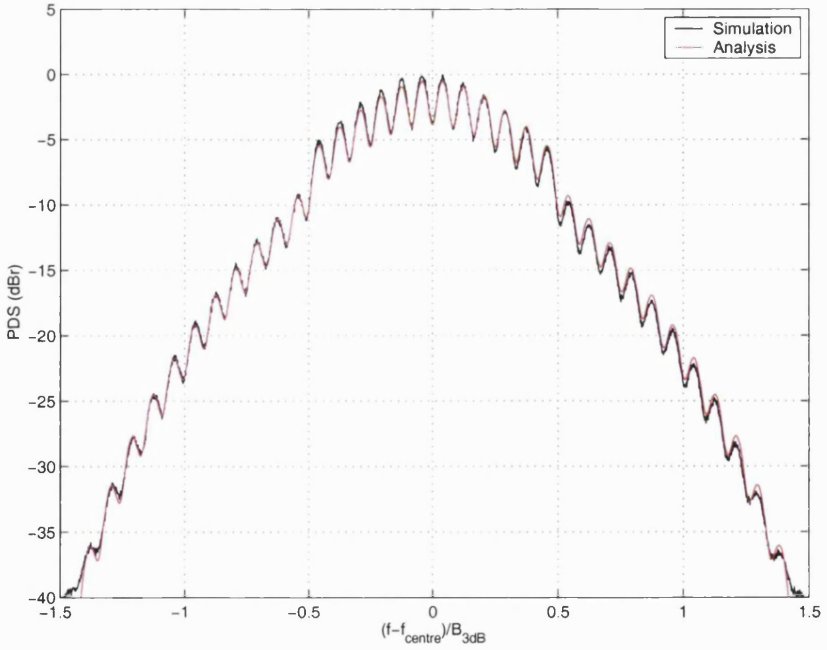

Figure 3.11: PDS of the response of the frequency dependent non-linearity to a 12 sub-channel OFDM/BPSK signal. Analytic results were obtained by considering the HPDSs $\overline{\Phi}_{xx_n}(f)$ of the input OFDM signal for $n=-3,\ldots,3$.

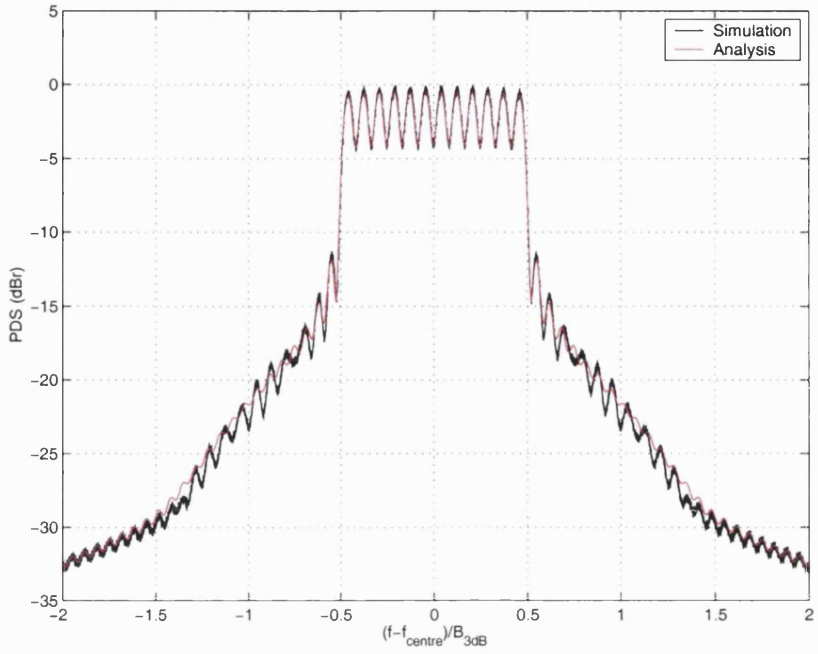

Figure 3.12: PDS of the response of the frequency independent non-linearity to a 12 sub-channel OFDM/BPSK signal. Analytic results were obtained by considering only the average PDS of the input OFDM signal.

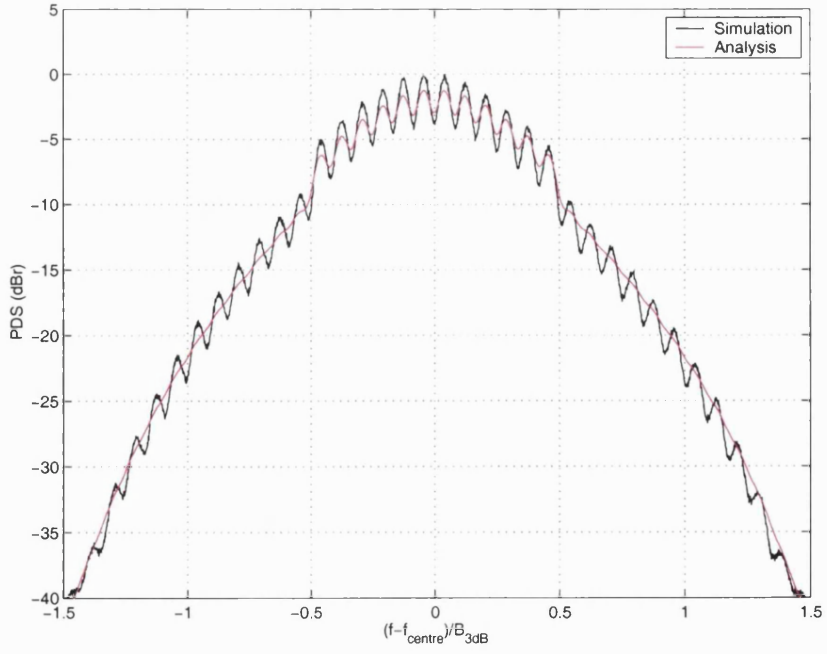

Figure 3.13: PDS of the response of the frequency dependent non-linearity to a 12 sub-channel OFDM/BPSK signal. Analytic results were obtained by considering only the average PDS of the input OFDM signal.

Table 3.1: Comparison of exact and approximated powers in an adjacent band.

	Case A	Case B	Case C	Case D
Exact Power	0.12 dBm	4.80 dBm	2.11 dBm	5.91 dBm
Approx. Power	0.21 dBm	4.99 dBm	1.92 dBm	6.28 dBm
Error (linear scale)	2.14 %	4.4 %	4.3 %	8.8 %

3.5 Summary

In this chapter, we have developed an analytic technique to assess the impact of non-linearities on the PDS of OFDM signals. Since we have modelled the non-linearities in the OFDM system by a Volterra series then this technique accounts for both frequency independent and frequency dependent non-linear behaviour. Accordingly, this technique can be used to provide a first-order approximation to the spectral spreading induced by fibre-radio system non-linearities on an OFDM signal without the need for time consuming simulations or costly experimentation. Moreover, this technique also provides insight into the different mechanisms responsible for the spectral spreading.

We have developed the analytic technique by taking into consideration the statistical properties of OFDM signals, i.e., we have considered an OFDM signal to be a zero-mean Gaussian cyclo-stationary stochastic process. First, expressions were derived to determine the mean value and the ACF of a non-linearly distorted OFDM signal and then, by realising that the non-linearly distorted OFDM signal is also a cyclo-stationary stochastic process, the expressions that give the average PDS of the distorted signal were determined by Fourier transforming the expressions that give the average ACF of the distorted signal. The derived expressions relate the statistics of the non-linearity output to the HACFs/HPDSs of the non-linearity input and to the kernels/transfer functions of the non-linearity. Moreover, the derived expressions take into account up to third-order non-linear behaviour.

Subsequently, we have investigated the application of the PDS expressions to specific OFDM signals distorted by both a frequency independent and a frequency dependent non-linearity exhibiting up to third-order non-linear behaviour. We have verified that analysis agrees perfectly with simulation provided that a sufficient number of HPDSs of the non-distorted OFDM signal are inserted into the mathematical expressions. We have also verified that analysis agrees perfectly with simulation both for OFDM signals with 48 sub-

almost

channels, for which the Gaussian approximation is highly accurate, and OFDM signals with 12 sub-channels, for which the Gaussian approximation is not so accurate.

Finally, we have demonstrated that by inserting only the average PDS of an OFDM signal into the mathematical expressions then relatively good agreement is already observed between analysis and simulation appropriate to many practical situations. We have noted that with this simplification our expressions, which apply to a zero-mean Gaussian cyclo-stationary process, reduce to the Bedrosian-Rice expressions, which apply to a zero-mean Gaussian stationary process. We have also noted that this simplification explains why previous researchers that have developed expressions to determine the PDS of non-linearly distorted OFDM signals, based only on considering an OFDM signal to be a stationary and not a cyclo-stationary stochastic process, have observed good agreement between analysis and simulation.

In the next chapter, we develop an analytic technique to assess the impact of non-linearities on the error probability of OFDM signals.

Chapter 4

Impact of non-linearities on the error probability of OFDM signals

4.1 Introduction

In the previous chapter, we have developed an analytic technique to assess the impact of non-linearities on the PDS of OFDM signals. This enabled us to capture one of the effects of a non-linearity on an OFDM signal, signal spectral spreading. In this chapter, we develop an analytic technique to assess the impact of non-linearities on the error probability of OFDM signals. This enables us to capture the other effect of a non-linearity on an OFDM signal, namely signal error probability degradation. We note that aspects of this research work have been published in the open literature in three papers [137-139].

The development of analytic techniques to determine the error probability of non-linearly distorted OFDM signals has been a subject of extensive previous research [13,14,16-18,21-25]. Yet again, since these techniques focused on the error rate of OFDM signals distorted by clipping devices and HPAs, which exhibit frequency independent behaviour, then they cannot generally be carried over to determine the error rate of OFDM signals distorted by fibre-radio system elements, which normally exhibit frequency dependent non-linear behaviour. To account for frequency dependent non-linear behaviour we use an equivalent baseband Volterra series to model the (bandpass) non-linearities encountered in the OFDM system. An introduction to the equivalent baseband Volterra series representation of (bandpass) non-linearities is the subject of section 4.2. The

development of the analytical method itself and then a critical analysis of the same method are considered in section 4.3 and section 4.4, respectively. Finally, section 4.5 summarises the main contributions of this chapter.

4.2 Equivalent baseband Volterra series representation of bandpass non-linearities

It is well known that for bandpass linear systems it is possible to develop an input-output relation involving the complex envelopes of the input and output signals and the equivalent baseband impulse response of the system [125,126]. Similarly, for bandpass non-linear systems it is also possible to develop an input-output relation involving the complex envelopes of the input and output signals and the equivalent baseband kernels of the system [125,126]. In this section, we introduce the equivalent baseband Volterra series representation of bandpass non-linearities which will be used throughout this chapter since it facilitates the analytical formulation of our problem.

We assume here that the non-linearity is bandpass and that both the input signal, $x(t)$, and the output signal, $y(t)$, are also bandpass so that they can be written in terms of complex envelope notation, respectively, as

$$x(t) = \mathrm{Re}\left\{\tilde{x}(t)e^{j2\pi f_c t}\right\} \tag{4.1}$$

and

$$y(t) = \mathrm{Re}\left\{\tilde{y}(t)e^{j2\pi f_c t}\right\} \tag{4.2}$$

where $\tilde{x}(t)$ is the complex envelope of the input signal, $\tilde{y}(t)$ is the complex envelope of the output signal and f_c is the carrier frequency. One may argue that a non-linearity strictly cannot be bandpass as its response to a sine wave with frequency f_c consists generally of several components with frequencies 0, f_c, $2f_c$, $3f_c$, ... To circumvent this difficulty we can take the non-linearity to be followed by a zonal filter whose purpose is to eliminate all the harmonics but the fundamental frequency f_c without introducing any distortion in the band of interest.

To develop an equivalent baseband Volterra series representation of a bandpass non-linearity it is first important to ascertain the properties of its kernels and its transfer functions. If the non-linearity excitation is

$$x(t) = \cos(2\pi f_c t) \tag{4.3}$$

then the non-linearity response is

$$y(t) = \sum_{n=1}^{\infty} y_n(t) \tag{4.4}$$

$$y_n(t) = \frac{1}{2^n} \sum H_n(\pm f_c, \pm f_c, \ldots, \pm f_c) e^{j2\pi(\pm f_c \pm f_c \pm \cdots \pm f_c)t} \tag{4.5}$$

where the summation in (4.5) runs through all the possible 2^n combinations of plus and minus signs in the argument of the nth-order transfer function of the non-linearity $H_n(\pm f_c, \pm f_c, \ldots, \pm f_c)$ and in the exponent of the complex exponential $e^{j2\pi(\pm f_c \pm f_c \cdots \pm f_c)t}$. Since the bandpass hypothesis demands that all contributions not centred around $\pm f_c$ are necessarily zero then we conclude from (4.4) and (4.5) that even-order transfer functions are zero as these would produce terms not around $\pm f_c$ but around 0, $\pm 2f_c$, $\pm 4f_c$, ... We also conclude from (4.4) and (4.5) that odd-order transfer functions exist only in a neighbourhood of the n-tuple $(\pm f_c, \pm f_c, \ldots, \pm f_c)$ in a 2^n-dimensional space such that the number of plus signs and the number of minus signs differs exactly by plus or minus one. Were this difference not plus or minus one then the contributions of the odd-order transfer functions would not be around $\pm f_c$ but around $\pm 3f_c$, $\pm 5f_c$, $\pm 7f_c$, ...

These properties reveal that the even-order transfer functions of the bandpass non-linearity are zero and the odd-order transfer functions of the bandpass non-linearity, $H_n(f_1, f_2, \ldots, f_n)$, can be written as the sum of 2^n baseband transfer functions, $\tilde{H}_n^{(\cdot)}(f_1, f_2, \ldots, f_n)$, as follows[11]

[11] For simplicity of notation we include terms $\tilde{H}_n^{(\cdot)}(f_1 \pm f_c, f_2 \pm f_c, \ldots, f_n \pm f_c)$ for which the number of plus signs and the number of minus signs does not differ by plus or minus one, although these are zero.

$$
\begin{aligned}
&H_n(f_1, f_2, \ldots, f_{n-1}, f_n) = \\
&= \widetilde{H}_n^{(1)}(f_1 - f_c, f_2 - f_c, \ldots, f_{n-1} - f_c, f_n - f_c) + \widetilde{H}_n^{(2)}(f_1 - f_c, f_2 - f_c, \ldots, f_{n-1} - f_c, f_n + f_c) + \cdots \\
&+ \widetilde{H}_n^{(2^n-1)}(f_1 + f_c, f_2 + f_c, \ldots, f_{n-1} + f_c, f_n - f_c) + \widetilde{H}_n^{(2^n)}(f_1 + f_c, f_2 + f_c, \ldots, f_{n-1} + f_c, f_n + f_c)
\end{aligned} \tag{4.6}
$$

where

$$
\widetilde{H}_n^{(\cdot)}(f_1 \mp f_c, f_2 \mp f_c, \ldots, f_n \mp f_c) = \begin{cases} H_n(f_1, f_2, \ldots, f_n), & \pm f_1, \pm f_2, \ldots, \pm f_n > 0 \\ 0, & \text{elsewhere} \end{cases} \tag{4.7}
$$

Similarly, the even-order kernels of the bandpass non-linearity are also zero and the odd-order kernels of the bandpass non-linearity, $h_n(\tau_1, \tau_2, \ldots, \tau_n)$, can also be written as the sum of 2^n baseband kernels, $\widetilde{h}_n^{(\cdot)}(\tau_1, \tau_2, \ldots, \tau_n)$, as follows[12]

$$
\begin{aligned}
&h_n(\tau_1, \tau_2, \ldots, \tau_{n-1}, \tau_n) = \\
&= \widetilde{h}_n^{(1)}(\tau_1, \tau_2, \ldots, \tau_{n-1}, \tau_n) e^{j2\pi f_c(\tau_1 + \tau_2 + \cdots + \tau_{n-1} + \tau_n)} + \widetilde{h}_n^{(2)}(\tau_1, \tau_2, \ldots, \tau_{n-1}, \tau_n) e^{j2\pi f_c(\tau_1 + \tau_2 + \cdots + \tau_{n-1} - \tau_n)} + \cdots \\
&+ \widetilde{h}_n^{(2^n-1)}(\tau_1, \tau_2, \ldots, \tau_{n-1}, \tau_n) e^{j2\pi f_c(-\tau_1 - \tau_2 - \cdots - \tau_{n-1} + \tau_n)} + \widetilde{h}_n^{(2^n)}(\tau_1, \tau_2, \ldots, \tau_{n-1}, \tau_n) e^{j2\pi f_c(-\tau_1 - \tau_2 - \cdots - \tau_{n-1} - \tau_n)}
\end{aligned} \tag{4.8}
$$

where $\widetilde{h}_n^{(\cdot)}(\tau_1, \tau_2, \ldots, \tau_n)$ is the n-dimensional inverse Fourier transform of $\widetilde{H}_n^{(\cdot)}(f_1, f_2, \ldots, f_n)$.

It is important to note that the baseband kernels in (4.8) are related to one another because the kernels of a non-linearity exhibit certain properties (see chapter 3). As the kernels of a non-linearity are symmetric then a baseband kernel that multiplies some complex exponential is equivalent to a baseband kernel that multiplies some other complex exponential provided that the complex exponentials are equivalent to one another by a permutation of the τ variables and that the same permutation of the τ variables is carried out in the arguments of the baseband kernels. As an example,

$$
\widetilde{h}_3^{(2)}(\tau_1, \tau_2, \tau_3) = \widetilde{h}_3^{(3)}(\tau_1, \tau_3, \tau_2) \tag{4.9}
$$

Moreover, as the kernels of a non-linearity are real then a baseband kernel that multiplies some complex exponential is the complex conjugate of a baseband kernel that multiplies the complex conjugate of the complex exponential under consideration. As an example,

---

[12] Again, for simplicity of notation we include terms $\widetilde{h}_n^{(\cdot)}(\tau_1, \tau_2, \ldots, \tau_n) e^{j2\pi f(\pm\tau 1 \pm \tau 2 \pm \ldots \pm \tau n)}$ for which the number of plus signs and the number of minus signs does not differ by plus or minus one, although these are zero.

$$\tilde{h}_3^{(2)}(\tau_1,\tau_2,\tau_3)=\tilde{h}_3^{(7)*}(\tau_1,\tau_2,\tau_3) \tag{4.10}$$

It is also important to note that the baseband transfer functions in (4.6) are also related to one another because the transfer functions of a non-linearity are symmetric and exhibit Hermitian symmetry (see chapter 3).

The input-output relationship involving equivalent baseband quantities is now obtained by substituting (4.1), (4.2) and the expressions for the kernels of the non-linearity, i.e., zero for even-order kernels or (4.8) for odd-order kernels, into the input-output relationship of the non-linearity (see (3.1) and (3.2) in chapter 3) and by exploring the relations between the baseband kernels. By carrying out these substitutions we find out that the (2n-1)th-order contribution of the bandpass non-linearity consists of $2^{2(2n-1)}$ terms of the form

$$\frac{1}{2^{2n-1}}\int_{-\infty}^{\infty}\cdots\int_{-\infty}^{\infty}\tilde{h}_{2n-1}^{(\cdot)}(\tau_1,\ldots,\tau_{2n-1})e^{j2\pi f_c(\pm\tau_1\pm\cdots\pm\tau_{2n-1})}\tilde{x}/\tilde{x}^*(t-\tau_1)e^{\pm j2\pi f_c(t-\tau_1)}\cdots\tilde{x}/\tilde{x}^*(t-\tau_{2n-1})e^{\pm j2\pi f_c(t-\tau_{2n-1})}d\tau_1\cdots d\tau_{2n-1} \tag{4.11}$$

and under the narrowband assumption it can be observed that integrands in (4.11) that contain any factor of the form $e^{\pm j2\pi f_c m\tau_k}$ for $m\neq 0$ vary much more rapidly than integrands that contain only factors of the form $e^{\pm j2\pi f_c m\tau_k}$ for $m=0$ so that the value of the integrals in the first case is much smaller than the value of the integrals in the second case. This result enables us to eliminate a number of terms. The remaining terms combine due to the relations between the baseband kernels yielding either

$$\frac{\binom{2n-1}{n-1}}{2^{2n-1}}\int_{-\infty}^{\infty}\cdots\int_{-\infty}^{\infty}\tilde{h}_{2n-1}^{(2^{n-1})}(\tau_1,\ldots,\tau_{2n-1})\tilde{x}(t-\tau_1)\cdots\tilde{x}(t-\tau_n)\tilde{x}^*(t-\tau_{n+1})\cdots\tilde{x}^*(t-\tau_{2n-1})d\tau_1\cdots d\tau_{2n-1}e^{j2\pi f_c t} \tag{4.12}$$

or

$$\frac{\binom{2n-1}{n-1}}{2^{2n-1}}\int_{-\infty}^{\infty}\cdots\int_{-\infty}^{\infty}\tilde{h}_{2n-1}^{(2^{2n-1}-2^{n-1}+1)}(\tau_1,\ldots,\tau_{2n-1})\tilde{x}^*(t-\tau_1)\cdots\tilde{x}^*(t-\tau_n)\tilde{x}(t-\tau_{n+1})\cdots\tilde{x}(t-\tau_{2n-1})d\tau_1\cdots d\tau_{2n-1}e^{-j2\pi f_c t} \tag{4.13}$$

which are complex conjugate pairs[13]. Accordingly, the complex envelope of the output signal, $\tilde{y}(t)$, is related to the complex envelope of the input signal, $\tilde{x}(t)$, as follows

$$\tilde{y}(t)=\sum_{n=1}^{\infty}\tilde{y}_{2n-1}(t) \tag{4.14}$$

$$\tilde{y}_{2n-1}(t)=\int_{-\infty}^{\infty}\cdots\int_{-\infty}^{\infty}\tilde{h}_{2n-1}(\tau_1,\ldots,\tau_{2n-1})\tilde{x}(t-\tau_1)\cdots\tilde{x}(t-\tau_n)\tilde{x}^*(t-\tau_{n+1})\cdots\tilde{x}^*(t-\tau_{2n-1})d\tau_1\cdots d\tau_{2n-1} \tag{4.15}$$

where $\tilde{h}_{2n-1}(\tau_1,\ldots,\tau_{2n-1})$ is the (2n-1)th-order equivalent baseband kernel of the bandpass non-linearity. This equivalent baseband kernel is given by

$$\tilde{h}_{2n-1}(\tau_1,\ldots,\tau_{2n-1})=\binom{2n-1}{n-1}\Big/2^{2n-2}\,\tilde{h}_{2n-1}^{(2^{n-1})}(\tau_1,\ldots,\tau_{2n-1}) \tag{4.16}$$

The spectrum of the complex envelope of the output signal, $\tilde{Y}(f)$, is related to the spectrum of the complex envelope of the input signal, $\tilde{X}(f)$, as follows

$$\tilde{Y}(f)=\sum_{n=1}^{\infty}\tilde{Y}_{2n-1}(f) \tag{4.17}$$

$$\tilde{Y}_{2n-1}(f)=\int_{-\infty}^{\infty}\cdots\int_{-\infty}^{\infty}\tilde{H}_{2n-1}(f_1,\ldots,f_{2n-1})\tilde{X}(f_1)\cdots\tilde{X}(f_n)\tilde{X}^*(-f_{n+1})\cdots\tilde{X}^*(-f_{2n-1})\delta(f-f_1-\cdots-f_{2n-1})df_1\cdots df_{2n-1} \tag{4.18}$$

where $\delta(\cdot)$ is the Dirac delta function and $\tilde{H}_{2n-1}(f_1,\ldots,f_{2n-1})$ is the (2n-1)th-order equivalent baseband transfer function of the bandpass non-linearity. This equivalent baseband transfer function is given by

$$\tilde{H}_{2n-1}(f_1,\ldots,f_{2n-1})=\binom{2n-1}{n-1}\Big/2^{2n-2}\,\tilde{H}_{2n-1}^{(2^{n-1})}(f_1,\ldots,f_{2n-1}) \tag{4.19}$$

---

[13] The binomial coefficient $\binom{2n-1}{n-1}=\frac{(2n-1)!}{n!(n-1)!}$.

The equivalent baseband kernels and the equivalent baseband transfer function are Fourier transform pairs.

4.2.1 Finding the equivalent baseband kernels/transfer functions of a bandpass non-linearity

In this section we review how to determine the equivalent baseband transfer functions of a bandpass non-linearity. The even-order equivalent baseband transfer functions are zero while the odd-order equivalent baseband transfer functions are given by

$$\tilde{H}_{2n-1}(f_1,\ldots,f_{2n-1}) = \binom{2n-1}{n-1} \Big/ 2^{2n-2}\, \tilde{H}_{2n-1}^{(2^{n-1})}(f_1,\ldots,f_{2n-1}) \tag{4.20}$$

where

$$\begin{aligned}\tilde{H}_{2n-1}^{(2^{n-1})}(f_1,\ldots,f_{2n-1}) = H_{2n-1}(f_1+f_c,\ldots,f_{2^{n-1}}+f_c,f_{2^{n-1}+1}-f_c,\ldots,f_{2n-1}-f_c)\\ u(f_1+f_c)\cdots u(f_{2^{n-1}}+f_c)u(-f_{2^{n-1}+1}+f_c)\cdots u(-f_{2n-1}+f_c)\end{aligned} \tag{4.21}$$

Here $u(\cdot)$ is the unit step function and $H_{2n-1}(f_1,\ldots,f_{2n-1})$ is the (2n-1)th-order transfer function of the bandpass non-linearity.

As an example, we determine the equivalent baseband transfer functions of a frequency independent non-linearity and a frequency dependent non-linearity, which will be used later in the thesis. The frequency independent non-linearity is shown in Figure 4.1, where $f(\cdot)$ represents a memoryless device whose characteristics can be expanded in a power series

$$f(z) = \sum_{i=1}^{\infty} c_i z^i \tag{4.22}$$

Note that this frequency independent non-linearity has already been considered in chapter 3 but here we have included a zonal filter to guarantee bandpass behaviour.

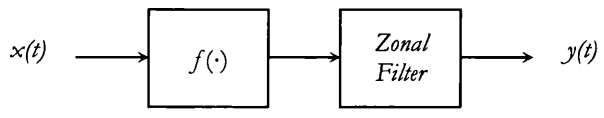

Figure 4.1: Frequency independent non-linearity model.

The equivalent baseband transfer functions of this non-linearity can be evaluated by noting that its transfer functions are given by (see (3.15))

$$H_n(f_1,\ldots,f_n)=c_n \tag{4.23}$$

Thus, the even-order equivalent baseband transfer functions are zero and the odd-order ones are

$$\tilde{H}_{2n-1}(f_1,\ldots,f_{2n-1})=\binom{2n-1}{n-1}\Big/2^{2n-2}\,c_{2n-1}\,u(f_1+f_c)\cdots u(f_{2^{n-1}}+f_c)u(-f_{2^{n-1}+1}+f_c)\cdots u(-f_{2n-1}+f_c) \tag{4.24}$$

The frequency dependent non-linearity is shown in Figure 4.2, where $H'(f)$ and $H''(f)$ are frequency responses of linear systems and $f(\cdot)$ again represents a memoryless device whose characteristics can be expanded in a power series

$$f(z)=\sum_{i=1}^{\infty}c_i z^i \tag{4.25}$$

Note also that this frequency dependent non-linearity has already been considered in chapter 3 but here we have included a zonal filter to guarantee bandpass behaviour. Again, the equivalent baseband transfer functions of this non-linearity can be evaluated by noting that its transfer functions are given by (see (3.20))

$$H_n(f_1,\ldots,f_n)=c_n H''(f_1+\cdots+f_n)H'(f_1)\cdots H'(f_n) \tag{4.26}$$

Thus, the even-order equivalent baseband transfer functions are zero and the odd-order ones are

$$\begin{aligned}\tilde{H}_{2n-1}(f_1,\ldots,f_{2n-1})=&\binom{2n-1}{n-1}\Big/2^{2n-2}\,c_{2n-1}\,H''(f_1+f_c+\cdots+f_{2^{n-1}}+f_c+f_{2^{n-1}+1}-f_c+\cdots+f_{2n-1}-f_c)\\ &H'(f_1+f_c)\cdots H'(f_{2^{n-1}}+f_c)H'(f_{2^{n-1}+1}-f_c)\cdots H'(f_{2n-1}-f_c)\\ &u(f_1+f_c)\cdots u(f_{2^{n-1}}+f_c)u(-f_{2^{n-1}+1}+f_c)\cdots u(-f_{2n-1}+f_c)\end{aligned} \tag{4.27}$$

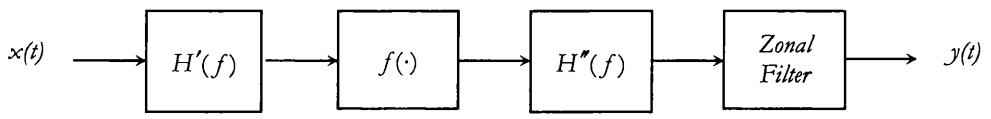

Figure 4.2: Frequency dependent non-linearity model.

The (2n-1)th-order equivalent baseband kernels of these non-linearities correspond to the (2n-1)-dimensional inverse Fourier transform of the (2n-1)th-order equivalent baseband transfer functions.

4.3 Analytic technique

In this section, we develop an analytic technique to determine the error probability of OFDM signals distorted by frequency independent and frequency dependent non-linearities in AWGN by deriving all the necessary mathematical relations and expressions. This development will be carried out with respect to the model shown in Figure 4.3. In this figure, $\tilde{s}(t)$ is the complex envelope of the transmitted OFDM signal, $\tilde{r}(t)$ is the complex envelope of the received OFDM signal, $\tilde{n}(t)$ is the additive white complex Gaussian noise (with power spectral density N_0) and the bandpass non-linearity is represented by an equivalent baseband Volterra series, i.e., the bandpass non-linearity is represented by its equivalent baseband kernels, $\tilde{h}_n(\tau_1,\ldots,\tau_n), n = 1,3,\ldots$, or by its equivalent baseband transfer functions, $\tilde{H}_n(f_1,\ldots,f_n), n = 1,3,\ldots$. $S_{k,n}$ is the complex transmitted symbol in time slot k and sub-channel n and $R_{k,n}$ is the complex received symbol in the same time slot and sub-channel; $g_n(t-kT)$ denotes the complex waveform used to convey the information in time slot k and sub-channel n and $g_n^*(t-kT)$ denotes its complex conjugate. The integrate and dump filter integrates from $kT+T_{CP}$ to $(k+1)T$, where T is the OFDM symbol duration and T_{CP} is the OFDM cyclic prefix duration; the nth equaliser multiplies the output of the nth integrator by a complex factor $H_{k,n}$ to compensate partially for the effects of the bandpass non-linearity. We consider a continuous time model, involving an oscillator based implementation of the OFDM transceiver, and not a discrete time model, involving an FFT based implementation of the same transceiver, because the input-output relation of the non-linearities encountered hereafter are expressed in continuous and not discrete time. However, both models are equivalent in the limit when the number of OFDM sub-channels tends to infinity [44,45].

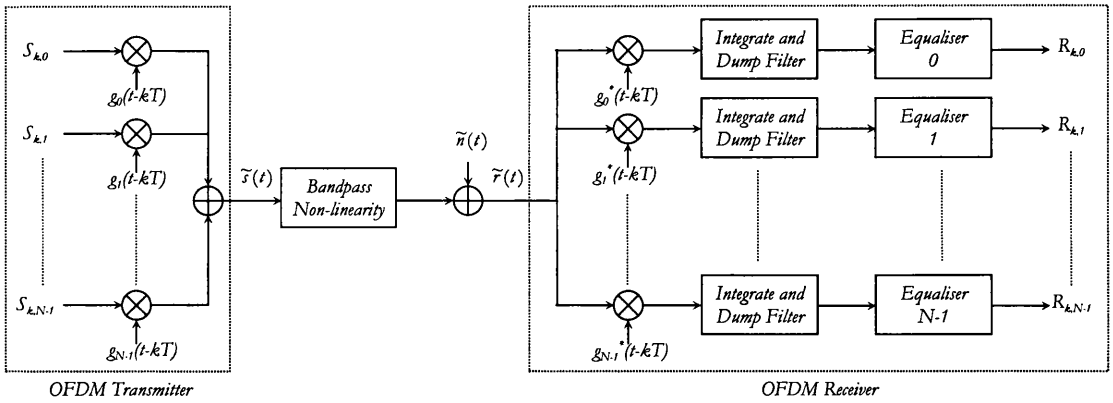

Figure 4.3: Model used to investigate the impact of non-linearities on the error probability of OFDM signals.

Conventionally, the error probability analysis of OFDM communication systems in the presence of frequency independent non-linearities has previously been carried out by noting that since the non-linearly distorted OFDM signal consists of a scaled replica of the OFDM signal and an uncorrelated distortion component, which is a consequence of Bussgang's theorem [13,14,16-18,21-25], then the PDS of the non-linearly distorted OFDM signal also consists of a scaled replica of the PDS of the OFDM signal and the PDS of the uncorrelated distortion component. From the PDSs, determined as described in chapter 3, a simple estimate of the signal-to-nonlinear-distortion power ratio can be obtained and hence a simple estimate of the error probability in AWGN can also be obtained by assuming the distortion to be Gaussian. The error probability analysis of OFDM communication systems in the presence of frequency dependent non-linearities cannot be carried out using such procedure because it is not possible to write the non-linearly distorted OFDM signal in this case as the sum of a scaled replica of the OFDM signal and an uncorrelated distortion component. Instead, to determine the error probability of non-linearly distorted OFDM signals in AWGN we first identify the various contributions to the received symbol in a particular sub-channel and we then express the error probability in that particular sub-channel as the statistical expectation with respect to the interference RV of the error probability in AWGN conditioned by a given value of the interference RV. Note that this method corresponds to that traditionally adopted to evaluate the error probability of digital communication systems in the presence of ISI [140-148] or other forms of interference [149] but differs from that traditionally adopted to

evaluate the error probability of non-linearly distorted OFDM signals in AWGN [13,14,16-18,21-25].

To identify the various contributions to the received symbol in a particular time slot and sub-channel we first observe that the transmitted OFDM signal is given by

$$\tilde{s}(t)=\sum_{k=-\infty}^{\infty}\sum_{n=0}^{N-1}S_{k,n}g_n(t-kT) \tag{4.28}$$

$$g_n(t)=\begin{cases}\dfrac{1}{\sqrt{T-T_{CP}}}e^{j\frac{2\pi n(t-T_{CP})}{T-T_{CP}}}, & t\in[0,T]\\ 0, & t\notin[0,T]\end{cases} \tag{4.29}$$

and that the received OFDM signal, which consists of the response of the non-linearity to the transmitted OFDM signal plus the additive white complex Gaussian noise, is given by

$$\tilde{r}(t)=\int_{-\infty}^{\infty}\tilde{h}_1(\tau_1)\tilde{s}(t-\tau_1)d\tau_1+\int_{-\infty}^{\infty}\int_{-\infty}^{\infty}\int_{-\infty}^{\infty}\tilde{h}_3(\tau_1,\tau_2,\tau_3)\tilde{s}(t-\tau_1)\tilde{s}(t-\tau_2)\tilde{s}^*(t-\tau_3)d\tau_1d\tau_2d\tau_3+\cdots+\tilde{n}(t) \tag{4.30}$$

Finally, we observe that the complex received symbol in time slot k and sub-channel n is obtained by multiplying the received OFDM signal by $g_n^*(t-kT)$, integrating from $kT+T_{CP}$ to $(k+1)T$ and multiplying the integrator output by the complex factor $H_{k,n}$, i.e.,

$$R_{k,n}=H_{k,n}\left[\int_{kT+T_{CP}}^{(k+1)T}\tilde{r}(t)g_n^*(t-kT)dt\right] \tag{4.31}$$

By using (4.28) and (4.29) in (4.30) and the resulting expression in (4.31) then a complex expression relating the complex received symbol in time slot k and sub-channel n to the complex transmitted symbols in different time slots and different sub-channels and to the kernels of the non-linearity results. To simplify such expression we assume that $\tilde{h}_1(\tau_1)$ is non-zero only when $\tau_1\in[0,T_{CP}]$, $\tilde{h}_3(\tau_1,\tau_2,\tau_3)$ is non-zero only when $\tau_1,\tau_2,\tau_3\in[0,T_{CP}]$, etc[14]. Thus,

[14] Note that for frequency independent non-linearities these conditions are always met because the kernels consist of Dirac delta impulses; for frequency dependent non-linearities these conditions are met provided that the cyclic prefix duration is sufficiently long. Note also that we have considered an OFDM signal with

$$R_{k,n} = H_{k,n}\sum_{n_1=0}^{N-1} S_{k,n_1}\frac{1}{(T-T_{CP})^0}\tilde{H}_1\left(\frac{n_1}{T-T_{CP}}\right)\delta(n_1-n)$$
$$+ H_{k,n}\sum_{n_1=0}^{N-1}\sum_{n_2=0}^{N-1}\sum_{n_3=0}^{N-1} S_{k,n_1}S_{k,n_2}S^*_{k,n_3}\frac{1}{(T-T_{CP})^1}\tilde{H}_3\left(\frac{n_1}{T-T_{CP}},\frac{n_2}{T-T_{CP}},-\frac{n_3}{T-T_{CP}}\right)\delta(n_1+n_2-n_3-n)$$
$$+\cdots$$
$$+ N_{k,n} \tag{4.32}$$

where $\delta(\cdot)$ is the Kronecker delta product and

$$N_{k,n} = H_{k,n}\left[\int_{kT+T_{CP}}^{(k+1)T}\tilde{n}(t)g_n^*(t-kT)dt\right] \tag{4.33}$$

Note that the various contributions to the received symbol in time slot k and sub-channel n can now be identified in (4.32): the first set of terms yields an attenuated/phase shifted version of the complex transmitted symbol in time slot k and sub-channel n; the second set of terms yields the different third-order IMPs; a third set of terms would yield the different fifth-order IMPs; etc. and $N_{k,n}$ is a complex Gaussian RV whose real and imaginary parts are uncorrelated zero-mean Gaussian RVs with common variance $|H_{k,n}|^2 N_0$, i.e.,

$$\mu_{\mathrm{Re}\{N_{k,n}\}} = E[\mathrm{Re}\{N_{k,n}\}] = \mu_{\mathrm{Im}\{N_{k,n}\}} = E[\mathrm{Im}\{N_{k,n}\}] = 0 \tag{4.34}$$

$$\sigma^2_{\mathrm{Re}\{N_{k,n}\}} = E\left[\left(\mathrm{Re}\{N_{k,n}\}-\mu_{\mathrm{Re}\{N_{k,n}\}}\right)^2\right] = \sigma^2_{\mathrm{Im}\{N_{k,n}\}} = E\left[\left(\mathrm{Im}\{N_{k,n}\}-\mu_{\mathrm{Im}\{N_{k,n}\}}\right)^2\right] = |H_{k,n}|^2 N_0 \tag{4.35}$$

$$\rho_{\mathrm{Re}\{N_{k,n}\}\mathrm{Im}\{N_{k,n}\}} = \frac{1}{\sigma_{\mathrm{Re}\{N_{k,n}\}}\sigma_{\mathrm{Im}\{N_{k,n}\}}}E\left[\left(\mathrm{Re}\{N_{k,n}\}-\mu_{\mathrm{Re}\{N_{k,n}\}}\right)\left(\mathrm{Im}\{N_{k,n}\}-\mu_{\mathrm{Im}\{N_{k,n}\}}\right)\right] = 0 \tag{4.36}$$

where μ, σ^2 and ρ denote the mean, variance and correlation coefficient of the RVs, respectively. The probability density function (PDF) of $N_{k,n}$ can then be written as follows

---

rectangular windowing and not an OFDM signal with raised cosine windowing, although the analysis is valid for either signal. The only effect of a raised cosine window with rolloff factor β is to reduce the upper limits defining the support of the equivalent baseband kernels by βT.

$$p(N_{k,n}) = \frac{1}{2\pi |H_{k,n}|^2 N_0} e^{-\frac{|N_{k,n}|^2}{2|H_{k,n}|^2 N_0}} \tag{4.37}$$

The statistical properties of $N_{k,n}$ in (4.34), (4.35) and (4.36) were obtained by using (4.33) in (4.34), (4.35) and (4.36) and the statistical properties of the additive white complex Gaussian noise (with power spectral density N_0), which are written below [42]

$$E[\mathrm{Re}\{\tilde{n}(t)\}] = E[\mathrm{Im}\{\tilde{n}(t)\}] = 0 \tag{4.38}$$

$$E[\mathrm{Re}\{\tilde{n}(t_1)\}\mathrm{Re}\{\tilde{n}(t_2)\}] = E[\mathrm{Im}\{\tilde{n}(t_1)\}\mathrm{Im}\{\tilde{n}(t_2)\}] = N_0\delta(t_1 - t_2) \tag{4.39}$$

$$E[\mathrm{Re}\{\tilde{n}(t_1)\}\mathrm{Im}\{\tilde{n}(t_2)\}] = 0 \tag{4.40}$$

where $\delta(\cdot)$ is the Dirac delta function.

To compensate for the constant attenuation/phase shift in the nth received symbol, $R_{k,n}$, the nth equaliser complex multiplicative factor, $H_{k,n}$, is set to

$$H_{k,n} = \left[\tilde{H}_1\left(\frac{n}{T - T_{CP}}\right)\right]^{-1} \tag{4.41}$$

Note that such a setting enables the transmission of M-PSK or M-QAM symbols without the need for modifying the decision regions at the receiver.

Finally, we observe that the characterisation of the received symbol in a particular time slot and sub-channel forms the basis for the development of a method to determine the error probability of non-linearly distorted OFDM signals in AWGN. The development of such a method for OFDM/BPSK and OFDM/QPSK signals is the subject of section 4.3.1 and section 4.3.2, respectively.

4.3.1 OFDM/BPSK signals

In this section, we present a method to evaluate the error probability of OFDM/BPSK signals by assuming that the complex transmitted symbols, $S_{k,n}$, take any value belonging to a BPSK signal constellation $\{Ae^{j2\pi(m-1)/2}; m = 1,2\}$ with equal probability.

The overall error probability of the OFDM signal, $P(e)$, is obtained by taking the average of the error probabilities in all OFDM sub-channels, i.e.,

$$P(e) = \frac{1}{N}\sum_{n=0}^{N-1} P(e_n) \tag{4.42}$$

where $P(e_n)$ is the error probability in the nth OFDM sub-channel. Since the complex transmitted symbols take any value belonging to a BPSK signal constellation with equal probability then the error probability in the nth OFDM sub-channel can be evaluated as follows

$$P(e_n) = \frac{1}{2}\sum_{m=1}^{2} P\left(e_n \middle| S_{k,n} = Ae^{j2\pi(m-1)/2}\right) \tag{4.43}$$

Finally, the conditional error probabilities on the right hand side of (4.43) are given by

$$P\left(e_n \middle| S_{k,n} = Ae^{j2\pi(m-1)/2}\right) = P\left(R_{k,n}^{m} \notin \text{Region m}\right) \tag{4.44}$$

where $R_{k,n}^{m}$ denotes the complex received symbol in time slot k and sub-channel n conditioned on $S_{k,n} = Ae^{j2\pi(m-1)/2}$ and the Region m denotes the region in the complex plane for which the symbol $Ae^{j2\pi(m-1)/2}$ is assumed to have been transmitted. The BPSK decision regions are shown in Figure 4.4. Note that these are the optimum regions that minimise the error probability for BPSK modulation in AWGN alone when the probability of transmitting any of the BPSK symbols is the same [42].

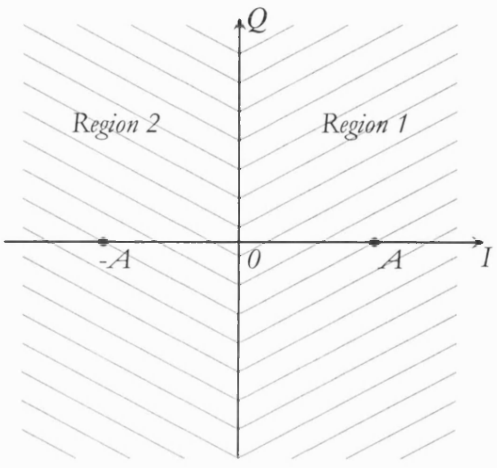

Figure 4.4: Optimum BPSK decision regions in AWGN.

To calculate the probabilities on the right hand side of (4.44) we write (4.32) as

$$R_{k,n} = S'_{k,n} + S''_{k,n} + N_{k,n} \tag{4.45}$$

where

$$\begin{aligned} S'_{k,n} &= H_{k,n} S_{k,n} \frac{1}{(T-T_{CP})^0} \widetilde{H}_1\left(\frac{n}{T-T_{CP}}\right)\delta(n-n) \\ &+ H_{k,n} S_{k,n} S_{k,n} S^*_{k,n} \frac{1}{(T-T_{CP})^1} \widetilde{H}_3\left(\frac{n}{T-T_{CP}}, \frac{n}{T-T_{CP}}, -\frac{n}{T-T_{CP}}\right)\delta(n+n-n-n) \\ &+ \cdots \end{aligned} \tag{4.46}$$

$$\begin{aligned} S''_{k,n} &= H_{k,n} \sum_{\substack{n_1=0 \\ n_1 \neq n}}^{N-1} S_{k,n_1} \frac{1}{(T-T_{CP})^0} \widetilde{H}_1\left(\frac{n_1}{T-T_{CP}}\right)\delta(n_1-n) \\ &+ H_{k,n} \sum_{\substack{n_1=0 \\ n_1,n_2,n_3 \neq n,n}}^{N-1} \sum_{n_2=0}^{N-1} \sum_{n_3=0}^{N-1} S_{k,n_1} S_{k,n_2} S^*_{k,n_3} \frac{1}{(T-T_{CP})^1} \widetilde{H}_3\left(\frac{n_1}{T-T_{CP}}, \frac{n_2}{T-T_{CP}}, -\frac{n_3}{T-T_{CP}}\right)\delta(n_1+n_2-n_3-n) \\ &+ \cdots \end{aligned} \tag{4.47}$$

and $N_{k,n}$ is the complex Gaussian RV. The justification for writing $R_{k,n}$ as the sum of $S'_{k,n}$, $S''_{k,n}$ and $N_{k,n}$ is that under symbol conditioning $R^m_{k,n}$ consists of a deterministic quantity $S'^m_{k,n}$, a random quantity $S''^m_{k,n}$ and the complex Gaussian RV $N_{k,n}$. Specifically, one can observe that $S'^m_{k,n}$ is the useful received symbol and $S''^m_{k,n}$ is the IMD RV. Thus, $R^m_{k,n}$ conditioned on $S''^m_{k,n}$, i.e., $R^m_{k,n} \mid S''^m_{k,n}$, is a complex Gaussian RV whose real and imaginary parts are uncorrelated Gaussian RVs with mean values $\mathrm{Re}\{S'^m_{k,n}\} + \mathrm{Re}\{S''^m_{k,n}\}$ and $\mathrm{Im}\{S'^m_{k,n}\} + \mathrm{Im}\{S''^m_{k,n}\}$, respectively, and common variance $|H_{k,n}|^2 N_0$. The PDF of $R^m_{k,n}$ conditioned on $S''^m_{k,n}$, i.e., $R^m_{k,n} \mid S''^m_{k,n}$, can then be written as follows

$$p\left(R^m_{k,n} \mid S''^m_{k,n}\right) = \frac{1}{2\pi |H_{k,n}|^2 N_0} e^{-\frac{\left|R^m_{k,n} - S'^m_{k,n} - S''^m_{k,n}\right|^2}{2|H_{k,n}|^2 N_0}} \tag{4.48}$$

Integrating (4.48) over the appropriate BPSK decision regions yields the conditional probabilities

$$P\left(R_{k,n}^{m} \notin \text{Region m} \middle| S_{k,n}^{''m}\right) = \frac{1}{2}\operatorname{erfc}\left(\cos\left(\frac{2\pi(m-1)}{2}\right) \frac{\operatorname{Re}\{S_{k,n}^{'m}\} + \operatorname{Re}\{S_{k,n}^{''m}\}}{\sqrt{2|H_{k,n}|^2 N_0}} \right) \tag{4.49}$$

and taking the expectation of (4.49) with respect to the IMD RV yields the probabilities

$$P\left(R_{k,n}^{m} \notin \text{Region m}\right) = E\left[\frac{1}{2}\operatorname{erfc}\left(\cos\left(\frac{2\pi(m-1)}{2}\right) \frac{\operatorname{Re}\{S_{k,n}^{'m}\} + \operatorname{Re}\{S_{k,n}^{''m}\}}{\sqrt{2|H_{k,n}|^2 N_0}} \right) \right] \tag{4.50}$$

where $\operatorname{erfc}(\cdot)$ is the complementary error function, given by

$$\operatorname{erfc}(x) = \frac{2}{\sqrt{\pi}} \int_{x}^{\infty} e^{-t^2} dt \tag{4.51}$$

Note that to determine the error probability of non-linearly distorted OFDM/BPSK signals in AWGN we have ultimately to compute the expectation of a function of the IMD RV. Note also that it suffices to take the expectation with respect to the real part of the IMD RV. Consequently, we do not need to consider complex valued RVs, which are described by two-dimensional PDFs, but real valued RVs, which are described by one-dimensional PDFs.

Conventionally, moment based methods, such as series expansion methods [140,141] or Gauss quadrature rules [142], have been used to compute the expectation of a function of a (real valued) RV to any desired degree of accuracy. Series expansion methods expand the function in some power series thereby approximating the expectation value in terms of a linear combination of a finite set of moments of the RV [140,141]. Gauss quadrature rules use a finite set of moments of the RV to define a quadrature rule that approximates the expectation value [142]. Consequently, the statistical expectations under consideration are computed by trading knowledge of the PDF of the RV for knowledge of a number of moments of the RV. This trade-off is justified by the fact that it is generally much easier to obtain a number of moments rather than the PDF of the RV. Obviously, the larger the set of moments the more accurate is the approximation. A method to determine the moments of the RVs needed to compute the error probability expectations in (4.50) is therefore developed in section 4.3.3.

4.3.2 OFDM/QPSK signals

In this section, we present a method to evaluate the error probability of OFDM/QPSK signals by assuming that the complex transmitted symbols, $S_{k,n}$, take any value belonging to a QPSK signal constellation $\left\{Ae^{j(2m-1)\pi/4}; m=1,2,3,4\right\}$ with equal probability.

The technique that we will outline in this section follows the technique outlined in the previous section. Specifically, the overall error probability of the OFDM signal, $P(e)$, is again obtained by taking the average of the error probabilities in all OFDM sub-channels, i.e.,

$$P(e)=\frac{1}{N}\sum_{n=0}^{N-1}P(e_n) \tag{4.52}$$

where $P(e_n)$ is the error probability in the nth OFDM sub-channel. Since the complex transmitted symbols take any value belonging to a QPSK signal constellation with equal probability then the error probability in each OFDM sub-channel can be evaluated as follows

$$P(e_n)=\frac{1}{4}\sum_{m=1}^{4}P\left(e_n \middle| S_{k,n}=Ae^{j(2m-1)\pi/4}\right) \tag{4.53}$$

Finally, the conditional error probabilities on the right hand side of (4.53) are given by

$$P\left(e_n \middle| S_{k,n}=Ae^{j(2m-1)\pi/4}\right)=P\left(R_{k,n}^{m}\notin \text{Region m}\right) \tag{4.54}$$

where $R_{k,n}^{m}$ denotes the complex received symbol in time slot k and sub-channel n conditioned on $S_{k,n}=Ae^{j(2m-1)\pi/4}$ and the Region m denotes the region in the complex plane for which the symbol $Ae^{j(2m-1)\pi/4}$ is assumed to have been transmitted. The QPSK decision regions are shown in Figure 4.5. Note that these are the optimum regions that minimise the error probability for QPSK modulation in AWGN alone when the probability of transmitting any of the QPSK symbols is the same [42].

To calculate the probabilities on the right hand side of (4.54) we repeat the steps of the previous section, i.e., we first integrate (4.48) over the appropriate QPSK decision regions to obtain

$$P\left(R_{k,n}^{m} \notin \text{Region m} \middle| S_{k,n}^{''m}\right) =$$
$$= \frac{1}{2}\operatorname{erfc}\left(\cos\left(\frac{(2m-1)\pi}{4}\right)\frac{\operatorname{Re}\left\{S_{k,n}^{'m}\right\}+\operatorname{Re}\left\{S_{k,n}^{''m}\right\}}{\sqrt{\left|H_{k,n}\right|^2 N_0}}\right)+\frac{1}{2}\operatorname{erfc}\left(\sin\left(\frac{(2m-1)\pi}{4}\right)\frac{\operatorname{Im}\left\{S_{k,n}^{'m}\right\}+\operatorname{Im}\left\{S_{k,n}^{''m}\right\}}{\sqrt{\left|H_{k,n}\right|^2 N_0}}\right)$$
$$-\frac{1}{2}\operatorname{erfc}\left(\cos\left(\frac{(2m-1)\pi}{4}\right)\frac{\operatorname{Re}\left\{S_{k,n}^{'m}\right\}+\operatorname{Re}\left\{S_{k,n}^{''m}\right\}}{\sqrt{\left|H_{k,n}\right|^2 N_0}}\right)\cdot\frac{1}{2}\operatorname{erfc}\left(\sin\left(\frac{(2m-1)\pi}{4}\right)\frac{\operatorname{Im}\left\{S_{k,n}^{'m}\right\}+\operatorname{Im}\left\{S_{k,n}^{''m}\right\}}{\sqrt{\left|H_{k,n}\right|^2 N_0}}\right) \tag{4.55}$$

and we then take the expectation of (4.55) with respect to the IMD RV to obtain

$$P\left(R_{k,n}^{m} \notin \text{Region m}\right) =$$
$$= E\left[\frac{1}{2}\operatorname{erfc}\left(\cos\left(\frac{(2m-1)\pi}{4}\right)\frac{\operatorname{Re}\left\{S_{k,n}^{'m}\right\}+\operatorname{Re}\left\{S_{k,n}^{''m}\right\}}{\sqrt{\left|H_{k,n}\right|^2 N_0}}\right)+\frac{1}{2}\operatorname{erfc}\left(\sin\left(\frac{(2m-1)\pi}{4}\right)\frac{\operatorname{Im}\left\{S_{k,n}^{'m}\right\}+\operatorname{Im}\left\{S_{k,n}^{''m}\right\}}{\sqrt{\left|H_{k,n}\right|^2 N_0}}\right)\right.$$
$$\left.-\frac{1}{2}\operatorname{erfc}\left(\cos\left(\frac{(2m-1)\pi}{4}\right)\frac{\operatorname{Re}\left\{S_{k,n}^{'m}\right\}+\operatorname{Re}\left\{S_{k,n}^{''m}\right\}}{\sqrt{\left|H_{k,n}\right|^2 N_0}}\right)\cdot\frac{1}{2}\operatorname{erfc}\left(\sin\left(\frac{(2m-1)\pi}{4}\right)\frac{\operatorname{Im}\left\{S_{k,n}^{'m}\right\}+\operatorname{Im}\left\{S_{k,n}^{''m}\right\}}{\sqrt{\left|H_{k,n}\right|^2 N_0}}\right)\right] \tag{4.56}$$

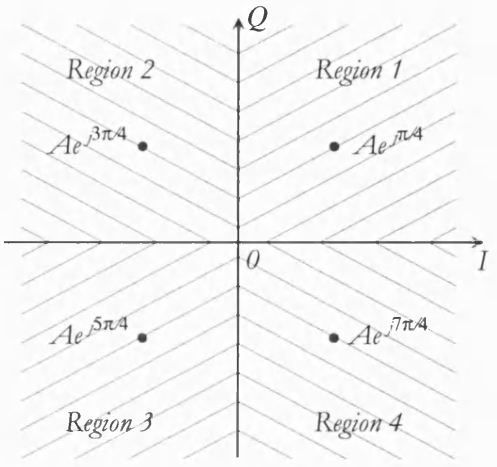

Figure 4.5: Optimum QPSK decision regions in AWGN.

Expression (4.56) can be simplified by noting that since the value of the complementary error functions is generally much less than one then the sum of the two complementary error functions is much larger than the product of the same two complementary error functions. Hence, neglecting the product term and writing the expectation of the sum of the remaining two terms as the sum of the expectations of each individual term we obtain

$$P\left(R_{k,n}^{m} \notin \text{Region m}\right) \approx$$
$$\approx E\left[\frac{1}{2}\operatorname{erfc}\left(\cos\left(\frac{(2m-1)\pi}{4}\right)\frac{\operatorname{Re}\left\{S_{k,n}^{\prime m}\right\}+\operatorname{Re}\left\{S_{k,n}^{\prime\prime m}\right\}}{\sqrt{\left|H_{k,n}\right|^{2}N_{0}}}\right)\right]+E\left[\frac{1}{2}\operatorname{erfc}\left(\sin\left(\frac{(2m-1)\pi}{4}\right)\frac{\operatorname{Im}\left\{S_{k,n}^{\prime m}\right\}+\operatorname{Im}\left\{S_{k,n}^{\prime\prime m}\right\}}{\sqrt{\left|H_{k,n}\right|^{2}N_{0}}}\right)\right] \tag{4.57}$$

This simplification implies that it suffices to carry out the first expectation only with respect to the real part of the IMD RV and the second expectation only with respect to the imaginary part of the IMD RV. Consequently, we do need not to consider complex valued RVs but real valued RVs and hence the discussion concerning the computation of the expectations in the OFDM/BPSK case directly applies to the computation of the expectations in the OFDM/QPSK case. A method to determine the moments of the RVs needed to compute the error probability expectations in (4.57) is therefore developed in the next section.

Finally, it is important to note that the derivations in the previous section and in this section only considered the determination of the symbol error probability of OFDM/BPSK and OFDM/QPSK signals, respectively, not mentioning the bit error probability of the same signals. In the OFDM/BPSK case, since each BPSK symbol conveys exactly one bit then the bit error probability is equal to the symbol error probability. In the OFDM/QPSK case, since each QPSK symbol conveys two bits then the bit error probability is not equal to the symbol error probability and the relation between these two performance metrics depends on the exact assignment of the two bits to the four possible QPSK symbols. If the two bits are assigned to the four possible QPSK symbols using Gray coding (see chapter 2), whereby binary digit words assigned to adjacent symbol states differ by one binary digit only, then the bit error probability is approximately equal to one half the symbol error probability because the most probable errors result in the selection of an adjacent phase to the true phase and hence a single bit error in the two binary digit word.

4.3.3 Moments of the IMD RV

In this section, we describe a method to determine the moments of the RVs needed for error probability evaluation, i.e., the real part of the IMD RV in the OFDM/BPSK case and both the real part and the imaginary part of the IMD RV in the OFDM/QPSK case. This method, applicable to non-linearly distorted OFDM signals, is an adaptation of the method proposed by Benedetto et al. [125,126], applicable to non-linearly distorted M-PSK signals. To determine the moments of these RVs we write for simplicity of notation the IMD RV and its complex conjugate as follows

$$S_{k,n}^{m} = \sum_{i=0}^{\infty} \sum_{n_1=0}^{N-1} \cdots \sum_{n_{1+2i}=0}^{N-1} S_{k,n_1} \cdots S_{k,n_{1+i}} S_{k,n_{2+i}}^{*} \cdots S_{k,n_{1+2i}}^{*} P_{1+2i}(n_1,\ldots,n_{1+2i}) \tag{4.58}$$

$$\left(S_{k,n}^{m}\right)^{*} = \sum_{i=0}^{\infty} \sum_{n_1=0}^{N-1} \cdots \sum_{n_{1+2i}=0}^{N-1} S_{k,n_1} \cdots S_{k,n_i} S_{k,n_{1+i}}^{*} \cdots S_{k,n_{1+2i}}^{*} Q_{1+2i}(n_1,\ldots,n_{1+2i}) \tag{4.59}$$

where $P_{1+2i}(n_1,\ldots,n_{1+2i})$ is given by

$$P_{1+2i}(n_1,\ldots,n_{1+2i}) = H_{k,n} \frac{1}{(T-T_{CP})^{i}} \tilde{H}_{1+2i}\left(\frac{n_1}{T-T_{CP}},\ldots,\frac{n_{1+i}}{T-T_{CP}},-\frac{n_{2+i}}{T-T_{CP}},\ldots,-\frac{n_{1+2i}}{T-T_{CP}}\right) \delta(n_1+\cdots+n_{1+i}-n_{2+i}-\cdots-n_{1+2i}-n) \tag{4.60}$$

when $n_1,\ldots,n_{1+2i} \neq n,\ldots,n$ and is zero otherwise, and $Q_{1+2i}(n_1,\ldots,n_{1+2i})$ is given by

$$Q_{1+2i}(n_1,\ldots,n_{1+2i}) = H_{k,n}^{*} \frac{1}{(T-T_{CP})^{i}} \tilde{H}_{1+2i}^{*}\left(\frac{n_{1+i}}{T-T_{CP}},\ldots,\frac{n_{1+2i}}{T-T_{CP}},-\frac{n_1}{T-T_{CP}},\ldots,-\frac{n_i}{T-T_{CP}}\right) \delta(n_{1+i}+\cdots+n_{1+2i}-n_1-\cdots-n_i-n) \tag{4.61}$$

when $n_1,\ldots,n_{1+2i} \neq n,\ldots,n$ and is zero otherwise.

The qth moment of the real part and the imaginary part of the IMD RV are given by

$$E\left[\mathrm{Re}\left\{S_{k,n}^{m}\right\}^{q}\right] = E\left[\left(\frac{S_{k,n}^{m}+\left(S_{k,n}^{m}\right)^{*}}{2}\right)^{q}\right] = \frac{1}{2^{q}}\sum_{p=0}^{q}\binom{q}{p} E\left[\left(S_{k,n}^{m}\right)^{q-p}\left(S_{k,n}^{m}\right)^{*p}\right] \tag{4.62}$$

$$E\left[\mathrm{Im}\left\{S_{k,n}^{m}\right\}^{q}\right] = E\left[\left(\frac{S_{k,n}^{m}-\left(S_{k,n}^{m}\right)^{*}}{2j}\right)^{q}\right] = \frac{1}{(2j)^{q}}\sum_{p=0}^{q}\binom{q}{p} E\left[\left(S_{k,n}^{m}\right)^{q-p}\left(S_{k,n}^{m}\right)^{*p}\right](-1)^{p} \tag{4.63}$$

where

$$\binom{q}{p} = \frac{q!}{p!(q-p)!} \tag{4.64}$$

The computation of these moments therefore reduces to the calculation of expectations of the form

$$E\left[\left(S_{k,n}^{\#m}\right)^{l_1}\left(S_{k,n}^{\#m}\right)^{*l_2}\right] \tag{4.65}$$

where l_1 and l_2 are appropriate integers. To calculate these expectations we note that just as the IMD RV and its complex conjugate have the form of a discrete Volterra series so do their powers [125,126]. The lth power of $S_{k,n}^{\#m}$ and $\left(S_{k,n}^{\#m}\right)^*$, i.e., $\left(S_{k,n}^{\#m}\right)^l$ and $\left(S_{k,n}^{\#m}\right)^{*l}$, are given by

$$\left(S_{k,n}^{\#m}\right)^l = \sum_{i=0}^{\infty}\sum_{n_1=0}^{N-1}\cdots\sum_{n_{l+2i}=0}^{N-1} S_{k,n_1}\cdots S_{k,n_{l+i}} S_{k,n_{l+i+1}}^*\cdots S_{k,n_{l+2i}}^* P_{l+2i}^{(l)}\left(n_1,\ldots,n_{l+2i}\right) \tag{4.66}$$

$$\left(S_{k,n}^{\#m}\right)^{*l} = \sum_{i=0}^{\infty}\sum_{n_1=0}^{N-1}\cdots\sum_{n_{l+2i}=0}^{N-1} S_{k,n_1}\cdots S_{k,n_i} S_{k,n_{i+1}}^*\cdots S_{k,n_{l+2i}}^* Q_{l+2i}^{(l)}\left(n_1,\ldots,n_{l+2i}\right) \tag{4.67}$$

where

$$P_{l+2i}^{(l)}\left(n_1,\ldots,n_{l+2i}\right) = \sum_{i'=0}^{i} P_{2i'+1}\left(n_1,\ldots,n_{i'+1},n_{l+i+1},\ldots,n_{l+i+i'}\right) P_{l-1+2(i-i')}^{(l-1)}\left(n_{i'+2},\ldots,n_{l+i},n_{l+i+i'+1},\ldots,n_{l+2i}\right) \tag{4.68}$$

$$Q_{l+2i}^{(l)}\left(n_1,\ldots,n_{l+2i}\right) = \sum_{i'=0}^{i} Q_{2i'+1}\left(n_1,\ldots,n_{i'},n_{i+1},\ldots,n_{i+i'+1}\right) Q_{l-1+2(i-i')}^{(l-1)}\left(n_{i'+1},\ldots,n_i,n_{i+i'+2},\ldots,n_{l+2i}\right) \tag{4.69}$$

and $P_i^{(1)}(\cdot) = P_i(\cdot)$ and $Q_i^{(1)}(\cdot) = Q_i(\cdot)$. Thus, substituting the appropriate powers of the IMD RV and its complex conjugate in (4.65) then

$$E\left[\left(S_{k,n}^{\#m}\right)^{l_1}\left(S_{k,n}^{\#m}\right)^{*l_2}\right] = \sum_{i_1=0}^{\infty}\sum_{i_2=0}^{\infty}\sum_{n_1=0}^{N-1}\cdots\sum_{n_{l_1/2+2i_1+2i_2}=0}^{N-1} E\left[S_{k,n_1}\cdots S_{k,n_{l_1+i_1+i_2}} S_{k,n_{l_1+i_1+i_2+1}}^*\cdots S_{k,n_{l_1/2+2i_1+2i_2}}^* \,\middle|\, S_{k,n}^{m}\right]$$
$$P_{l_1+2i_1}^{(l_1)}\left(n_1,\ldots,n_{l_1+i_1},n_{l_1+i_1+i_2+1},\ldots,n_{l_1+2i_1+i_2}\right) Q_{l_2+2i_2}^{(l_2)}\left(n_{l_1+i_1+1},\ldots,n_{l_1+i_1+i_2},n_{l_1+2i_1+i_2+1},\ldots,n_{l_1+l_2+2i_1+2i_2}\right) \tag{4.70}$$

where $S_{k,n}^{m}$ denotes the complex transmitted symbol in time slot k and sub-channel n conditioned on either the mth BPSK symbol or the mth QPSK symbol.

The final step towards knowledge of the moments of the real part and the imaginary part of the IMD RV therefore involves computation of conditional expectations of the form

$$E\left[S_{k,n_1}\cdots S_{k,n_{l_1+i_1+i_2}} S^{*}_{k,n_{l_1+i_1+i_2+1}}\cdots S^{*}_{k,n_{l_1+l_2+2i_1+2i_2}} \,\middle|\, S^{m}_{k,n}\right] \tag{4.71}$$

To calculate these conditional expectations we denote by $r_{n'}$ and $s_{n'}$ the number of elements of the form $S_{k,n'}$ and $S^{*}_{k,n'}$ respectively in (4.71). Thus, assuming that the complex transmitted symbols in different sub-channels are independent[15] and noting that n' runs from 0 to $N-1$ then

$$E\left[S_{k,n_1}\cdots S_{k,n_{l_1+i_1+i_2}} S^{*}_{k,n_{l_1+i_1+i_2+1}}\cdots S^{*}_{k,n_{l_1+l_2+2i_1+2i_2}} \,\middle|\, S^{m}_{k,n}\right] = \left(S^{m}_{k,n}\right)^{r_n}\left(S^{m*}_{k,n}\right)^{s_n}\prod_{\substack{n'=0\\ n'\neq n}}^{N-1} E\left[\left(S_{k,n'}\right)^{r_{n'}}\left(S^{*}_{k,n'}\right)^{s_{n'}}\right] \tag{4.72}$$

In the BPSK case, where the complex transmitted symbols take any value belonging to a BPSK signal constellation $\left\{Ae^{j2\pi(m-1)/2};\, m=1,2\right\}$ with equal probability, the expectations on the right hand side of (4.72) are given by

$$E\left[\left(S_{k,n'}\right)^{r_{n'}}\left(S^{*}_{k,n'}\right)^{s_{n'}}\right] = \begin{cases} A^{r_{n'}+s_{n'}}, & r_{n'}-s_{n'}=\ldots,-4,-2,0,2,4,\ldots \\ 0, & \text{otherwise} \end{cases} \tag{4.73}$$

In the QPSK case, where the complex transmitted symbols take any value belonging to a QPSK signal constellation $\left\{Ae^{j(2m-1)\pi/4};\, m=1,2,3,4\right\}$ with equal probability, the expectations on the right hand side of (4.72) are given by

$$E\left[\left(S_{k,n'}\right)^{r_{n'}}\left(S^{*}_{k,n'}\right)^{s_{n'}}\right] = \begin{cases} A^{r_{n'}+s_{n'}}, & r_{n'}-s_{n'}=\ldots,-16,-8,0,8,16,\ldots \\ -A^{r_{n'}+s_{n'}}, & r_{n'}-s_{n'}=\ldots,-12,-4,4,12,\ldots \\ 0, & \text{otherwise} \end{cases} \tag{4.74}$$

[15] Again, independence is satisfied in a variety of situations including COFDM systems provided that an interleaver is employed. Independence would not be satisfied in situations where PAPR reduction codes are employed.

To summarise, the error probability evaluation of non-linearly distorted OFDM/BPSK and OFDM/QSPK signals involves the following steps:

1. Determination of a number of moments of the real part and the imaginary part of the IMD RV in each OFDM sub-channel conditioned on each transmitted symbol according to the procedure described in this section.

2. Evaluation of the error probability in each OFDM sub-channel conditioned on each transmitted symbol according to (4.50) (BPSK case) or (4.57) (QPSK case) by using the moments of the appropriate RVs in conjunction with some moment based technique.

3. Evaluation of the error probability in each OFDM sub-channel according to (4.43) (in the BPSK case) or (4.53) (in the QPSK case).

4. Evaluation of the overall error probability of the OFDM signal according to (4.42) (in the BPSK case) or (4.52) (in the QPSK case).

4.4 Discussion

An examination of the moment computation procedure reveals that this is extremely time consuming. For example, calculation of the qth moment of either the real part or the imaginary part of the IMD RV requires $q+1$ expectations of the form (4.65) to be computed and calculation of each of these expectations for a non-linearity of order n and for an OFDM signal with N sub-channels requires $N^q\left[\left(N^{n+1}-1\right)/\left(N^2-1\right)\right]^2$ expectations of the form (4.71) to be computed. Overall, we need to calculate approximately $(q+1)N^qN^{2(n-1)}$ expectations of the form (4.71) which implies that the computation time grows exponentially with the order q of the moment and the order n of the non-linearity and it grows polynomially with the number N of OFDM sub-channels. We have verified that such a computation is not feasible for $q>2$, $n>3$ and $N>128$.

The inefficiency of the moment computation procedure suggests that, to evaluate the expectations that will ultimately yield the error probability of non-linearly distorted OFDM signals in AWGN, we cannot rely on series expansion methods [140,141] or Gauss quadrature rules [142] because these moment based methods typically require a large

number of moments, but rather on alternative approximations/estimations for the IMD distribution which require a limited number of moments.

To understand the origins of the inefficiency of this moment computation procedure let us concentrate on the expression that defines the IMD RV (see (4.58)). Clearly, this RV cannot be written as the sum of a number of statistically independent components and consequently a fast recursive method to compute its moments cannot be devised [126]. In contrast, a fast recursive method to compute the moments of an ISI RV can be devised because this RV can be written as the sum of a number of statistically independent components [126]. Incidentally, the fact that the IMD RV cannot be written as a sum of independent contributions also prevents us from determining its moment generating function, which is required to use other methods that approximate or bound the value of the expectation of a function of a RV such as Chernoff bounds [143,144], modified Chernoff bounds [145-147] and saddle-point approximations [148].

4.5 Summary

In this chapter, we have developed an analytic technique to assess the impact of non-linearities on the error probability of OFDM signals. Since we have modelled the non-linearities in the OFDM system by a Volterra series then this technique accounts for both frequency independent and frequency dependent non-linear behaviour. Accordingly, this technique can be used to provide a first-order approximation to the error probability degradation induced by fibre-radio system non-linearities on an OFDM signal without the need for time consuming simulations or costly experimentation. Moreover, this technique also provides insight into the different mechanisms responsible for the error probability degradation.

Initially, we have determined the relation between transmitted and received symbols in an OFDM communication system in the presence of non-linearities and AWGN. Subsequently, we have derived expressions to evaluate the error probability of non-linearly distorted OFDM/BPSK and OFDM/QPSK signals in AWGN. The overall error probability of an OFDM signal was given as the average of the error probability in all OFDM sub-channels. In turn, the error probability in each OFDM sub-channel was given as the statistical expectation with respect to the IMD RV of the error probability in AWGN conditioned by a given value of the IMD RV. We have also derived expressions to

evaluate the moments of the IMD RV in each OFDM sub-channel. Finally, we have confirmed that the moment computation procedure was extremely time consuming (moment computation is limited to the first and the second moments, non-linearities exhibiting up to third-order non-linear behaviour and OFDM signals with up to 128 sub-channels). Hence, to compute the error probability expectations, one could not rely on series expansion methods or Gauss quadrature rules, which require a large number of moments, but on alternative approximations/estimation methods for the IMD distribution requiring only a limited number of moments.

In the next chapter, we investigate specific approximation/estimation techniques for the IMD distribution and the error probability of non-linearly distorted OFDM signals.

Chapter 5

The distribution of the IMD and the error probability of non-linearly distorted OFDM signals

5.1 Introduction

In the previous chapter, we have developed expressions to determine the error probability of non-linearly distorted OFDM/BPSK and OFDM/QPSK signals in AWGN. Such expressions relate the error probability of the OFDM signal to the error probabilities of the OFDM sub-channels, each of which is given as the expectation with respect to the IMD RV of the error probability in AWGN conditioned by a given value of the IMD RV. We have also developed expressions to determine the moments of the IMD RV. However, we have argued that since the moment computation procedure was extremely time consuming then to compute the error probability expectations we could not rely on series expansion methods or Gauss quadrature rules because these moment based methods typically require a large number of moments, but rather on alternative approximations/estimations for the IMD distribution which require a limited number of moments.

Accordingly, an investigation of specific approximation/estimation techniques for the IMD distribution and the error probability of non-linearly distorted OFDM signals is the subject of this chapter. In section 5.2 and in section 5.3, we analyse the different

approximation/estimation techniques for the IMD distribution and the error probability of non-linearly distorted OFDM signals, respectively. In section 5.4, we present new results related to the behaviour of non-linearly distorted OFDM signals. Finally, section 5.5 summarises the main contributions of this chapter. Four papers have resulted from the research work presented in this chapter [150-153].

5.2 Distribution of the IMD

In this section, we assess different approximations/estimations for the IMD distribution as a means to compute the error probability expectations. To identify appropriate approximation/estimation techniques the properties of the IMD RV are examined in section 5.2.1 while in sections 5.2.2 and 5.2.3 specific approximation/estimation techniques for the IMD distribution are examined.

5.2.1 Properties of the IMD RV

In this section, we examine the properties of the IMD RV for non-linearly distorted OFDM/BPSK and OFDM/QPSK signals with 16 to 256 sub-channels. Particularly, we consider the IMD RV in the sub-channel on the edge of the band, where the number of IMPs is lowest, and the IMD RV in the sub-channel in the centre of the band, where the number of IMPs is highest, because these represent the two extreme cases thereby providing sufficient insight into how to define appropriate approximations/estimations for the IMD distribution.

The complex modulation symbol conveyed in sub-channel n, where n corresponds to the sub-channel being examined, is set to A in the OFDM/BPSK case and to $Ae^{j\pi/4}$ in the OFDM/QPSK case, and the complex modulation symbols conveyed in the remaining sub-channels are assumed to be independent and to take any value belonging to the BPSK or the QPSK signal constellation with equal probability. Note that symmetry considerations suggest that a different symbol conditioning does not affect the basic properties of the IMD RV. Note also that although the IMD RV is a complex valued quantity, for error probability evaluation purposes it suffices to consider only the real part of this RV in the OFDM/BPSK case and both the real part and the imaginary part of this RV in the OFDM/QPSK case (see chapter 4). Thus, we do not examine the properties of the IMD RV per se but of its real part in the OFDM/BPSK case; since symmetry

considerations suggest that the properties of the real part and the imaginary part of the IMD RV are identical in the OFDM/QPSK case then here too we only examine the real part of the IMD RV. Hereafter, when we refer to the IMD in the OFDM/BPSK case we mean its real part conditioned on A and when we refer to the IMD in the OFDM/QPSK case we mean its real part conditioned on $Ae^{j\pi/4}$.

We have examined the properties of the IMD RVs for OFDM signals distorted both by a simple frequency independent and a simple frequency dependent non-linearity, which exhibit up to third-order non-linear behaviour. Higher-order non-linear behaviour is not considered because up to third-order non-linear behaviour often serves as a good approximation to a broad range of non-linearities encountered in practice and the moments of the RVs needed for error probability evaluation for non-linearities of order greater than three cannot be obtained. The frequency independent non-linearity is modelled as in Figure 4.1 where the characteristic of the memoryless device $f(\cdot)$ is given by

$$f(z) = c_1 z + c_2 z^2 + c_3 z^3 \tag{5.1}$$

with $c_1 = 1$, $c_2 = 0$ and $c_3 = -0.25$[16]. The equivalent baseband transfer functions for this non-linearity can be obtained from (4.24) by noting that $c_1 = 1$, $c_3 = -0.25$ and $c_{2n-1} = 0$ for $n > 2$.

The frequency dependent non-linearity is modelled as in Figure 4.2 where the characteristic of the memoryless device $f(\cdot)$ is also given by

$$f(z) = c_1 z + c_2 z^2 + c_3 z^3 \tag{5.2}$$

with $c_1 = 1$, $c_2 = 0$ and $c_3 = -0.25$, and $H'(f)$ and $H''(f)$ are frequency responses of two bandpass first-order Butterworth filters

$$H'(f) = H''(f) = \frac{1}{1 + j\frac{f_0}{B}\left(\frac{f}{f_0} - \frac{f_0}{f}\right)} \tag{5.3}$$

[16] Again, although a ratio $c_1/c_3 = -4$ is typical for non-linear elements encountered in communication systems (e.g. HPAs) [135], the analysis presented hereafter is independent of the actual value of the ratio.

where f_0 is the centre frequency and B is the 3 dB bandwidth of the bandpass filters. The centre frequency and the 3 dB bandwidth of the bandpass filters were set to be equal to the centre frequency and the 3 dB bandwidth of the OFDM signals, respectively. The equivalent baseband transfer functions for this non-linearity can be obtained from (4.27) by noting that $c_1 = 1$, $c_3 = -0.25$ and $c_{2n-1} = 0$ for $n > 2$, and $H'(f)$ and $H''(f)$ are given in (5.3).

To study the properties of the IMD RV we have examined its cumulants, $k_n, n = 1,2,\ldots$, which are defined by the identity in t [154]

$$e^{k_1 t + \frac{k_2 t^2}{2!} + \cdots + \frac{k_n t^n}{n!} + \cdots} = 1 + \mu_1' t + \frac{\mu_2' t^2}{2!} + \cdots + \frac{\mu_n' t^n}{n!} + \cdots \tag{5.4}$$

where $\mu_n', n = 1,2,\ldots$, are the moments of the RV[17]. The cumulants were estimated in MATLAB as follows: A large number of samples was generated of the IMD RV under consideration in accordance to (4.58), $X_1, X_2, \ldots, X_N$. Estimates $\hat{\mu}_n', n = 1,2,\ldots$, of the moments $\mu_n', n = 1,2,\ldots$, were then obtained through [136]

$$\hat{\mu}_n' = \frac{1}{N}\sum_{k=1}^{N} X_k^n, \quad n = 1,2,\ldots \tag{5.5}$$

Estimates $\hat{k}_n, n = 1,2,\ldots$, of the cumulants $k_n, n = 1,2,\ldots$, were finally obtained from the relation between cumulants and moments [154]

$$k_1 = \mu_1' \tag{5.6}$$

$$k_2 = \mu_2' - \mu_1'^2 \tag{5.7}$$

$$k_3 = \mu_3' - 3\mu_2'\mu_1' + 2\mu_1'^3 \tag{5.8}$$

$$k_4 = \mu_4' - 4\mu_3'\mu_1' - 3\mu_2'^2 + 12\mu_2'\mu_1'^2 - 6\mu_1'^4 \tag{5.9}$$

[17] The nth moment of a RV X is given by $\mu_n' = E[X^n]$.

$$k_5 = \mu_5' - 5\mu_4'\mu_1' - 10\mu_3'\mu_2' + 20\mu_3'\mu_1'^2 + 30\mu_2'^2\mu_1' - 60\mu_2'\mu_1'^3 + 24\mu_1'^5 \tag{5.10}$$

$$\begin{aligned} k_6 = {} & \mu_6' - 6\mu_5'\mu_1' - 15\mu_4'\mu_2' + 30\mu_4'\mu_1'^2 - 10\mu_3'^2 + 120\mu_3'\mu_2'\mu_1' - 120\mu_3'\mu_1'^3 \\ & + 30\mu_2'^3 - 270\mu_2'^2\mu_1'^2 + 360\mu_2'\mu_1'^4 - 120\mu_1'^6 \end{aligned} \tag{5.11}$$

The variance of the IMD RV was set to one in each case under consideration for comparison purposes.

Note that the cumulants are a useful set of descriptive constants of a RV because they enable us to identify the distribution of the RV straightforwardly. For example, for a Gaussian distribution the first cumulant corresponds to its mean, the second cumulant corresponds to its variance and all the other higher-order cumulants are zero; for a Poisson distribution the cumulants are all equal; and for other distributions interesting relations also exist [154].

To study the properties of the IMD RV we have also examined its CDF, $F(x)$, which is defined by [154]

$$F(x) = \int_{-\infty}^{x} f(t)dt \tag{5.12}$$

where $f(x)$ is the PDF of the RV. The CDF was estimated in MATLAB as follows: A large number of samples was generated of the IMD RV under consideration in accordance to (4.58), $X_1, X_2, \ldots, X_N$. An estimate $\hat{F}(x)$ of the CDF $F(x)$ was then obtained through [136]

$$\hat{F}(x) = \begin{cases} 0, & x < X_1 \\ \dfrac{k}{N}, & X_k \le x < X_{k+1}, k = 1,2,\ldots,N-1 \\ 1, & x \ge X_N \end{cases} \tag{5.13}$$

Note that it is implicitly assumed that the samples $X_1, X_2, \ldots, X_N$ are written in increasing order, i.e., $X_1 < X_2 < \cdots < X_N$.

A number of properties of the IMD RV can be inferred from Figure 5.1 and Figure 5.2. Figure 5.1 shows the cumulants of the IMD RV in the sub-channel on the edge of the band and in the sub-channel in the centre of the band against the number of OFDM sub-channels for OFDM/BPSK signals distorted by the frequency independent non-linearity. Figure 5.2 shows corresponding results for OFDM/QPSK signals distorted by the same frequency independent non-linearity. Observation of the figures reveals that the higher-order cumulants of the IMD approach zero as the number of OFDM sub-channels is increased. Since for a Gaussian distribution the first cumulant corresponds to its mean, the second cumulant corresponds to its variance and all the other higher-order cumulants are zero then we conclude that the IMD distribution approaches a Gaussian distribution as the number of OFDM sub-channels is increased. This is not a surprising result because by increasing the number of OFDM sub-channels then the number of terms or IMPs that contribute to the IMD RV also increases and hence Gaussian convergence in line with the CLT is to be expected. It is appropriate to note that we do not refer to a strong form of the CLT, where independence among the terms is required, but a weaker form of the same theorem, where some degree of correlation among the terms is allowed [155]. Observation of the figures also reveals that the IMD distribution in an OFDM sub-channel on the edge of the band converges faster to a Gaussian distribution rather than the IMD distribution in an OFDM sub-channel in the centre of the band. This is a counter intuitive result because the number of IMPs that fall in the sub-channel on the edge of the band is lower than the number of IMPs that fall in the sub-channel in the centre of the band. This result suggests that significant correlation exists among the various IMPs that fall in a particular OFDM sub-channel. Finally, it is interesting to note that more rapid Gaussian convergence is observed for BPSK modulation than for QPSK modulation.

Similar trends are also observed in the frequency dependent non-linearity case, as shown in Figure 5.3 and Figure 5.4. Again, the first figure shows the cumulants of the IMD RV in the sub-channel on the edge of the band and in the sub-channel in the centre of the band against the number of OFDM sub-channels for non-linearly distorted OFDM/BPSK signals and the second figure shows corresponding results for non-linearly distorted OFDM/QPSK signals.

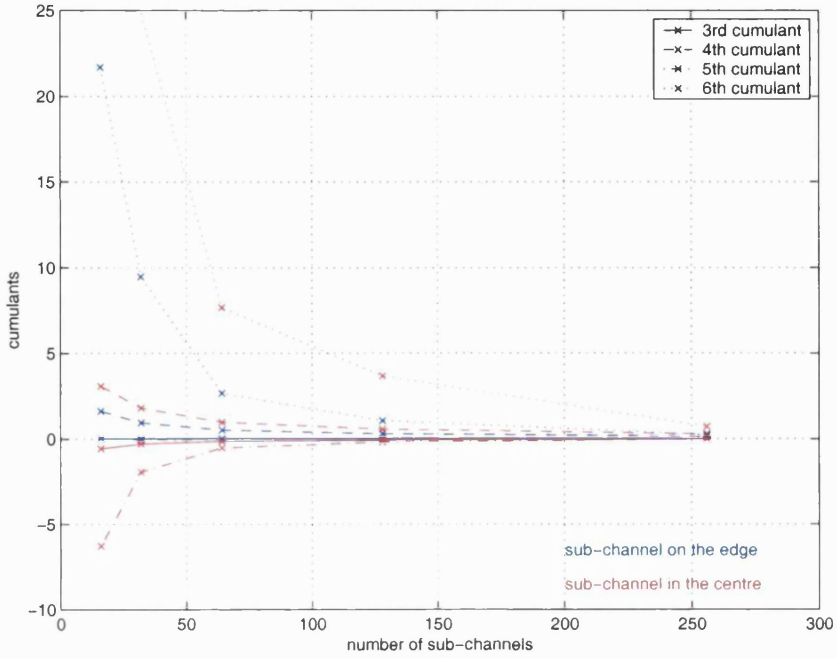

Figure 5.1: Cumulants of the IMD in the sub-channel on the edge of the band and in the sub-channel in the centre of the band vs. number of OFDM sub-channels for OFDM/BPSK signals distorted by the frequency independent non-linearity.

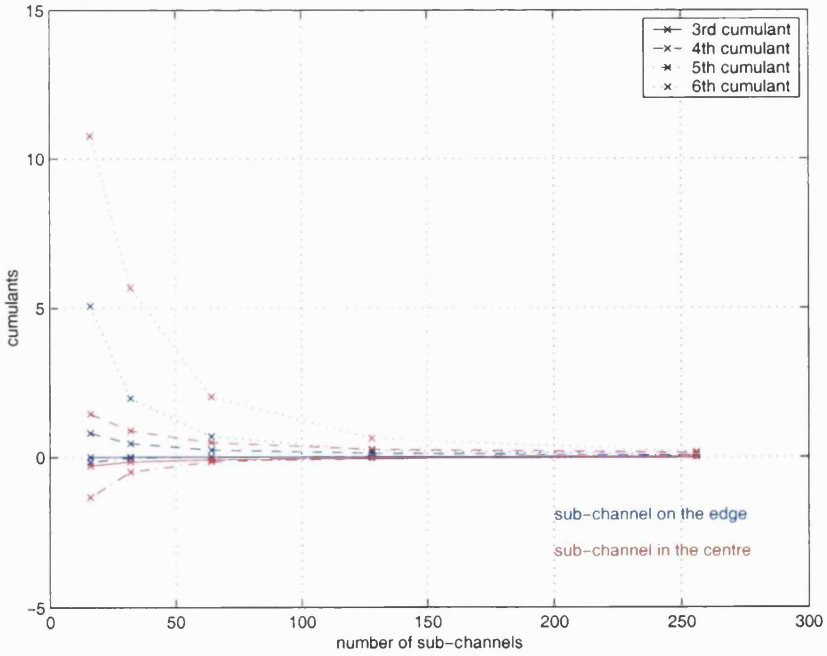

Figure 5.2: Cumulants of the IMD in the sub-channel on the edge of the band and in the sub-channel in the centre of the band vs. number of OFDM sub-channels for OFDM/QPSK signals distorted by the frequency independent non-linearity.

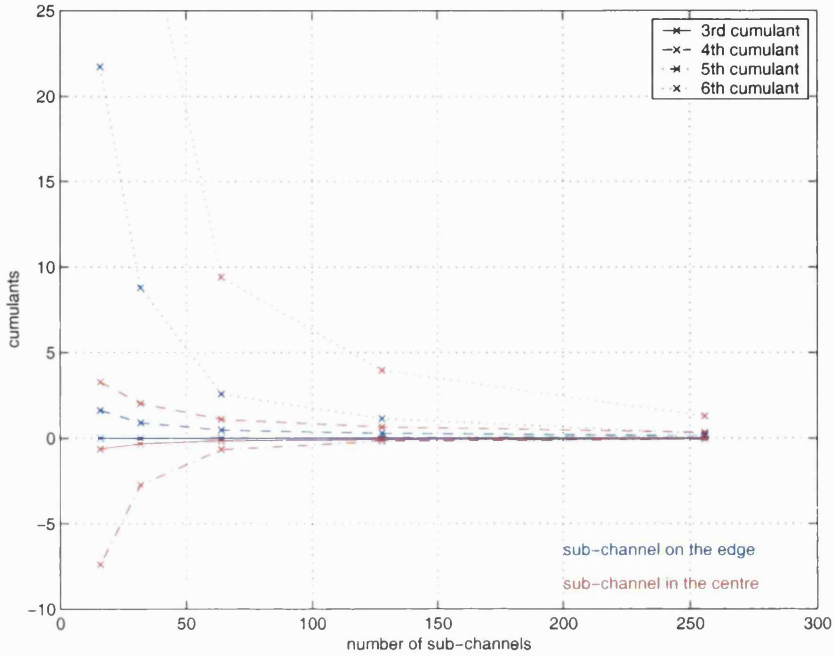

Figure 5.3: Cumulants of the IMD in the sub-channel on the edge of the band and in the sub-channel in the centre of the band vs. number of OFDM sub-channels for OFDM/BPSK signals distorted by the frequency dependent non-linearity.

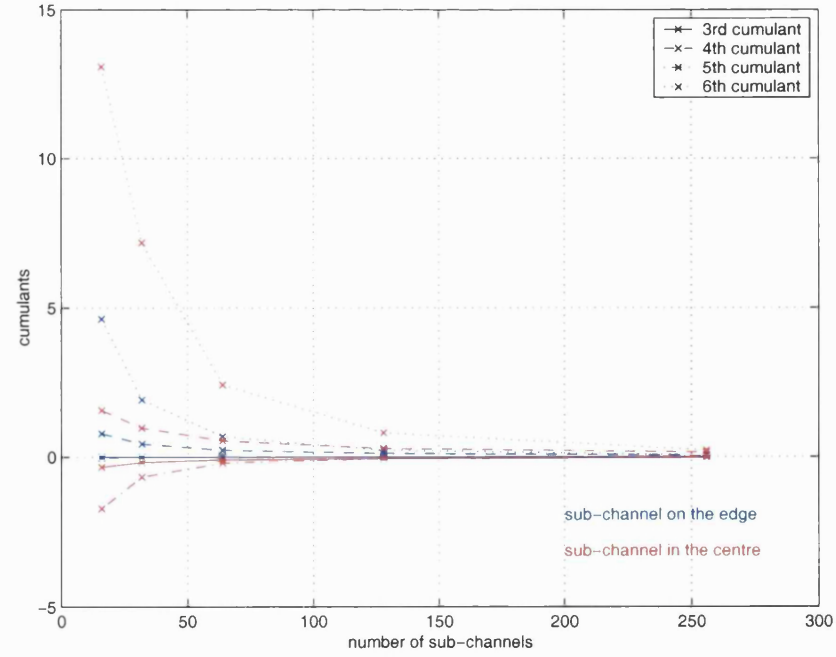

Figure 5.4: Cumulants of the IMD in the sub-channel on the edge of the band and in the sub-channel in the centre of the band vs. number of OFDM sub-channels for OFDM/QPSK signals distorted by the frequency dependent non-linearity.

Further properties of the IMD RV can be inferred from Figure 5.5 through Figure 5.8. These figures show the CDF of the IMD RV for the different situations under consideration. Note that the x-axis is normalised to the mean μ and the standard deviation σ of the distributions in these figures. We can infer from these figures that the distribution of the IMD does indeed approach a Gaussian distribution as the number of OFDM sub-channels is increased and that the speed of convergence depends on both the location of the OFDM sub-channel (edge or centre) and the type of modulation (BPSK or QPSK). We can also infer from these figures that the distribution of the IMD is characterised by different rates of tail decay. Distributions with heavier tails correspond to a lower number of OFDM sub-channels, the sub-channel in the centre of the band and BPSK modulation. Conversely, distributions with lighter tails correspond to a higher number of OFDM sub-channels, the sub-channel on the edge of the band and QPSK modulation. These trends hold both in the frequency independent non-linearity case and in the frequency dependent non-linearity case.

Finally, it is interesting to note that the speed of convergence of the IMD distribution to a Gaussian distribution is rather slow. For example, for a 64 sub-channel non-linearly distorted OFDM signal the IMD RV in any sub-channel consists of hundreds of IMPs and yet, contrary to what might expected, its distribution does not match the Gaussian distribution over the range shown in each figure. Again, this result suggests that significant correlation exists among the various IMPs that fall in a particular OFDM sub-channel.

The properties of the IMD RV suggest that appropriate approximations/estimations for the IMD distribution have to allow for PDFs with different rates of tail decay and for a Gaussian PDF as a particular case. However, the realisation of such approximations/estimations is a daunting task frustrated by the fact that all we have to define them is the first and the second moments of the IMD RV (see chapter 4).

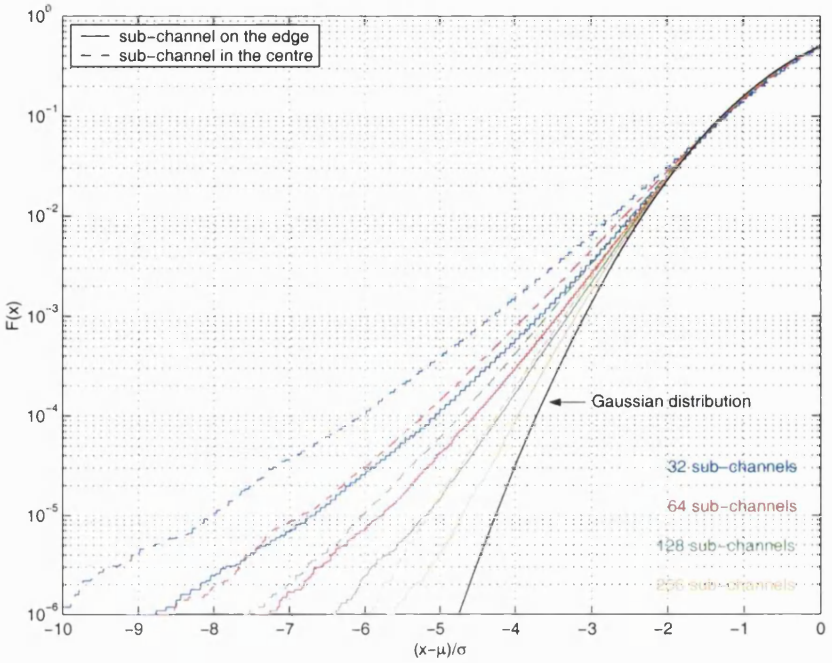

Figure 5.5: CDFs, *F(x)*, of the IMD in the sub-channel on the edge of the band and in the sub-channel in the centre of the band for OFDM/BPSK signals with 32 to 256 sub-channels distorted by the frequency independent non-linearity.

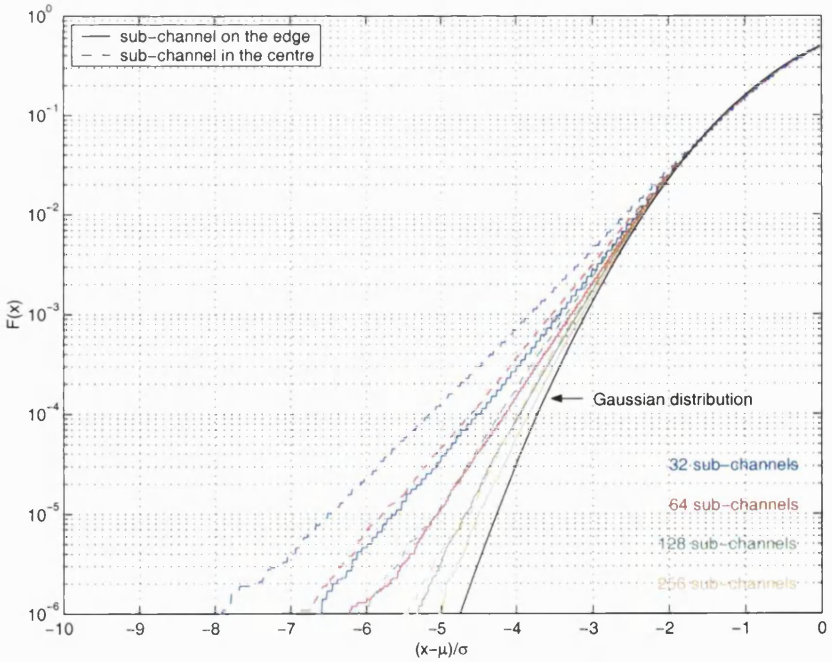

Figure 5.6: CDFs, *F(x)*, of the IMD in the sub-channel on the edge of the band and in the sub-channel in the centre of the band for OFDM/QPSK signals with 32 to 256 sub-channels distorted by the frequency independent non-linearity.

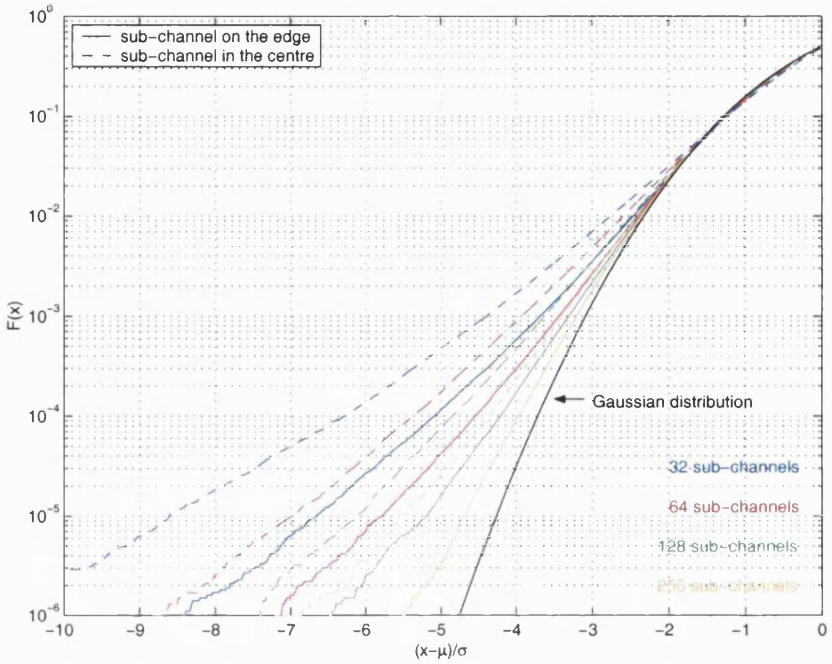

Figure 5.7: CDFs, *F(x)*, of the IMD in the sub-channel on the edge of the band and in the sub-channel in the centre of the band for OFDM/BPSK signals with 32 to 256 sub-channels distorted by the frequency dependent non-linearity.

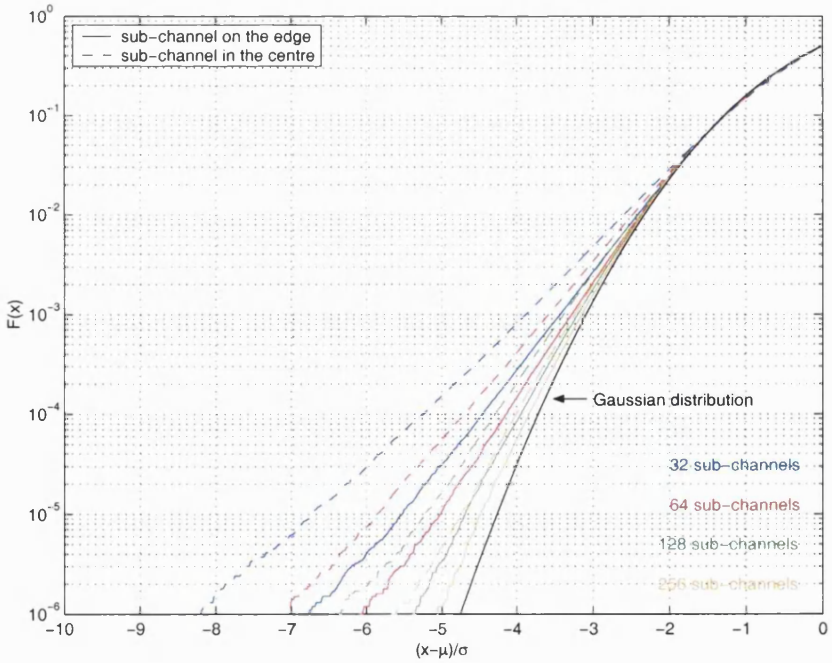

Figure 5.8: CDFs, *F(x)*, of the IMD in the sub-channel on the edge of the band and in the sub-channel in the centre of the band for OFDM/QPSK signals with 32 to 256 sub-channels distorted by the frequency dependent non-linearity.

A possible solution to the IMD approximation/estimation problem is found by noting that the coefficients of skewness and kurtosis of the IMD RV do not depend significantly on the type of non-linearity, as shown in Figure 5.9 through Figure 5.12. The coefficient of skewness β_1 is a measure of the symmetry of a distribution and the coefficient of kurtosis β_2 is a measure of the peakness/flatness of a distribution [154]. These coefficients are defined by [154]

$$\beta_1 = \frac{\mu_3^2}{\mu_2^3} \tag{5.14}$$

and

$$\beta_2 = \frac{\mu_4}{\mu_2^2} \tag{5.15}$$

where $\mu_n, n = 1,2,\ldots$, are the central moments of the RV[18]. The coefficients of skewness and kurtosis were estimated in MATLAB as follows: by generating a large number of samples of the IMD RV under consideration in accordance to (4.58), $X_1, X_2, \ldots, X_N$, then estimates $\hat{\mu}_n', n = 1,2,\ldots$, of the moments $\mu_n', n = 1,2,\ldots$, were obtained through (5.5) and then estimates $\hat{\mu}_n, n = 1,2,\ldots$, of the central moments $\mu_n, n = 1,2,\ldots$, were obtained from the relation between central moments and moments [154]

$$\mu_n = \sum_{k=0}^{n} \binom{n}{k} (-1)^{n-k} \mu_k' \mu_1'^{n-k} \tag{5.16}$$

where

$$\binom{n}{k} = \frac{n!}{k!(n-k)!} \tag{5.17}$$

Finally, an estimate $\hat{\beta}_1$ of the coefficient of skewness β_1 and an estimate $\hat{\beta}_2$ of the coefficient of kurtosis β_2 were obtained from the central moments through (5.14) and (5.15), respectively.

The independence of skewness and kurtosis values on the non-linearity type suggests that were these values known *a priori* for some reference non-linearity then they could be

[18] The nth central moment of a RV X is given by $\mu_n = E\left[(X-\mu)^n\right]$, where $\mu = \mu_1'$ is the mean of the RV.

used to enhance the approximations/estimations for the IMD distribution. One would therefore be able to use the first four moments of the IMD RV or, equivalently, four quantities related to the first four moments of the IMD RV, to define appropriate approximations/estimations for the IMD distribution. Note that it is always possible to work backwards and recover the first four moments from the first moment, the second moment and the coefficients of skewness and kurtosis[19]. Clearly, one may argue that the match between skewness and kurtosis values for the frequency independent and the frequency dependent cases is specific for this particular frequency dependent non-linearity. Indeed, one may always conceive a hypothetical frequency dependent non-linearity that eliminates all IMPs but a particular one so that skewness and kurtosis values would differ in the frequency independent and the frequency dependent cases. However, we will show in chapter 6 that other frequency dependent non-linearities do in fact still yield the same skewness and kurtosis values.

Skewness and kurtosis values of the real part of the IMD RV (conditioned on each possible complex modulation symbol) in selected sub-channels for non-linearly distorted OFDM/BPSK signals with 16 to 128 sub-channels are given in Appendix B. Skewness and kurtosis values of both the real part and the imaginary part of the IMD RV (conditioned on each possible complex modulation symbol) in selected sub-channels for non-linearly distorted OFDM/QPSK signals with 16 to 128 sub-channels are also given in Appendix B. A frequency independent non-linearity has been adopted as a reference non-linearity. Note that the exact value of the (third-order) transfer function of the frequency independent non-linearity is irrelevant because the coefficients of skewness and kurtosis are normalised quantities.

Finally, it is important to emphasise that the analysis in this section is restricted to non-linearities that exhibit up to third-order non-linear behaviour. It is fortunate that third-order non-linear behaviour often serves as a good approximation to a broad range of non-linearities encountered in practice because the moments of the RVs needed for error probability evaluation are not readily obtained for non-linearities of orders greater than three.

---

[19] Strictly speaking, to obtain the first four moments of the IMD RV, the first moment, the second moment and $\sqrt{\beta_1}$ and β_2 of the IMD RV are required. The value of β_1 is known whereas the value of $\sqrt{\beta_1}$ is not entirely known because it can be either positive or negative depending on the value of the third central moment. Extensive simulations have shown that in the IMD case if the first moment is positive then $\sqrt{\beta_1}>0$ and if the first moment is negative then $\sqrt{\beta_1}<0$.

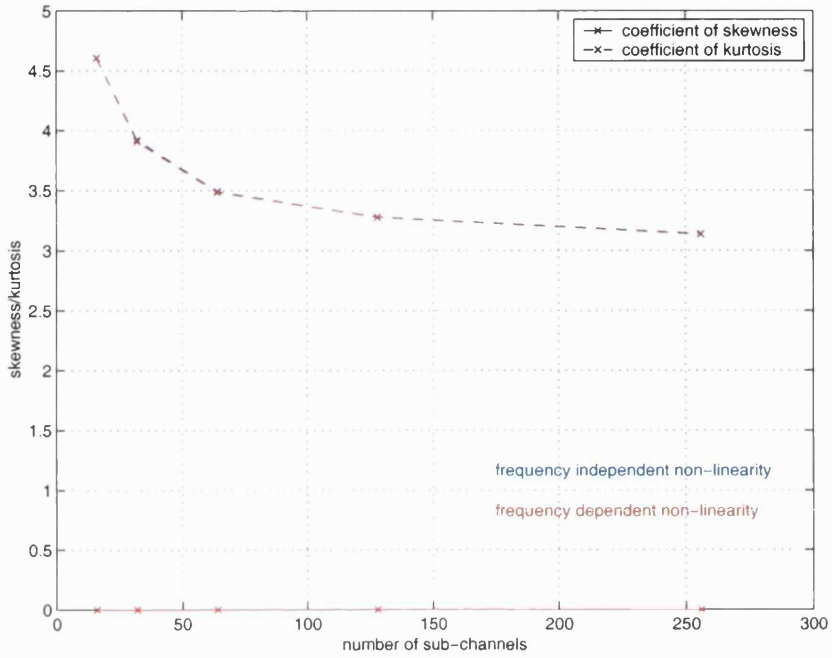

Figure 5.9: Skewness and kurtosis of the IMD in the sub-channel on the edge of the band vs. number of OFDM sub-channels for OFDM/BPSK signals distorted by the frequency independent and the frequency dependent non-linearities.

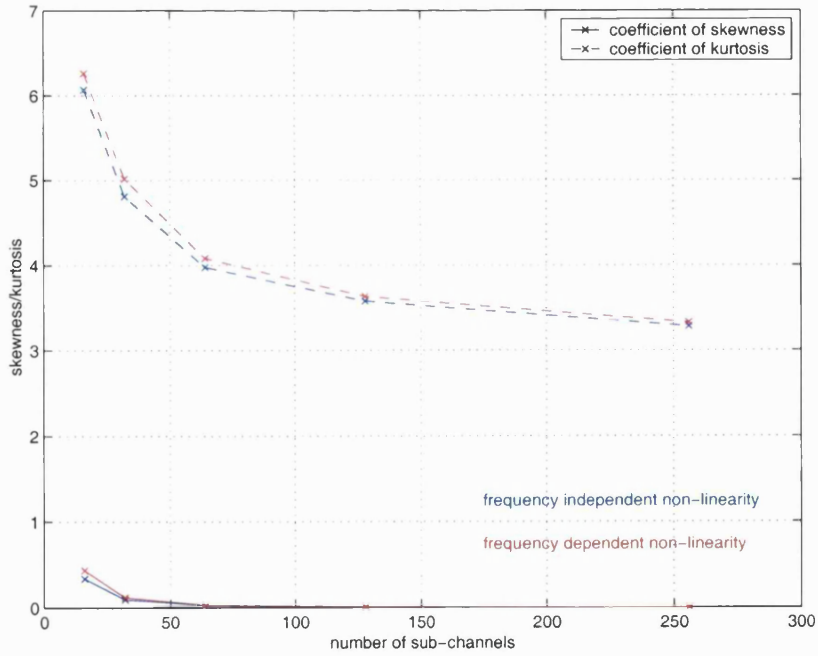

Figure 5.10: Skewness and kurtosis of the IMD in the sub-channel in the centre of the band vs. number of OFDM sub-channels for OFDM/BPSK signals distorted by the frequency independent and the frequency dependent non-linearities.

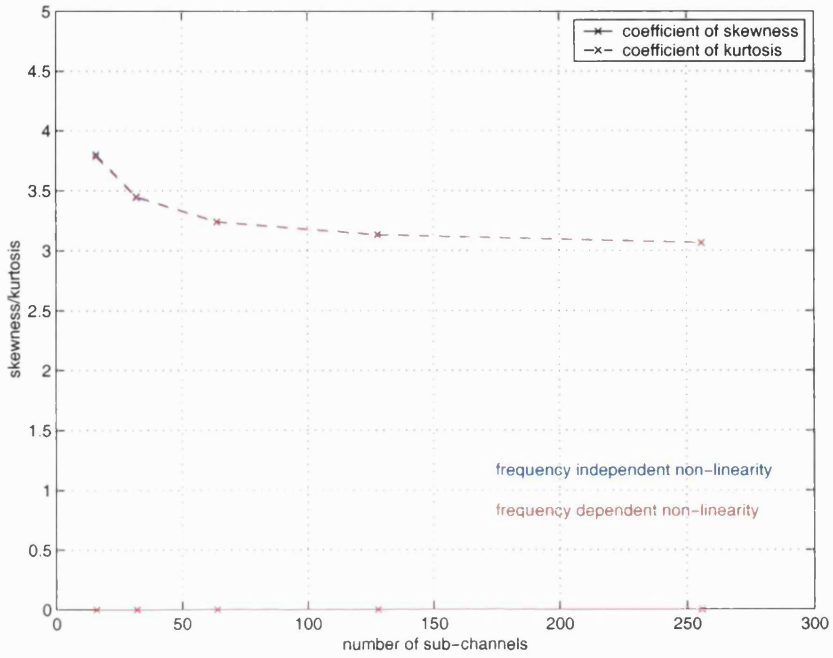

Figure 5.11: Skewness and kurtosis of the IMD in the sub-channel on the edge of the band vs. number of OFDM sub-channels for OFDM/QPSK signals distorted by the frequency independent and the frequency dependent non-linearities.

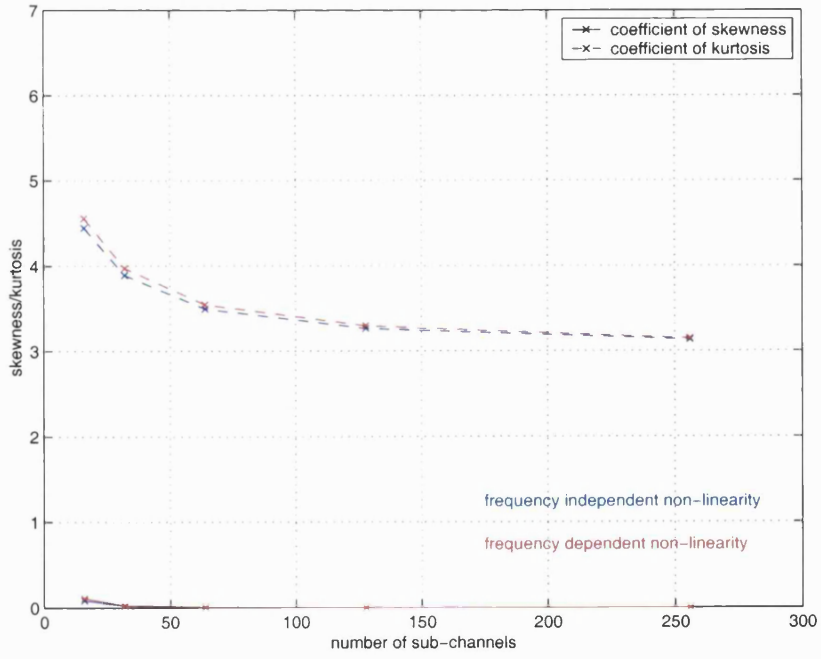

Figure 5.12: Skewness and kurtosis of the IMD in the sub-channel in the centre of the band vs. number of OFDM sub-channels for OFDM/QPSK signals distorted by the frequency independent and the frequency dependent non-linearities.

5.2.2 Approximations for the IMD distribution

In this section, we examine various approximations for the IMD distribution. The observations in section 5.2.1 suggest that to model the IMD distribution we have to select a method that allows for PDFs with different rates of tail decay while encompassing a Gaussian PDF as a particular case. Moreover, the method has to rely only upon the first four moments of the IMD RV or, equivalently, on four quantities related to the first four moments of the IMD RV.

To realise such a method we consider systems of distributions, i.e., mathematical frameworks which accommodate a number of distributions exhibiting certain properties. Particularly, we consider the generalised Gaussian system of distributions and the Pearson system of distributions because these systems have been used in a variety of applications to model distributions whose behaviour deviates from Gaussian behaviour [154,156]. We also consider Gaussian and Laplace distributions for comparison purposes because the former exhibits light tails whereas the later exhibits heavy tails.

In the following paragraphs, we first describe these distributions/systems of distributions and we then investigate the approximation performance of these methods.

Gaussian and Laplace distributions

The PDF of a Gaussian distributed RV is given by [154]

$$f(x)=\frac{1}{\sqrt{2\pi\sigma^2}}e^{-\frac{(x-\mu)^2}{2\sigma^2}} \tag{5.18}$$

where μ is the mean value and σ^2 is the variance of the distribution. The parameters of this distribution are determined from the first moment, μ_1', and the second moment, μ_2', of the RV as follows

$$\mu=\mu_1' \tag{5.19}$$

$$\sigma^2=\mu_2'-\mu_1'^2 \tag{5.20}$$

The PDF of a Laplace distributed RV is given by [154]

$$f(x)=\frac{1}{2\beta}e^{-\left|\frac{x-\alpha}{\beta}\right|} \tag{5.21}$$

where α is the mean value and $2\beta^2$ is the variance of the distribution. Again, the parameters of this distribution are determined from the first two moments, μ_1' and μ_2', of the RV as follows

$$\alpha = \mu_1' \tag{5.22}$$

$$2\beta^2 = \mu_2' - \mu_1'^2 \tag{5.23}$$

Generalised Gaussian system of distributions

The generalised Gaussian system of distributions is characterised by the PDF given below [156]

$$f(x) = \frac{c\gamma}{2\Gamma(1/c)} e^{-\gamma^c |x-\mu|^c} \tag{5.24}$$

where

$$\gamma = \frac{1}{\sigma}\left[\frac{\Gamma(3/c)}{\Gamma(1/c)}\right]^{1/2} \tag{5.25}$$

and μ is the mean of the distribution, σ^2 is the variance of the distribution, c is a parameter that controls the shape of the distribution and the gamma function $\Gamma(\cdot)$ is defined as

$$\Gamma(n) = \int_0^\infty t^{n-1} e^{-t} dt \tag{5.26}$$

for $n > 0$. This system of distributions includes several PDFs with different rates of tail decay. For example, $c = 1$ represents a Laplace distribution and $c = 2$ represents a Gaussian distribution.

The parameters μ and σ^2 of the generalised Gaussian distribution are obtained from the first moment, μ_1', and the second moment, μ_2', of the RV as follows

$$\mu = \mu_1' \tag{5.27}$$

$$\sigma^2 = \mu_2' - \mu_1'^2 \tag{5.28}$$

The central moments of a generalised Gaussian distributed RV are given by

$$\mu_n = \int_{-\infty}^{\infty}(x-\mu)^n f(x)dx = \begin{cases} 0, & \text{n odd} \\ \dfrac{\Gamma((n+1)/c)}{\gamma^n \Gamma(1/c)}, & \text{n even} \end{cases} \tag{5.29}$$

and hence the coefficients of skewness and kurtosis, defined in (5.14) and (5.15) respectively, are given by

$$\beta_1 = \frac{\mu_3^2}{\mu_2^3} = 0 \tag{5.30}$$

and

$$\beta_2 = \frac{\mu_4}{\mu_2^2} = \frac{\Gamma(5/c)\Gamma(1/c)}{\Gamma(3/c)^2} \tag{5.31}$$

The parameter c is therefore obtained from the coefficient of kurtosis of the RV. Finally, it is interesting to note that since the coefficient of skewness of the RV is zero, which implies symmetry, then the generalised Gaussian system of distributions cannot accommodate skewed or asymmetric behaviour.

Pearson system of distributions

The Pearson system of distributions is characterised by the differential equation given below [154]

$$\frac{d\ln f(x)}{dx} = \frac{x-a}{b_0 + b_1 x + b_2 x^2} \tag{5.32}$$

where $f(x)$ is the PDF of the distribution, a is the mode or antimode of the distribution and b_0, b_1 and b_2 are parameters that control the shape of the distribution. This system of distributions includes several important PDFs with different rates of tail decay such as Gaussian, Cauchy, t, F, χ^2, uniform, γ, exponential and β PDFs [154].

The parameters in the Pearson differential equation are obtained by the moment method, i.e., by equating the moment expressions to the moment values [154]. To explain such a procedure the Pearson differential equation is written as follows

$$\left(b_0 + b_1 x + b_2 x^2\right)\frac{df(x)}{dx} = (x-a)f(x) \tag{5.33}$$

Multiplying each side of (5.33) by x^n and integrating the resulting expression with respect to x then we find that the moments μ'_n, if defined, obey the recursive relationship[20]

$$nb_0\mu'_{n-1} + [(n+1)b_1 - a]\mu'_n + [(n+2)b_2 + 1]\mu'_{n+1} = 0 \tag{5.34}$$

and by putting $n = 0,1,2,3$ successively in (5.34) we obtain a system of four linear equations that enables us to find the parameters a, b_0, b_1 and b_2 in terms of the first four moments.

Typically, the parameters in the Pearson differential equation are not given in terms of the first four moments but in terms of the first four central moments. Accordingly, if the mean $\mu = \mu'_1$ is transferred to the origin then we find that the central moments μ_n obey the recursive relationship

$$nb_0\mu_{n-1} + [(n+1)b_1 - a]\mu_n + [(n+2)b_2 + 1]\mu_{n+1} = 0 \tag{5.35}$$

and by putting $n = 0,1,2,3$ successively in (5.35) we obtain a system of four linear equations that enables us to find the parameters a, b_0, b_1 and b_2 in terms of the first four central moments. The parameters in the Pearson differential equation are therefore given by

$$b_1 = a = -\frac{\mu_3\left(\mu_4 + 3\mu_2^2\right)}{10\mu_4\mu_2 - 18\mu_2^3 - 12\mu_3^2} = -\frac{\sigma\sqrt{\beta_1}(\beta_2 + 3)}{10\beta_2 - 18 - 12\beta_1} \tag{5.36}$$

$$b_0 = -\frac{\mu_2\left(4\mu_2\mu_4 - 3\mu_3^2\right)}{10\mu_4\mu_2 - 18\mu_2^3 - 12\mu_3^2} = -\frac{\sigma^2(4\beta_2 - 3\beta_1)}{10\beta_2 - 18 - 12\beta_1} \tag{5.37}$$

$$b_2 = -\frac{\left(2\mu_2\mu_4 - 3\mu_3^2 - 6\mu_2^3\right)}{10\mu_4\mu_2 - 18\mu_2^3 - 12\mu_3^2} = -\frac{(2\beta_2 - 3\beta_1 - 6)}{10\beta_2 - 18 - 12\beta_1} \tag{5.38}$$

where σ^2 is the variance of the distribution and β_1 and β_2 are the coefficients of skewness and kurtosis of the distribution defined in (5.14) and (5.15), respectively.

---

[20] To derive this recursive relation it was assumed that $\lim_{x\to\pm\infty} x^{n+2} f(x) = 0$ if the range of $f(x)$ is infinite [154].

Explicit forms to the Pearson PDF are obtained by integrating the Pearson differential equation. Solutions to the Pearson differential equation depend on the nature of the roots of the denominator on the right hand side of (5.32), i.e., whether the roots are real and of different sign, complex or real and of the same sign, and the nature of the roots of the denominator on the right hand side of (5.32) depends on the value of k given by

$$k = \frac{b_1^2}{4b_0b_2} = \frac{\beta_1(\beta_2+3)^2}{4(2\beta_2-3\beta_1-6)(4\beta_2-3\beta_1)} \tag{5.39}$$

If k is negative the roots are real and of different sign and we get the first main type of curve or Pearson's Type I; if k is positive and less than unity the roots are complex and we get the second main type of curve or Pearson's Type IV; finally, if k is positive and greater than unity the roots are real and of the same sign and we get the third main type of curve or Pearson's Type VI. The main types of Pearson distributions are discussed in the following paragraphs.

Pearson's Type I: This corresponds to the case where the roots of the quadratic are real and of different sign. In this case, it is possible to expand the denominator on the right hand side of (5.32) in real factors and hence to write the Pearson differential equation as follows

$$\frac{d\ln f(x)}{dx} = \frac{1}{b_2}\frac{x-a}{(x+A_1)(x-A_2)} = \frac{1}{b_2}\frac{A_1+a}{A_1+A_2}\frac{1}{A_1+x} - \frac{1}{b_2}\frac{A_2-a}{A_1+A_2}\frac{1}{A_2-x} \tag{5.40}$$

where $A_1, A_2 > 0$. Note that $-A_1$ and A_2 are the roots of the quadratic. Integration of (5.40) yields

$$f(x) = c(A_1+x)^{\frac{1}{b_2}\frac{A_1+a}{A_1+A_2}}(A_2-x)^{\frac{1}{b_2}\frac{A_2-a}{A_1+A_2}} \tag{5.41}$$

The support of the PDF is from $-A_1$ to A_2 and the value of the integration constant c is chosen so that the area under the PDF is one.

Pearson's Type IV: In this case, the roots of the quadratic are complex and it is not possible to expand the denominator on the right hand side of (5.32) in real factors. Consequently, we write the Pearson differential equation alternatively as follows

$$\frac{d\ln f(x)}{dx} = \frac{x-a}{b_2\left[(x+\gamma)^2+\delta^2\right]} \tag{5.42}$$

where $\gamma \pm j\delta$ are the complex conjugate roots of the quadratic. Integration of (5.42) then gives

$$f(x) = c\left[(x+\gamma)^2+\delta^2\right]^{\frac{1}{2b_2}} e^{-\frac{a+\gamma}{b_2\delta}\tan^{-1}\frac{x+\gamma}{\delta}} \tag{5.43}$$

where the value of the integration constant c is chosen so that the area under the PDF is one. The support of this PDF is from $-\infty$ to ∞.

Pearson's Type VI: This corresponds to the case where the roots of the quadratic are real and of the same sign. In this case, it is possible to expand the denominator on the right hand side of (5.32) in real factors and hence to write the Pearson differential equation as follows

$$\frac{d\ln f(x)}{dx} = \frac{1}{b_2}\frac{x-a}{(x-A_1)(x-A_2)} = \frac{1}{b_2}\frac{A_1-a}{A_1-A_2}\frac{1}{x-A_1} - \frac{1}{b_2}\frac{A_2-a}{A_1-A_2}\frac{1}{x-A_2} \tag{5.44}$$

where A_1 and A_2 are the roots of the quadratic. Integration of (5.44) yields

$$f(x) = c(x-A_1)^{\frac{1}{b_2}\frac{A_1-a}{A_1-A_2}}(x-A_2)^{-\frac{1}{b_2}\frac{A_2-a}{A_1-A_2}} \tag{5.45}$$

The support of the PDF is from $\max(A_1, A_2)$ to ∞ and the value of the integration constant c is chosen so that the area under the PDF is one.

It is important to mention that the various Pearson PDFs discussed in the preceding paragraphs are normally written in the literature by centring them at appropriate points and by scaling them [154]. These procedures were not carried out here because the aim was only to show how to obtain an explicit form to the Pearson PDF. It is also important to mention that the main types of Pearson distributions discussed in the preceding paragraphs cover the whole field of solutions to the Pearson differential equation but in limiting cases when one type changes into another we reach simpler forms of transition curves. For example, the Gaussian curve corresponds to $k = 0$ when $b_1 = b_2 = 0$ [154].

Comparison of the approximation methods

To evaluate the efficacy of these methods we have compared the approximated IMD CDF to the true IMD CDF. We have considered the same cases considered in the previous section, i.e., the real part of the IMD in the sub-channel on the edge of the band and the real part of the IMD in the sub-channel in the centre of the band for non-linearly distorted OFDM/BPSK and OFDM/QPSK signals with different numbers of sub-channels. We have also considered the same symbol conditioning and the same frequency independent and frequency dependent non-linearities[21].

The Gaussian and the Laplace approximations were defined by using the first two moments of the IMD RV to specify the parameters of the Gaussian and the Laplace PDFs in (5.18) and (5.21), respectively, as explained previously. The generalised Gaussian approximation was defined by using the first two moments plus the kurtosis value of the IMD RV to specify the parameters of the generalised Gaussian PDF in (5.24) and (5.25), as explained previously. Finally, the Pearson approximation was characterised first by using the first two moments of the IMD RV plus its skewness and kurtosis values to obtain the parameters of the Pearson differential equation, then by integrating the Pearson differential equation to obtain the Pearson PDF and finally by shifting this PDF from the origin to the mean. It is interesting to note that a Pearson's type IV distribution resulted in each case under consideration. The first two moments of the IMD RV were calculated as described in chapter 4 and the skewness and kurtosis values were read from the tables in Appendix B. The CDFs were obtained from the PDFs by numerical integration in accordance to (5.12).

A comparison of the approximation effectiveness of these methods for the different situations under consideration is shown in Figure 5.13 through Figure 5.20. Note that the x-axis is normalised to the mean μ and the standard deviation σ of the distributions in these figures. Observation of these figures reveals that the generalised Gaussian system does not yield a good approximation to the IMD distribution, except in particular cases where the IMD distribution is practically Gaussian (e.g., see Figure 5.15 and Figure 5.19). The Pearson system, on the other hand, is capable of providing a very good approximation

[21] Again, when we refer to the IMD distribution in the OFDM/BPSK case we mean its real part conditioned on A and when we refer to the IMD distribution in the OFDM/QPSK case we mean its real part conditioned on $Ae^{j\pi/4}$.

to the IMD distribution in each case. This is an interesting result because both systems include distributions with different rates of tail decay and a Gaussian distribution as a particular case while the former does not serve as an appropriate approximation technique whereas the later does. The explanation of this result must ultimately lie in the nature of the IMD RV and the nature of the distributions that the generalised Gaussian system and the Pearson system include. Observation of these figures also reveals that Gaussian and Laplace approximations are only justified in particular cases. The Gaussian approximation is appropriate when light tail behaviour is observed which occurs for a high number of OFDM sub-channels, the sub-channel on the edge of the band and QPSK modulation. The Laplace approximation, on the other hand, is appropriate when heavy tail behaviour is observed which occurs for a low number of OFDM sub-channels, the sub-channel in the centre of the band and BPSK modulation.

Finally, it is important to note that any of these approximations would yield equivalent results in situations where high error rates are expected. For example, if the error rate is 10^{-2} then it is clear that values of the IMD RV that occur with a probability of 10^{-2} or less will make no contribution whatsoever to define this error rate. However, the various approximations are equivalent for values that do not occur with a probability of 10^{-2} or less. In practice, this implies that in wireless systems, where a high error rate is expected, any of these approximations is appropriate; in optical systems, where low error rates are commonly expected, a Pearson approximation ought to be used.

Gaussian approximations to the IMD distribution have been used extensively in the literature [13,14,16-18,21-25]. Obviously, a Gaussian approximation can be justified for high error rates or for OFDM signals with a very large number of sub-channels, as shown in this chapter. A Gaussian approximation can also be justified for OFDM signals distorted by non-linearities exhibiting non-linear behaviour of orders higher than three due to accelerated Gaussian convergence due to the increased number of IMPs, as shown in the next chapter. However, in the literature such an approximation has been suggested also to estimate relatively low error rates for a 64 sub-channel OFDM signal distorted by non-linearities exhibiting up to third-order non-linear behaviour [157].

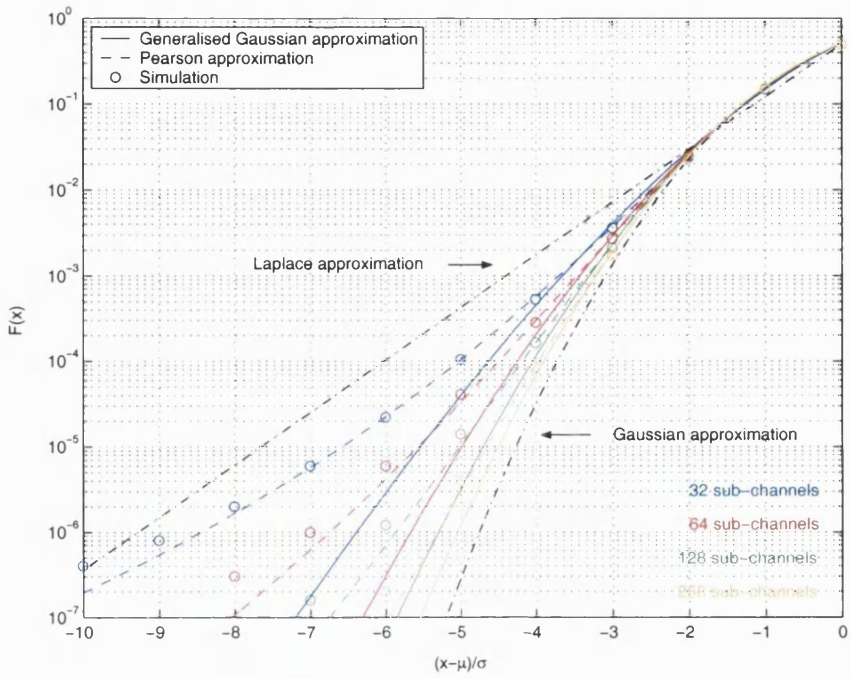

Figure 5.13: Approximations for the CDFs, *F(x)*, of the IMD in the sub-channel on the edge of the band for OFDM/BPSK signals with 32 to 256 sub-channels in the frequency independent non-linearity case.

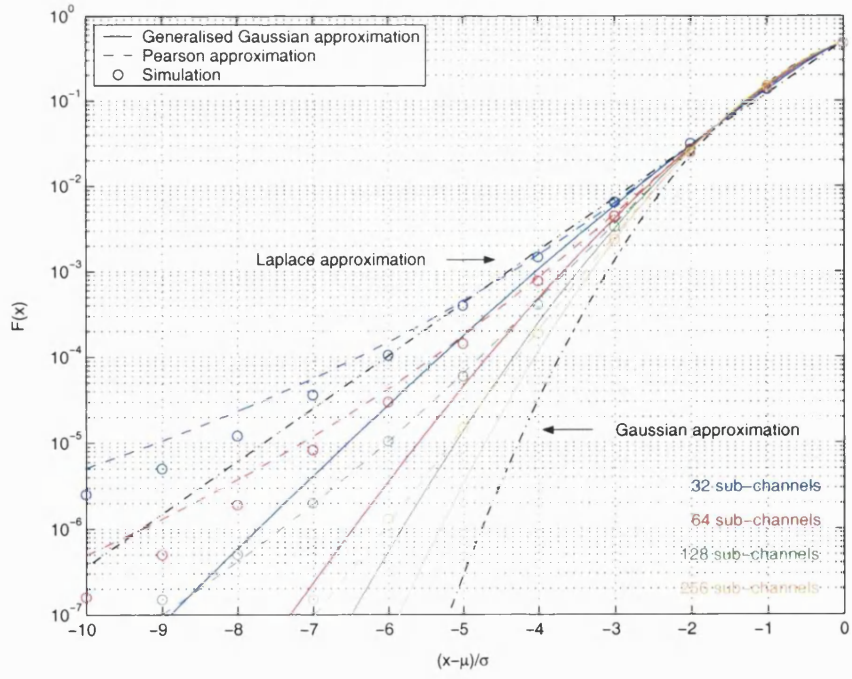

Figure 5.14: Approximations for the CDFs, *F(x)*, of the IMD in the sub-channel in the centre of the band for OFDM/BPSK signals with 32 to 256 sub-channels in the frequency independent non-linearity case.

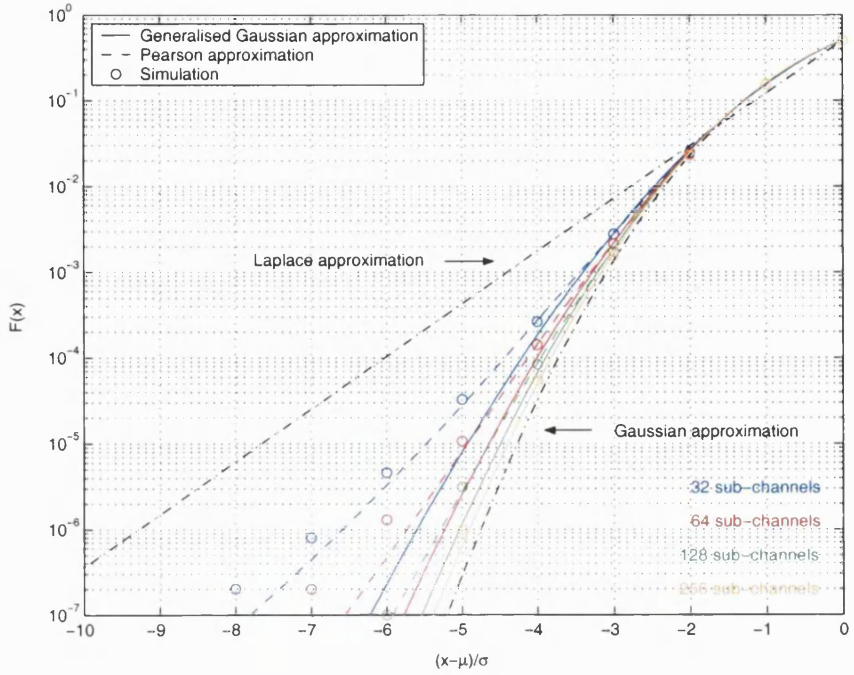

Figure 5.15: Approximations for the CDFs, *F(x)*, of the IMD in the sub-channel on the edge of the band for OFDM/QPSK signals with 32 to 256 sub-channels in the frequency independent non-linearity case.

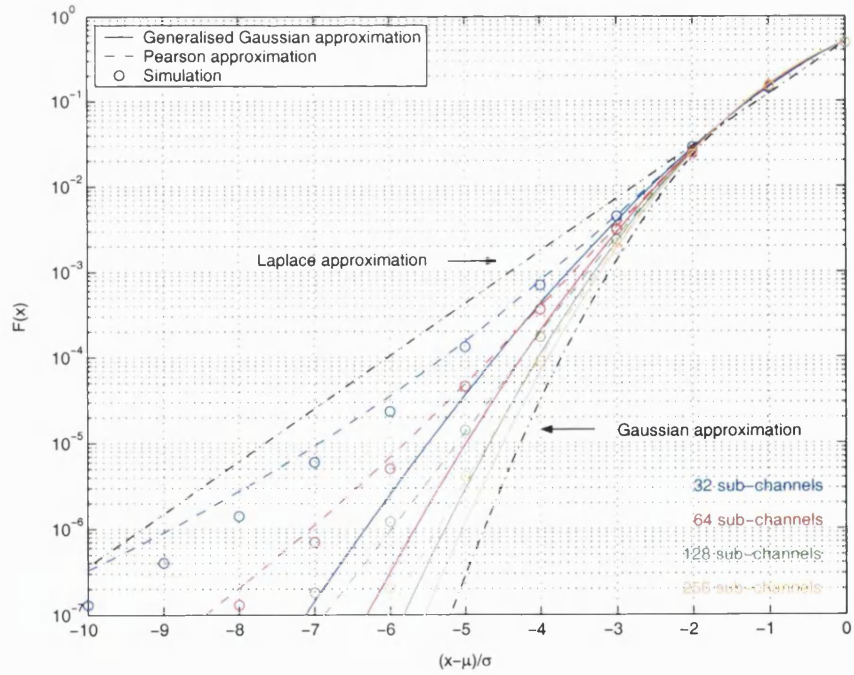

Figure 5.16: Approximations for the CDFs, *F(x)*, of the IMD in the sub-channel in the centre of the band for OFDM/QPSK signals with 32 to 256 sub-channels in the frequency independent non-linearity case.

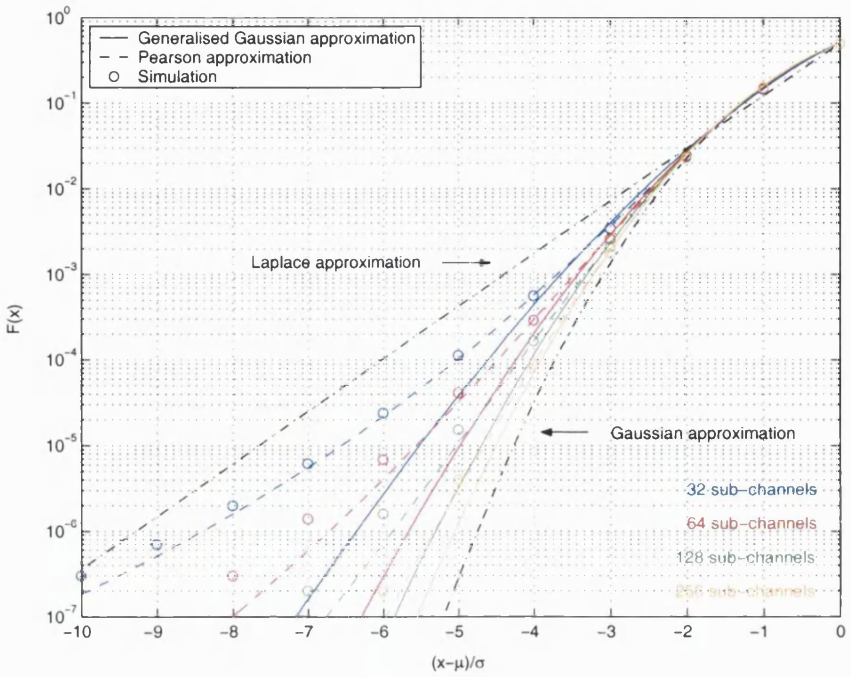

Figure 5.17: Approximations for the CDFs, *F(x)*, of the IMD in the sub-channel on the edge of the band for OFDM/BPSK signals with 32 to 256 sub-channels in the frequency dependent non-linearity case.

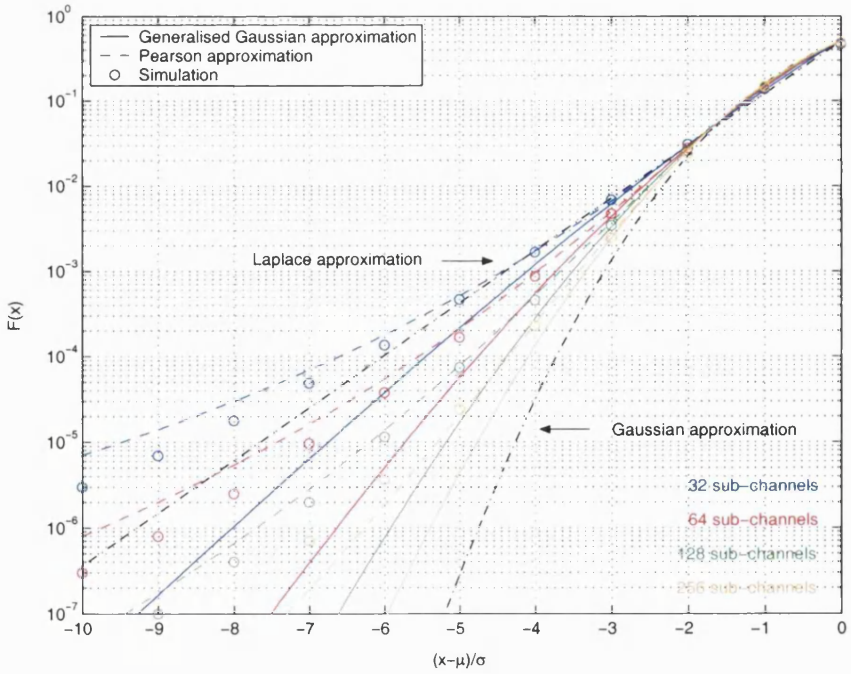

Figure 5.18: Approximations for the CDFs, *F(x)*, of the IMD in the sub-channel in the centre of the band for OFDM/BPSK signals with 32 to 256 sub-channels in the frequency dependent non-linearity case.

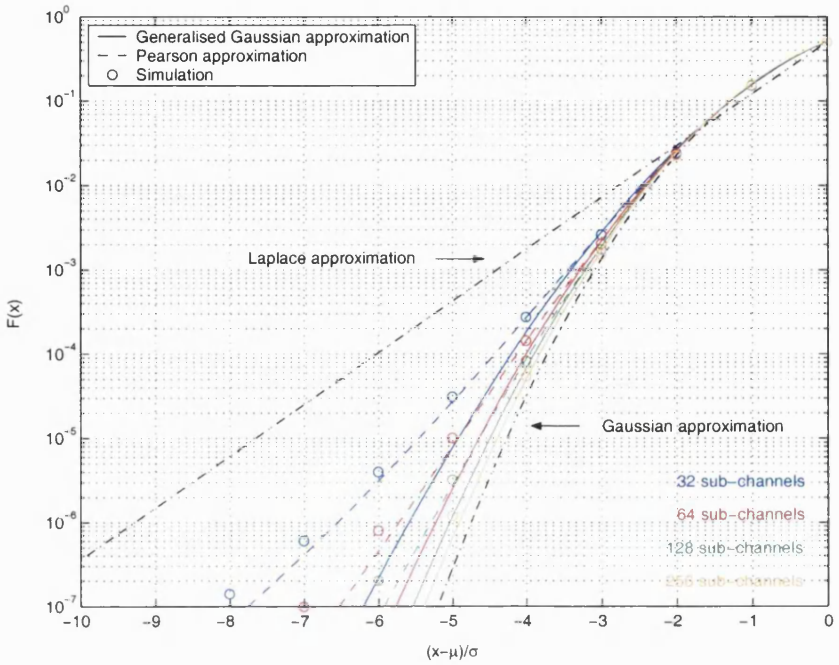

Figure 5.19: Approximations for the CDFs, *F(x)*, of the IMD in the sub-channel on the edge of the band for OFDM/QPSK signals with 32 to 256 sub-channels in the frequency dependent non-linearity case.

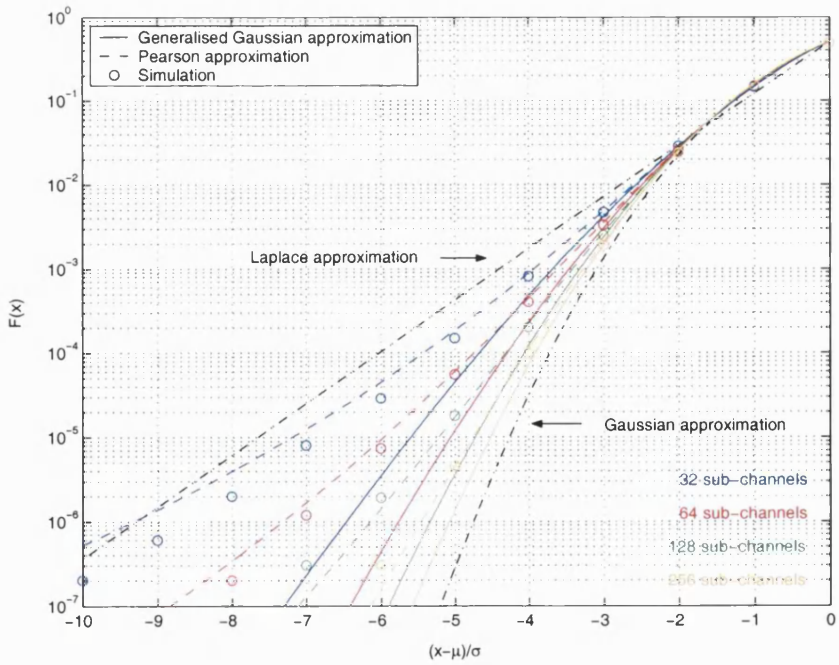

Figure 5.20: Approximations for the CDFs, *F(x)*, of the IMD in the sub-channel in the centre of the band for OFDM/QPSK signals with 32 to 256 sub-channels in the frequency dependent non-linearity case.

5.2.3 Maximum entropy and minimum relative entropy estimations for the IMD distribution

In this section, we explore maximum entropy and minimum relative entropy estimations for the IMD distribution. Special attention is devoted to the maximum entropy method (MEM) and the minimum relative entropy method (MREM) because a number of researchers have shown that among moment based techniques these two require far less moments than others, such as series expansion methods or Gauss quadrature rules [158,159].

In the MEM we maximise the entropy function [158,159]

$$H(f)=\int_a^b f(x)\ln\frac{1}{f(x)}dx=-\int_a^b f(x)\ln f(x)dx \tag{5.46}$$

with respect to the unknown PDF $f(x)$, subject to a set of moments constraints

$$\mu_n'=\int_a^b x^n f(x)dx,\quad n=1,\ldots,N \tag{5.47}$$

and subject to the normalisation condition

$$\int_a^b f(x)dx=1 \tag{5.48}$$

Here a and b define the support of the unknown PDF.

Maximisation of the entropy of the unknown PDF is motivated by the fact that a number of distributions occurring in practice are maximum entropy distributions given appropriate moment constraints [158,159]. For example, the maximum entropy density under the constraints of a first moment equal to zero and a second moment equal to σ^2 is a Gaussian density with zero mean and σ^2 variance. It seems therefore appropriate to explore maximising the entropy of the IMD PDF given a set of moment constraints.

This constrained optimisation problem can be solved using calculus of variations techniques [160], whereby the unknown PDF is found by requiring that

$$\frac{d}{d\alpha}\left[-\int_a^b(f(x)+\alpha h(x))\ln(f(x)+\alpha h(x))dx+\sum_{n=0}^{N}\lambda_n\int_a^b x^n(f(x)+\alpha h(x))dx\right]_{\alpha=0}=0,\quad \forall h(x) \tag{5.49}$$

where $\lambda_n, n = 0,1,\ldots,N$, are the Lagrange multipliers. By solving (5.49) for $f(x)$ then

$$f(x) = e^{-1+\sum_{n=0}^{N}\lambda_n x^n}, \quad a \le x \le b \tag{5.50}$$

The values of the Lagrange multipliers in (5.50) are determined by requiring that the constraint equations (5.47) and (5.48) are satisfied.

In the MREM we minimise the relative entropy function [158,159]

$$\mathrm{R}(f) = \int_a^b f(x)\ln\frac{f(x)}{g(x)}dx \tag{5.51}$$

with respect to the unknown PDF $f(x)$, given a prior estimate $g(x)$ of the unknown PDF $f(x)$, a set of moment constraints

$$\mu_n' = \int_a^b x^n f(x)dx, \quad n = 1,\ldots,N \tag{5.52}$$

and the normalisation condition

$$\int_a^b f(x)dx = 1 \tag{5.53}$$

Note that a and b define the support of $f(x)$. Note also that the relative entropy function is finite if and only if the support of $f(x)$ is contained in the support of $g(x)$.

The minimum relative entropy principle is a generalisation of the maximum entropy principle and applies to cases where a prior estimate of the unknown PDF in addition to the moment constraints is known. It is interesting to note that minimisation of the relative entropy is equivalent to maximisation of the entropy when the prior estimate is uniform.

This constrained optimisation problem can also be solved using calculus of variations techniques [160], whereby the unknown PDF is found by requiring that

$$\frac{d}{d\alpha}\left[\int_a^b (f(x)+\alpha h(x))\ln\left(\frac{f(x)+\alpha h(x)}{g(x)}\right)dx + \sum_{n=0}^{N}\lambda_n\int_a^b x^n(f(x)+\alpha h(x))dx\right]\Bigg|_{\alpha=0} = 0, \quad \forall h(x) \tag{5.54}$$

where $\lambda_n, n = 0,1,\ldots,N$, are the Lagrange multipliers. By solving (5.54) for $f(x)$ then

$$f(x) = g(x)e^{-1-\sum_{n=0}^{N}\lambda_n x^n}, \quad a \le x \le b \tag{5.55}$$

The values of the Lagrange multipliers in (5.55) are also determined by requiring that the constraint equations (5.52) and (5.53) are satisfied.

To evaluate the efficacy of these methods we have compared the estimated IMD CDF to the true IMD CDF. We have considered the same cases considered in the previous section, i.e., the real part of the IMD in the sub-channel on the edge of the band and the real part of the IMD in the sub-channel in the centre of the band for non-linearly distorted OFDM/BPSK and OFDM/QPSK signals with different numbers of sub-channels. We have also considered the same symbol conditioning and the same frequency independent and frequency dependent non-linearities[22].

The MEM and the MREM estimations were defined by using the first four moments of the IMD RV under consideration. The first two moments were calculated as described in chapter 4 and the remaining moments were calculated by using the skewness and kurtosis values, which were read from the tables in Appendix B. In the MEM case the limits of integration a and b were set to the minimum and maximum value of the IMD RV, respectively. Extensive simulations have shown that for the frequency independent non-linearity these extremes correspond to the following two cases: either the symbols conveyed in the other sub-channels are all equal to the symbol conveyed in the sub-channel being examined or the symbols conveyed in the other sub-channels are symmetric to the symbol conveyed in the sub-channel being examined. The one that corresponds to the minimum and the one that corresponds to the maximum depends on the actual symbol transmitted in the sub-channel being examined and the sign of the transfer function of the frequency independent non-linearity. Difficulties in determining the maximum and minimum values of the IMD RV for the frequency dependent non-linearity led us not to explore the performance of the MEM method in this case. In the MREM case we have used a Laplace distribution as a prior estimate to try to capture the heavy-tailed nature of the IMD distribution. Moreover, in the MREM case the limits of integration a and b were set to $-\infty$ and ∞, respectively.

As explained previously, the values of the Lagrange multipliers in the MEM and the MREM case are determined by requiring that the constraint equations are satisfied. The Lagrange multiplier λ_0 is found in terms of the Lagrange multipliers $\lambda_n = 1,\ldots,N$ from

---

[22] Again, when we refer to the IMD distribution in the OFDM/BPSK case we mean its real part conditioned on A and when we refer to the IMD distribution in the OFDM/QPSK case we mean its real part conditioned on $Ae^{j\pi/4}$.

the normalisation constraint equation. The Lagrange multipliers $\lambda_n = 1,\ldots,N$ are then found by solving simultaneously the N moment constraint equations using the iterative method described in [158,159]. The method starts with an initial guess to the Lagrange multiplier values $\boldsymbol{\lambda}^{(1)} = \{\lambda_1^{(1)},\ldots,\lambda_N^{(1)}\}$, e.g., $\boldsymbol{\lambda}^{(1)} = \{0,\ldots,0\}$, and generates iterative approximate solutions $\boldsymbol{\lambda}^{(2)}$, $\boldsymbol{\lambda}^{(3)}$, ... sequentially. The (r+1)th Lagrange multiplier values are obtained from the rth Lagrange multiplier values by requiring that $\Delta\boldsymbol{\lambda}^{(r)} = \boldsymbol{\lambda}^{(r+1)} - \boldsymbol{\lambda}^{(r)}$ is a solution to

$$\boldsymbol{\mu}'^{(r)} - \boldsymbol{\mu}' = \mathbf{H}^{(r)} \cdot \Delta\boldsymbol{\lambda}^{(r)} \tag{5.56}$$

where $\boldsymbol{\mu}' = \{\mu_1',\ldots,\mu_N'\}$ are the true moment values, $\boldsymbol{\mu}'^{(r)} = \{\mu_1'^{(r)},\ldots,\mu_N'^{(r)}\}$ are the estimated moment values in iteration r and $\mathbf{H}^{(r)}$ is the Hessian matrix in iteration r. The elements of the Hessian matrix are given by

$$H_{ij} = \mu_{i+j}'^{(r)} - \mu_i'^{(r)}\mu_j'^{(r)}, \quad i,j = 1,\ldots,N \tag{5.57}$$

It is interesting to note that this iterative method is an application of the Newton-Raphson iterative method, which is used to compute solutions to systems of non-linear equations, to the present case [158,159]. It is also interesting to note that this problem has a unique solution [158,159]. Once the values of the Lagrange multipliers were obtained the estimated CDF was determined from the estimated PDF by numerical integration in accordance to (5.12).

A comparison of the estimation effectiveness of the MEM and the MREM for the different situations under consideration is shown in Figure 5.21 through Figure 5.28. Note that the x-axis is normalised to the mean μ and the standard deviation σ of the distributions in these figures. From these figures we can conclude that the MEM fails to provide a reasonable estimate of the IMD distribution in each case. This is particularly evident for the highest number of OFDM sub-channels where there is a substantial discrepancy between the MEM distribution and the true distribution. From these figures we can also conclude that the MREM also fails to estimate reasonably the IMD distribution in each case. This last finding is particularly interesting given that a Laplace distribution was used as a prior estimate and yet the method fails to capture the heavy-tailed nature of the IMD distribution. Accordingly, both the MEM and the MREM are inadequate for the present application if only four moments are available. If more moments were available both the MEM and the MREM might possibly provide a reasonable estimate of the IMD distribution.

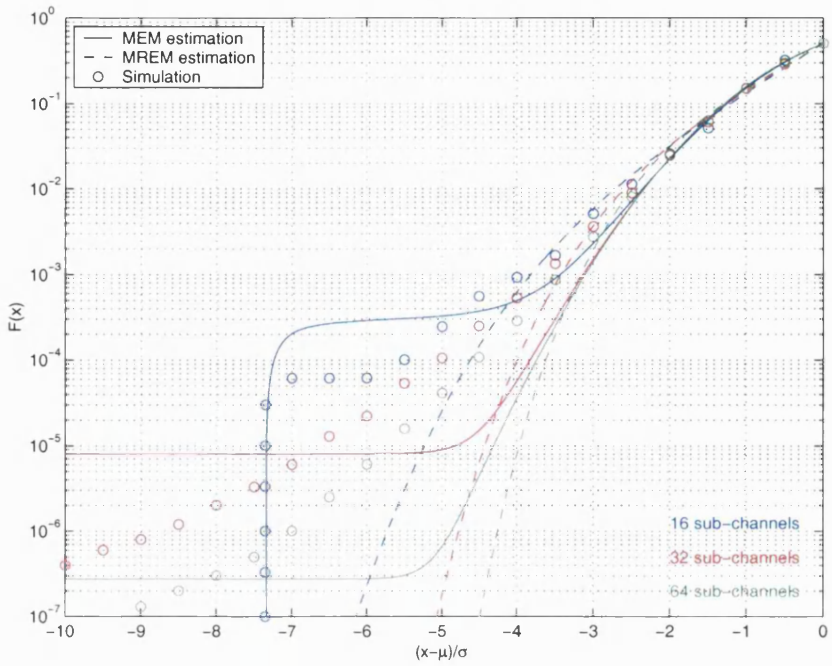

Figure 5.21: Estimations for the CDFs, *F(x)*, of the IMD in the sub-channel on the edge of the band for OFDM/BPSK signals with 16 to 64 sub-channels in the frequency independent non-linearity case.

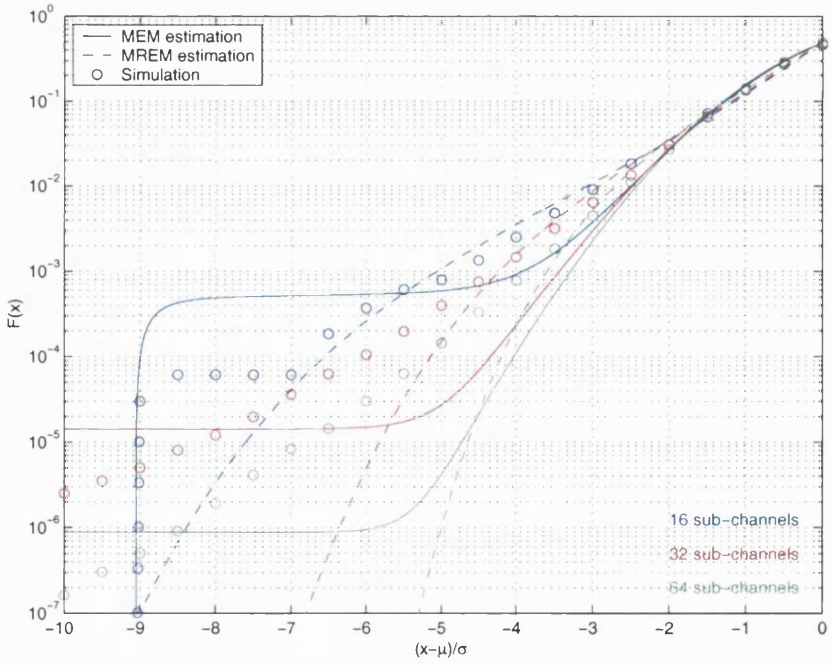

Figure 5.22: Estimations for the CDFs, *F(x)*, of the IMD in the sub-channel in the centre of the band for OFDM/BPSK signals with 16 to 64 sub-channels in the frequency independent non-linearity case.

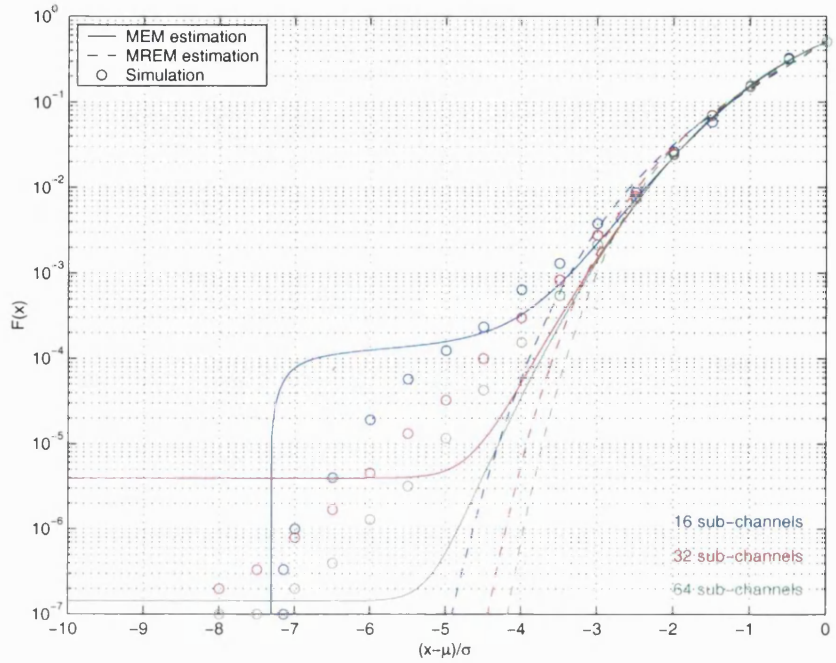

Figure 5.23: Estimations for the CDFs, *F(x)*, of the IMD in the sub-channel on the edge of the band for OFDM/QPSK signals with 16 to 64 sub-channels in the frequency independent non-linearity case.

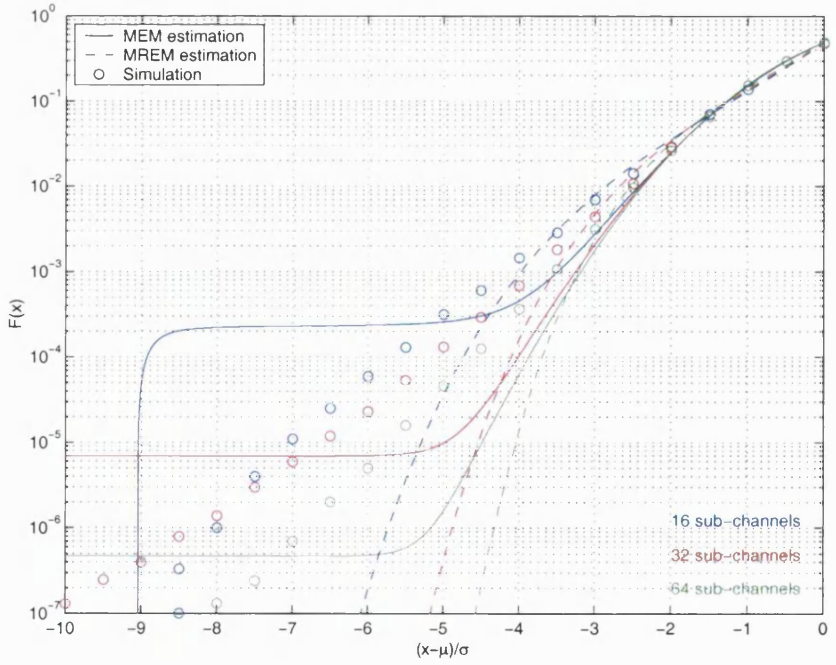

Figure 5.24: Estimations for the CDFs, *F(x)*, of the IMD in the sub-channel in the centre of the band for OFDM/QPSK signals with 16 to 64 sub-channels in the frequency independent non-linearity case.

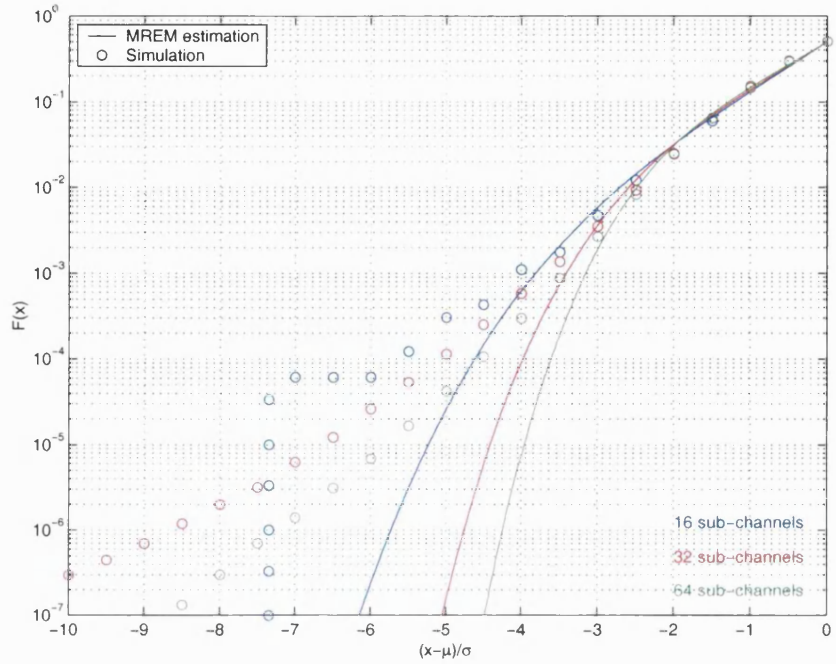

Figure 5.25: Estimations for the CDFs, *F(x)*, of the IMD in the sub-channel on the edge of the band for OFDM/BPSK signals with 16 to 64 sub-channels in the frequency dependent non-linearity case.

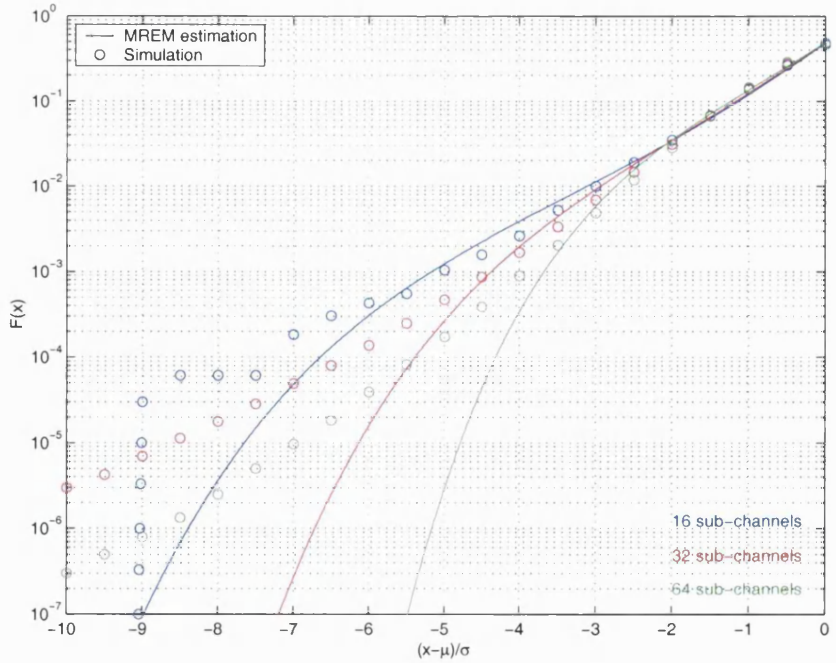

Figure 5.26: Estimations for the CDFs, *F(x)*, of the IMD in the sub-channel in the centre of the band for OFDM/BPSK signals with 16 to 64 sub-channels in the frequency dependent non-linearity case.

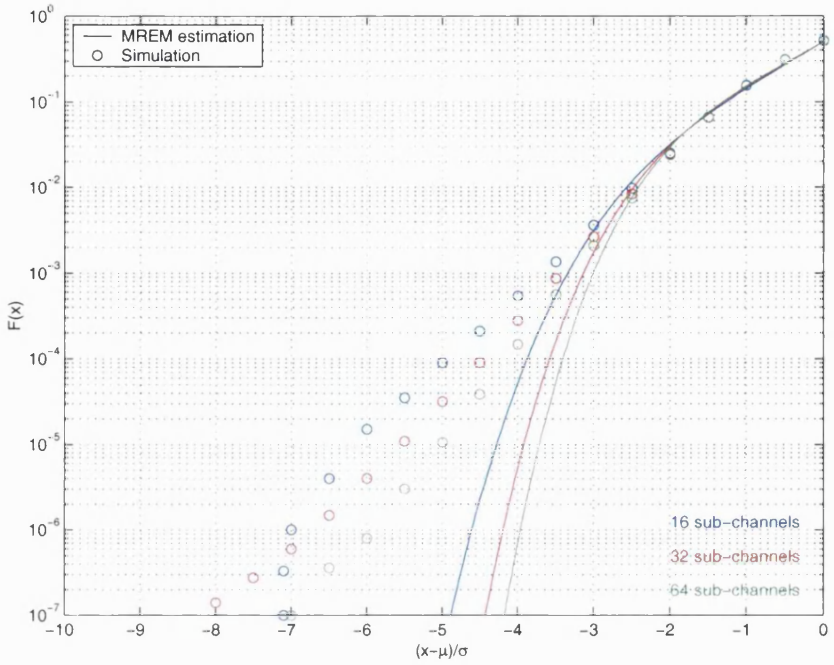

Figure 5.27: Estimations for the CDFs, *F(x)*, of the IMD in the sub-channel on the edge of the band for OFDM/QPSK signals with 16 to 64 sub-channels in the frequency dependent non-linearity case.

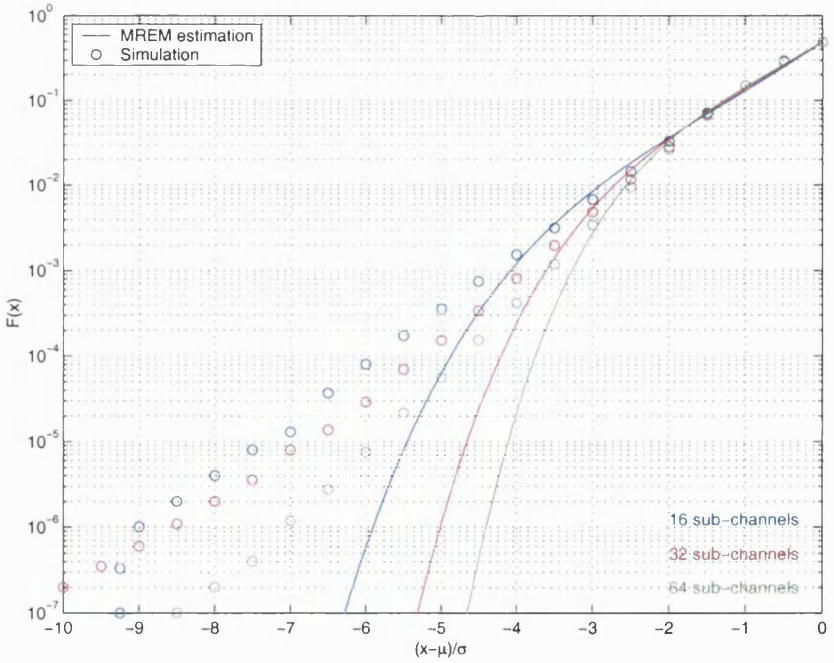

Figure 5.28: Estimations for the CDFs, *F(x)*, of the IMD in the sub-channel in the centre of the band for OFDM/QPSK signals with 16 to 64 sub-channels in the frequency dependent non-linearity case.

5.3 Error probability

Error probability evaluation of non-linearly distorted OFDM signals provided the primary motivation behind the investigation of specific approximation/estimation schemes for the IMD distribution. In this section, we compare the error probability approximation performance of such schemes. Particularly, we consider Gaussian, Laplace, generalised Gaussian and Pearson approximations. We do not consider MEM and MREM estimations because we have shown that these estimation methods are very ineffective.

To evaluate the error probability approximation performance of the various schemes we have obtained the overall BER, the BER in the sub-channel on the edge of the band and the BER in the sub-channel in the centre of the band by analytic and simulation means for the OFDM communication system model depicted in Figure 5.29. We have considered the same frequency independent and frequency dependent bandpass non-linearities. We have also considered an OFDM signal with the following parameters: $f_c = 1GHz$, $T = 4\,\mu s$, $T_{CP} = 0.8\,\mu s$ and $N = 48$. The modulation symbols conveyed in different time slots and different sub-channels were assumed to take any value from a BPSK signal constellation with equal probability or from a Gray coded QPSK signal constellation with equal probability and were assumed to be independent. For illustration we consider specifically OFDM signals with 48 sub-channels because many of the recently proposed wireless networks employ OFDM signals with such a number of sub-channels [44,45].

The BERs were obtained for E_b/N_0 values in the range of 0-30 dB, where E_b denotes the average received energy per bit and N_0 denotes the one-sided power spectral density of the AWGN. The BERs were also obtained for an OBO value of 3 dB in the frequency independent non-linearity case and for an OBO value of 4 dB in the frequency dependent non-linearity case. The OBO was set by varying the power in the constellations of each OFDM sub-channel until a specified value, as given by (3.84), was achieved. Note that once the OBO value is set so is the average power of the received OFDM signal and hence the average energy of the received OFDM symbols. The E_b/N_0 ratio is then given by dividing the average energy of the received OFDM symbols by the total number of bits conveyed per OFDM symbol and by the one-sided power spectral density of the AWGN.

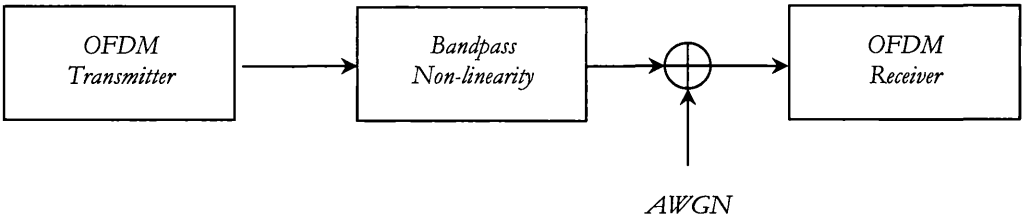

Figure 5.29: OFDM communication system model.

Analytic results were obtained in MATLAB by using the PDF of the approximation method under consideration, which was defined in the manner described in section 5.2.2, to carry out the expectations that will ultimately yield the BERs (see chapter 4).

Simulation results were obtained in MATLAB as follows: Initially, the transmitted OFDM signal was generated given a set of randomly generated BPSK or QPSK symbols; subsequently, the OFDM signal was distorted both by the bandpass non-linearity and AWGN; finally, the received OFDM signal was detected in accordance to the procedure described in chapter 4, giving a set of BPSK or QPSK symbols. The overall BER, the BER in the sub-channel on the edge of the band and the BER in the sub-channel in the centre of the band were obtained by comparing the appropriate transmitted symbols to the appropriate received symbols using Monte Carlo techniques [136]. In the BPSK case, the comparison of transmitted to received symbols yielded directly the BERs. In the QPSK case, we have compared the bits that correspond to the transmitted symbols to the bits that correspond to the received symbols by assuming Gray coding. For example, if $A^{j\pi/4}$ was transmitted (which, for example, conveys the two-bit word 11) and $A^{j3\pi/4}$ was received (which, for example, conveys the two-bit word 10) then a single bit error in the two-bit word results. The simulation sampling frequency was chosen so that the highest frequency component in the non-linearly distorted OFDM signal could be accounted for[23].

A comparison of the error probability approximation performance of the various schemes in the frequency independent non-linearity case is shown in Figure 5.30 and Figure 5.31. The first figure shows the overall BER, the BER in the sub-channel on the

[23] Again, note that we have used MATLAB to obtain both analytic and simulation results. Analytic BER results were determined by using MATLAB as a calculator, where we have effectively implemented and solved all the mathematical relations and expressions. Simulation BER results were determined by using MATLAB as a simulator, where we have implemented all the underlying processes unfolding in time.

edge of the band and the BER in the sub-channel in the centre of the band against E_b/N_0 for non-linearly distorted OFDM/BPSK signals whereas the second figure shows identical results for non-linearly distorted OFDM/QPSK signals. Essentially, these results confirm the observations of section 5.2.2. For low E_b/N_0 values, when the error rate is normally high, the various approximations yield identical results because in this case the tails of the approximation distributions, where they mostly differ, do not play any significant role in defining such an error rate. Conversely, for high E_b/N_0 values, when the error rate is normally low, the various approximations do not yield identical results anymore. In this case, one can notice that the generalised Gaussian approximation does not give such accurate results as does the Pearson approximation. Moreover, the Pearson approximation not only estimates properly the error rate in the sub-channel on the edge of the band and the error rate in the sub-channel in the centre of the band but also the overall error rate, giving us confidence that such an approximation is in fact appropriate for each sub-channel. One can also notice that for a 48 sub-channel OFDM system a Laplace approximation tends to give better results when compared to a Gaussian approximation because for such a number of OFDM sub-channels the IMD distribution is characterised by relatively heavy tails.

Finally, it is important to note that it has occasionally been suggested that the error probability performance of each OFDM sub-channel is practically the same [23-25,65,66]. For low E_b/N_0 values, when the noise contribution to the error rate dominates with respect to the non-linearity contribution, then the error probability of each sub-channel is indeed similar. However, for high E_b/N_0 values, when it is not the noise contribution but the non-linearity contribution that is the dominant one, then the error probability of each OFDM sub-channel is not similar anymore (see Figure 5.30 and Figure 5.31, where the error rate in the sub-channel on the edge of the band differs from the error rate in the sub-channel in the centre of the band by about two orders of magnitude). This is not an unexpected result because the variance of the IMD for the sub-channel in the centre is larger than the variance of the IMD for the sub-channel on the edge (see Table 5.1). Moreover, the tails of the IMD distribution in the sub-channel in the centre are heavier than the tails of the IMD distribution in the sub-channel on the edge (see section 5.2.2). The error probability performance of each OFDM sub-channel is different not only for systems that exhibit third-order non-linear behaviour but also for systems that exhibit higher-order non-linear behaviour, as shown in the next chapter.

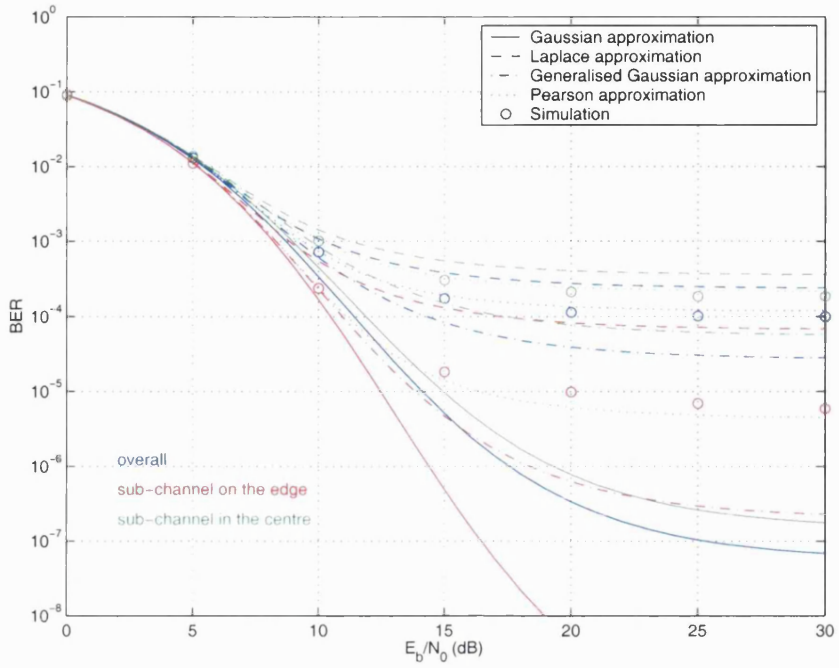

Figure 5.30: Approximations for the overall BER, the BER in the sub-channel on the edge of the band, and the BER in the sub-channel in the centre of the band of a 48 sub-channel OFDM/BPSK signal distorted by the frequency independent non-linearity.

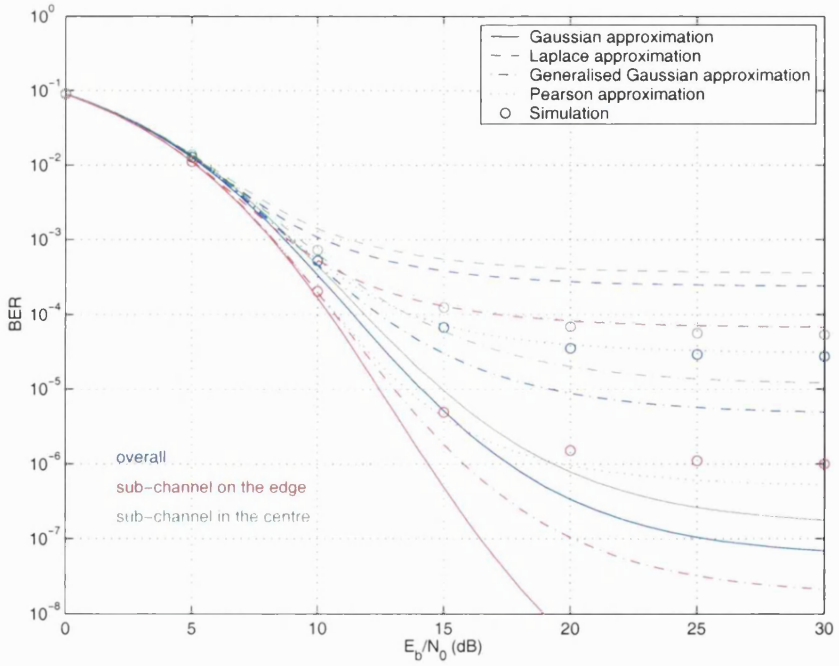

Figure 5.31: Approximations for the overall BER, the BER in the sub-channel on the edge of the band, and the BER in the sub-channel in the centre of the band of a 48 sub-channel OFDM/QPSK signal distorted by the frequency independent non-linearity.

Table 5.1: Variances of the real part of the IMD in selected sub-channels for the 48 sub-channel OFDM/BPSK and OFDM/QPSK signals distorted by the frequency independent non-linearity.

	Sub-channel on the edge	Sub-channel in the centre
OFDM/BPSK	0.62×10^{-9}	0.96×10^{-9}
OFDM/QPSK	0.32×10^{-9}	0.48×10^{-9}

Table 5.2: Variances of the real part of the IMD in selected sub-channels for the 48 sub-channel OFDM/BPSK and OFDM/QPSK signals distorted by the frequency dependent non-linearity.

	Sub-channel on the edge	Sub-channel in the centre
OFDM/BPSK	1.02×10^{-9}	0.90×10^{-9}
OFDM/QPSK	0.53×10^{-9}	0.44×10^{-9}

Similar trends are also observed in the frequency dependent non-linearity case, as shown in Figure 5.32 and Figure 5.33. Again, the first figure shows the overall BER, the BER in the sub-channel on the edge of the band and the BER in the sub-channel in the centre of the band against E_b/N_0 for non-linearly distorted OFDM/BPSK signals whereas the second figure shows identical results for non-linearly distorted OFDM/QPSK signals. However, there is a fundamental difference between the frequency independent and the frequency dependent non-linearity cases. In the former, the error rate performance in each sub-channel is equal at low E_b/N_0 values and differs only at high E_b/N_0. In the later, more complex behaviour arises because not only does the receiver's equaliser enhance the noise variance differently in each sub-channel but it also enhances the IMD variance differently in each sub-channel. For example, in the frequency independent non-linearity case the IMD variance in the sub-channel in the centre is larger than the IMD variance in the sub-channel on the edge (see Table 5.1). In the frequency dependent non-linearity case the IMD variance in the sub-channel on the edge is larger than the IMD variance in the sub-channel in the centre (see Table 5.2).

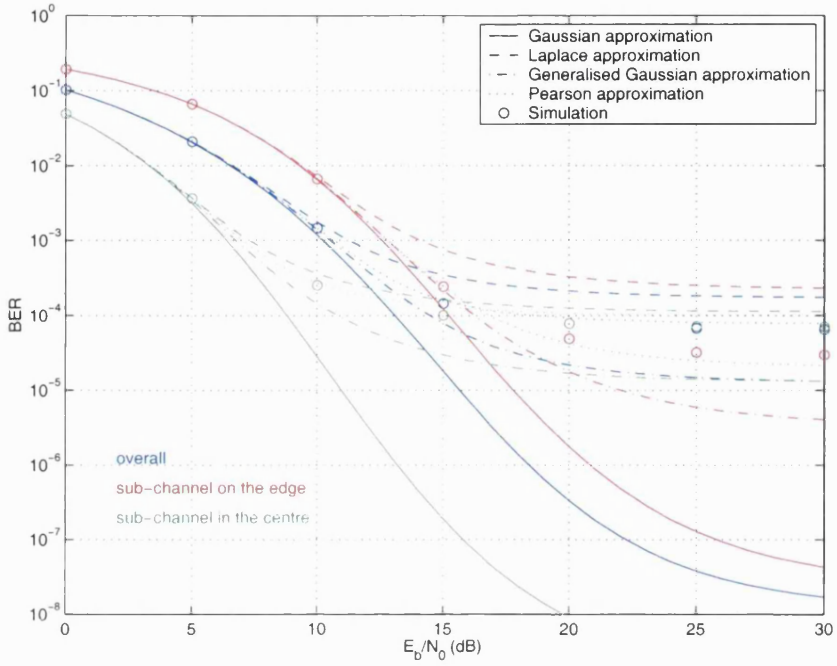

Figure 5.32: Approximations for the overall BER, the BER in the sub-channel on the edge of the band, and the BER in the sub-channel in the centre of the band of a 48 sub-channel OFDM/BPSK signal distorted by the frequency dependent non-linearity.

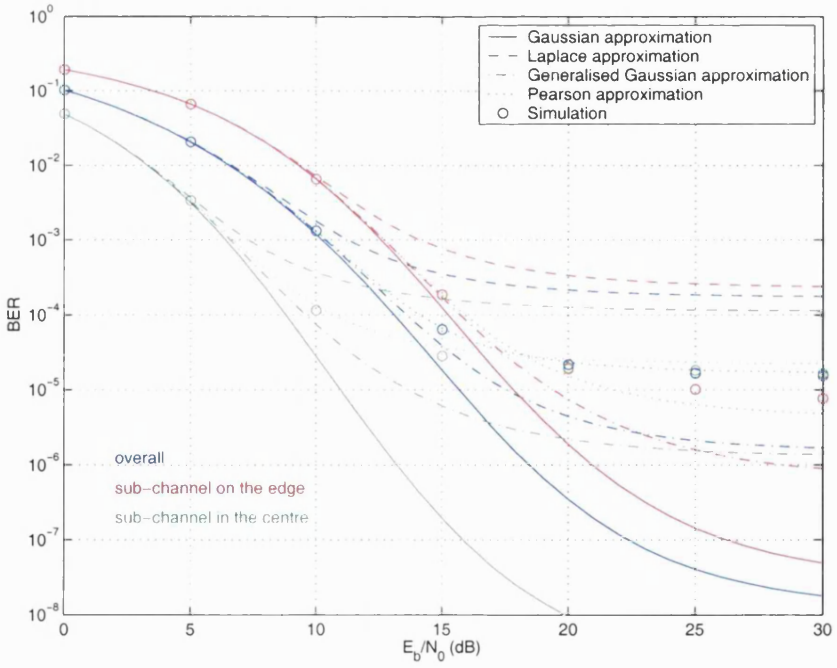

Figure 5.33: Approximations for the overall BER, the BER in the sub-channel on the edge of the band, and the BER in the sub-channel in the centre of the band of a 48 sub-channel OFDM/QPSK signal distorted by the frequency dependent non-linearity.

5.4 Considerations on the behaviour of non-linearly distorted OFDM signals

In this chapter, we have presented a variety of results which have provided further insight into the behaviour of non-linearly distorted OFDM signals. For example, we have shown in section 5.2 that a Gaussian approximation to the IMD distribution is not always appropriate and we have shown in section 5.3 that the error probability performance in each OFDM sub-channel is not always identical. In this section, we present another result related to the behaviour of non-linearly distorted OFDM signals.

The origin of this result rests on the following argument: On the one hand, by increasing the number of OFDM sub-channels the number of IMPs also increases and hence so do the support and the variance of the IMD distribution. On the other hand, by increasing the number of OFDM sub-channels the heaviness of the tails of the IMD distribution diminishes. An increase in the support and the variance of the IMD distribution implies an increase in the error rate whereas a decrease in the heaviness of the tails of the IMD distribution implies a decrease in the error rate. Consequently, it is feasible that a worst number of OFDM sub-channels may exist from the error rate point of view in the presence of non-linear distortion and AWGN. To verify this conjecture we have obtained by means of simulation the overall BER for OFDM/BPSK signals with 8 to 256 sub-channels distorted by the same frequency independent and frequency dependent non-linearities and corrupted by AWGN (see Figure 5.29). We have obtained the BER for different OBO values and different E_b/N_0 values. Observation of Figure 5.34 and Figure 5.35 reveals that there is indeed a worst number of OFDM sub-channels both in the frequency independent and the frequency dependent non-linearity cases. It is interesting to note that this trend is particularly evident for high E_b/N_0 values for which the non-linearity contribution to the error rate dominates with respect to the noise contribution. It is also interesting to note that this trend is valid for the different OBO values and hence for different degrees of intensity of non-linear behaviour. Essentially, this result shows that, in the presence of non-linear distortion and AWGN, an OFDM signal with a relatively high number of sub-channels N_1 performs better that an OFDM signal with a relatively low number of sub-channels N_2 provided that both N_1 and N_2 are greater than the worst number of OFDM sub-channels. This important result should be the subject of future investigations in the field.

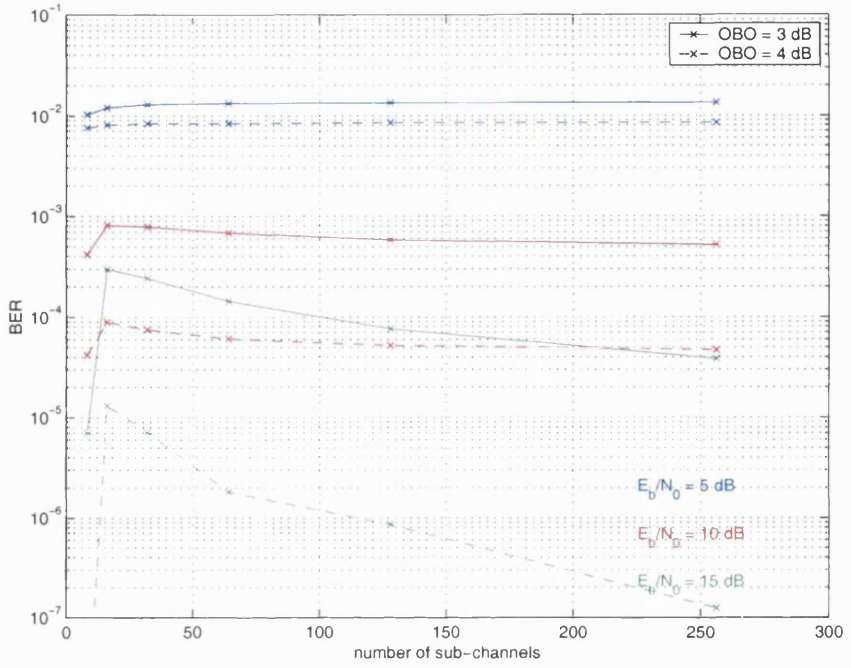

Figure 5.34: BER against number of OFDM sub-channels for OFDM/BPSK signals distorted by the frequency independent non-linearity.

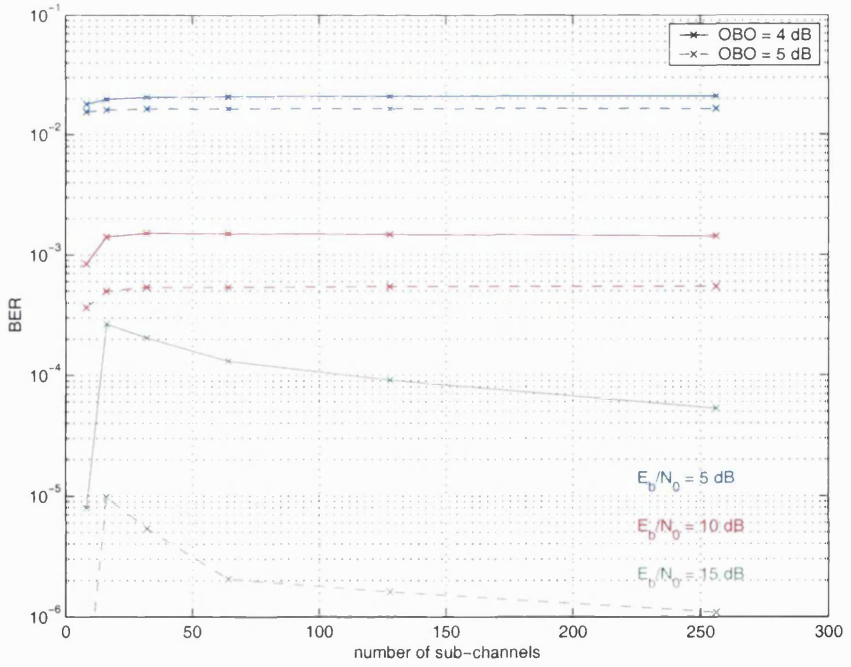

Figure 5.35: BER against number of OFDM sub-channels for OFDM/BPSK signals distorted by the frequency dependent non-linearity.

5.5 Summary

In this chapter, we have analysed different approximation/estimation techniques for the IMD distribution and the error probability of non-linearly distorted OFDM/BPSK and OFDM/QPSK signals.

Initially, as a means to select appropriate approximations/estimations for the IMD distribution, we have examined the properties of the IMD RV for OFDM/BPSK and OFDM/QPSK signals with different numbers of sub-channels distorted by both a frequency independent and a frequency dependent non-linearity exhibiting up to third-order non-linear behaviour. We have shown that the IMD distribution is generally characterised by different rates of tail decay, which depend on the number of OFDM sub-channels, the location of the specific OFDM sub-channel (e.g., edge or centre) and the type of modulation (e.g., BPSK or QPSK). Particularly, we have verified that heavy tailed behaviour corresponds to a low number of OFDM sub-channels, the sub-channel in the centre and BPSK modulation whereas approximately Gaussian behaviour corresponds to a high number of OFDM sub-channels, the sub-channel on the edge and QPSK modulation. Moreover, we have also shown that skewness and kurtosis values of the IMD RVs do not significantly depend on the non-linearity type and hence, if known *a priori* for a reference non-linearity, these statistical measures could be used to enhance the approximation/estimation for the IMD distribution.

Subsequently, we have analysed approximation techniques to describe the IMD behaviour that, on the one hand, allow for distributions with different rates of tail decay and, on the other hand, allow for a Gaussian distribution as a particular case. These included Gaussian, Laplace, generalised Gaussian and Pearson approximations. We have also analysed estimation techniques that require a limited number of moments to describe the IMD behaviour, such as maximum entropy and minimum relative entropy estimations. We have investigated the relative performance of the various approximation and estimation techniques for the IMD distribution of a range of OFDM signals distorted both by a frequency independent and a dependent non-linearity linearity exhibiting up to third-order non-linear behaviour. We have verified that Gaussian, Laplace and generalised Gaussian approximations only apply to particular cases whereas Pearson approximations always apply. We have also verified that maximum entropy and minimum relative entropy estimations always fail to provide adequate approximations in this case.

Finally, we have investigated the relative performance of the various approximation techniques for the error probability of a range of OFDM signals distorted both by the frequency independent and the frequency dependent non-linearity exhibiting up to third-order non-linear behaviour. Again, we have verified that Gaussian, Laplace and generalised Gaussian approximations only apply to particular cases whereas Pearson approximations always apply.

In this chapter, we have also provided further insight into the behaviour of non-linearly distorted OFDM signals, which has been overlooked in the open literature. For example, we have established that a Gaussian approximation to the IMD distribution is not always appropriate and that the error probability performance of each OFDM sub-channel is not always identical. We have also established that, in the presence of non-linear distortion and AWGN, there is a worst number of OFDM sub-channels from the error probability point of view.

In the next chapter, we investigate the application of the techniques developed in this thesis to two particular IM/DD fibre-radio systems. One of the systems relies on the direct modulation of a laser source and exhibits frequency dependent non-linear behaviour. The other system relies on the external modulation of a laser source and exhibits frequency independent non-linear behaviour.

Chapter 6

Applications to IM/DD fibre-radio systems

6.1 Introduction

The main motivation behind the development of the analytic techniques detailed in chapters 3, 4 and 5 was the application to fibre-radio systems. In this chapter, we consider the application of such analytic techniques to two particular IM/DD fibre-radio systems, where one relies on the direct modulation of the intensity of a laser source and the other relies on the external modulation of the intensity of a laser source to generate the OFDM signals bearing optical waves to be delivered over optical fibre between CSs and BSs.

This chapter is organised as follows: Section 6.2 introduces the fibre-radio concept. Section 6.3 and section 6.4 consider the application of the PDS and the error probability techniques to the fibre-radio systems under consideration. In these sections, merits and demerits of the techniques are discussed by comparing analytic to simulation results and further new results related to the behaviour of non-linearly distorted OFDM signals are presented. Finally, section 6.5 summarises the main contributions of this chapter. Two papers have resulted from the research work presented in this chapter [161,162].

6.2 The fibre-radio concept

Recently, fibre-radio technology has been proposed to interconnect CSs and BSs in a number of wireless systems such as mobile communication systems, fixed broadband access communication systems, wireless LANs and also traffic monitoring and guidance systems [8-12].

The topology of a generic fibre-radio based wireless system is shown in Figure 6.1. On the downlink, the CS generates an optical wave bearing the outgoing RF signal to be delivered to the BS over an optical network. The BS retrieves the RF signal using standard optical technology and then amplifies it and radiates it to an MS. On the uplink, it is the BS that generates the optical wave bearing the incoming RF signal to be delivered to the CS over an optical network and it is the CS that retrieves the RF signal using standard optical technology.

A fibre-radio based wireless system offers potential benefits when compared to conventional wireless systems [8-12]. Major benefits are:

- Low loss and high bandwidth transmission. These properties are associated with the optical fibre transmission mechanisms.

- Simplification of the BS. The BS does not perform radio interface operations such as coding/decoding, modulation/demodulation and up-conversions/down-conversions to/from RF. The BS merely retrieves the RF signal from the incoming optical wave to be transmitted to the MS and generates an outgoing optical wave bearing the RF signal received from the MS using standard optical technology.

- Centralisation and sharing of complex equipment at the CS. Radio interface equipment is centralised at the CS and hence it is shared among a number of BSs.

- Lower complexity and costs. Simplification of the BS and centralisation and sharing of complex equipment at the CS are associated with lower complexity and costs.

These potential benefits are particularly important for wireless systems with micro-cell (around 1 km diameter) and pico-cell (around 100 m diameter or less) architectures for which lowering of complexity and costs are of utmost importance.

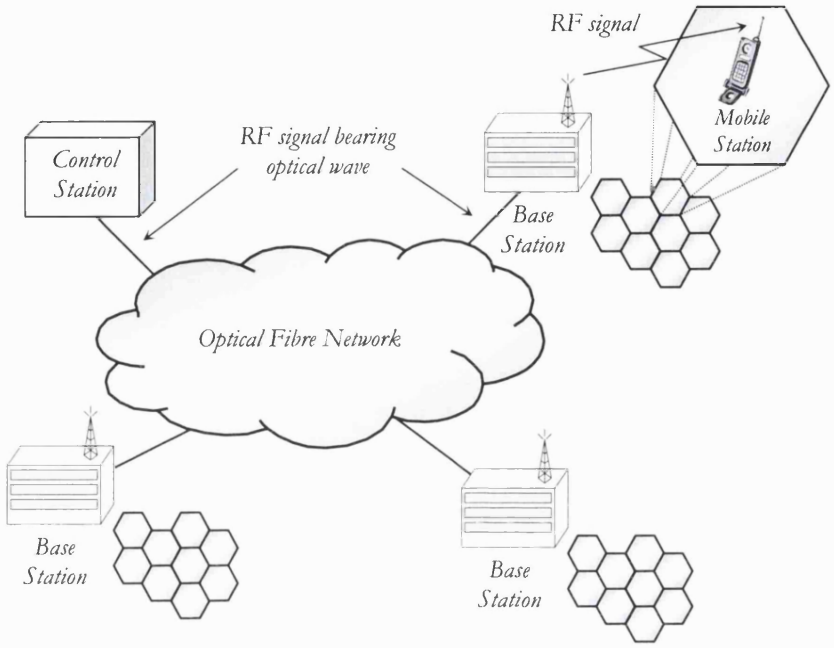

Figure 6.1: Topology of a generic fibre-radio based wireless system.

Over the years, a number of alternatives have been proposed to realise optical transport of an RF signal between CSs and BSs. At lower RF frequencies, direct modulation or external modulation of a laser source can be used to generate an RF intensity modulated optical wave for transmission over the fibre. Direct detection of the RF intensity modulated optical wave in a PIN photodiode then yields a photocurrent which is a replica of the RF bearing information signal [8-10]. At higher RF frequencies, optical transport of an RF signal between CSs and BSs is realised by using self-heterodyne techniques [11,12].

In the following sections, we will consider specifically the application of the analytic techniques detailed in chapters 3, 4 and 5 to two particular IM/DD fibre-radio systems. The first system (section 6.3) relies on the direct modulation of the intensity of a laser source and the second system (section 6.4) on the external modulation of the intensity of a laser source to generate the OFDM signals bearing optical waves to be delivered over optical fibre between CSs and BSs. The former exhibits frequency dependent non-linear behaviour while the later frequency independent non-linear behaviour. We shall not

consider a comparison of the relative merits of each system but merely the application of the PDS and the error probability techniques.

6.3 IM/DD fibre-radio system based on the direct modulation of an LD

In this section, we apply the results developed in chapter 3, chapter 4 and chapter 5 to the IM/DD fibre-radio system model shown in Figure 6.2, which relies on the direct modulation of an LD to generate an OFDM intensity modulated optical wave to be delivered over optical fibre to a remote location. Direct detection of the intensity modulated optical wave in a PIN photodiode then yields a photocurrent which is a replica of the OFDM signal. Note that we are specifically addressing the downlink case. Analysis of the uplink case is more complex because the certainly frequency selective radio channel induces different attenuations and phase rotations in each sub-carrier of the incoming RF OFDM signal, a situation that the developed analytical treatments do not account for.

Some of degradation factors that may exist in this fibre-radio system are LD induced non-linear distortion [163,164], laser intensity and phase noise [163,164], laser chirp-fibre dispersion interaction and receiver shot and thermal noise [165,166]. In out study, however, the only impairments considered are LD non-linearities and receiver thermal noise.

In the following sections, we start by describing the model of the non-linear element in the system, the LD model, so as to derive its transfer functions. Finally, analysis of the application of the PDS and the error probability techniques to the fibre-radio system under consideration is carried out by comparing analytical to simulation results. This analysis is carried out at the output of the bandpass filter.

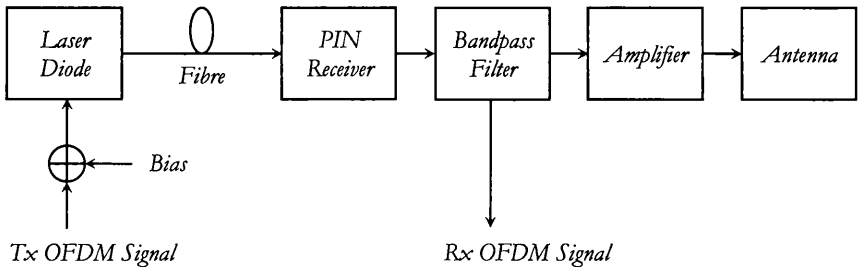

Figure 6.2: Fibre-radio system based on the direct modulation of an LD.

6.3.1 LD model

A laser is a device that emits radiation with high spatial and temporal coherence. Laser action can occur when light interacts with matter and is the result of three basic processes: photon absorption, spontaneous emission and stimulated emission. These three processes are represented for a simple two-energy-level system in Figure 6.3. In this figure, E_1 is the ground state energy and E_2 is the excited state energy, the circles represent electrons and incident photons are shown on the left and emitted photons are shown on the right. According to Planck's law, electron transitions between these two energy states involve the absorption or emission of a photon of energy $E_2 - E_1 = h\nu_{12}$, where h is the Planck's constant and ν_{12} is the frequency of the photon. If an electron is initially in the ground state it can make a transition to the higher energy state when a photon with energy $E_2 - E_1 = h\nu_{12}$ is absorbed. Conversely, if an electron is initially in the excited state it can make a transition to the lower energy state when a photon with energy $E_2 - E_1 = h\nu_{12}$ is emitted. This last process can occur either by spontaneous emission, when the electron returns to the lower energy state in an entirely random manner, or by stimulated emission, when it is a second photon of the same energy $E_2 - E_1 = h\nu_{12}$ that triggers the emission of the first photon. Spontaneous emissions are isotropic and of random phase and hence are associated with the non-coherent emission of light. Stimulated emissions, on the other hand, are associated with the coherent emission of light since both photons involved in the process have exactly the same frequency, phase and polarization. Stimulated emission processes are therefore exploited by lasers to achieve the emission of radiation of high spatial and temporal coherence.

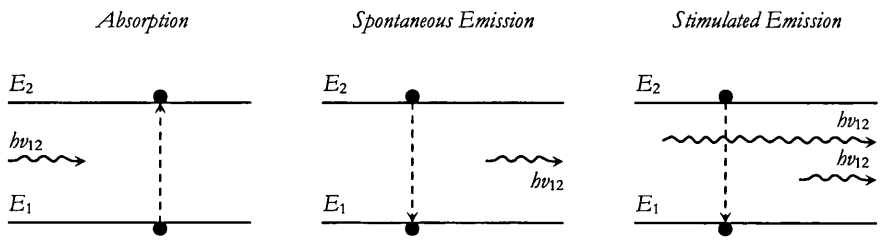

Figure 6.3: Energy state diagram for a simple two-energy-level system showing photon absorption, spontaneous emission and stimulated emission.

The basic structure of a laser is shown in Figure 6.4. The external energy source, or the pumping mechanism, is required to increase the number of electrons in the excited energy state beyond the number of electrons in the ground energy state (a situation known as population inversion) so that stimulated emission processes outnumber absorption processes[24]. The pair of partially transmitting mirrors, or the feedback mechanism, is required to contain a number of photons in the laser cavity so that stimulated emission processes outnumber spontaneous emission processes. Lasing operation therefore occurs for wavelengths that correspond to the laser cavity resonance frequencies provided that the gain in the laser cavity due to stimulated emission is greater than the losses in the cavity due to spontaneous emission and scattering [167].

The principles described above are common to different classes of lasers, i.e., gas, liquid and solid-state lasers and semiconductor LDs. In LDs, however, transitions occur between continuous distributions of energy states in the conduction and valence bands in the active region of a forward biased p-n junction and population inversion is achieved by injecting current into the active region of the forward biased p-n junction. Different LD structures have been proposed throughout the years to improve deficiencies associated with LDs [168]. Although different LD structures have different operational parameters, the basis of operation is the same and the model discussed below applies to most LDs.

The modulation dynamics of an LD are modelled by the laser rate equations which relate the injected current I into the laser active region to the carrier density N and the photon density P in the laser active region. The laser rate equations are given by [169-172]

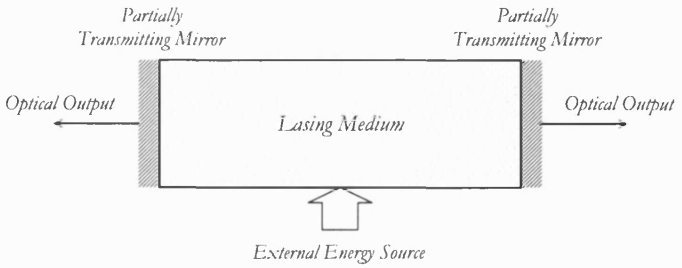

Figure 6.4: Basic structure of a laser.

[24] Note that in thermal equilibrium the number of electrons in the ground energy state is greater than the number of electrons in the excited energy state so that absorption processes outnumber stimulated emission processes.

$$\frac{dN}{dt} = \frac{I}{qV} - \frac{N}{\tau_s} - g_0(N - N_{0m})(1 - \varepsilon P)P \tag{6.1}$$

$$\frac{dP}{dt} = \left[\Gamma g_0(N - N_{0m})(1 - \varepsilon P) - \frac{1}{\tau_p}\right]P + \Gamma\beta\frac{N}{\tau_s} \tag{6.2}$$

where Γ is the optical confinement factor, g_0 is the gain slope constant, N_{0m} is the carrier density at which the net gain is zero, τ_p is the photon lifetime, τ_s is the electron lifetime, β is the fraction of spontaneous emission coupled into the lasing mode, V is the volume of the active region and q is the electronic charge. The parameter ε specifies the gain compression characteristics of the active region.

Equation (6.1) states that the time rate of change of carrier density in the laser active region is proportional to the rate of injected carriers, the rate of reduction in carriers due to spontaneous emission and the rate of reduction in carriers due to stimulated emission. Equation (6.2) states that the time rate of change of photon density in the laser active region is proportional to the fraction Γ of stimulated emitted photons which are confined into the laser active region, the rate of loss of photons and the fraction β of spontaneous emitted photons which are coupled into the lasing mode. Gain compression enters the laser rate equations by the factor $(1 - \varepsilon P)$ and has important implications for the linearity characteristics of an LD [171,172].

The laser rate equations have been conventionally used to model the effect of laser non-linearity in certain optical fibre communication systems such as sub-carrier multiplexing (SCM) optical fibre communication systems [129-131,173]. These equations cannot be used to model the laser static and clipping non-linearities but the laser dynamic non-linearity. Static non-linearity is associated with the imperfect linearity in the static light-power versus current laser characteristics whereas dynamic non-linearity is associated with a resonant frequency in the laser frequency response [171,172]. Clipping non-linearity occurs when the LD p-n junction is reverse biased [171,172]. The exact region of validity of the laser rate equations model depends on the laser modulation frequency. For high modulation frequencies (more than 1 GHz) the dynamic non-linearity is the most important and hence the rate equations are adequate. Conversely, for low modulation frequencies (a couple of MHz) the static and the clipping non-linearities are the most important and hence the rate equations are not adequate.

Table 6.1: Parameter values for the Ortel-1510B laser.

$V\,(m^3)$	0.80×10^{-16}
β	2×10^{-3}
Γ	0.37
$\varepsilon\,(m^3)$	3.1×10^{-23}
$g_0\,(m^3 s^{-1})$	3.5×10^{-12}
$N_{0m}\,(m^{-3})$	1.27×10^{24}
$\tau_s\,(ns)$	1.64
$\tau_p\,(ps)$	1.0
η_i	1
η_d	0.0255
$I_{th}\,(mA)$	16.0

The LD output optical power is given by [169-172]

$$P_{out} = \frac{h\nu\eta_d VP}{2\Gamma\eta_i\tau_p} \tag{6.3}$$

where h is Planck's constant, ν is the frequency of operation (optical frequency), η_i is the internal quantum efficiency of the laser and η_d is the differential quantum efficiency of the laser.

In our modelling, we consider a specific LD (Ortel 1510B) designed for microwave applications in the frequency range 0.01-6 GHz [174]. The parameter values for this LD are shown in Table 6.1. The drive circuit and the chip and package parasitics for this LD can be modelled using a first-order Butterworth filter with a 3 dB bandwidth of 4 GHz. The threshold current of this LD, i.e., the current at which stimulated emission starts, is equal to 16.0 mA.

6.3.2 LD transfer functions

In the IM/DD fibre-radio system under consideration the LD output lightwave intensity is directly modulated about a bias point by the time-varying OFDM signal. This is shown in Figure 6.5 where we use the static output power (P_{out}) versus input current (I)

characteristics of an LD to illustrate such concept. Thus, the input current I consists of a steady-state component I_0 plus a time-varying component $I(t)$, i.e.,

$$I = I_0 + I(t) \tag{6.4}$$

and similarly the carrier density N and the photon density P also consist of a steady-state component, N_0 and P_0, respectively, plus a time-varying component, $N(t)$ and $P(t)$, respectively, i.e,

$$N = N_0 + N(t) \tag{6.5}$$

and

$$P = P_0 + P(t) \tag{6.6}$$

The steady-state components satisfy the following system of equations

$$\frac{dN_0}{dt} = \frac{I_0}{qV} - \frac{N_0}{\tau_s} - g_0(N_0 - N_{0m})(1 - \varepsilon P_0)P_0 = 0 \tag{6.7}$$

$$\frac{dP_0}{dt} = \left[\Gamma g_0(N_0 - N_{0m})(1 - \varepsilon P_0) - \frac{1}{\tau_p}\right]P_0 + \Gamma\beta\frac{N_0}{\tau_s} = 0 \tag{6.8}$$

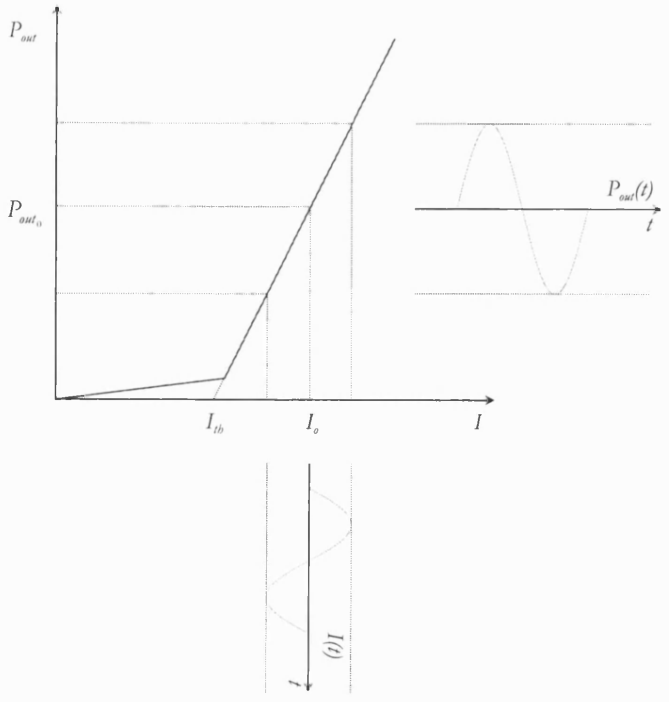

Figure 6.5: Analogue modulation of an LD.

and the time-varying components satisfy the following system of differential equations

$$\frac{dN(t)}{dt} = \frac{(I_0 + I(t))}{qV} - \frac{(N_0 + N(t))}{\tau_s} - g_0((N_0 + N(t)) - N_{0m})(1 - \varepsilon(P_0 + P(t)))(P_0 + P(t)) \quad (6.9)$$

$$\frac{dP(t)}{dt} = \left[\Gamma g_0((N_0 + N(t)) - N_{0m})(1 - \varepsilon(P_0 + P(t))) - \frac{1}{\tau_p}\right](P_0 + P(t)) + \Gamma\beta\frac{(N_0 + N(t))}{\tau_s} \quad (6.10)$$

We shall now determine the transfer functions of the LD that relate the time-varying component of the current to the time-varying component of the carrier density and the photon density and hence ultimately the transmitted OFDM signal and the received OFDM signal in the fibre-radio system under consideration, as shown later. The transfer functions of the LD are determined by applying the harmonic input method (described in chapter 3) to (6.9) and (6.10) simultaneously. Thus, the nth-order transfer functions $G_n(f_1,\ldots,f_n)$ and $H_n(f_1,\ldots,f_n)$ associated with the time-varying components of the carrier density and the photon density, respectively, are obtained by letting the time-varying component of the current be the sum of n complex exponentials

$$I(t) = \sum_{k=1}^{n} e^{j2\pi f_k t} \quad (6.11)$$

and noting that the time-varying components of the carrier density and the photon density are given by

$$N(t) = \sum_{k_1=1}^{n} G_1(f_{k_1}) e^{j2\pi f_{k_1} t} + \sum_{k_1=1}^{n}\sum_{k_2=1}^{n} G_2(f_{k_1}, f_{k_2}) e^{j2\pi(f_{k_1}+f_{k_2})t} + \cdots \quad (6.12)$$

$$P(t) = \sum_{k_1=1}^{n} H_1(f_{k_1}) e^{j2\pi f_{k_1} t} + \sum_{k_1=1}^{n}\sum_{k_2=1}^{n} H_2(f_{k_1}, f_{k_2}) e^{j2\pi(f_{k_1}+f_{k_2})t} + \cdots \quad (6.13)$$

By substituting (6.11), (6.12) and (6.13) in (6.9) and (6.10) we find that the nth-order transfer functions $G_n(f_1,\ldots,f_n)$ and $H_n(f_1,\ldots,f_n)$ satisfy the system of equations given below

$$G_n(f_1,\ldots,f_n)\psi(f_1+\cdots+f_n) = -D_n - H_n(f_1,\ldots,f_n)g_0(N_0 - N_{0m})(1 - 2\varepsilon P_0) \quad (6.14)$$

$$H_n(f_1,\ldots,f_n)\chi(f_1+\cdots+f_n) = \Gamma C_n + G_n(f_1,\ldots,f_n)\Gamma[g_0(1-\varepsilon P_0)P_0 + \beta/\tau_s] \quad (6.15)$$

Table 6.2: Terms in (6.16) and (6.17): $C_1 = 0$, $C_2 = D_2$ and $C_3 = D_3$.

n	D_n
1	$-\frac{1}{qV}$
2	$\frac{1}{2}g_0(1-2\varepsilon P_0)[G_1(f_1)H_1(f_2)+G_1(f_2)H_1(f_1)]-g_0\varepsilon(N_0-N_{0m})H_1(f_1)H_1(f_2)$
3	$\frac{1}{3}g_0(1-2\varepsilon P_0)[G_1(f_1)H_2(f_2,f_3)+G_1(f_2)H_2(f_1,f_3)+G_1(f_3)H_2(f_1,f_2)$ $+G_2(f_1,f_2)H_1(f_3)+G_2(f_1,f_3)H_1(f_2)+G_2(f_2,f_3)H_1(f_1)]$ $-\frac{2}{3}g_0\varepsilon(N_0-N_{0m})[H_1(f_1)H_2(f_2,f_3)+H_1(f_2)H_2(f_1,f_3)+H_1(f_3)H_2(f_1,f_2)]$ $-\frac{1}{3}g_0\varepsilon[G_1(f_1)H_1(f_2)H_1(f_3)+G_1(f_2)H_1(f_1)H_1(f_3)+G_1(f_3)H_1(f_1)H_1(f_2)]$

Solving (6.14) and (6.15) for $G_n(f_1,\ldots,f_n)$ and $H_n(f_1,\ldots,f_n)$ yields

$$G_n(f_1,\ldots,f_n)=\frac{-D_n\chi(f_1+\cdots+f_n)-C_n\Gamma g_0(N_0-N_{0m})(1-2\varepsilon P_0)}{\varphi(f_1+\cdots+f_n)} \tag{6.16}$$

$$H_n(f_1,\ldots,f_n)=\frac{-D_n\Gamma[g_0(1-\varepsilon P_0)P_0+\beta/\tau_s]+C_n\Gamma\psi(f_1+\cdots+f_n)}{\varphi(f_1+\cdots+f_n)} \tag{6.17}$$

where

$$\psi(f)=j2\pi(f)+g_0(1-\varepsilon P_0)P_0+1/\tau_s \tag{6.18}$$

$$\chi(f)=j2\pi(f)-\Gamma g_0(N_0-N_{0m})(1-2\varepsilon P_0)+1/\tau_p \tag{6.19}$$

$$\varphi(f)=\psi(f)\chi(f)+\Gamma[g_0(1-\varepsilon P_0)P_0+\beta/\tau_s]g_0(N_0-N_{0m})(1-2\varepsilon P_0) \tag{6.20}$$

and a number of terms D_n and C_n are given in Table 6.2. Note that (6.16), (6.17), (6.18), (6.19) and (6.20) are recursive expressions to compute $G_n(f_1,\ldots,f_n)$ and $H_n(f_1,\ldots,f_n)$ as a function of $G_{n-1}(f_1,\ldots,f_{n-1})$ and $H_{n-1}(f_1,\ldots,f_{n-1})$. Note also that from the transfer functions in (6.16) and in (6.17) we can clearly see that an LD exhibits frequency dependent non-linear behaviour and hence the fibre-radio system under consideration also exhibits such a type of non-linear behaviour, as mentioned earlier. The transfer functions of the LD determined in this section are used in the next section to obtain analytic results.

Finally, we note that the effect of the laser drive circuit and the laser chip and package parasitics are included in the analysis by letting $D_1 = -H_P(f)/qV$, where $H_P(f)$ is the frequency response of the parasitics [173].

6.3.3 Analytic and simulation results

6.3.3.1 PDS

In this section, we determine the PDS of an OFDM signal at the output of the bandpass filter of the fibre-radio system under consideration both by analysis and simulation. We have considered OFDM signals with $f_c = 2.5\,GHz$, $T = 1\,\mu s$, $T_{CP} = 0.2\,\mu s$, $N = 48$ and $\beta = 0.1$ (β is the raised cosine window rolloff factor). The modulation symbols conveyed in different time slots and different sub-channels were assumed to take any value from a BPSK signal constellation with equal probability and were assumed to be independent. The LD biasing current was set to $I_0 = 1.5I_{th}$ so as to achieve a relatively low resonance frequency and hence observable non-linear effects, the optical fibre was assumed only to attenuate the intensity of the optical signal by a factor A and the photodiode responsivity was set to $R = 0.8\,A/W$. No receiver thermal noise was considered in this study.

The PDS was obtained for specific modulation indices, which we have defined as follows

$$m_i = \frac{\sigma_I}{I_0 - I_{th}} \tag{6.21}$$

where I_0 is the LD biasing current, I_{th} is the LD threshold current and σ_I is the standard deviation of the time-varying component of the input current to the LD, i.e., the standard deviation of the OFDM signal. The modulation index was set by varying the power in the constellations of each OFDM sub-channel until a specified value, as given by (6.21), was achieved.

Analytic results were obtained by inserting the first three transfer functions of the fibre-radio system and the average PDS of the OFDM signal (see chapter 2) into the PDS expressions developed in chapter 3 and by carrying out the integrations numerically. The transfer functions of the fibre-radio system are given by

$$T_n(f_1, f_2, \ldots, f_n) = R\frac{1}{A}\frac{h\nu\eta_d V}{2\Gamma\eta_i\tau_p} H_n(f_1, f_2, \ldots, f_n) H_{bandpass}(f_1 + f_2 + \cdots + f_n) \tag{6.22}$$

where R is the photodiode responsivity, A is the fibre attenuation, $h\nu\eta_d V/2\Gamma\eta_i\tau_p$ is the LD photon density to output optical power conversion factor, $H_n(f_1, \ldots, f_n)$ is the LD

nth-order transfer function associated with the photon density and $H_{bandpass}(f)$ is the bandpass filter frequency response which is assumed to be ideal. Note that we have not included the effect of the HPDSs of the OFDM signal because we have shown in chapter 3 that these do not produce any significant difference. Note also that we have not included the effect of transfer functions of orders higher than three because our analytical treatment does not accommodate non-linear behaviour of order higher than three.

Simulation results were obtained by implementing the system shown in Figure 6.2 in MATLAB. Initially, the transmitted OFDM signal was generated given a set of randomly generated BPSK symbols; subsequently, the OFDM signal was conveyed through the fibre-radio system model; finally, the PDS of the received OFDM signal was estimated using the periodogram or direct method [136]. The rate equations model was implemented in SIMULINK by using a normalised version of the rate equations for numerical purposes [173]. The sampling frequency used in the simulations was chosen so that up to eleventh-order non-linear effects could be observed.

Figure 6.6 and Figure 6.7 show the PDS of the received OFDM signal for a modulation index of 0.3 and 0.5, respectively. Note that the horizontal axis has been normalised to the centre frequency and the 3 dB bandwidth of the OFDM signal, given by (2.34) and (2.35) respectively, and the vertical axis has been normalised to the maximum value of the PDS. For the lower modulation index, LD non-linear contributions of orders higher than three are negligible and hence analysis matches simulation. This is particularly the case in the normalised frequency range from – 1.5 to 1.5. Outside this frequency range there is a minor difference between analysis and simulation because a third-order representation of a non-linearity cannot predict IMD spectral components outside the normalised frequency range from – 1.5 to 1.5 as these are due to higher-order non-linear behaviour. For the higher modulation index, LD non-linear contributions of orders higher than three are not negligible and hence analysis does not match simulation. Differences between analytic and simulation results can be observed both in the normalised frequency range from – 1.5 to 1.5 and outside this frequency range. Consequently, we conclude that the analytic technique is appropriate as long as the modulation index is kept low when higher-order non-linear behaviour is negligible in comparison to third-order non-linear behaviour.

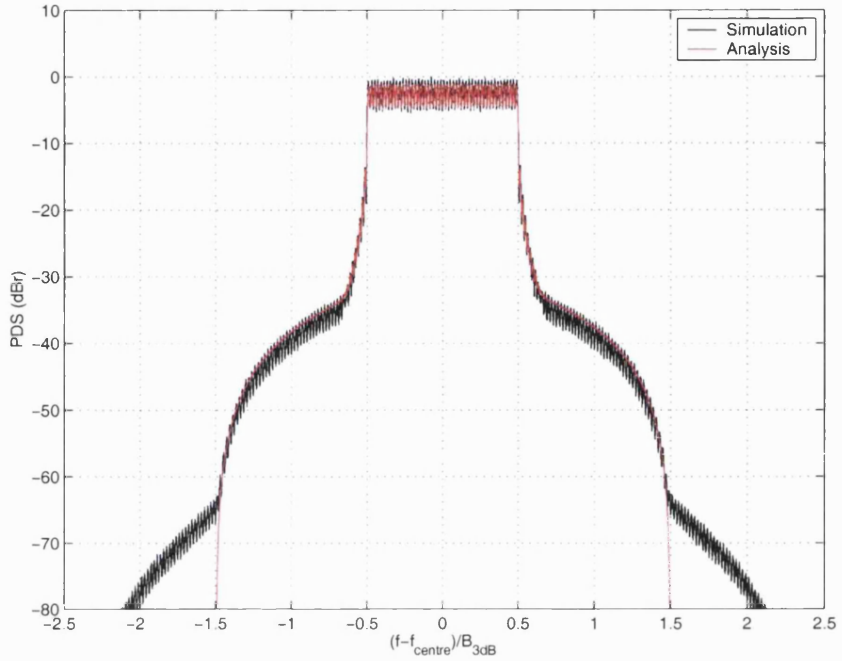

Figure 6.6: PDS of the received OFDM/BPSK signal for a modulation index equal to 0.3.

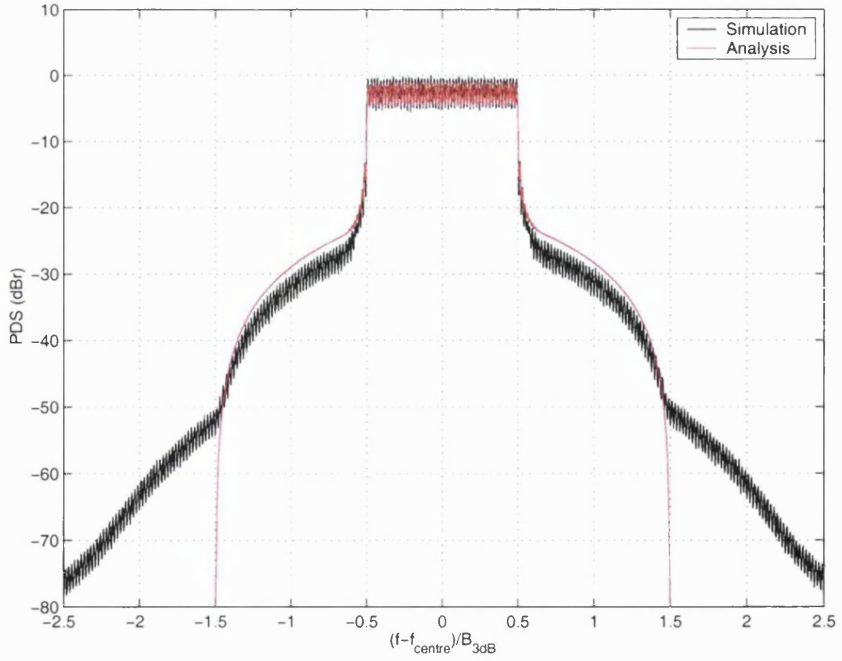

Figure 6.7: PDS of the received OFDM/BPSK signal for a modulation index equal to 0.5.

6.3.3.2 Distribution of the IMD and error probability

In this section, we determine the IMD distribution and the error probability of an OFDM signal at the output of the bandpass filter of the fibre-radio system under consideration both by analysis and simulation. Analytic results were obtained using Pearson approximations as these have proved to be the most accurate.

We have considered OFDM signals with $f_c = 2.5\,GHz$, $T = 1\,\mu s$, $T_{CP} = 0.2\,\mu s$, $N = 48$ and $\beta = 0.1$ (β is the raised cosine window rolloff factor). The modulation symbols conveyed in different time slots and different sub-channels were assumed to take any value from a BPSK signal constellation with equal probability or from a Gray coded QPSK signal constellation with equal probability and were assumed to be independent. Again, the LD biasing current was set to $I_0 = 1.5I_{th}$ so as to achieve a relatively low resonance frequency and hence observable non-linear effects, the optical fibre was assumed only to attenuate the intensity of the optical signal by a factor A and the photodiode responsivity was set to $R = 0.8\,A/W$. The power spectral density of the receiver's thermal noise, which was assumed to be white and Gaussian, was set to $100\times10^{-24}\,A^2/Hz$.

We have obtained the CDF of the real part of the IMD in the sub-channel on the edge of the band and in the sub-channel in the centre of the band conditioned on A in the OFDM/BPSK case and on $Ae^{j\pi/4}$ in the OFDM/QPSK case for various modulation indices as given by (6.21). We have also obtained the overall BER and the BERs in the sub-channel on the edge of the band and in the sub-channel in the centre of the band for various modulation indices as given by (6.21). The unmodulated optical power at the input of the photodiode was set to – 33.0 dBm in the OFDM/BPSK case and to – 31.5 dBm in the OFDM/QSPK case.

The Pearson approximation to the CDF of the real part of the IMD was defined first by using the first two moments of the real part of the IMD RV and its skewness and kurtosis values to obtain the parameters of the Pearson differential equation, then by integrating the Pearson differential equation to obtain the Pearson PDF and finally by shifting this PDF from the origin to the mean, as explained in chapter 5. The CDF was determined from the PDF by numerical integration in accordance to (5.12). The first two moments of the real part of the IMD RV were calculated as described in chapter 4 and its

skewness and kurtosis values were read from the tables in Appendix B. The Pearson approximation to the BERs was determined by using the Pearson PDFs to carry out the expectations that ultimately yield the BERs, as explained in chapter 5.

The equivalent baseband transfer functions of the fibre-radio system needed to calculate the moments of the RVs were determined from the transfer functions of the same system (see (6.22)), as described in chapter 4. Note that the bandpass filter in the fibre-radio system under consideration acts as a zonal filter. The fibre-radio system was represented by its first-order and third-order equivalent baseband transfer functions because our analytical treatment does not accommodate non-linear behaviour of orders higher than three.

Simulation results were determined from the fibre-radio system model implemented in MATLAB. An estimate to the CDF of the real part of the IMD in sub-channel n was obtained as follows: Initially, the transmitted OFDM signal was generated given a set of randomly generated BPSK or QPSK symbols and by setting the information conveyed in sub-channel n to A in the BPSK case or to $Ae^{j\pi/4}$ in the QPSK case; subsequently, the OFDM signal was conveyed through the fibre-radio system model in the absence of receiver's thermal noise; finally, the OFDM signal was detected in accordance to the procedure described in chapter 4 (without regeneration of the received symbols), giving a set of non-regenerated BPSK or QPSK symbols. Approximate samples of the real part of the IMD RV in sub-channel n were found by taking the difference of the real part of the non-regenerated received symbol in sub-channel n and the real part of the transmitted symbol in sub-channel n (see (4.45)). Given a large number of samples of the real part of the IMR RV in sub-channel n, $X_1, X_2, \ldots, X_N$, then an estimate $\hat{F}(x)$ to the CDF $F(x)$ of the real part of the IMD RV in sub-channel n was found through [136]

$$\hat{F}(x) = \begin{cases} 0, & x < X_1 \\ \dfrac{k}{N}, & X_k \le x < X_{k+1}, k = 1,2,\ldots,N-1 \\ 1, & x \ge X_N \end{cases} \tag{6.23}$$

Note that it is implicitly assumed that the samples $X_1, X_2, \ldots, X_N$ are written in increasing order, i.e., $X_1 < X_2 < \cdots < X_N$. Note also that this procedure differs from the procedure employed in chapter 5 because computation of samples of the RV under consideration in

accordance to (4.58) is extremely time consuming for non-linearities that exhibit non-linear behaviour of orders higher than three.

An estimate to the overall BER and the BERs in the sub-channel on the edge of the band and the sub-channel in the centre of the band were obtained as follows: Initially, the transmitted OFDM signal was generated given a set of randomly generated BPSK or QPSK symbols; subsequently, the OFDM signal was conveyed through the fibre-radio system model in the presence of receiver's thermal noise; finally, the OFDM signal was detected in accordance to the procedure described in chapter 4 (with regeneration of the received symbols), giving a set of regenerated BPSK or QPSK symbols. The overall BER, the BER in the sub-channel on the edge of the band and the BER in the sub-channel in the centre of the band were found by comparing the appropriate transmitted symbols to the appropriate received symbols using Monte Carlo techniques [136]. In the BPSK case, the comparison of transmitted to received symbols yielded directly the BERs. In the QPSK case, we have compared the bits that correspond to the transmitted symbols to the bits that correspond to the received symbols by assuming Gray coding. For example, if $A^{j\pi/4}$ was transmitted (which, for example, conveys the two-bit word 11) and $A^{j3\pi/4}$ was received (which, for example, conveys the two-bit word 10) then a single bit error in the two-bit word results.

The sampling frequency used in the IMD and the error probability simulations was chosen so that up to eleventh order non-linear effects could be accounted for.

Figure 6.8 through Figure 6.11 compare the CDF of the real part of the IMD obtained by analysis and simulation for specific modulation indices for each case under consideration. The distributions corresponding to different modulation indices were plotted by normalising the x-axis in the figures to the mean μ and the standard deviation σ obtained by analysis of the same distributions. Observation of these figures reveals that the Pearson approximation is appropriate at low modulation indices but it rapidly fails at higher modulation indices because higher-order non-linear behaviour not accounted for by analysis becomes increasingly important. The Pearson approximation fails in the strong signal regime because not only do the mean and variance obtained by analysis differ from the true mean and variance but also the skewness and kurtosis values used in analysis differ from the true skewness and kurtosis values. This can be verified by comparing the figures in Table 6.3 and Table 6.4 to the figures in Appendix B.

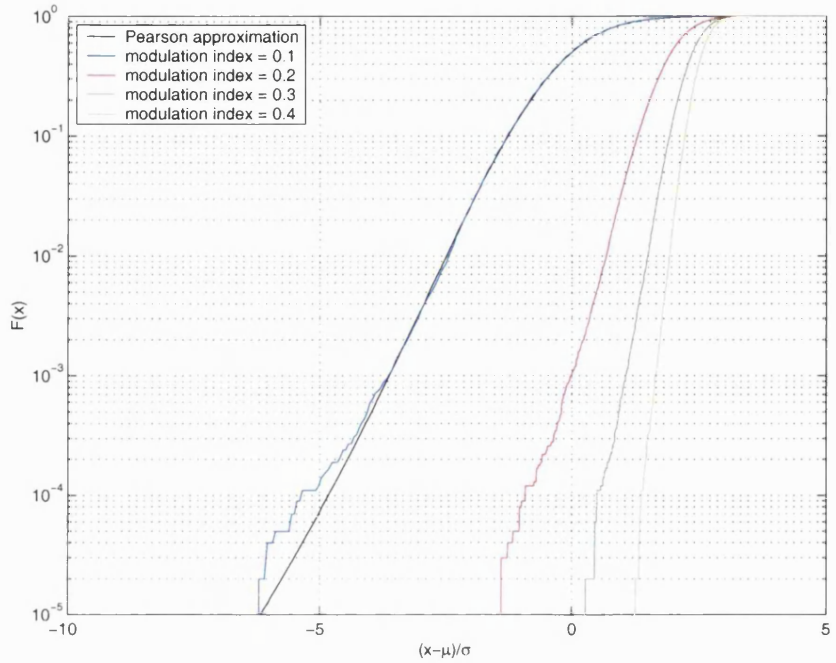

Figure 6.8: Pearson approximation for the CDF, *F(x)*, of the real part of the IMD in the sub-channel on the edge of the band for various modulation indices. OFDM/BPSK case.

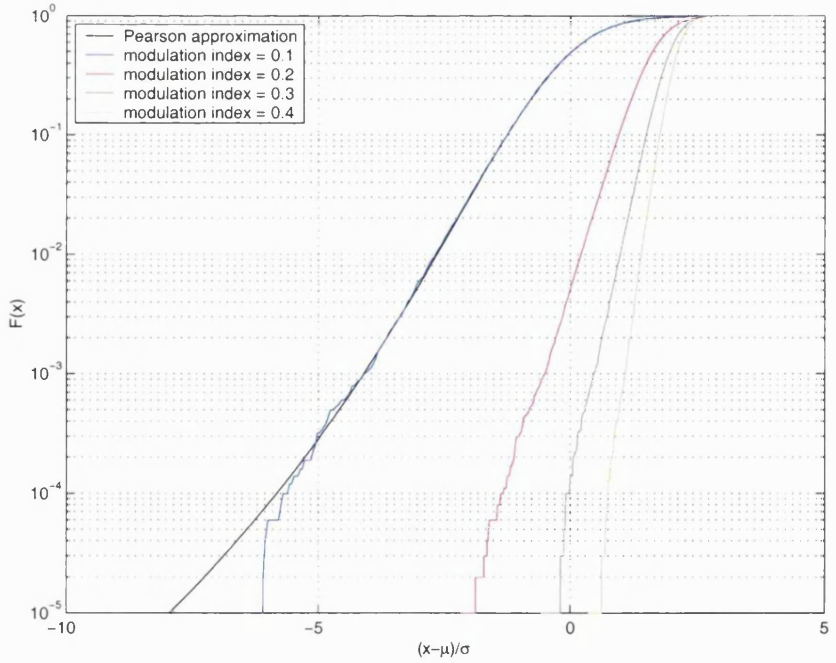

Figure 6.9: Pearson approximation for the CDF, *F(x)*, of the real part of the IMD in the sub-channel in the centre of the band for various modulation indices. OFDM/BPSK case.

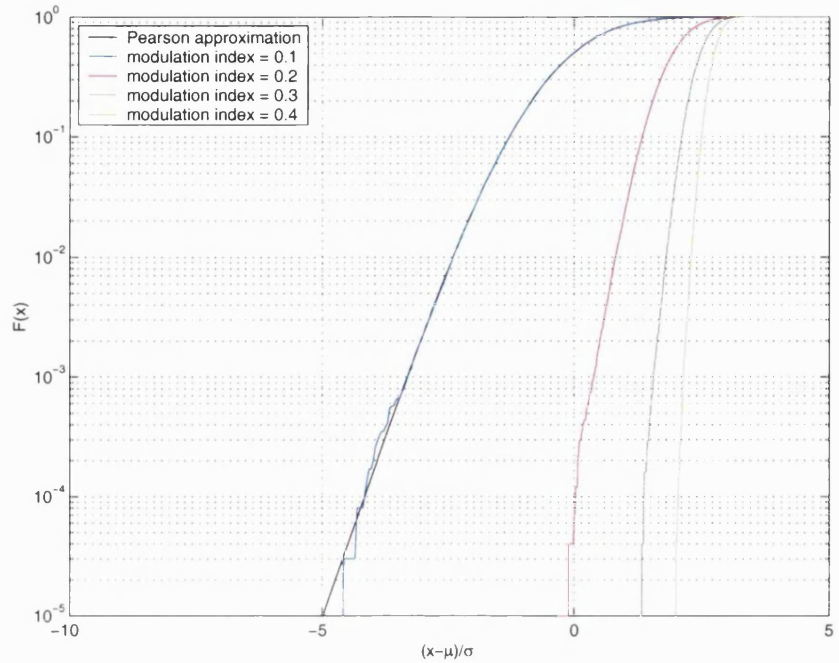

Figure 6.10: Pearson approximation for the CDF, *F(x)*, of the real part of the IMD in the sub-channel on the edge of the band for various modulation indices. OFDM/QPSK case.

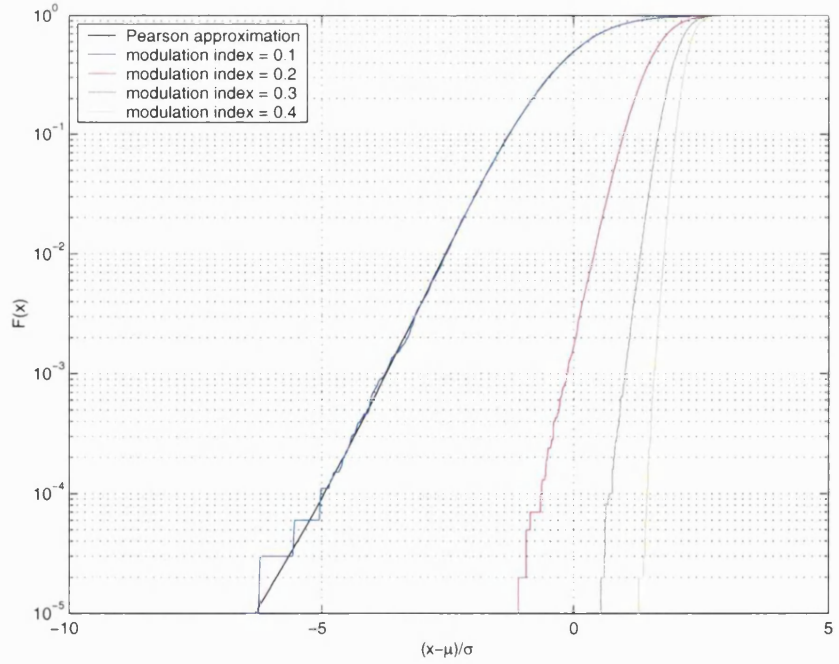

Figure 6.11: Pearson approximation for the CDF, *F(x)*, of the real part of the IMD in the sub-channel in the centre of the band for various modulation indices. OFDM/QPSK case.

Table 6.3: Skewness and kurtosis values of the real part of the IMD in selected sub-channels in the OFDM/BPSK case.

	$m_i = 0.1$	$m_i = 0.2$	$m_i = 0.3$	$m_i = 0.4$
Skewness, Edge	≈ 0	≈ 0	≈ 0	≈ 0
Skewness, Centre	0.05	0.05	0.05	0.03
Kurtosis, Edge	3.72	3.80	3.65	3.42
Kurtosis, Centre	4.28	4.37	4.27	3.89

Table 6.4: Skewness and kurtosis values of the real part of the IMD in selected sub-channels in the OFDM/QPSK case.

	$m_i = 0.1$	$m_i = 0.2$	$m_i = 0.3$	$m_i = 0.4$
Skewness, Edge	≈ 0	≈ 0	≈ 0	≈ 0
Skewness, Centre	0.02	0.01	≈ 0	≈ 0
Kurtosis, Edge	3.28	3.23	3.13	3.06
Kurtosis, Centre	3.64	3.53	3.41	3.33

From the IMD results we can also verify a number of issues already mentioned in chapter 5. For example, from Table 6.3 and Table 6.4 we can see that for other frequency dependent non-linearities skewness and kurtosis values are identical to those for the reference non-linearity for low modulation indices. Moreover, from Table 6.3 and Table 6.4 we can also see that as the modulation index is increased skewness and kurtosis values tend to zero and three, i.e., the skewness and kurtosis values corresponding to a Gaussian distribution, thereby suggesting that higher-order non-linear behaviour does accelerate Gaussian convergence. Gaussian convergence is illustrated in Figure 6.12 through Figure 6.15. The distributions corresponding to different modulation indices were now plotted by normalising the x-axis in the figures to the true mean μ and the true standard deviation σ of the same distributions.

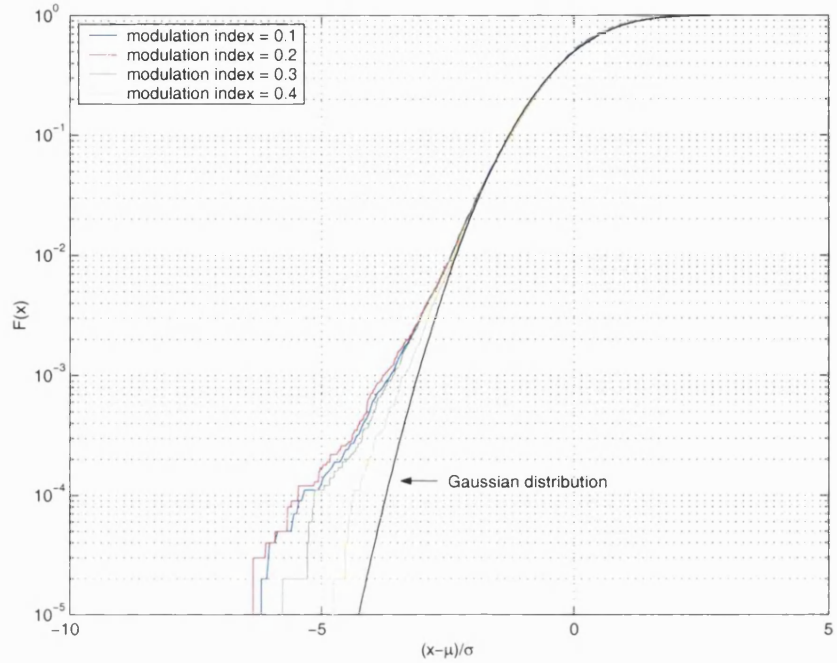

Figure 6.12: CDF, *F(x)*, of the real part of the IMD in the sub-channel on the edge of the band for various modulation indices. OFDM/BPSK case.

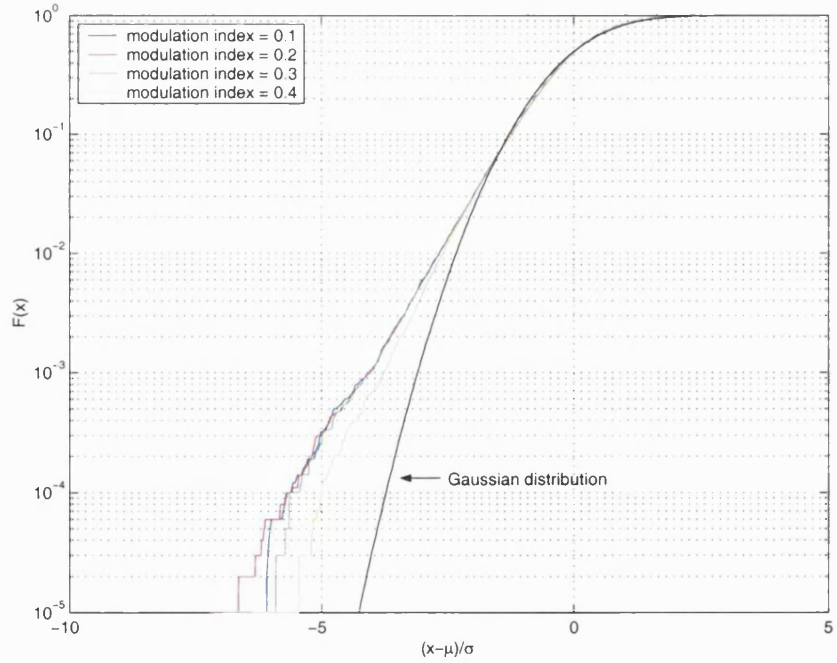

Figure 6.13: CDF, *F(x)*, of the real part of the IMD in the sub-channel in the centre of the band for various modulation indices. OFDM/BPSK case.

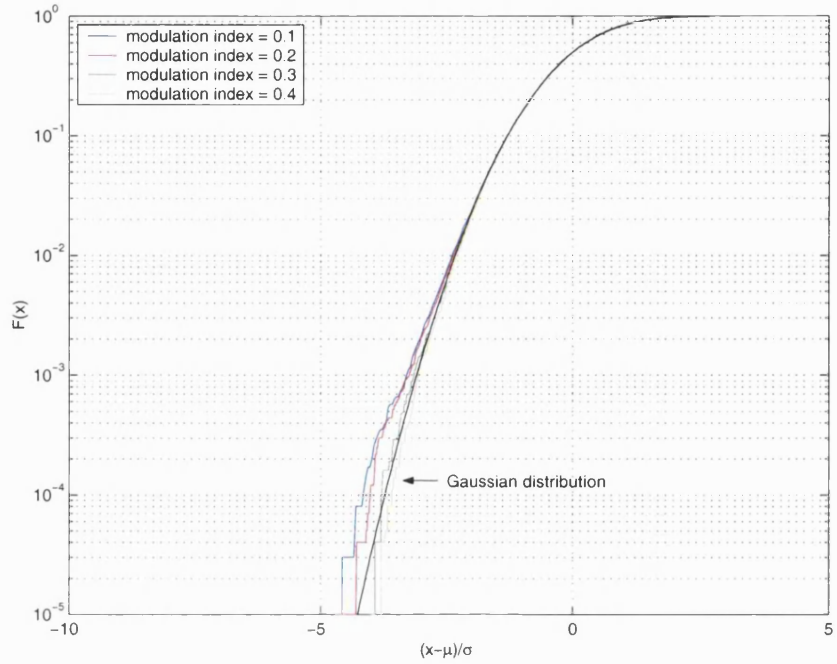

Figure 6.14: CDF, *F(x)*, of the real part of the IMD in the sub-channel on the edge of the band for various modulation indices. OFDM/QPSK case.

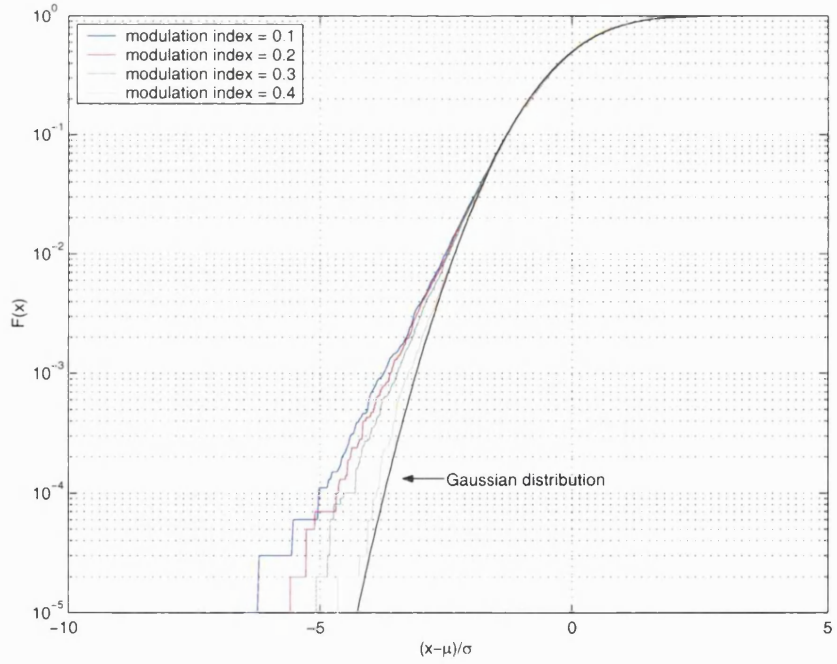

Figure 6.15: CDF, *F(x)*, of the real part of the IMD in the sub-channel in the centre of the band for various modulation indices. OFDM/QPSK case.

Table 6.5: Standard deviations of the real part of the IMD in selected sub-channels for the 48 sub-channel OFDM/BPSK and OFDM/QPSK signals.

	$m_i = 0.1$	$m_i = 0.2$	$m_i = 0.3$	$m_i = 0.4$
Edge, BPSK	0.27×10^{-9}	0.26×10^{-8}	0.79×10^{-8}	1.87×10^{-8}
Centre, BPSK	0.34×10^{-9}	0.28×10^{-8}	0.99×10^{-8}	2.33×10^{-8}
Edge, QPSK	0.36×10^{-9}	0.28×10^{-8}	0.86×10^{-8}	1.84×10^{-8}
Centre, QPSK	0.45×10^{-9}	0.35×10^{-8}	1.08×10^{-8}	2.42×10^{-8}

Figure 6.16 and Figure 6.17 compare the BERs obtained by analysis and simulation in the OFDM/BPSK and the OFDM/QPSK case, respectively[25]. Observation of these figures also reveals that the Pearson approximation rapidly fails at higher modulation indices because higher-order non-linear behaviour not accounted for by analysis becomes increasingly important. However, it is still possible to obtain an estimate of an optimum modulation index in the presence of non-linear distortion and Gaussian noise. This optimum modulation index arises because by increasing the modulation index both the SNR and the signal-to-distortion ratio (SDR) also increase, the former implying a better error rate performance and the later a worse error rate performance.

From the error probability results we can also verify that the error probability performance of different OFDM sub-channels is different not only for systems that exhibit third-order non-linear behaviour but also for systems that exhibit higher-order non-linear behaviour, as mentioned in chapter 5. For example, in the present case differences between the performance of the sub-channel on the edge of the band and the sub-channel in the centre of the band are expected because not only is the standard deviation of the real part of the IMD higher for the sub-channel in the centre, as shown in Table 6.5, but also the tails of its distribution are heavier. Considerable differences in the error probability performance of the sub-channel on the edge of the band and the sub-channel in the centre of the band cannot, however, be observed from Figure 6.16 and Figure 6.17 because very high BERs were simulated.

[25] Very high BERs were simulated due to time consuming simulations. Since simulation is based on the computation of successive numerical solutions of the rate equations then error rate points of 10^{-4} would take in excess of one month of simulation time on a sun workstation.

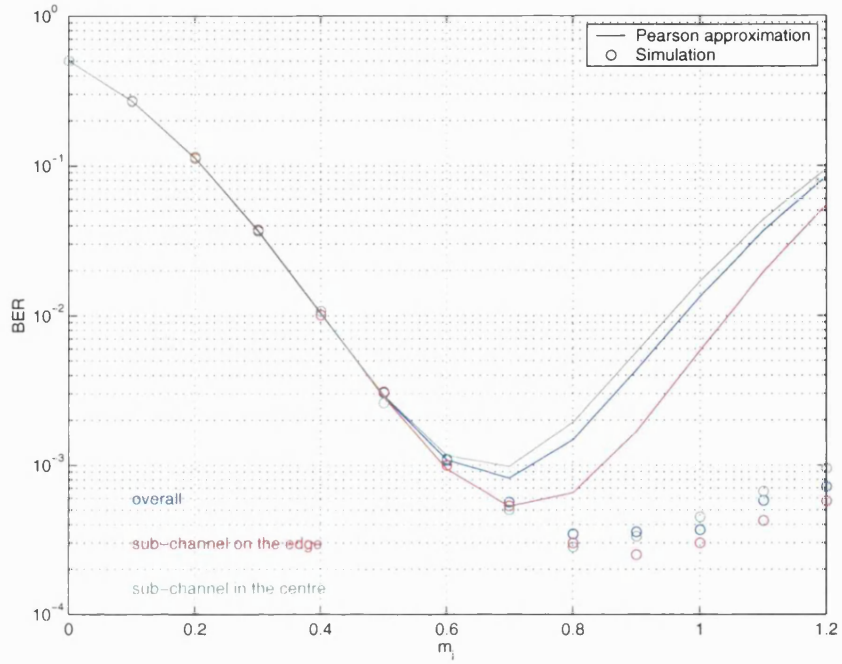

Figure 6.16: Pearson approximation for the overall BER, the BER in the sub-channel on the edge of the band, and the BER in the sub-channel in the centre of the band of the received OFDM/BPSK signal.

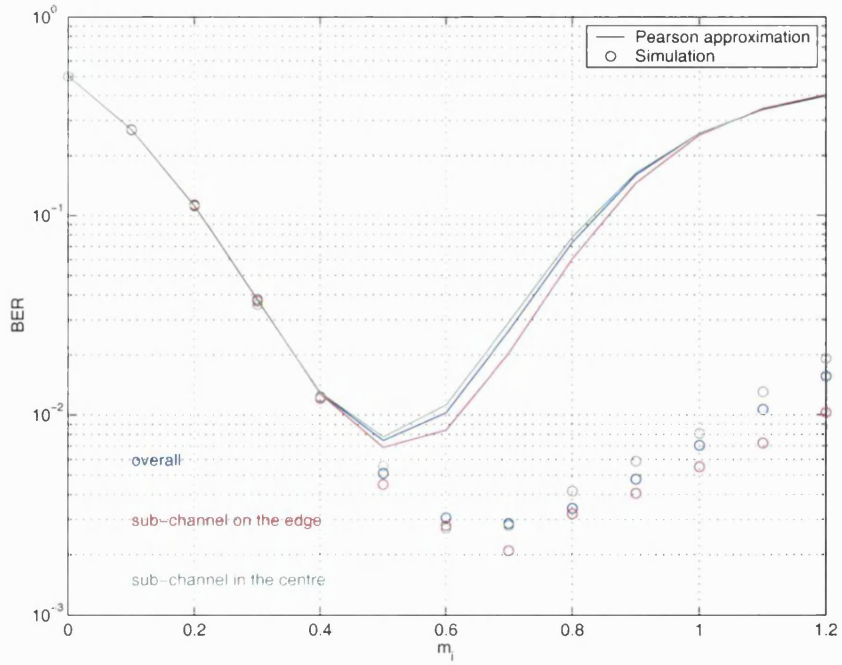

Figure 6.17: Pearson approximation for the overall BER, the BER in the sub-channel on the edge of the band, and the BER in the sub-channel in the centre of the band of the received OFDM/QPSK signal.

6.4 IM/DD fibre-radio system based on the external modulation of an LD

In this section, we apply the results developed in chapter 3, chapter 4 and chapter 5 to the IM/DD fibre-radio system model shown in Figure 6.18, which relies on the external modulation of an LD to generate an OFDM intensity modulated optical wave to be delivered over optical fibre to a remote location. Again, direct detection of the intensity modulated optical wave in a PIN photodiode then yields a photocurrent which is a replica of the OFDM signal. As in the previous fibre-radio system, note that we are specifically addressing the downlink case.

Mach-Zehnder modulator (MZM) induced non-linear distortion [163], residual chirp-fibre dispersion interaction and receiver shot and thermal noise [165,166] are some of the degradation factors that may exist in this fibre-radio system. In out study, however, the only impairments considered are MZM non-linearities and receiver thermal noise.

In the following sections, we start by describing the model of the non-linear element in the system, the MZM model, so as to derive its transfer functions. Finally, analysis of the application of the PDS and the error probability techniques to the fibre-radio system under consideration is carried out by comparing analytical to simulation results. Again, this analysis is carried out at the output of the bandpass filter.

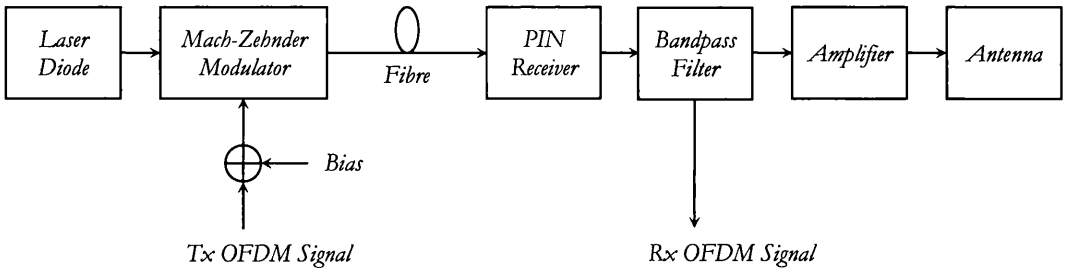

Figure 6.18: Fibre-radio system based on the external modulation of an LD.

6.4.1 MZM model

A number of physical effects (electro-optic, acousto-optic, magneto-optic) in conjunction with a number of different materials (GaAs, InP, $LiNbO_3$) can be used to produce intensity modulators. An MZM uses, however, the electro-optic effect and either GaAs or $LiNbO_3$ [167].

The electro-optic effect is a physical phenomenon that arises in materials where the application of an electric field causes a change in the refractive index proportional to the electric field [167]. A phase change $\Delta\phi$ in a lightwave propagating through the material will therefore be induced by the refractive index change Δn which is related to the interaction length L by [167]

$$\Delta\phi = \frac{2\pi}{\lambda}\Delta nL \tag{6.24}$$

where λ is the wavelength of the lightwave.

An MZM explores this phenomenon to achieve intensity modulation of a lightwave passing through it. The basic structure of an MZM is shown in Figure 6.19. In such a device the incoming lightwave is split into two equal components by a Y-junction 3 dB splitter which are later recombined by a Y-junction 3 dB combiner to yield the outgoing lightwave. Electrodes are normally laid down along both of the interferometer arms in a "push-pull" placement (see Figure 6.19) so that when the driving voltage V is applied one of the arms exhibits a change in the refractive index of Δn and the other arm exhibits a change in the refractive index of $-\Delta n$. The changes in refractive index then induce changes in the phase of the optical waves travelling in each of the interferometer arms. The phase modulated optical waves finally recombine at the output of the Y-junction either constructively or destructively resulting in amplitude modulation at the output of the waveguide. Hence, in an MZM phase modulation is converted to intensity modulation.

The E-field response of a perfectly balanced MZM is given by [175]

$$E_{out} = E_{in}\cos\left(\frac{\pi}{2}\frac{V}{V_\pi}\right) \tag{6.25}$$

where E_{out} is the E-field value of the output optical wave, E_{in} is the E-field value of the input optical wave, V is the applied voltage and V_π is the applied voltage required to induce a relative phase shift of π between the lightwaves in the two arms of the MZM.

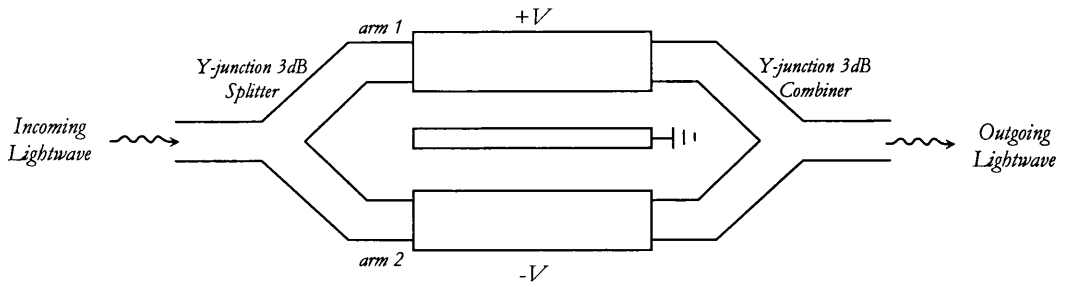

Figure 6.19: Basic structure of an MZM.

The intensity response of a perfectly balanced MZM is given by [175]

$$P_{out} = P_{in} \cos^2\left(\frac{\pi}{2}\frac{V}{V_\pi}\right) \tag{6.26}$$

where P_{out} is the intensity value of the output optical wave and P_{in} is the intensity value of the input optical wave. Note that these expressions neglect losses in the device such as coupling losses and the inherent 3 dB waveguide loss at the Y-junction 3 dB combiner [163]. Note also that since these expressions refer to a perfectly balanced MZM then they neglect phenomena such as non-perfect extinction ratio and chirp [163].

The E-field and the intensity responses of an MZM are intrinsically non-linear as shown in Figure 6.20. Therefore, in intensity modulation applications an MZM is normally biased at the point of maximum intensity linearity, i.e., $V_\pi/2$.

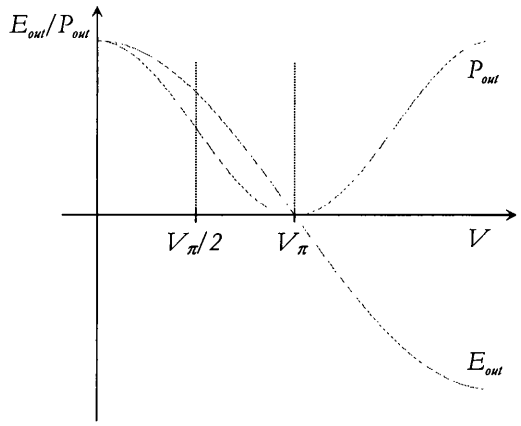

Figure 6.20: E-field and intensity responses of an MZM.

6.4.2 MZM transfer functions

In the IM/DD fibre-radio system under consideration the LD output lightwave intensity is externally modulated about a bias point by the time-varying OFDM signal. This is shown in Figure 6.21 where we use the output intensity versus modulating voltage characteristics of an MZM to illustrate such concept. Both the modulating voltage V applied to the MZM and the output intensity P_{out} of the MZM therefore consist of a steady state component, V_0 and P_{out_0}, respectively, and a time-varying component, $V(t)$ and $P_{out}(t)$, respectively, i.e.,

$$V = V_0 + V(t) \tag{6.27}$$

and

$$P_{out} = P_{out_0} + P_{out}(t) \tag{6.28}$$

The steady-state components are related by

$$P_{out_0} = P_{in} \cos^2\left(\frac{\pi}{2}\frac{V_0}{V_\pi}\right) \tag{6.29}$$

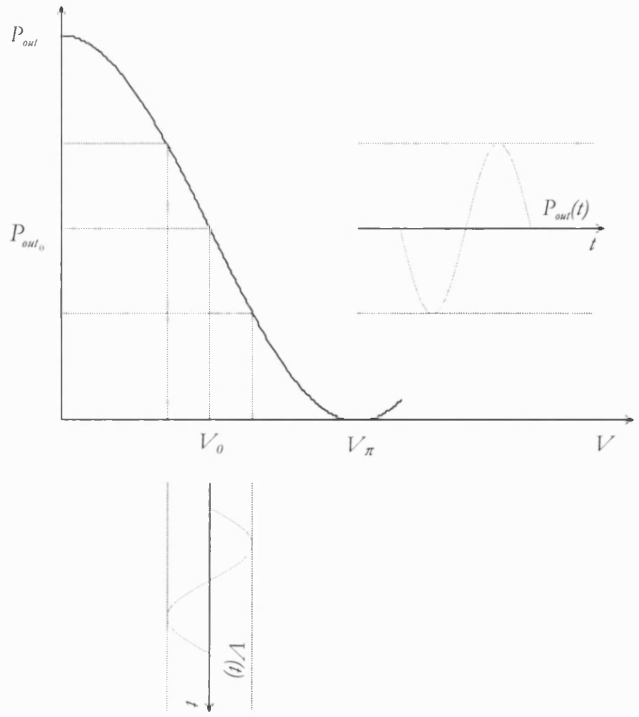

Figure 6.21: Analogue modulation of an MZM.

and the time-varying components are related by

$$P_{out}(t)=\sum_{n=1}^{\infty}P_{in}\frac{V^n(t)}{n!}\left[\frac{1}{2}\left(2\frac{\pi}{2}\frac{1}{V_\pi}\right)^n\cos\left(2\frac{\pi}{2}\frac{V_0}{V_\pi}+\frac{n\pi}{2}\right)\right] \tag{6.30}$$

Note that (6.30) is obtained by expanding the intensity response of the MZM in a Taylor series and collecting the terms that correspond to the time-varying component of the intensity response.

We shall now determine the transfer functions of the MZM that relate the time-varying component of the modulating voltage to the time-varying component of the output intensity and hence ultimately the transmitted OFDM signal and the received OFDM signal in the fibre-radio system under consideration, as shown later. The transfer functions of the MZM are obtained by applying the harmonic input method (described in chapter 3) to (6.30). Thus, the nth-order transfer function $H_n(f_1,\ldots,f_n)$ is obtained by letting the time-varying component of the modulating voltage be the sum of n complex exponentials

$$V(t)=\sum_{k=1}^{n}e^{j2\pi f_k t} \tag{6.31}$$

and by noting that the time-varying component of the output intensity is given by

$$P_{out}(t)=\sum_{k_1=1}^{n}H_1(f_{k_1})e^{j2\pi f_{k_1}t}+\sum_{k_1=1}^{n}\sum_{k_2=1}^{n}H_2(f_{k_1},f_{k_2})e^{j2\pi(f_{k_1}+f_{k_2})t}+\cdots \tag{6.32}$$

By substituting (6.31) and (6.32) in (6.30) we find that the nth-order transfer function $H_n(f_1,\ldots,f_n)$ is given by

$$H_n(f_1,\ldots,f_n)=P_{in}\frac{1}{n!}\left[\frac{1}{2}\left(2\frac{\pi}{2}\frac{1}{V_\pi}\right)^n\cos\left(2\frac{\pi}{2}\frac{V_0}{V_\pi}+\frac{n\pi}{2}\right)\right] \tag{6.33}$$

Note that from the transfer functions in (6.33) we can clearly see that an MZM exhibits frequency independent non-linear behaviour and hence the fibre-radio system under consideration also exhibits such a type of non-linear behaviour, as mentioned earlier. The transfer functions of the MZM determined in this section are used in the next section to obtain analytic results.

6.4.3 Analytic and simulation results

6.4.3.1 PDS

In this section, we determine the PDS of the OFDM/BPSK signal already considered in section 6.3.3.1 at the output of the bandpass filter of the fibre-radio system shown in Figure 6.18 both by analysis and simulation. The MZM biasing voltage was set to

$V_0 = 0.5V_\pi$ and V_π to a typical value of 4 V, the optical fibre was assumed only to attenuate the intensity of the optical signal by a factor A and the photodiode responsivity was set to $R = 0.8\ A/W$. No receiver thermal noise was considered in this study.

As in section 6.3.3.1, the PDS was obtained for specific modulation indices, which we have defined as follows

$$m_i = \frac{\sigma_V}{0.5V_\pi} \tag{6.34}$$

where V_π is the voltage required to induce a relative phase shift of π between the lightwaves in the two arms of the MZM and σ_V is the standard deviation of the time-varying component of the modulating voltage of the MZM, i.e., the standard deviation of the OFDM signal. The modulation index was set by varying the power in the constellations of each OFDM sub-channel until a specified value, as given by (6.34), was achieved.

Analytic results were obtained by following the procedures described in section 6.3.3.1. In this case, the transfer functions needed to obtain these results are given by

$$T_n(f_1, f_2, \ldots, f_n) = R\frac{1}{A} H_n(f_1, f_2, \ldots, f_n) H_{bandpass}(f_1 + f_2 + \cdots + f_n) \tag{6.35}$$

where R is the photodiode responsivity, A is the fibre attenuation, $H_n(f_1, \ldots, f_n)$ is the MZM nth-order transfer function and $H_{bandpass}(f)$ is the bandpass filter frequency response which is assumed to be ideal. Again, the effect of HPDSs of the OFDM signal and the effect of transfer functions of orders higher than three were not included in the analysis.

Simulation results were obtained by implementing the system under consideration in MATLAB, as described in section 6.3.3.1. The sampling frequency used in the simulations was set so that up to eleventh-order non-linear effects could be accounted for.

Figure 6.22 and Figure 6.23 show the PDS of the received OFDM signal for a modulation index of 0.3 and 0.5, respectively. Note that the horizontal axis has been normalised to the centre frequency and the 3 dB bandwidth of the OFDM signal, given by (2.34) and (2.35) respectively, and the vertical axis has been normalised to the maximum value of the PDS. We can observe that for the lower modulation index analytic results agree with simulation results in the normalised frequency range from – 1.5 to 1.5 but slightly disagree outside this frequency range. We can also observe that for the higher modulation index analysis does not match simulation over the entire frequency range shown. Consequently, we conclude again that the analytic technique is appropriate as long as the modulation index is kept low when higher-order non-linear behaviour is negligible in comparison to third-order non-linear behaviour.

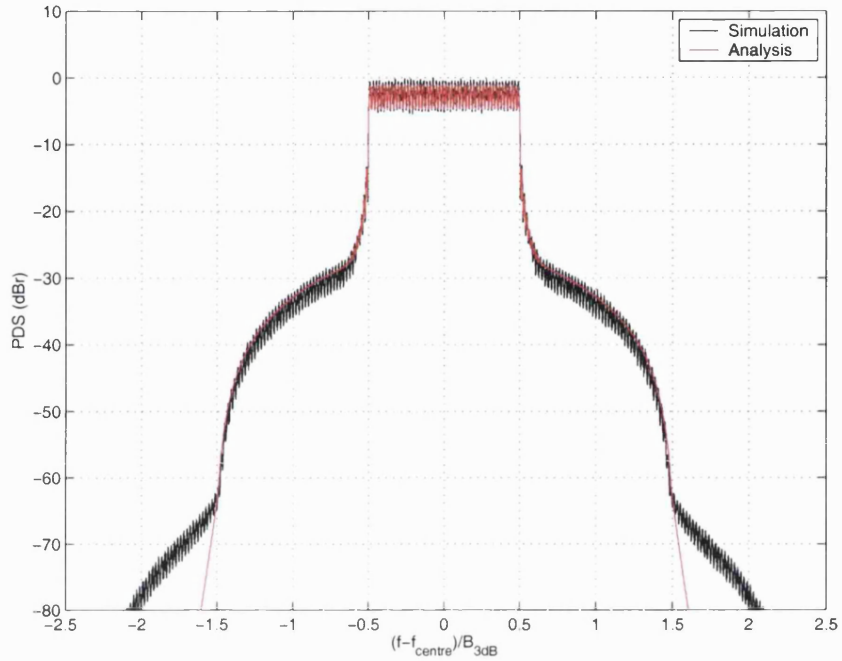

Figure 6.22: PDS of the received OFDM/BPSK signal for a modulation index equal to 0.3.

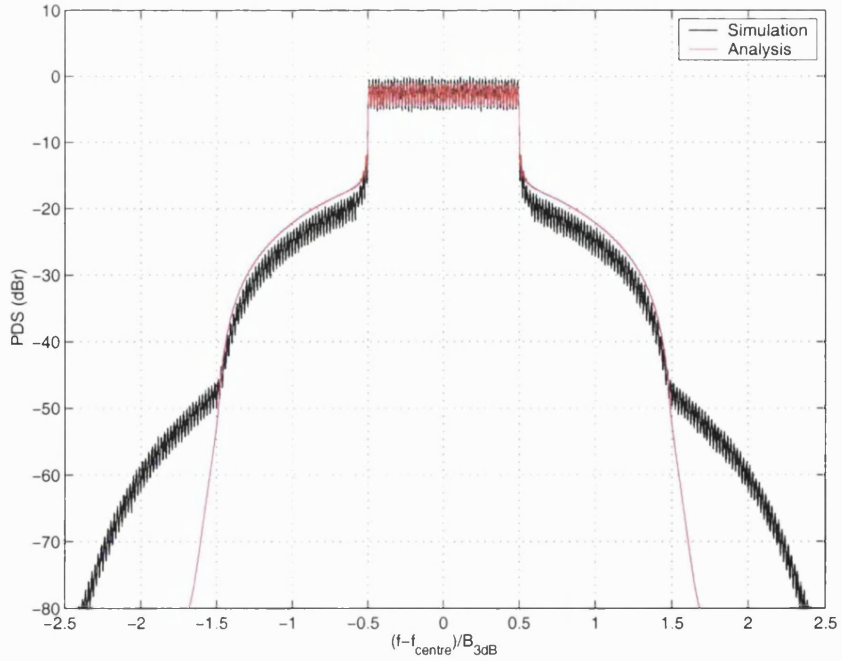

Figure 6.23: PDS of the received OFDM/BPSK signal for a modulation index equal to 0.5.

6.4.3.2 Distribution of the IMD and error probability

In this section, we determine the IMD distribution and the error probability of the OFDM/BPSK and the OFDM/QPSK signals already considered in section 6.3.3.2 at the output of the bandpass filter of the fibre-radio system shown in Figure 6.18 both by analysis and simulation. Analytic results were obtained using Pearson approximations as these have proved to be the most accurate.

Again, the MZM modulator biasing voltage was set to $V_0 = 0.5V_\pi$ and V_π to a typical value of 4 V, the optical fibre was assumed only to attenuate the intensity of the optical signal by a factor A and the photodiode responsivity was set to $R = 0.8\,A/W$. The power spectral density of the receiver's thermal noise, which was assumed to be white and Gaussian, was set to $36\times10^{-24}\,A^2/Hz$.

As in section 6.3.3.2, we have obtained the CDF of the real part of the IMD in the sub-channel on the edge of the band and in the sub-channel in the centre of the band conditioned on A in the OFDM/BPSK case and on $Ae^{j\pi/4}$ in the OFDM/QPSK case for various modulation indices as given by (6.34). We have also obtained the overall BER and the BERs in the sub-channel on the edge of the band and in the sub-channel in the centre of the band for various modulation indices as given by (6.34). The unmodulated optical power at the input of the photodiode was set to – 33.0 dBm in the OFDM/BPSK case and to – 31.5 dBm in the OFDM/QSPK case.

The Pearson approximation to the CDF of the real part of the IMD and the Pearson approximation to the BERs were determined by following the procedure described in section 6.3.3.2. In this case, the equivalent baseband transfer functions of the fibre-radio system needed to obtain these results were determined from the transfer functions of the same system (see (6.35)), as described in chapter 4. Again, the fibre-radio system was represented by its first-order and third-order equivalent baseband transfer functions.

Simulation results were determined from the fibre-radio system model implemented in MATLAB, as described in section 6.3.3.2. The sampling frequency used in the simulations was set so that up to eleventh-order non-linear effects could be accounted for.

Table 6.6: Skewness and kurtosis values of the real part of the IMD in selected sub-channels in the OFDM/BPSK case.

	$m_i = 0.1$	$m_i = 0.2$	$m_i = 0.3$	$m_i = 0.4$
Skewness, Edge	≈ 0	≈ 0	≈ 0	≈ 0
Skewness, Centre	0.03	0.03	0.02	0.01
Kurtosis, Edge	3.57	3.48	3.36	3.21
Kurtosis, Centre	4.19	4.06	3.90	3.65

Table 6.7: Skewness and kurtosis values of the real part of the IMD in selected sub-channels in the OFDM/QPSK case.

	$m_i = 0.1$	$m_i = 0.2$	$m_i = 0.3$	$m_i = 0.4$
Skewness, Edge	≈ 0	≈ 0	≈ 0	≈ 0
Skewness, Centre	0.01	0.01	0.01	≈ 0
Kurtosis, Edge	3.30	3.25	3.17	3.12
Kurtosis, Centre	3.61	3.55	3.44	3.32

We can conclude that the Pearson approximation to the CDF of the real part of the IMD is appropriate at low modulation indices but deteriorates as the modulation index is increased, as shown in Figure 6.24 through Figure 6.27. The distributions corresponding to different modulation indices were plotted by normalising the x-axis in the figures to the mean μ and the standard deviation σ obtained by analysis of the same distributions. Disagreement between analysis and simulation in the strong signal regime is caused by failure of the analytical treatment to estimate the true mean and the true variance and by not using in the analytical treatment the true skewness and kurtosis values. This can be verified by comparing the values shown in Table 6.6 and Table 6.7 to the values in Appendix B. Moreover, from the IMD results we can again observe that higher-order non-linear behaviour does accelerate Gaussian convergence, as shown in Figure 6.28 through Figure 6.31 The distributions corresponding to different modulation indices were now plotted by normalising the x-axis in the figures to the true mean μ and the true standard deviation σ of the distributions.

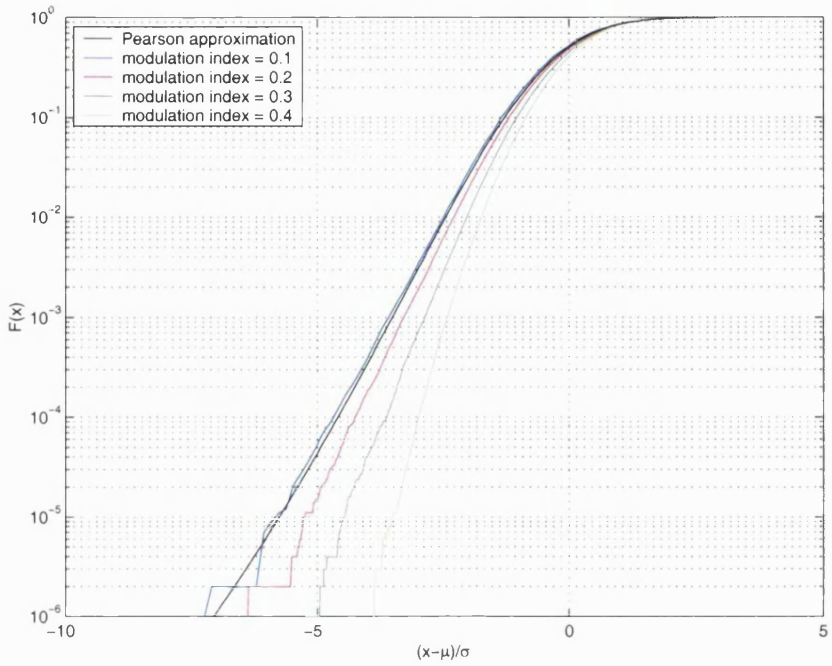

Figure 6.24: Pearson approximation for the CDF, *F(x)*, of the real part of the IMD in the sub-channel on the edge of the band for different modulation indices. OFDM/BPSK case.

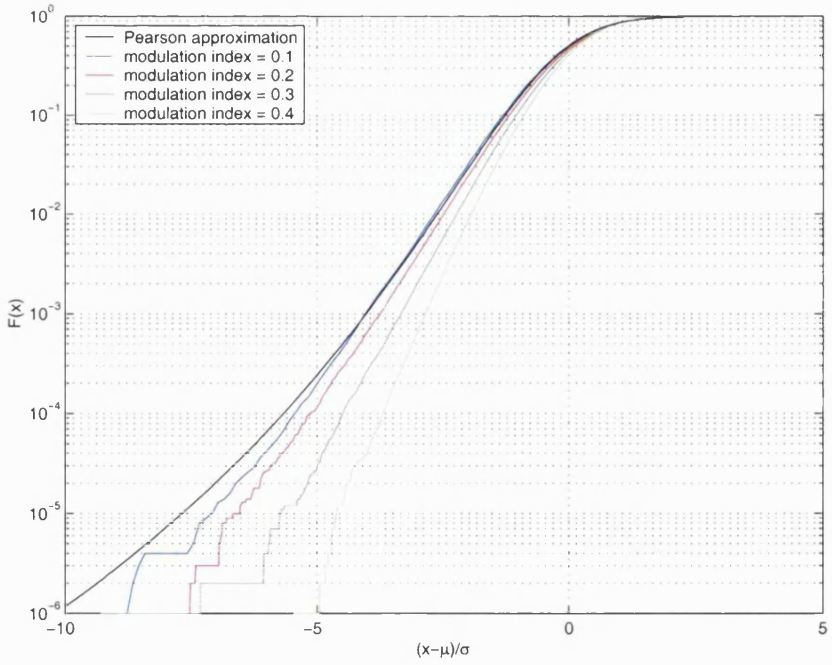

Figure 6.25: Pearson approximation for the CDF, *F(x)*, of the real part of the IMD in the sub-channel in the centre of the band for different modulation indices. OFDM/BPSK case.

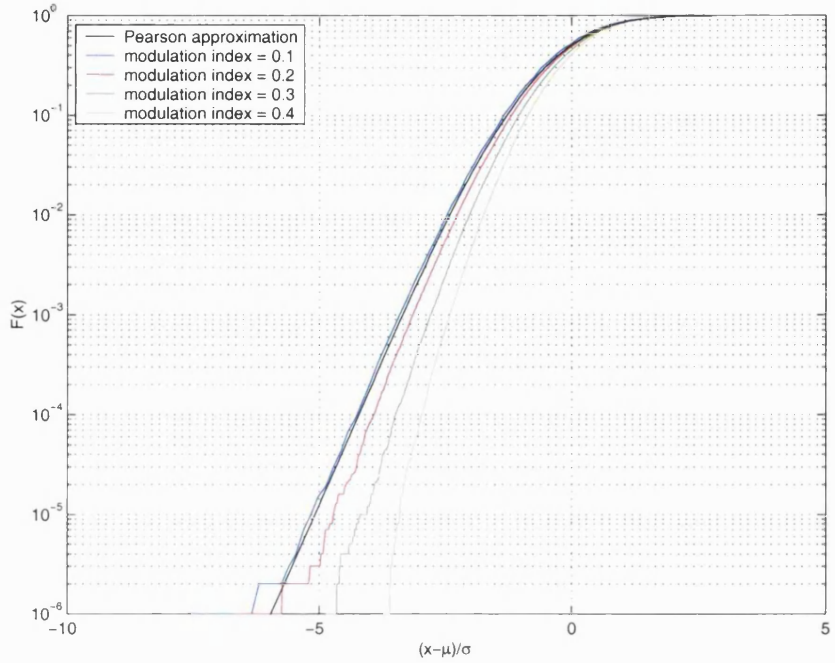

Figure 6.26: Pearson approximation for the CDF, *F(x)*, of the real part of the IMD in the sub-channel on the edge of the band for different modulation indices. OFDM/QPSK case.

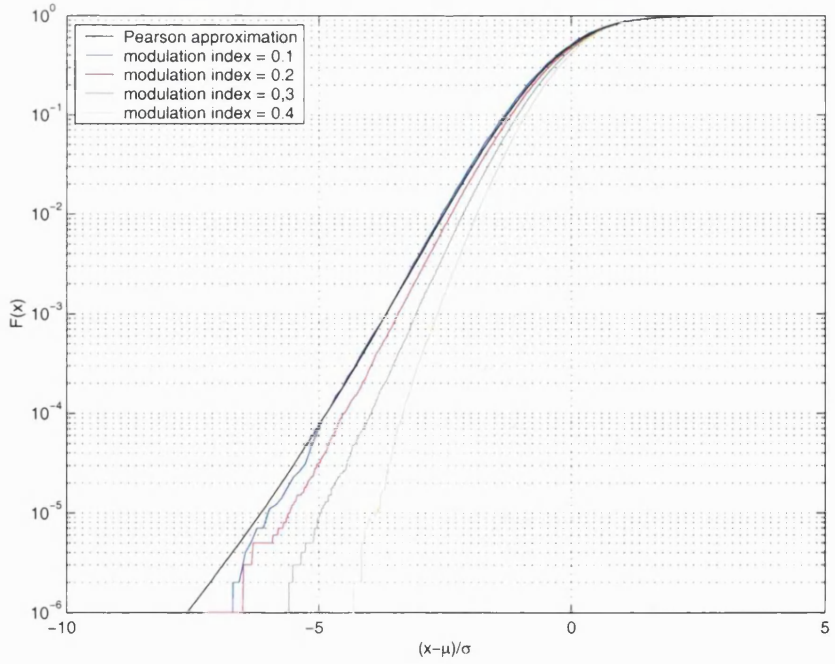

Figure 6.27: Pearson approximation for the CDF, *F(x)*, of the real part of the IMD in the sub-channel in the centre of the band for different modulation indices. OFDM/QPSK case.

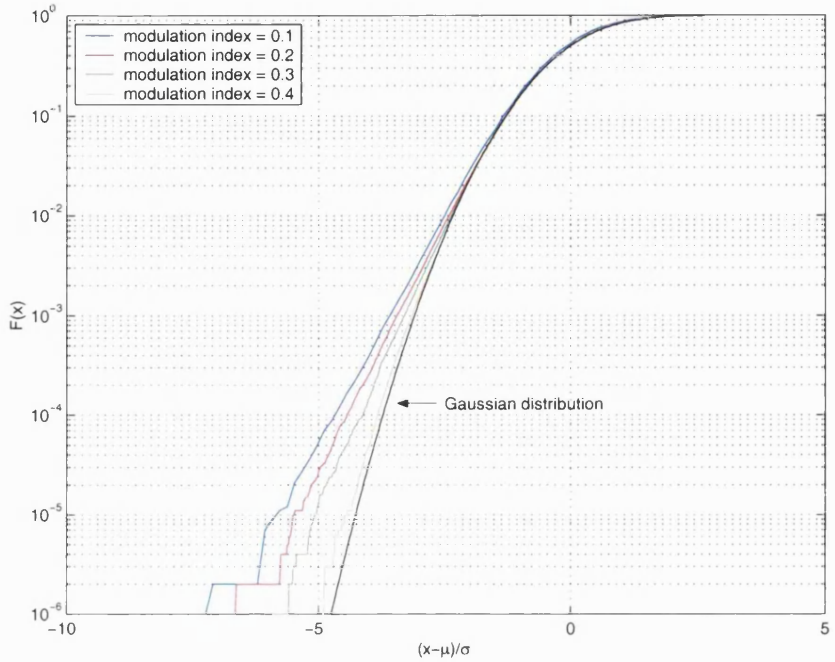

Figure 6.28: CDF, *F(x)*, of the real part of the IMD in the sub-channel on the edge of the band for different modulation indices. OFDM/BPSK case.

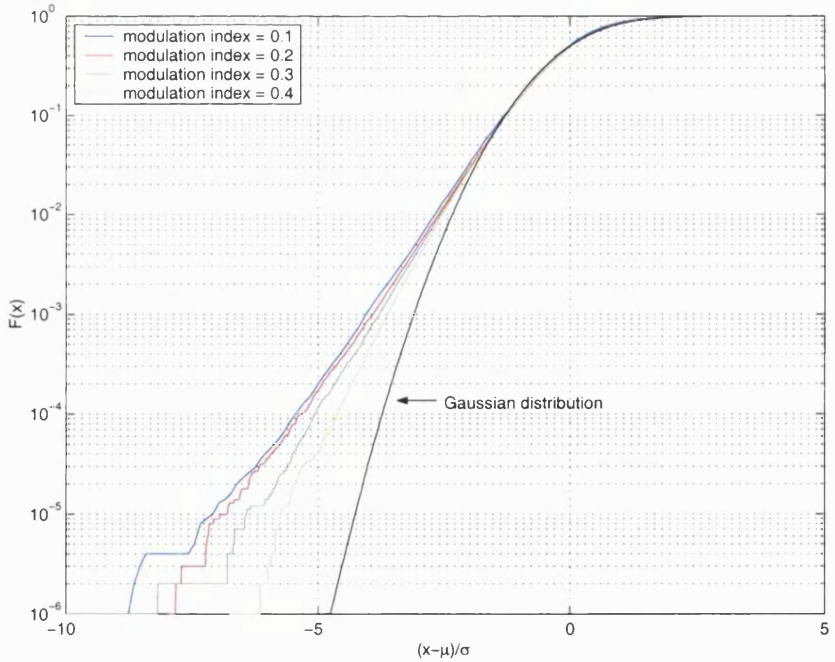

Figure 6.29: CDF, *F(x)*, of the real part of the IMD in the sub-channel in the centre of the band for different modulation indices. OFDM/BPSK case.

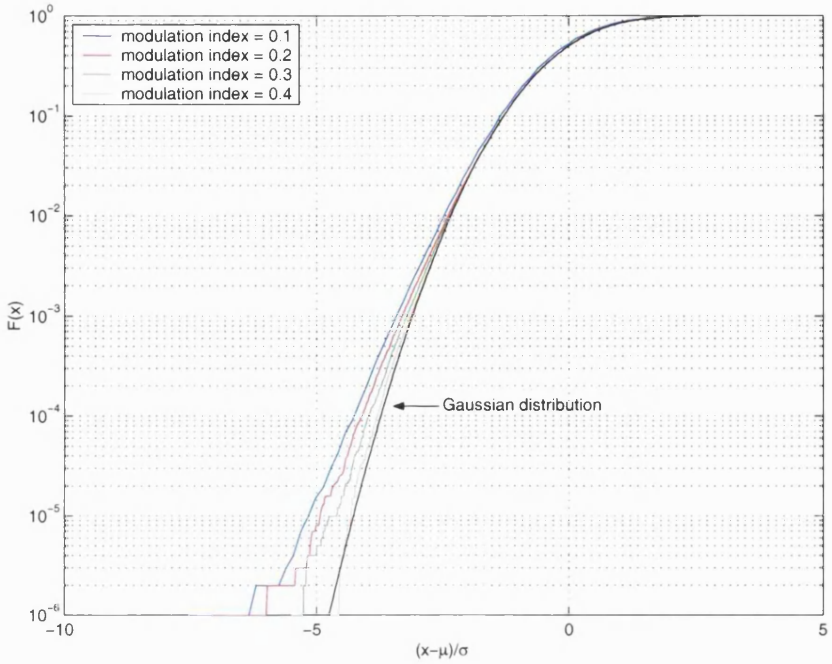

Figure 6.30: CDF, *F(x)*, of the real part of the IMD in the sub-channel on the edge of the band for different modulation indices. OFDM/QPSK case.

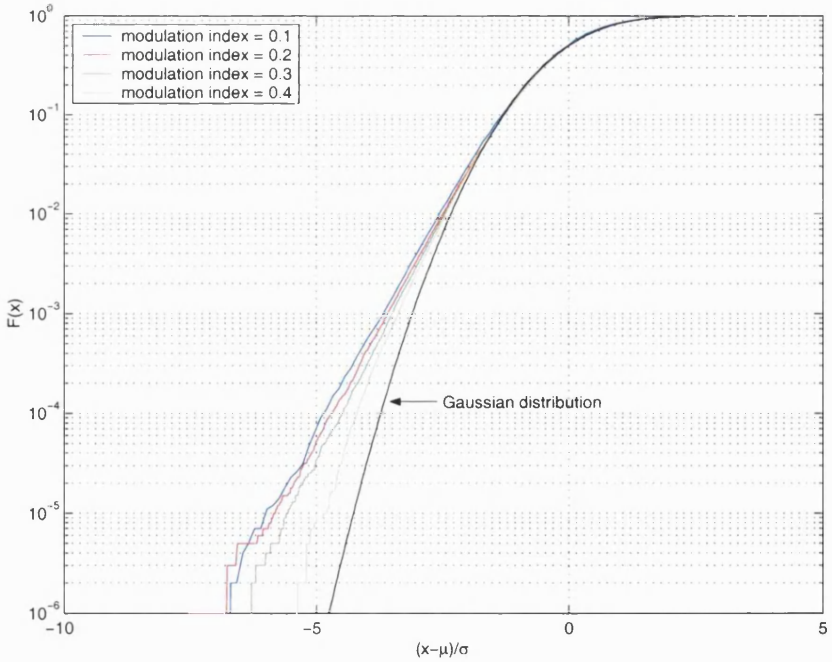

Figure 6.31: CDF, *F(x)*, of the real part of the IMD in the sub-channel in the centre of the band for different modulation indices. OFDM/QPSK case.

Table 6.8: Standard deviations of the real part of the IMD in selected sub-channels for the 48 sub-channel OFDM/BPSK and OFDM/QPSK signals.

	$m_i = 0.1$	$m_i = 0.2$	$m_i = 0.3$	$m_i = 0.4$
Edge, BPSK	0.22×10^{-6}	1.66×10^{-6}	5.26×10^{-6}	1.15×10^{-5}
Centre, BPSK	0.27×10^{-6}	2.05×10^{-6}	6.48×10^{-6}	1.41×10^{-5}
Edge, QPSK	0.15×10^{-6}	1.18×10^{-6}	3.73×10^{-6}	8.13×10^{-6}
Centre, QPSK	0.19×10^{-6}	1.45×10^{-6}	4.59×10^{-6}	9.99×10^{-6}

We can also conclude that the Pearson approximation to the BERs deteriorates as the modulation index is increased, as shown in Figure 6.32 and Figure 6.33[26]. However, it is still possible to obtain an estimate of an optimum modulation index in the presence of non-linear distortion and Gaussian noise. Again, this optimum modulation index arises because by increasing the modulation index both the SNR and the SDR also increase, the former implying a better error rate performance and the later a worse error rate performance. Moreover, from the error probability results we can again verify that the error probability performance of different OFDM sub-channels differs not only for systems exhibiting third-order non-linear behaviour but also for systems exhibiting higher-order non-linear behaviour. For example, the error probability in the sub-channel in the centre of the band is higher than the error probability in the sub-channel on the edge of the band because not only is the standard deviation of the real part of the IMD higher for the sub-channel in the centre, as shown in Table 6.8, but also the tails of its distribution are heavier.

Finally, it is interesting to note that the accuracy of the Pearson approximation deteriorates much faster in the LD based IM/DD system rather than in the MZM based IM/DD system, as the modulation index is increased. This leads us to conclude that a three term description of the LD non-linearity may not always be appropriate in contrast to what has been suggested previously [173].

[26] Again, very high BERs were simulated due to time consuming simulations.

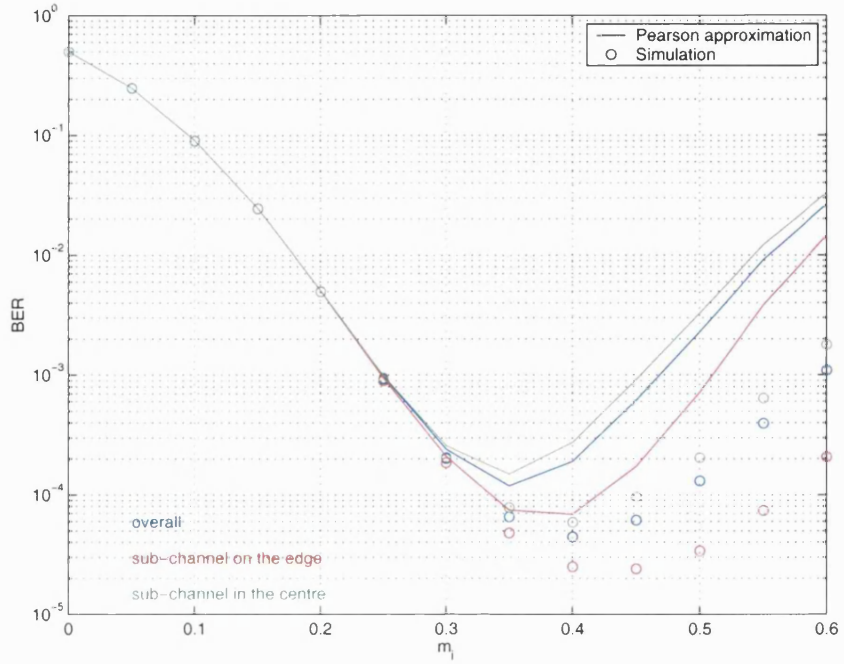

Figure 6.32: Pearson approximation for the overall BER, the BER in the sub-channel on the edge of the band, and the BER in the sub-channel in the centre of the band of the received OFDM/BPSK signal.

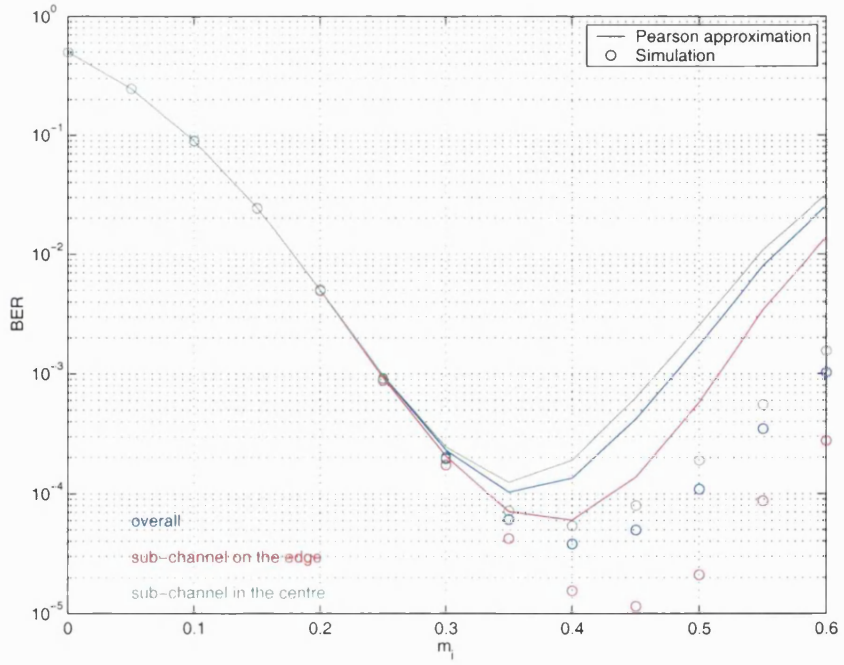

Figure 6.33: Pearson approximation for the overall BER, the BER in the sub-channel on the edge of the band, and the BER in the sub-channel in the centre of the band of the received OFDM/QPSK signal.

6.5 Summary

In this chapter, we have considered the application of the techniques developed in chapters 3, 4 and 5 to two particular IM/DD fibre-radio systems. The first system was based on the direct modulation of an LD and it exhibited frequency dependent non-linear behaviour. The second system was based on the external modulation of an LD and it exhibited frequency independent non-linear behaviour.

Initially, we have introduced the fibre-radio concept and we have discussed the potential benefits of a fibre-radio based wireless network. Subsequently, we have investigated the application of the PDS, the IMD and the error probability techniques to the referred IM/DD fibre-radio systems. We have represented each fibre-radio system by its first three transfer functions, which have been related to the transfer functions of the non-linear element in the system (the LD in one case and the MZM in the other case). We have shown that for low modulation indices, for which a three term representation of the system non-linearity is adequate, analysis agrees with simulation. However, for high modulation indices, for which a three term representation of the system non-linearity is not adequate, analysis does not agree with simulation. We have also shown that in the error probability case analysis can still provide an estimate of an optimum modulation index in the presence of non-linear distortion and noise. Finally, from the IMD and the error probability results we have verified a number of issues previously mentioned in chapter 5. For example, we have demonstrated that for other frequency dependent non-linearities skewness and kurtosis values are identical to those for the reference non-linearity and that higher-order non-linear behaviour does accelerate the IMD Gaussian convergence. We have also demonstrated that the error probability performance of different OFDM sub-channels is different not only for systems that exhibit third-order non-linear behaviour but also for systems that exhibit higher-order non-linear behaviour.

Chapter 7

Concluding remarks

This work is concerned with the development of powerful, yet tractable, analytic techniques to investigate the impact of fibre-radio system non-linearities on the performance of OFDM signals. Volterra series techniques are used to model both the frequency independent and frequency dependent behaviour typical of fibre-radio system non-linearities. The developed techniques aim at capturing the two main effects of a non-linearity on an OFDM signal, which are signal spectral spreading and signal error probability degradation.

The basic principles and characteristics of OFDM signals and communication systems were reviewed in chapter 2. Particularly, an FOFDM scheme with twice the bandwidth efficiency of conventional OFDM schemes was proposed.

The development of a Volterra series based analytic technique to assess the impact of frequency independent and frequency dependent non-linearities on the PDS of OFDM signals was the subject of chapter 3. The analytic technique was developed by taking into consideration the statistical properties of OFDM signals, i.e., it was considered that an OFDM signal is a zero-mean Gaussian cyclo-stationary process. First, expressions were derived to determine the mean value and the ACF of a non-linearly distorted OFDM signal and then, by proving that the non-linearly distorted OFDM signal is also a cyclo-stationary stochastic process, the expressions that give the output average PDS were determined by Fourier transforming the expressions that give the output average ACF. The derived expressions relate the statistics of the non-linearity output (the non-linearly distorted OFDM signal) to the HACFs/HPDSs of the non-linearity input (the non-distorted OFDM signal) and the kernels/transfer functions of the non-linearity. Moreover, the derived

expressions take into account up to third-order non-linear behaviour. The application of the PDS expressions was investigated to specific OFDM signals distorted by both a frequency independent and a frequency dependent non-linearity exhibiting up to third-order non-linear behaviour. Particularly, it was shown that analysis perfectly agrees with simulation provided that a sufficient number of HPDSs of the non-distorted OFDM signal are inserted into the mathematical expressions. It was also shown that analysis perfectly agrees with simulation both for OFDM signals with 48 sub-channels, for which the Gaussian approximation is highly accurate, and OFDM signals with 12 sub-channels, for which the Gaussian approximation is not so accurate. It was finally established that the use of just the average PDS of the non-distorted OFDM signal in the mathematical expressions already yields very good agreement between analysis and simulation, such a simplification suggesting that an OFDM signal can be treated as a stationary stochastic process in practice.

The development of a Volterra series based analytic technique to assess the impact of frequency independent and frequency dependent non-linearities on the error probability of OFDM signals was the subject of chapter 4. First, the relation between transmitted and received symbols in an OFDM communication system in the presence of non-linearities and AWGN was determined and only then, based on this relation, were expressions to evaluate the error probability of non-linearly distorted OFDM/BPSK and OFDM/QPSK signals in AWGN derived. The overall error probability of an OFDM signal was given as the average of the error probabilities in all OFDM sub-channels. In turn, the error probability in each OFDM sub-channel was given as the statistical expectation with respect to the IMD RV of the error probability in AWGN conditioned by a given value of the IMD RV. Expressions were also derived to evaluate the moments of the IMD RV in each OFDM sub-channel. It was confirmed that the moment computation procedure was extremely time consuming (moment computation is limited to the first and the second moments, non-linearities exhibiting up to third-order non-linear behaviour and OFDM signals with up to 128 sub-channels). Hence, to compute the error probability expectations, one could not rely on series expansion methods or Gauss quadrature rules, which require a large number of moments, but on alternative approximation/estimation methods for the IMD distribution requiring only a limited number of moments.

The time consuming nature of the moment computation method prompted the investigation of specific approximations/estimations for the IMD distribution and the

error probability, which was carried out in chapter 5. The properties of the IMD RV were initially examined for OFDM/BPSK and OFDM/QPSK signals with different numbers of sub-channels distorted both by a frequency independent and a frequency dependent non-linearity (exhibiting up to third-order non-linear behaviour), as a means to select appropriate approximations/estimations for the IMD distribution. It was established that the IMD distribution is generally characterised by different rates of tail decay, which depend on the total number of OFDM sub-channels, the location of the specific OFDM sub-channel (e.g., edge or centre) and the type of modulation (e.g., BPSK or QPSK). Specifically, it was shown that heavy tailed behaviour is associated with a low number of OFDM sub-channels, the sub-channel in the centre and BPSK modulation whereas approximately Gaussian behaviour is associated with a high number of OFDM sub-channels, the sub-channel on the edge and QPSK modulation. Moreover, it was also established that skewness and kurtosis values of the IMD RV do not significantly depend on the non-linearity type and hence, if known *a priori* for a reference non-linearity, these statistical measures could be used to enhance the approximations/estimations for the IMD distribution. Approximation/estimation techniques that, on the one hand, allow for distributions with different rates of tail decay and, on the other hand, allow for a Gaussian distribution as a particular case were selected as a means to describe the IMD distribution behaviour. Particularly, generalised Gaussian, Pearson, Gaussian and Laplace approximations were considered. Maximum entropy and minimum relative entropy estimations were also considered. The relative performance of the different approximation and estimation techniques for the IMD distribution and the error probability were examined for OFDM/BPSK and OFDM/QSPK signals with different numbers of sub-channels distorted both by a frequency independent and frequency dependent non-linearity (exhibiting up to third-order non-linear behaviour) by comparing analytic to simulation results. Specifically, it was shown that Gaussian, Laplace and generalised Gaussian approximations only apply to particular cases whereas Pearson approximations always apply. It was also shown that maximum entropy and minimum relative entropy estimations never applied.

The application of the developed techniques to two particular IM/DD fibre-radio systems was the subject of chapter 6. The first system relied on the direct modulation of a laser source to generate an OFDM intensity modulated optical wave to be delivered by optical fibre to the remote location, and it exhibited frequency dependent non-linear

behaviour. The second system relied on the external modulation of a laser source to generate an OFDM intensity modulated optical wave to be delivered by optical fibre to the remote location, and it exhibited frequency independent non-linear behaviour. Each IM/DD fibre-radio system was represented by its first three transfer functions, which have been related to the transfer functions of the non-linear elements in the system (the LD in the first system and the MZM in the second system). It was shown that in the small signal regime (for low modulation indices), for which a three term representation of the system non-linearity is adequate, analysis agrees with simulation. However, in the strong signal regime (for high modulation indices), for which a three term representation of the system non-linearity is not adequate, analysis does not agree with simulation. It was also shown that in the error probability case the analytical treatment can still provide a first-order approximation to an optimum modulation index in the presence of non-linear distortion and noise.

Overall, this thesis has provided a range of analytic tools to assess the effects of mild non-linearities on performance of fibre-radio based wireless networks employing OFDM signalling. Moreover, this thesis has also provided new insight into the behaviour of non-linearly distorted OFDM signals that has not been previously reported in the literature. For example, it was shown that a Gaussian approximation to the IMD distribution is not always appropriate and that, in the presence of non-linearities, the error probability performance of each OFDM sub-channel is not always identical. It was also shown that, in the presence of non-linearities, the error probability performance of an OFDM signal with a high number of sub-channels, which exhibits a high PAPR, can be better than the error probability performance of an OFDM signal with a low number of sub-channels, which exhibits a low PAPR.

7.1 Recommendations for future research

Based on the experience and knowledge acquired during this research work, several areas for future research can be suggested. These are:

- Extension of the techniques reported in this thesis to deal with OFDM/M-PSK, OFDM/M-QAM and OFDM/M-DPSK signals. Extension of the techniques to OFDM/M-QAM and OFDM/M-PSK signals seems to be straightforward. For PDS, the derived expressions directly apply. For error probability, expressions can

also be derived that relate the error probability of an OFDM/M-PSK or an OFDM/M-QAM signal to the error probabilities of the OFDM sub-channels, each of which is given as the expectation with respect to the IMD RV of the error probability in AWGN conditioned by a given value of the IMD RV [150]. Therefore, it suffices to carry out an analysis of the properties of the IMD RV and potential approximations/estimations for the IMD distribution and the error probability for these two new cases [152]. Extension of the techniques to OFDM/M-DPSK signals does not seem to be so straightforward. Consideration of higher-order and differential modulation schemes is important because many practical systems do not only use OFDM/BPSK or OFDM/QPSK signals but also OFDM signals with higher-order or differential modulation [3-7].

- Integration of higher-order non-linear effects in the expressions. In the PDS case, the inclusion of higher-order non-linear effects requires extra algebraic work. However, it is important to note that the numerical computation of the resulting multi-dimensional integrals may be extremely time-consuming. In the error probability case, integration of higher-order non-linear effects requires a whole new formulation for the moment computation procedure. A fast method to compute a large number of moments of the IMD RV in conjunction with series expansion methods or Gauss quadrature rules would yield accurate error probability values. Alternatively, a not so fast method to compute a relatively small number of moments of the IMD RV in conjunction with appropriate approximation/estimation techniques would yield approximate error probability values. It is important to note, however, that the development of such moment computation procedures may be extremely difficult or even impossible. The integration of higher-order non-linear effects in the expressions would clearly allow one to consider both the effect of mild and strong non-linearities on an OFDM communication system.

- Extension of the techniques reported in this thesis to accommodate the effects of non-linear distortion and multi-path fading channels on coded OFDM schemes. Jong and Stark have already developed an analytic technique to deal with the effects of non-linear distortion and multi-path fading channels on coded multi-carrier spread-spectrum systems [135]. Likewise, an identical treatment could be adopted to extend

the techniques reported in this thesis to accommodate the effects of such impairments on coded OFDM schemes.

- Comparison of merits and demerits of potential fibre-radio system architectures to convey OFDM signals between CSs and BSs [8-12]. For example, one could investigate the suitability of fibre-radio systems to support indoor wireless LANs employing OFDM signalling such as IEEE 802.11 or HIPERLAN2. If the effects of both multi-path fading and non-linear distortion on the OFDM signals were considered then one would be able to evaluate the performance both of the downlink (from the CS to the BS) and of the uplink (from the BS to the CS). Evaluation of the performance of the uplink is of particular importance because the OFDM signal to be conveyed from the BS to the CS has been previously transmitted over a multi-path fading channel, which has certainly induced different attenuations and phase shifts in different OFDM sub-carriers. Therefore, upon non-linear distortion the weakest sub-carriers will experience a very low SDR whereas the strongest sub-carriers will experience a relatively higher SDR. The overall performance of the link is therefore dictated by the weakest sub-carriers.

- Investigation of a range of techniques to ameliorate the performance of non-linearly distorted OFDM signals in fibre-radio systems. Most techniques apply only to OFDM signals distorted by frequency independent non-linearities and not by frequency dependent non-linearities. It is therefore natural to ask whether these are extensible to frequency dependent non-linearities. Possible techniques to be investigated include pre-distortion [82-84], PAPR reduction [67-81] and non-linear equalisation [176].

- Investigation of the interaction of non-linear distortion with channel estimation and synchronisation operations in an OFDM communication system. Channel estimation and synchronisation operations rely on the transmission of known symbols or a pilot structure embedded in the OFDM signal from which channel state and synchronisation information can be retrieved [87-98]. Obviously, any non-linearity will alter the known symbols or the pilot structure in such a way that channel estimation and synchronisation information may not be retrieved reliably. Therefore, besides the non-linear degradation there is also non-linear induced synchronisation

and channel estimation degradation in the OFDM communication system. Consideration of such possible interactions and the identification or development of robust channel estimation and synchronisation operations is therefore an important topic.

- Investigation of the interaction of non-linear distortion with adaptive OFDM systems. Adaptive OFDM systems rely on the transmission of higher-order modulation formats in high SNR OFDM sub-channels and lower-order modulation formats in low SNR OFDM sub-channels. Alternatively, the overall transmitted power is allocated differently to different OFDM sub-channels depending on their current SNR state [101]. Obviously, any non-linearity will interfere with the allocation procedure because different OFDM sub-channels experience different non-linear distortion levels. Consideration of such possible interactions and the identification or development of robust allocation algorithms is therefore an important topic.

- Acquisition of a more solid understanding of the influence of non-linearities on the performance of OFDM signals. Surprisingly, we have shown in this thesis that, in the presence of non-linearities, the error probability performance of OFDM signals with higher PAPRs can be better than the error probability performance of OFDM signals with lower PAPRs, because the probability of error of an OFDM signal is ultimately related to the IMD behaviour and not to the PAPR behaviour. This suggests that it may be more beneficial to rely on IMD minimisation techniques instead of PAPR reduction techniques [67-81] to improve the performance of non-linearly distorted OFDM signals. PAPR reduction codes introduce a set of redundant symbols in the set of data symbols to eliminate combinations that produce high peaks [77-81]. A hypothetical IMD reduction code would introduce a set of redundant symbols in the set of data symbols to cancel out different IMPs upon OFDM signal non-linear distortion. Cancellation of out-of-band IMPs would limit signal spectral spreading whereas cancellation of in-band IMPs would improve signal error probability performance. Whether or not the development of such a code is feasible should be the subject of further work.

- Further development of the FOFDM scheme [106]. FOFDM exhibits two drawbacks when compared to OFDM such as vulnerability to synchronisation errors and linear distortion [177]. Consideration of such issues would therefore provide a starting point for the further development of the FOFDM scheme.

Appendix A

Fast OFDM

This appendix includes the paper written by the author which introduces the basics of the fast orthogonal frequency division multiplexing signalling scheme and its advantages and disadvantages. FOFDM is a scheme with twice the bandwidth efficiency of conventional OFDM schemes because in FOFDM a $1/2T$ inter-carrier frequency spacing is used whereas in OFDM the inter-carrier frequency spacing is $1/T$ (T is the useful symbol duration). In this appendix, we show that whilst each OFDM sub-carrier can be modulated by complex modulation symbols drawn from any M-PSK or any M-QAM signal constellation, each FOFDM sub-carrier can only be modulated by real modulation symbols drawn from a BPSK or an M-ASK signal constellation otherwise severe ICI results upon demodulation. We also show that FOFDM exhibits two drawbacks when compared to OFDM such as vulnerability to synchronisation errors and linear distortion.

Fast OFDM: A Proposal for Doubling the Data Rate of OFDM Schemes

M. R. D. Rodrigues and I. Darwazeh

Department of Electronic and Electrical Engineering
University College London
Torrington Place, London WC1E 7JE, England
Phone: +44 20 7679 3980, Fax: +44 20 7388 9325, Email: mrodrigu@ee.ucl.ac.uk

ABSTRACT

In this paper, we present a novel OFDM proposal, which under specific modulation schemes, achieves twice the bandwidth efficiency. We show that one-dimensional modulation schemes (e.g., BPSK or M-ASK) can be transmitted with no degradation in the BER whereas two-dimensional modulation schemes (e.g., M-PSK or M-QAM) can not. Finally, a qualitative discussion of the expected performance of FOFDM in relation to OFDM is carried out.

I. INTRODUCTION

In recent years, the wireless industry has shown great interest in OFDM systems. Indeed, such systems have been adopted in a variety of wireless applications such as digital audio broadcasting (DAB) and digital video broadcasting (DVB). Moreover, OFDM has also been proposed for indoor wireless networks and fixed wireless broadband access [1],[2]. This growing interest was due to the realisation that OFDM is an efficient scheme to convey information in a frequency selective fading channel without requiring complex equalisers [3]. Moreover, OFDM uses the available bandwidth efficiently and can be efficiently generated and detected using the IFFT and the FFT, respectively [4].

Future wireless communication systems need to provide very high data rate services. Since the radio spectrum is a limited resource then highly bandwidth efficient modulation schemes need to be developed. Accordingly, in this paper we propose a "fast" orthogonal frequency division multiplexing (FOFDM) modulation scheme with twice the bandwidth efficiency.

This paper is organised as follows: In section II, the FOFDM modulation scheme is described. In section III, the FOFDM concept is demonstrated by comparing analytic results to simulation results. Section IV qualitatively discusses the expected performance of FOFDM in relation to OFDM, particularly, in the presence of frequency selective fading and synchronisation errors. Finally, section V concludes the paper.

II. FAST OFDM

In OFDM the high data rate stream is partitioned into N lower data rate sub-streams using a serial-to-parallel converter. These sub-streams then modulate a set of N complex sub-carriers that are in turn linearly added prior to transmission. The frequency separation between adjacent sub-carriers is equal to 1/T, where T is the duration of the signalling interval. With this frequency separation the sub-carriers are orthogonal over the signalling interval of length T and hence the complex data can be recovered without inter-carrier interference (ICI)[1].

We write the OFDM signal as follows

$$s(t)=\sum_{k=-\infty}^{\infty}\sum_{n=0}^{N-1}S_{kn}\,g_n(t-kT) \tag{1}$$

$$g_n(t)=\begin{cases}\dfrac{1}{\sqrt{T}}e^{j\frac{2\pi nt}{T}}, & t\in[0,T]\\ 0, & t\notin[0,T]\end{cases} \tag{2}$$

where S_{kn} denotes the complex data conveyed in time slot k and sub-channel n and $g_n(t-kT)$ denotes the complex waveform (the complex sub-carrier) used to convey the complex data in the same time slot and sub-channel. The complex received symbol in time slot k and sub-channel n, R_{kn}, is recovered by multiplying the received OFDM signal, $r(t)$, by the complex conjugate of the waveform used to convey this complex symbol, $g_n^*(t-kT)$, and integrating from kT to $(k+1)T$, i.e.,

$$R_{kn}=\int_{kT}^{(k+1)T}r(t)g_n^*(t-kT)dt \tag{3}$$

Assuming that the received OFDM signal $r(t)$ is ideal (noiseless and with no distortion), then from equations (1), (2) and (3) the complex received symbol can be expressed by the equation below:

[1] A frequency separation of 1/T is the minimum frequency separation that ensures orthogonality between two sub-carriers over a signalling interval of length T.

Published in the Proceedings of the International Conference on Telecommunications, vol. 2, pp. 484-487, June 2002. (Beijing, China)

$$R_{kn} = \int_{kT}^{(k+1)T} \left[\sum_{k'=-\infty}^{\infty} \sum_{n'=0}^{N-1} S_{k'n'} g_{n'}(t-k'T) \right] g_n^*(t-kT)dt$$
$$= \sum_{n'=0}^{N-1} S_{kn'} \mathrm{sinc}(n'-n) e^{j\pi(n'-n)} \quad (4)$$
$$= S_{kn}$$

As mentioned before, in this case the data is recovered without ICI.

The difference between OFDM and FOFDM is in the frequency separation between adjacent sub-carriers. In the OFDM case a 1/T frequency separation is used whereas in the FOFDM case a 1/2T frequency separation is employed. We will show that, with this new frequency separation, one-dimensional modulation schemes (e.g., BPSK or M-ASK) can be transmitted without any degradation in the BER whereas two-dimensional modulation schemes (e.g., M-PSK or M-QAM) cannot

.

We write the FOFDM signal as follows

$$s(t) = \sum_{k=-\infty}^{\infty} \sum_{n=0}^{N-1} S_{kn} g_n(t-kT) \quad (5)$$

$$g_n(t) = \begin{cases} \frac{1}{\sqrt{T}} e^{j\frac{2\pi nt}{2T}}, & t \in [0,T] \\ 0, & t \notin [0,T] \end{cases} \quad (6)$$

Again, S_{kn} represents the complex data conveyed in time slot k and sub-channel n and $g_n(t-kT)$ represents the complex waveform (the complex sub-carrier) used to convey the complex data in the same time slot and sub-channel. The complex received symbol in time slot k and sub-channel n, R_{kn}, is recovered by multiplying the received FOFDM signal, $r(t)$, by the complex conjugate of the waveform used to convey this complex symbol, $g_n^*(t-kT)$, and integrating over kT and $(k+1)T$, i.e.,

$$R_{kn} = \int_{kT}^{(k+1)T} r(t) g_n^*(t-kT)dt \quad (7)$$

Again, by assuming that the received fast OFDM signal is ideal then

$$R_{kn} = \int_{kT}^{(k+1)T} \left[\sum_{k'=-\infty}^{\infty} \sum_{n'=0}^{N-1} S_{k'n'} g_{n'}(t-k'T) \right] g_n^*(t-kT)dt$$
$$= \sum_{n'=0}^{N-1} S_{kn'} \mathrm{sinc}\left(\frac{n'-n}{2}\right) e^{j\frac{\pi(n'-n)}{2}} \quad (8)$$

If the complex transmitted symbols S_{kn} belong to a one-dimensional signal constellation, which implies that $\mathrm{Re}\{S_{kn}\} \neq 0$ and $\mathrm{Im}\{S_{kn}\} = 0$, then the real part and the imaginary part of the complex received symbols are given by:

$$\mathrm{Re}\{R_{kn}\} = \sum_{n'=0}^{N-1} \mathrm{Re}\{S_{kn'}\} \mathrm{sinc}\left(\frac{n'-n}{2}\right) \cos\left(\frac{\pi(n'-n)}{2}\right) \quad (9)$$
$$= \mathrm{Re}\{S_{kn}\}$$

$$\mathrm{Im}\{R_{kn}\} = \sum_{n'=0}^{N-1} \mathrm{Re}\{S_{kn'}\} \mathrm{sinc}\left(\frac{n'-n}{2}\right) \sin\left(\frac{\pi(n'-n)}{2}\right) \quad (10)$$
$$\neq 0$$

In this case, the real part of the data is received without ICI whereas the imaginary part of the data is not. Thus, no degradation in the BER is expected for BPSK or M-ASK schemes transmitted using fast OFDM since the information is conveyed in $\mathrm{Re}\{S_{kn}\}$ and not in $\mathrm{Im}\{S_{kn}\}$. Alternatively, if the complex transmitted symbols S_{kn} belong to a two-dimensional signal constellation, which implies that $\mathrm{Re}\{S_{kn}\} \neq 0$ and $\mathrm{Im}\{S_{kn}\} \neq 0$, then the real part and the imaginary part of the complex received symbols are given by:

$$\mathrm{Re}\{R_{kn}\} = \sum_{n'=0}^{N-1} \mathrm{Re}\{S_{kn'}\} \mathrm{sinc}\left(\frac{n'-n}{2}\right) \cos\left(\frac{\pi(n'-n)}{2}\right)$$
$$- \sum_{n'=0}^{N-1} \mathrm{Im}\{S_{kn'}\} \mathrm{sinc}\left(\frac{n'-n}{2}\right) \sin\left(\frac{\pi(n'-n)}{2}\right) \quad (11)$$
$$\neq \mathrm{Re}\{S_{kn}\}$$

$$\mathrm{Im}\{R_{kn}\} = \sum_{n'=0}^{N-1} \mathrm{Re}\{S_{kn'}\} \mathrm{sinc}\left(\frac{n'-n}{2}\right) \sin\left(\frac{\pi(n'-n)}{2}\right)$$
$$+ \sum_{n'=0}^{N-1} \mathrm{Im}\{S_{kn'}\} \mathrm{sinc}\left(\frac{n'-n}{2}\right) \cos\left(\frac{\pi(n'-n)}{2}\right) \quad (12)$$
$$\neq \mathrm{Im}\{S_{kn}\}$$

In this case, there is ICI in the real and imaginary parts of the data. Thus, degradation in the BER is expected for M-PSK or M-QAM schemes transmitted using fast OFDM.

We conclude that one-dimensional modulation schemes can be transmitted with twice the bandwidth efficiency without any additional degradation using FOFDM whereas two-dimensional modulation schemes cannot.

Finally, it is interesting to note that a frequency separation of 1/2T between tones is also used in minimum shift keying (MSK) or in M-ary frequency shift keying (M-FSK) in order to achieve high bandwidth efficiency [5]. It is also interesting to note that a multi-carrier CDMA scheme that achieves twice the bandwidth efficiency has already been proposed elsewhere [6]. Essentially, it has been observed that in the binary case the IDFT output exhibits certain symmetries that enable the DFT input to be reconstructed based on approximately half the number of samples. Accordingly, by transmitting approximately half the number of

Published in the Proceedings of the International Conference on Telecommunications, vol. 2, pp. 484-487, June 2002. (Beijing, China)

samples the bandwidth was reduced by approximately a factor of two.

III. Results

In this section, we demonstrate the FOFDM concept by comparing our analytical predictions above (equations 9-12) to simulation results. We show both the demodulated points and the error probability for a 48 sub-channel FOFDM signal. We consider both one-dimensional (BPSK) and two-dimensional (QPSK) modulation of each FOFDM sub-channel.

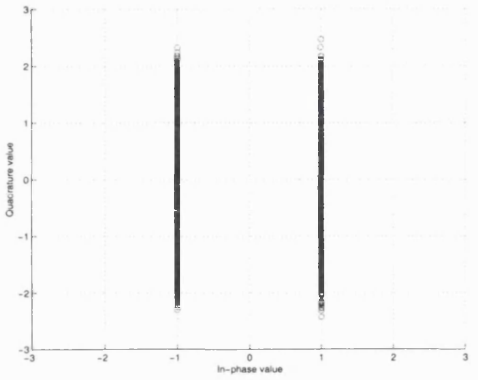

Figure 1: Demodulated points for a 48 sub-channel FOFDM/BPSK signal.

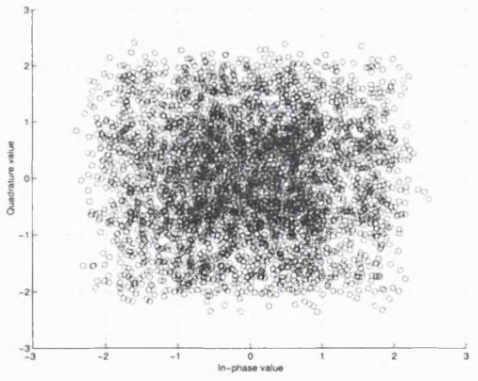

Figure 2: Demodulated points for a 48 sub-channel FOFDM/QPSK signal.

Figure 1 and Figure 2 show the demodulated points for a 48 sub-channel FOFDM signal using BPSK and QPSK modulation in each sub-channel, respectively. In the BPSK case, the real part of the data is received without ICI whereas the imaginary part of the data is not (in the graph this is evident from receiving a series of vertically aligned demodulated points). Thus, the transmitted data can be recovered without BER performance degradation when compared to OFDM. In the QPSK case, there is ICI both in the real part and the imaginary part of the data. Thus, we cannot recover the transmitted data and hence we expect severe degradation in the BER performance of the FOFDM scheme. Note that these results agree with the observations made in section II.

Figure 3 and Figure 4 show the error probability for a 48 sub-channel FOFDM signal using BPSK and QPSK modulation in each sub-channel, respectively. The OFDM error probability has also been included in these figures for comparison purposes. As expected, in the BPSK case the FOFDM signal error probability matches the OFDM signal error rate; in the QPSK case, the FOFDM signal error rate differs from the OFDM signal error rate. Again, these results agree with the observations made in section II.

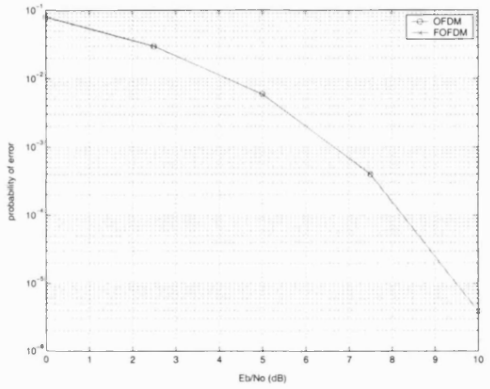

Figure 3: Error probability for a 48 sub-channel FOFDM/BPSK signal.

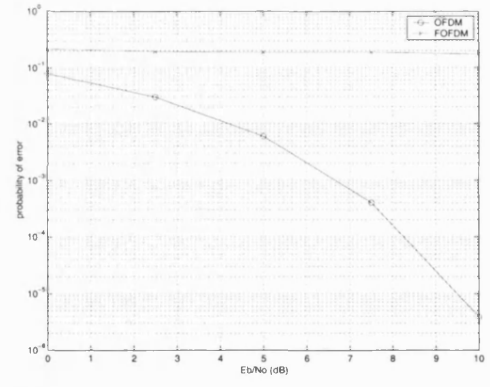

Figure 4: Error probability for a 48 sub-channel FOFDM/QPSK signal.

IV. Discussion

Having introduced the FOFDM concept it is now important to highlight the advantages and disadvantages of such a scheme. Particularly, a comparison of FOFDM to OFDM ought to be carried out.

Obviously, FOFDM with M-ASK modulation is entirely equivalent to OFDM with M-QAM modulation both from bandwidth efficiency and error probability points of view. This suggests that there may not be any advantage in using the former in comparison to the later. Yet, FOFDM may allow simpler implementation as it can be used with less complex data elements.

Other factors that must be taken into account when implementing a possible FOFDM system are

Published in the Proceedings of the International Conference on Telecommunications, vol. 2, pp. 484-487, June 2002. (Beijing, China)

its performance in a frequency selective fading environment and in the presence of synchronisation errors. These issues are separately discussed below.

A. Frequency selective fading

As explained before, the main advantage of OFDM modulation schemes is that they handle frequency selective fading efficiently without requiring complex equalisation procedures at the receiver. Essentially, by inserting a cyclic prefix whose duration is longer than the delay spread of the frequency selective fading channel, then the received symbol in time slot k and sub-channel n, R_{kn}, is related to the transmitted symbol in the same time slot and the same sub-channel, S_{kn}, as follows

$$R_{kn} = S_{kn} H_{kn} + N_{kn} \tag{13}$$

where H_{kn} is the channel transfer function in time slot k and sub-channel n and N_{kn} is the noise sample in the same time slot and sub-channel. Clearly, insertion of a cyclic prefix eliminates both inter-symbol interference and inter-carrier interference in a frequency selective fading environment. Moreover, insertion of a cyclic prefix allows the use of a simple one-tap equaliser at the receiver to correct for a possible attenuation/phase rotation of the received symbols.

In FOFDM such a simple relation between the received symbols and the transmitted symbols does not exist in a frequency selective fading channel even if an appropriate cyclic prefix is used. Essentially, FOFDM demands perfect alignment between the sub-carriers in order for inter-carrier interference to be eliminated which does not necessarily happen since a frequency selective channel will introduce different phase rotations in different sub-carriers.

A possible solution to this problem is to equalise the signal prior to demodulation. Yet, such an approach would be highly complex. Another possible solution to this problem is to employ pre-equalisation. Pre-equalisation has also been suggested for OFDM schemes in order to avoid the noise enhancement introduced by the equalisation procedure [7]. However, this approach requires knowledge of the channel transfer function which may not be always easy to obtain.

Further research is needed to assess the applicability of FOFDM in frequency selective fading environments.

B. Synchronisation error

The effects of synchronisation errors on OFDM modulation schemes have been the subject of intensive research [7]. Particularly, frequency offset errors and phase noise have been shown to introduce considerable inter-carrier interference and hence an increased degradation of the performance of these modulation schemes.

We anticipate that FOFDM may be more vulnerable to synchronisation errors due to the smaller inter-carrier frequency spacing.

A comparison of the performance of both schemes under such impairments ought to be the subject of future research.

V. Conclusions

In this paper, we have proposed a novel OFDM scheme with twice the bandwidth efficiency. We have shown that one-dimensional modulation schemes (e.g., BPSK or M-ASK) can be transmitted without any degradation in the BER whereas two-dimensional modulation schemes (e.g., M-PSK or M-QAM) cannot. We have also observed that although FOFDM with M-ASK modulation is equivalent to OFDM with M-QAM modulation, the former needs to handle only real data elements whereas the later needs to handle complex data elements. Accordingly, simpler implementations may be possible for FOFDM.

Acknowledgements

This work has been supported by the Fundação para a Ciência e a Tecnologia (Portugal) through the PRAXIS XXI scholarship programme.

References

[1] J. A. C. Bingham, "Multicarrier modulation for data transmission: an idea whose time has come," IEEE Communications Magazine, vol. 28, pp. 5-14, May 1990.

[2] W. Y. Zou and Y. Wu, "COFDM: an overview," IEEE Transactions on Broadcasting, vol. 41, pp. 1-8, March 1995.

[3] L. J. Cimini, "Analysis and simulation of a digital mobile channel using orthogonal frequency division multiplexing," IEEE Transactions on Communications, vol. 33, pp. 665-675, July 1985.

[4] S. B. Weinstein and P. M. Ebert, "Data transmission by frequency-division multiplexing using the discrete Fourier transform," IEEE Transactions on Communication Technology, vol. 19, pp. 628-634, October 1971.

[5] J. G. Proakis. *Digital Communications, 3rd ed.* Singapore: McGraw-Hill, 1995.

[6] J. Oh and M. Lim, "The bandwidth efficiency increasing method of multicarrier CDMA and its performance evaluation in comparison with DS-CDMA with rake receivers," Proc. of the IEEE VTC, vol. 1, pp. 561-565, May 1999.

[7] T. Keller and L. Hanzo, "Adaptive multicarrier modulation: A convenient framework for time-frequency processing in wireless communications," Proceedings of the IEEE, vol. 88, pp. 611-640, May 2000.

Appendix B

Skewness and kurtosis values of the IMD RV

In this appendix, we list skewness and kurtosis values of the RVs needed for error probability evaluation, i.e., the real part of the IMD RV in the OFDM/BPSK case and both the real part and the imaginary part of the IMD RV in the OFDM/QPSK case. Table B.1 and Table B.2 list skewness and kurtosis values, respectively, of the real part of the IMD RV in selected sub-channels for OFDM/BPSK signals with 16 to 128 sub-channels distorted by a reference non-linearity. Table B.3 and Table B.4 list skewness and kurtosis values, respectively, of both the real part and the imaginary part of the IMD RV in selected sub-channels for OFDM/QPSK signals distorted by a reference non-linearity. Note that skewness and kurtosis values do not depend on the symbol conditioning, i.e., A or $-A$ in the OFDM/BPSK case and $Ae^{j\pi/4}$, $Ae^{j3\pi/4}$, $Ae^{j5\pi/4}$ or $Ae^{j7\pi/4}$ in the OFDM/QPSK case. Note also that in the OFDM/QPSK case skewness and kurtosis values of the real part and the imaginary part of the IMD RV are identical. A frequency independent non-linearity has been adopted as a reference non-linearity.

Table B.1: Skewness values of the real part of the IMD RV in selected sub-channels (n) for OFDM/BPSK signals with 16 to 128 sub-channels (N).

n \ N	16	24	32	40	48	56	64	72	80	88	96	104	112	120	128
1	≅ 0	≅ 0	≅ 0	≅ 0	≅ 0	≅ 0	≅ 0	≅ 0	≅ 0	≅ 0	≅ 0	≅ 0	≅ 0	≅ 0	≅ 0
2	0.0293	0.0058	0.0020	0.0013	0.0004	0.0002	≅ 0	0.0001	≅ 0	0.0001	≅ 0	0.0001	≅ 0	≅ 0	≅ 0
3	0.0820	0.0167	0.0068	0.0024	0.0011	0.0009	0.0005	0.0002	0.0003	0.0001	≅ 0	≅ 0	0.0001	0.0001	≅ 0
4	0.1312	0.0358	0.0119	0.0055	0.0032	0.0019	0.0009	0.0007	0.0004	0.0003	0.0003	0.0002	0.0002	0.0002	0.0001
5	0.1854	0.0516	0.0170	0.0075	0.0045	0.0022	0.0018	0.0011	0.0008	0.0005	0.0004	0.0002	0.0002	0.0001	0.0001
6	0.2228	0.0639	0.0227	0.0116	0.0068	0.0031	0.0021	0.0019	0.0010	0.0006	0.0003	0.0004	0.0002	0.0002	0.0003
7	0.2775	0.0775	0.0358	0.0179	0.0077	0.0040	0.0027	0.0019	0.0015	0.0012	0.0005	0.0007	0.0006	0.0003	0.0002
8	0.3292	0.0853	0.0345	0.0180	0.0101	0.0072	0.0038	0.0024	0.0016	0.0010	0.0009	0.0008	0.0005	0.0001	0.0004
9	0.3292	0.1121	0.0447	0.0224	0.0115	0.0067	0.0040	0.0033	0.0021	0.0013	0.0013	0.0009	0.0008	0.0006	0.0005
10	0.2775	0.1158	0.0500	0.0266	0.0125	0.0075	0.0050	0.0025	0.0021	0.0018	0.0014	0.0010	0.0005	0.0005	0.0004
11	0.2228	0.1377	0.0524	0.0284	0.0149	0.0093	0.0051	0.0049	0.0025	0.0019	0.0018	0.0011	0.0010	0.0007	0.0005
12	0.1854	0.1513	0.0666	0.0317	0.0170	0.0105	0.0069	0.0044	0.0034	0.0019	0.0020	0.0014	0.0011	0.0009	0.0008
13	0.1312	0.1513	0.0693	0.0336	0.0202	0.0113	0.0078	0.0049	0.0033	0.0031	0.0014	0.0016	0.0015	0.0013	0.0007
14	0.0820	0.1377	0.0805	0.0336	0.0220	0.0126	0.0093	0.0051	0.0049	0.0031	0.0022	0.0015	0.0014	0.0010	0.0010
15	0.0293	0.1158	0.0822	0.0390	0.0236	0.0137	0.0091	0.0062	0.0034	0.0028	0.0027	0.0016	0.0013	0.0009	0.0009
16	≅ 0	0.1121	0.0943	0.0434	0.0230	0.0148	0.0106	0.0071	0.0045	0.0032	0.0031	0.0017	0.0016	0.0013	0.0008
17	-	0.0853	0.0943	0.0458	0.0270	0.0155	0.0103	0.0069	0.0049	0.0037	0.0024	0.0025	0.0017	0.0013	0.0015
18	-	0.0775	0.0822	0.0487	0.0278	0.0173	0.0108	0.0090	0.0057	0.0041	0.0032	0.0022	0.0020	0.0012	0.0010
19	-	0.0639	0.0805	0.0528	0.0320	0.0172	0.0108	0.0088	0.0054	0.0039	0.0037	0.0025	0.0020	0.0014	0.0012
20	-	0.0516	0.0693	0.0557	0.0309	0.0198	0.0121	0.0090	0.0067	0.0051	0.0035	0.0032	0.0021	0.0018	0.0014
21	-	0.0358	0.0666	0.0557	0.0346	0.0199	0.0136	0.0085	0.0075	0.0044	0.0041	0.0029	0.0021	0.0021	0.0015
22	-	0.0167	0.0524	0.0528	0.0358	0.0220	0.0142	0.0099	0.0079	0.0053	0.0041	0.0032	0.0024	0.0018	0.0016
23	-	0.0058	0.0500	0.0487	0.0367	0.0247	0.0152	0.0113	0.0068	0.0061	0.0042	0.0033	0.0025	0.0023	0.0018
24	-	≅ 0	0.0447	0.0458	0.0392	0.0232	0.0167	0.0103	0.0075	0.0056	0.0042	0.0030	0.0024	0.0024	0.0014
25	-	-	0.0345	0.0434	0.0392	0.0251	0.0162	0.0114	0.0084	0.0059	0.0046	0.0036	0.0029	0.0027	0.0014
26	-	-	0.0358	0.0390	0.0367	0.0251	0.0165	0.0112	0.0083	0.0052	0.0049	0.0035	0.0034	0.0021	0.0022
27	-	-	0.0227	0.0336	0.0358	0.0286	0.0181	0.0131	0.0090	0.0064	0.0054	0.0040	0.0029	0.0025	0.0019
28	-	-	0.0170	0.0336	0.0346	0.0282	0.0196	0.0133	0.0090	0.0066	0.0055	0.0041	0.0036	0.0029	0.0020
29	-	-	0.0119	0.0317	0.0309	0.0282	0.0200	0.0134	0.0099	0.0073	0.0068	0.0048	0.0033	0.0027	0.0021
30	-	-	0.0068	0.0284	0.0320	0.0286	0.0206	0.0138	0.0092	0.0077	0.0056	0.0045	0.0043	0.0028	0.0021
31	-	-	0.0020	0.0266	0.0278	0.0251	0.0222	0.0156	0.0110	0.0078	0.0054	0.0046	0.0037	0.0022	0.0025
32	-	-	≅ 0	0.0224	0.0270	0.0251	0.0236	0.0164	0.0118	0.0083	0.0060	0.0044	0.0041	0.0031	0.0028
33	-	-	-	0.0180	0.0230	0.0232	0.0236	0.0172	0.0109	0.0089	0.0070	0.0048	0.0041	0.0034	0.0027
34	-	-	-	0.0179	0.0236	0.0247	0.0222	0.0156	0.0135	0.0079	0.0062	0.0047	0.0041	0.0034	0.0029
35	-	-	-	0.0116	0.0220	0.0220	0.0206	0.0181	0.0131	0.0097	0.0072	0.0057	0.0047	0.0033	0.0029
36	-	-	-	0.0075	0.0202	0.0199	0.0200	0.0183	0.0134	0.0094	0.0067	0.0052	0.0046	0.0040	0.0029
37	-	-	-	0.0055	0.0170	0.0198	0.0196	0.0183	0.0135	0.0095	0.0068	0.0062	0.0042	0.0035	0.0027
38	-	-	-	0.0024	0.0149	0.0172	0.0181	0.0181	0.0140	0.0105	0.0082	0.0056	0.0039	0.0040	0.0033
39	-	-	-	0.0013	0.0125	0.0173	0.0165	0.0156	0.0142	0.0105	0.0074	0.0070	0.0053	0.0044	0.0036
40	-	-	-	≅ 0	0.0115	0.0155	0.0162	0.0172	0.0154	0.0106	0.0082	0.0067	0.0051	0.0042	0.0029
41	-	-	-	-	0.0101	0.0148	0.0167	0.0164	0.0154	0.0115	0.0091	0.0061	0.0060	0.0041	0.0034
42	-	-	-	-	0.0077	0.0137	0.0152	0.0156	0.0142	0.0117	0.0087	0.0071	0.0052	0.0039	0.0040
43	-	-	-	-	0.0068	0.0126	0.0142	0.0138	0.0140	0.0117	0.0094	0.0067	0.0057	0.0047	0.0036
44	-	-	-	-	0.0045	0.0113	0.0136	0.0134	0.0135	0.0123	0.0102	0.0077	0.0056	0.0048	0.0037
45	-	-	-	-	0.0032	0.0105	0.0121	0.0133	0.0134	0.0123	0.0102	0.0079	0.0059	0.0052	0.0037
46	-	-	-	-	0.0011	0.0093	0.0108	0.0131	0.0131	0.0117	0.0093	0.0073	0.0064	0.0051	0.0040
47	-	-	-	-	0.0004	0.0075	0.0108	0.0112	0.0135	0.0117	0.0109	0.0080	0.0060	0.0049	0.0035
48	-	-	-	-	≅ 0	0.0067	0.0103	0.0114	0.0109	0.0115	0.0102	0.0078	0.0066	0.0054	0.0038
49	-	-	-	-	-	0.0072	0.0106	0.0103	0.0118	0.0106	0.0102	0.0078	0.0067	0.0054	0.0044
50	-	-	-	-	-	0.0040	0.0091	0.0113	0.0110	0.0105	0.0109	0.0083	0.0065	0.0051	0.0044
51	-	-	-	-	-	0.0031	0.0093	0.0099	0.0092	0.0105	0.0093	0.0085	0.0065	0.0059	0.0046
52	-	-	-	-	-	0.0022	0.0078	0.0085	0.0099	0.0095	0.0102	0.0095	0.0074	0.0060	0.0040
53	-	-	-	-	-	0.0019	0.0069	0.0090	0.0090	0.0094	0.0102	0.0095	0.0063	0.0056	0.0047
54	-	-	-	-	-	0.0009	0.0051	0.0088	0.0090	0.0097	0.0094	0.0085	0.0071	0.0058	0.0056
55	-	-	-	-	-	0.0002	0.0050	0.0090	0.0083	0.0079	0.0087	0.0083	0.0074	0.0067	0.0046
56	-	-	-	-	-	≅ 0	0.0040	0.0069	0.0084	0.0089	0.0091	0.0078	0.0079	0.0061	0.0043
57	-	-	-	-	-	-	0.0038	0.0071	0.0075	0.0083	0.0082	0.0078	0.0079	0.0059	0.0058
58	-	-	-	-	-	-	0.0027	0.0062	0.0068	0.0078	0.0074	0.0080	0.0074	0.0062	0.0057
59	-	-	-	-	-	-	0.0021	0.0051	0.0079	0.0077	0.0082	0.0073	0.0071	0.0067	0.0051
60	-	-	-	-	-	-	0.0018	0.0049	0.0075	0.0073	0.0068	0.0079	0.0063	0.0069	0.0060
61	-	-	-	-	-	-	0.0009	0.0044	0.0067	0.0066	0.0067	0.0077	0.0074	0.0069	0.0056
62	-	-	-	-	-	-	0.0005	0.0049	0.0054	0.0064	0.0072	0.0067	0.0065	0.0067	0.0056
63	-	-	-	-	-	-	≅ 0	0.0025	0.0057	0.0052	0.0062	0.0071	0.0065	0.0062	0.0058
64	-	-	-	-	-	-	≅ 0	0.0033	0.0049	0.0059	0.0070	0.0061	0.0067	0.0059	0.0068

n \ N	16	24	32	40	48	56	64	72	80	88	96	104	112	120	128
65	-	-	-	-	-	-	-	0.0024	0.0045	0.0056	0.0060	0.0067	0.0066	0.0061	0.0068
66	-	-	-	-	-	-	-	0.0019	0.0034	0.0061	0.0054	0.0070	0.0060	0.0067	0.0058
67	-	-	-	-	-	-	-	0.0019	0.0049	0.0053	0.0056	0.0056	0.0064	0.0058	0.0056
68	-	-	-	-	-	-	-	0.0011	0.0033	0.0044	0.0068	0.0062	0.0059	0.0056	0.0056
69	-	-	-	-	-	-	-	0.0007	0.0034	0.0051	0.0055	0.0052	0.0056	0.0060	0.0060
70	-	-	-	-	-	-	-	0.0002	0.0025	0.0039	0.0054	0.0057	0.0057	0.0059	0.0051
71	-	-	-	-	-	-	-	0.0001	0.0021	0.0041	0.0049	0.0047	0.0052	0.0051	0.0057
72	-	-	-	-	-	-	-	≅ 0	0.0021	0.0037	0.0046	0.0048	0.0060	0.0054	0.0058
73	-	-	-	-	-	-	-	-	0.0016	0.0032	0.0042	0.0044	0.0051	0.0054	0.0043
74	-	-	-	-	-	-	-	-	0.0015	0.0028	0.0042	0.0046	0.0053	0.0049	0.0046
75	-	-	-	-	-	-	-	-	0.0010	0.0031	0.0041	0.0045	0.0039	0.0051	0.0056
76	-	-	-	-	-	-	-	-	0.0008	0.0031	0.0041	0.0048	0.0042	0.0052	0.0047
77	-	-	-	-	-	-	-	-	0.0004	0.0019	0.0035	0.0041	0.0046	0.0048	0.0040
78	-	-	-	-	-	-	-	-	0.0003	0.0019	0.0037	0.0040	0.0047	0.0047	0.0046
79	-	-	-	-	-	-	-	-	≅ 0	0.0018	0.0032	0.0035	0.0041	0.0039	0.0044
80	-	-	-	-	-	-	-	-	≅ 0	0.0013	0.0024	0.0036	0.0041	0.0041	0.0044
81	-	-	-	-	-	-	-	-	-	0.0010	0.0031	0.0030	0.0041	0.0042	0.0038
82	-	-	-	-	-	-	-	-	-	0.0012	0.0027	0.0033	0.0037	0.0044	0.0035
83	-	-	-	-	-	-	-	-	-	0.0006	0.0022	0.0032	0.0043	0.0040	0.0040
84	-	-	-	-	-	-	-	-	-	0.0005	0.0014	0.0029	0.0033	0.0035	0.0037
85	-	-	-	-	-	-	-	-	-	0.0003	0.0020	0.0032	0.0036	0.0040	0.0037
86	-	-	-	-	-	-	-	-	-	0.0001	0.0018	0.0025	0.0029	0.0033	0.0036
87	-	-	-	-	-	-	-	-	-	0.0001	0.0014	0.0022	0.0034	0.0034	0.0040
88	-	-	-	-	-	-	-	-	-	≅ 0	0.0013	0.0025	0.0029	0.0034	0.0034
89	-	-	-	-	-	-	-	-	-	-	0.0009	0.0017	0.0024	0.0031	0.0029
90	-	-	-	-	-	-	-	-	-	-	0.0005	0.0016	0.0025	0.0022	0.0036
91	-	-	-	-	-	-	-	-	-	-	0.0003	0.0015	0.0024	0.0028	0.0033
92	-	-	-	-	-	-	-	-	-	-	0.0004	0.0016	0.0021	0.0027	0.0027
93	-	-	-	-	-	-	-	-	-	-	0.0003	0.0014	0.0021	0.0029	0.0029
94	-	-	-	-	-	-	-	-	-	-	≅ 0	0.0011	0.0020	0.0025	0.0029
95	-	-	-	-	-	-	-	-	-	-	≅ 0	0.0010	0.0020	0.0021	0.0029
96	-	-	-	-	-	-	-	-	-	-	≅ 0	0.0009	0.0017	0.0027	0.0027
97	-	-	-	-	-	-	-	-	-	-	-	0.0008	0.0016	0.0024	0.0028
98	-	-	-	-	-	-	-	-	-	-	-	0.0007	0.0013	0.0023	0.0025
99	-	-	-	-	-	-	-	-	-	-	-	0.0004	0.0014	0.0018	0.0021
100	-	-	-	-	-	-	-	-	-	-	-	0.0002	0.0015	0.0021	0.0021
101	-	-	-	-	-	-	-	-	-	-	-	0.0002	0.0011	0.0018	0.0020
102	-	-	-	-	-	-	-	-	-	-	-	≅ 0	0.0010	0.0014	0.0019
103	-	-	-	-	-	-	-	-	-	-	-	0.0001	0.0005	0.0012	0.0022
104	-	-	-	-	-	-	-	-	-	-	-	≅ 0	0.0008	0.0013	0.0014
105	-	-	-	-	-	-	-	-	-	-	-	-	0.0005	0.0013	0.0014
106	-	-	-	-	-	-	-	-	-	-	-	-	0.0006	0.0009	0.0018
107	-	-	-	-	-	-	-	-	-	-	-	-	0.0002	0.0010	0.0016
108	-	-	-	-	-	-	-	-	-	-	-	-	0.0002	0.0013	0.0015
109	-	-	-	-	-	-	-	-	-	-	-	-	0.0002	0.0009	0.0014
110	-	-	-	-	-	-	-	-	-	-	-	-	0.0001	0.0007	0.0012
111	-	-	-	-	-	-	-	-	-	-	-	-	≅ 0	0.0005	0.0010
112	-	-	-	-	-	-	-	-	-	-	-	-	≅ 0	0.0006	0.0015
113	-	-	-	-	-	-	-	-	-	-	-	-	-	0.0001	0.0008
114	-	-	-	-	-	-	-	-	-	-	-	-	-	0.0003	0.0009
115	-	-	-	-	-	-	-	-	-	-	-	-	-	0.0002	0.0010
116	-	-	-	-	-	-	-	-	-	-	-	-	-	0.0001	0.0007
117	-	-	-	-	-	-	-	-	-	-	-	-	-	0.0002	0.0008
118	-	-	-	-	-	-	-	-	-	-	-	-	-	0.0001	0.0005
119	-	-	-	-	-	-	-	-	-	-	-	-	-	≅ 0	0.0004
120	-	-	-	-	-	-	-	-	-	-	-	-	-	≅ 0	0.0005
121	-	-	-	-	-	-	-	-	-	-	-	-	-	-	0.0004
122	-	-	-	-	-	-	-	-	-	-	-	-	-	-	0.0002
123	-	-	-	-	-	-	-	-	-	-	-	-	-	-	0.0003
124	-	-	-	-	-	-	-	-	-	-	-	-	-	-	0.0001
125	-	-	-	-	-	-	-	-	-	-	-	-	-	-	0.0001
126	-	-	-	-	-	-	-	-	-	-	-	-	-	-	≅ 0
127	-	-	-	-	-	-	-	-	-	-	-	-	-	-	≅ 0
128	-	-	-	-	-	-	-	-	-	-	-	-	-	-	≅ 0

Table B.2: Kurtosis values of the real part of the IMD RV in selected sub-channels (n) for OFDM/BPSK signals with 16 to 128 sub-channels (N).

n \ N	16	24	32	40	48	56	64	72	80	88	96	104	112	120	128
1	4.5979	4.1606	3.8867	3.7413	3.6286	3.5415	3.4961	3.4475	3.4173	3.3721	3.3545	3.3345	3.3209	3.2906	3.2666
2	5.2068	4.4919	4.1115	3.8881	3.7090	3.5999	3.5475	3.4937	3.4371	3.4202	3.3864	3.3593	3.3283	3.3050	3.2863
3	5.5203	4.6925	4.2423	3.9829	3.7936	3.6925	3.5895	3.5327	3.4901	3.4442	3.4017	3.3693	3.3513	3.3465	3.2945
4	5.6937	4.8560	4.3529	4.0489	3.8599	3.7335	3.6221	3.5738	3.5007	3.4888	3.4380	3.4066	3.3833	3.3483	3.3148
5	5.8938	4.9738	4.4515	4.1400	3.9052	3.7755	3.6892	3.6121	3.5354	3.5081	3.4567	3.4019	3.3806	3.3641	3.3333
6	5.9896	5.0348	4.5621	4.1651	3.9530	3.8050	3.7127	3.6453	3.5676	3.5102	3.4844	3.4360	3.4044	3.3754	3.3457
7	6.0311	5.0882	4.5963	4.2611	4.0277	3.8374	3.7419	3.6590	3.6041	3.5402	3.4673	3.4418	3.4027	3.3835	3.3594
8	6.0512	5.1984	4.6089	4.2480	4.0250	3.8831	3.7679	3.6764	3.6093	3.5521	3.4909	3.4551	3.4245	3.3926	3.3725
9	6.0512	5.3369	4.6749	4.2934	4.0537	3.8974	3.7952	3.6982	3.6257	3.5597	3.5242	3.4674	3.4420	3.3996	3.3625
10	6.0311	5.1999	4.6575	4.3135	4.0944	3.9199	3.7821	3.6957	3.6514	3.5843	3.5371	3.4951	3.4426	3.4254	3.3663
11	5.9896	5.2720	4.7375	4.3926	4.1002	3.9268	3.8231	3.7308	3.6664	3.5866	3.5370	3.4913	3.4414	3.4101	3.3861
12	5.8938	5.2904	4.7716	4.3647	4.1167	3.9521	3.8421	3.7278	3.6561	3.5931	3.5598	3.4998	3.4562	3.4277	3.3911
13	5.6937	5.2904	4.8362	4.4282	4.1385	3.9876	3.8652	3.7663	3.6829	3.6178	3.5647	3.5054	3.4775	3.4329	3.4052
14	5.5203	5.2720	4.7713	4.4197	4.1795	3.9809	3.8724	3.7691	3.7016	3.6102	3.5783	3.5255	3.4782	3.4533	3.4060
15	5.2068	5.1999	4.8221	4.4411	4.1616	4.0269	3.8602	3.7761	3.7040	3.6435	3.5557	3.5328	3.5024	3.4603	3.4098
16	4.5979	5.3369	4.8777	4.4391	4.1718	4.0087	3.9234	3.8011	3.7346	3.6389	3.5800	3.5441	3.5071	3.4678	3.4296
17	-	5.1984	4.8777	4.4560	4.2352	4.0226	3.8863	3.8118	3.7306	3.6540	3.5995	3.5550	3.5089	3.4796	3.4458
18	-	5.0882	4.8221	4.4571	4.2187	4.0447	3.9332	3.8135	3.7319	3.6850	3.6118	3.5570	3.5213	3.4815	3.4479
19	-	5.0348	4.7713	4.5250	4.2172	4.0233	3.8747	3.8106	3.7191	3.6707	3.6184	3.5693	3.5253	3.4808	3.4338
20	-	4.9738	4.8362	4.5002	4.1921	4.0593	3.9235	3.8387	3.7484	3.6764	3.6311	3.5573	3.5299	3.4974	3.4538
21	-	4.8560	4.7716	4.5002	4.2826	4.0432	3.9088	3.8140	3.7505	3.6984	3.6322	3.5516	3.5414	3.4717	3.4551
22	-	4.6925	4.7375	4.5250	4.2256	4.0174	3.9152	3.8258	3.7530	3.6766	3.6432	3.5817	3.5319	3.4904	3.4573
23	-	4.4919	4.6575	4.4571	4.2252	4.0595	3.9407	3.8357	3.7540	3.7030	3.6514	3.5697	3.5291	3.5046	3.4677
24	-	4.1606	4.6749	4.4560	4.2414	4.0876	3.9255	3.8365	3.7564	3.6671	3.6335	3.5652	3.5218	3.4800	3.4590
25	-	-	4.6089	4.4391	4.2414	4.0536	3.9495	3.8517	3.7757	3.7007	3.6492	3.6023	3.5318	3.5063	3.4730
26	-	-	4.5963	4.4411	4.2252	4.0893	3.9598	3.8425	3.7722	3.7115	3.6333	3.5941	3.5515	3.5086	3.4737
27	-	-	4.5621	4.4197	4.2256	4.1010	3.9624	3.8740	3.7862	3.7183	3.6430	3.5991	3.5608	3.5018	3.4818
28	-	-	4.4515	4.4282	4.2826	4.0802	3.9541	3.8938	3.7665	3.7038	3.6558	3.6013	3.5691	3.5121	3.5013
29	-	-	4.3529	4.3647	4.1921	4.0802	3.9650	3.8706	3.7739	3.7162	3.6569	3.6327	3.5828	3.5170	3.4818
30	-	-	4.2423	4.3926	4.2172	4.1010	3.9420	3.8738	3.8138	3.7036	3.6478	3.6163	3.5730	3.5261	3.4887
31	-	-	4.1115	4.3135	4.2187	4.0893	3.9904	3.8551	3.7754	3.7212	3.6833	3.6055	3.5671	3.5393	3.5105
32	-	-	3.8867	4.2934	4.2352	4.0536	3.9729	3.8813	3.8100	3.7105	3.6893	3.6240	3.5870	3.5318	3.4886
33	-	-	-	4.2480	4.1718	4.0876	3.9729	3.8788	3.8148	3.7529	3.6870	3.6340	3.5789	3.5398	3.5126
34	-	-	-	4.2611	4.1616	4.0595	3.9904	3.9159	3.8221	3.7292	3.6726	3.6376	3.5926	3.5273	3.5139
35	-	-	-	4.1651	4.1795	4.0174	3.9420	3.9077	3.7997	3.7513	3.6878	3.6467	3.5905	3.5713	3.4967
36	-	-	-	4.1400	4.1385	4.0432	3.9650	3.8839	3.8141	3.7523	3.6731	3.6187	3.5966	3.5552	3.5089
37	-	-	-	4.0489	4.1167	4.0593	3.9541	3.8839	3.8349	3.7487	3.6926	3.6474	3.5781	3.5559	3.5187
38	-	-	-	3.9829	4.1002	4.0233	3.9624	3.9077	3.7976	3.7751	3.6848	3.6374	3.6089	3.5571	3.5204
39	-	-	-	3.8881	4.0944	4.0447	3.9598	3.9159	3.8165	3.7614	3.6998	3.6531	3.5929	3.5670	3.5121
40	-	-	-	3.7413	4.0537	4.0226	3.9495	3.8788	3.8299	3.7458	3.6901	3.6700	3.6029	3.5561	3.5256
41	-	-	-	-	4.0250	4.0087	3.9255	3.8813	3.8299	3.7776	3.7079	3.6374	3.6053	3.5667	3.5105
42	-	-	-	-	4.0277	4.0269	3.9407	3.8551	3.8165	3.7591	3.7027	3.6613	3.6078	3.5656	3.5367
43	-	-	-	-	3.9530	3.9809	3.9152	3.8738	3.7976	3.7732	3.7070	3.6660	3.6246	3.5780	3.5325
44	-	-	-	-	3.9052	3.9876	3.9088	3.8706	3.8349	3.7611	3.7312	3.6738	3.6096	3.5724	3.5408
45	-	-	-	-	3.8599	3.9521	3.9235	3.8938	3.8141	3.7611	3.7254	3.6702	3.6112	3.5791	3.5473
46	-	-	-	-	3.7936	3.9268	3.8747	3.8740	3.7997	3.7732	3.7170	3.7085	3.6254	3.5724	3.5508
47	-	-	-	-	3.7090	3.9199	3.9332	3.8425	3.8221	3.7591	3.7213	3.6763	3.6264	3.5706	3.5222
48	-	-	-	-	3.6286	3.8974	3.8863	3.8517	3.8148	3.7776	3.7085	3.6542	3.6265	3.5871	3.5517
49	-	-	-	-	-	3.8831	3.9234	3.8365	3.8100	3.7458	3.7085	3.6897	3.6099	3.5890	3.5355
50	-	-	-	-	-	3.8374	3.8602	3.8357	3.7754	3.7614	3.7213	3.6665	3.6165	3.5731	3.5440
51	-	-	-	-	-	3.8050	3.8724	3.8258	3.8138	3.7751	3.7170	3.6729	3.6395	3.5858	3.5332
52	-	-	-	-	-	3.7755	3.8652	3.8140	3.7739	3.7487	3.7254	3.6638	3.6349	3.5961	3.5325
53	-	-	-	-	-	3.7335	3.8421	3.8387	3.7665	3.7523	3.7312	3.6638	3.6510	3.5772	3.5485
54	-	-	-	-	-	3.6925	3.8231	3.8106	3.7862	3.7513	3.7070	3.6729	3.6504	3.6032	3.5574
55	-	-	-	-	-	3.5999	3.7821	3.8135	3.7722	3.7292	3.7027	3.6665	3.6247	3.5879	3.5555
56	-	-	-	-	-	3.5415	3.7952	3.8118	3.7757	3.7529	3.7079	3.6897	3.6192	3.6004	3.5510
57	-	-	-	-	-	-	3.7679	3.8011	3.7564	3.7105	3.6901	3.6542	3.6192	3.6026	3.5637
58	-	-	-	-	-	-	3.7419	3.7761	3.7540	3.7212	3.6998	3.6763	3.6247	3.5917	3.5618
59	-	-	-	-	-	-	3.7127	3.7691	3.7530	3.7036	3.6848	3.7085	3.6504	3.5945	3.5692
60	-	-	-	-	-	-	3.6892	3.7663	3.7505	3.7162	3.6926	3.6702	3.6510	3.6004	3.5712
61	-	-	-	-	-	-	3.6221	3.7278	3.7484	3.7038	3.6731	3.6738	3.6349	3.6004	3.5417
62	-	-	-	-	-	-	3.5895	3.7308	3.7191	3.7183	3.6878	3.6660	3.6395	3.5945	3.5668
63	-	-	-	-	-	-	3.5475	3.6957	3.7319	3.7115	3.6726	3.6613	3.6165	3.5917	3.5513
64	-	-	-	-	-	-	3.4961	3.6982	3.7306	3.7007	3.6870	3.6374	3.6099	3.6026	3.5829

n \ N	16	24	32	40	48	56	64	72	80	88	96	104	112	120	128
65	-	-	-	-	-	-	-	3.6764	3.7346	3.6671	3.6893	3.6700	3.6265	3.6004	3.5829
66	-	-	-	-	-	-	-	3.6590	3.7040	3.7030	3.6833	3.6531	3.6264	3.5879	3.5513
67	-	-	-	-	-	-	-	3.6453	3.7016	3.6766	3.6478	3.6374	3.6254	3.6032	3.5668
68	-	-	-	-	-	-	-	3.6121	3.6829	3.6984	3.6569	3.6474	3.6112	3.5772	3.5417
69	-	-	-	-	-	-	-	3.5738	3.6561	3.6764	3.6558	3.6187	3.6096	3.5961	3.5712
70	-	-	-	-	-	-	-	3.5327	3.6664	3.6707	3.6430	3.6467	3.6246	3.5858	3.5692
71	-	-	-	-	-	-	-	3.4937	3.6514	3.6850	3.6333	3.6376	3.6078	3.5731	3.5618
72	-	-	-	-	-	-	-	3.4475	3.6257	3.6540	3.6492	3.6340	3.6053	3.5890	3.5637
73	-	-	-	-	-	-	-	-	3.6093	3.6389	3.6335	3.6240	3.6029	3.5871	3.5510
74	-	-	-	-	-	-	-	-	3.6041	3.6435	3.6514	3.6055	3.5929	3.5706	3.5555
75	-	-	-	-	-	-	-	-	3.5676	3.6102	3.6432	3.6163	3.6089	3.5724	3.5574
76	-	-	-	-	-	-	-	-	3.5354	3.6178	3.6322	3.6327	3.5781	3.5791	3.5485
77	-	-	-	-	-	-	-	-	3.5007	3.5931	3.6311	3.6013	3.5966	3.5724	3.5325
78	-	-	-	-	-	-	-	-	3.4901	3.5866	3.6184	3.5991	3.5905	3.5780	3.5332
79	-	-	-	-	-	-	-	-	3.4371	3.5843	3.6118	3.5941	3.5926	3.5656	3.5440
80	-	-	-	-	-	-	-	-	3.4173	3.5597	3.5995	3.6023	3.5789	3.5667	3.5355
81	-	-	-	-	-	-	-	-	-	3.5521	3.5800	3.5652	3.5870	3.5561	3.5517
82	-	-	-	-	-	-	-	-	-	3.5402	3.5557	3.5697	3.5671	3.5670	3.5222
83	-	-	-	-	-	-	-	-	-	3.5102	3.5783	3.5817	3.5730	3.5571	3.5508
84	-	-	-	-	-	-	-	-	-	3.5081	3.5647	3.5516	3.5828	3.5559	3.5473
85	-	-	-	-	-	-	-	-	-	3.4888	3.5598	3.5573	3.5691	3.5552	3.5408
86	-	-	-	-	-	-	-	-	-	3.4442	3.5370	3.5693	3.5608	3.5713	3.5325
87	-	-	-	-	-	-	-	-	-	3.4202	3.5371	3.5570	3.5515	3.5273	3.5367
88	-	-	-	-	-	-	-	-	-	3.3721	3.5242	3.5550	3.5318	3.5398	3.5105
89	-	-	-	-	-	-	-	-	-	-	3.4909	3.5441	3.5218	3.5318	3.5256
90	-	-	-	-	-	-	-	-	-	-	3.4673	3.5328	3.5291	3.5393	3.5121
91	-	-	-	-	-	-	-	-	-	-	3.4844	3.5255	3.5319	3.5261	3.5204
92	-	-	-	-	-	-	-	-	-	-	3.4567	3.5054	3.5414	3.5170	3.5187
93	-	-	-	-	-	-	-	-	-	-	3.4380	3.4998	3.5299	3.5121	3.5089
94	-	-	-	-	-	-	-	-	-	-	3.4017	3.4913	3.5253	3.5018	3.4967
95	-	-	-	-	-	-	-	-	-	-	3.3864	3.4951	3.5213	3.5086	3.5139
96	-	-	-	-	-	-	-	-	-	-	3.3545	3.4674	3.5089	3.5063	3.5126
97	-	-	-	-	-	-	-	-	-	-	-	3.4551	3.5071	3.4800	3.4886
98	-	-	-	-	-	-	-	-	-	-	-	3.4418	3.5024	3.5046	3.5105
99	-	-	-	-	-	-	-	-	-	-	-	3.4360	3.4782	3.4904	3.4887
100	-	-	-	-	-	-	-	-	-	-	-	3.4019	3.4775	3.4717	3.4818
101	-	-	-	-	-	-	-	-	-	-	-	3.4066	3.4562	3.4974	3.5013
102	-	-	-	-	-	-	-	-	-	-	-	3.3693	3.4414	3.4808	3.4818
103	-	-	-	-	-	-	-	-	-	-	-	3.3593	3.4426	3.4815	3.4737
104	-	-	-	-	-	-	-	-	-	-	-	3.3345	3.4420	3.4796	3.4730
105	-	-	-	-	-	-	-	-	-	-	-	-	3.4245	3.4678	3.4590
106	-	-	-	-	-	-	-	-	-	-	-	-	3.4027	3.4603	3.4677
107	-	-	-	-	-	-	-	-	-	-	-	-	3.4044	3.4533	3.4573
108	-	-	-	-	-	-	-	-	-	-	-	-	3.3806	3.4329	3.4551
109	-	-	-	-	-	-	-	-	-	-	-	-	3.3833	3.4277	3.4538
110	-	-	-	-	-	-	-	-	-	-	-	-	3.3513	3.4101	3.4338
111	-	-	-	-	-	-	-	-	-	-	-	-	3.3283	3.4254	3.4479
112	-	-	-	-	-	-	-	-	-	-	-	-	3.3209	3.3996	3.4458
113	-	-	-	-	-	-	-	-	-	-	-	-	-	3.3926	3.4296
114	-	-	-	-	-	-	-	-	-	-	-	-	-	3.3835	3.4098
115	-	-	-	-	-	-	-	-	-	-	-	-	-	3.3754	3.4060
116	-	-	-	-	-	-	-	-	-	-	-	-	-	3.3641	3.4052
117	-	-	-	-	-	-	-	-	-	-	-	-	-	3.3483	3.3911
118	-	-	-	-	-	-	-	-	-	-	-	-	-	3.3465	3.3861
119	-	-	-	-	-	-	-	-	-	-	-	-	-	3.3050	3.3663
120	-	-	-	-	-	-	-	-	-	-	-	-	-	3.2906	3.3625
121	-	-	-	-	-	-	-	-	-	-	-	-	-	-	3.3725
122	-	-	-	-	-	-	-	-	-	-	-	-	-	-	3.3594
123	-	-	-	-	-	-	-	-	-	-	-	-	-	-	3.3457
124	-	-	-	-	-	-	-	-	-	-	-	-	-	-	3.3333
125	-	-	-	-	-	-	-	-	-	-	-	-	-	-	3.3148
126	-	-	-	-	-	-	-	-	-	-	-	-	-	-	3.2945
127	-	-	-	-	-	-	-	-	-	-	-	-	-	-	3.2863
128	-	-	-	-	-	-	-	-	-	-	-	-	-	-	3.2666

Table B.3: Skewness values of the real and imaginary parts of the IMD RV in selected sub-channels (n) for OFDM/QPSK signals with 16 to 128 sub-channels (N).

n \ N	16	24	32	40	48	56	64	72	80	88	96	104	112	120	128
1	≅ 0	≅ 0	≅ 0	≅ 0	≅ 0	≅ 0	≅ 0	≅ 0	≅ 0	≅ 0	≅ 0	≅ 0	≅ 0	≅ 0	≅ 0
2	0.0081	0.0017	0.0005	0.0002	0.0001	≅ 0	≅ 0	≅ 0	≅ 0	≅ 0	≅ 0	≅ 0	≅ 0	≅ 0	≅ 0
3	0.0199	0.0046	0.0018	0.0007	0.0002	0.0003	0.0002	0.0001	0.0001	≅ 0	0.0001	≅ 0	≅ 0	≅ 0	≅ 0
4	0.0294	0.0083	0.0029	0.0013	0.0006	0.0004	0.0003	0.0003	0.0001	0.0001	0.0001	≅ 0	0.0001	≅ 0	≅ 0
5	0.0453	0.0120	0.0053	0.0022	0.0015	0.0007	0.0002	0.0003	0.0003	0.0001	0.0001	0.0001	≅ 0	≅ 0	0.0001
6	0.0570	0.0171	0.0068	0.0035	0.0017	0.0011	0.0005	0.0005	0.0002	0.0002	0.0002	0.0001	0.0001	0.0001	≅ 0
7	0.0677	0.0178	0.0075	0.0037	0.0022	0.0013	0.0008	0.0004	0.0004	0.0002	0.0002	0.0001	0.0001	≅ 0	0.0001
8	0.0804	0.0217	0.0082	0.0044	0.0027	0.0015	0.0010	0.0007	0.0005	0.0001	0.0003	0.0001	0.0001	0.0001	0.0001
9	0.0804	0.0252	0.0116	0.0047	0.0030	0.0018	0.0008	0.0008	0.0004	0.0005	0.0002	0.0004	0.0002	0.0001	0.0001
10	0.0677	0.0290	0.0118	0.0060	0.0033	0.0022	0.0012	0.0009	0.0007	0.0004	0.0004	0.0003	0.0001	0.0002	0.0002
11	0.0570	0.0329	0.0136	0.0072	0.0041	0.0020	0.0016	0.0009	0.0010	0.0004	0.0004	0.0004	0.0003	0.0004	0.0001
12	0.0453	0.0365	0.0163	0.0074	0.0040	0.0025	0.0021	0.0011	0.0008	0.0006	0.0006	0.0003	0.0003	0.0002	0.0002
13	0.0294	0.0365	0.0174	0.0081	0.0046	0.0032	0.0019	0.0012	0.0006	0.0007	0.0004	0.0003	0.0003	0.0002	0.0002
14	0.0199	0.0329	0.0182	0.0088	0.0053	0.0025	0.0021	0.0016	0.0011	0.0006	0.0007	0.0003	0.0003	0.0003	0.0003
15	0.0081	0.0290	0.0207	0.0104	0.0055	0.0035	0.0025	0.0014	0.0011	0.0007	0.0006	0.0006	0.0004	0.0002	0.0002
16	≅ 0	0.0252	0.0221	0.0113	0.0059	0.0037	0.0028	0.0018	0.0014	0.0010	0.0007	0.0006	0.0004	0.0003	0.0002
17	-	0.0217	0.0221	0.0113	0.0067	0.0044	0.0029	0.0021	0.0014	0.0009	0.0006	0.0005	0.0005	0.0003	0.0003
18	-	0.0178	0.0207	0.0137	0.0074	0.0044	0.0029	0.0019	0.0014	0.0011	0.0009	0.0005	0.0003	0.0004	0.0002
19	-	0.0171	0.0182	0.0138	0.0073	0.0052	0.0030	0.0025	0.0013	0.0012	0.0009	0.0010	0.0003	0.0004	0.0003
20	-	0.0120	0.0174	0.0139	0.0075	0.0050	0.0032	0.0020	0.0016	0.0009	0.0009	0.0006	0.0006	0.0004	0.0004
21	-	0.0083	0.0163	0.0139	0.0088	0.0058	0.0032	0.0024	0.0017	0.0014	0.0010	0.0009	0.0007	0.0005	0.0005
22	-	0.0046	0.0136	0.0138	0.0089	0.0056	0.0038	0.0031	0.0021	0.0018	0.0010	0.0009	0.0007	0.0006	0.0004
23	-	0.0017	0.0118	0.0137	0.0084	0.0056	0.0035	0.0030	0.0020	0.0014	0.0008	0.0009	0.0007	0.0007	0.0005
24	-	≅ 0	0.0116	0.0113	0.0111	0.0060	0.0045	0.0028	0.0019	0.0017	0.0014	0.0007	0.0010	0.0007	0.0004
25	-	-	0.0082	0.0113	0.0111	0.0055	0.0036	0.0033	0.0022	0.0014	0.0012	0.0007	0.0008	0.0007	0.0005
26	-	-	0.0075	0.0104	0.0084	0.0073	0.0043	0.0029	0.0022	0.0017	0.0013	0.0011	0.0007	0.0007	0.0004
27	-	-	0.0068	0.0088	0.0089	0.0069	0.0048	0.0030	0.0022	0.0018	0.0014	0.0011	0.0008	0.0010	0.0005
28	-	-	0.0053	0.0081	0.0088	0.0071	0.0056	0.0033	0.0024	0.0019	0.0014	0.0011	0.0010	0.0008	0.0005
29	-	-	0.0029	0.0074	0.0075	0.0071	0.0054	0.0033	0.0027	0.0018	0.0017	0.0012	0.0008	0.0008	0.0005
30	-	-	0.0018	0.0072	0.0073	0.0069	0.0053	0.0035	0.0026	0.0021	0.0014	0.0012	0.0011	0.0008	0.0006
31	-	-	0.0005	0.0060	0.0074	0.0073	0.0054	0.0035	0.0029	0.0021	0.0016	0.0011	0.0010	0.0007	0.0006
32	-	-	≅ 0	0.0047	0.0067	0.0055	0.0059	0.0038	0.0029	0.0018	0.0018	0.0013	0.0010	0.0009	0.0006
33	-	-	-	0.0044	0.0059	0.0060	0.0059	0.0040	0.0031	0.0020	0.0016	0.0013	0.0010	0.0007	0.0007
34	-	-	-	0.0037	0.0055	0.0056	0.0054	0.0046	0.0033	0.0023	0.0014	0.0013	0.0011	0.0009	0.0007
35	-	-	-	0.0035	0.0053	0.0056	0.0053	0.0042	0.0035	0.0024	0.0019	0.0015	0.0013	0.0010	0.0008
36	-	-	-	0.0022	0.0046	0.0058	0.0054	0.0042	0.0035	0.0029	0.0016	0.0013	0.0012	0.0007	0.0007
37	-	-	-	0.0013	0.0040	0.0050	0.0056	0.0042	0.0030	0.0026	0.0020	0.0014	0.0013	0.0008	0.0006
38	-	-	-	0.0007	0.0041	0.0052	0.0048	0.0042	0.0034	0.0023	0.0020	0.0015	0.0013	0.0009	0.0010
39	-	-	-	0.0002	0.0033	0.0044	0.0043	0.0046	0.0032	0.0027	0.0023	0.0015	0.0011	0.0009	0.0008
40	-	-	-	≅ 0	0.0030	0.0044	0.0036	0.0040	0.0034	0.0029	0.0020	0.0014	0.0013	0.0010	0.0008
41	-	-	-	-	0.0027	0.0037	0.0045	0.0038	0.0034	0.0029	0.0021	0.0019	0.0014	0.0010	0.0008
42	-	-	-	-	0.0022	0.0035	0.0035	0.0035	0.0032	0.0027	0.0021	0.0018	0.0017	0.0012	0.0008
43	-	-	-	-	0.0017	0.0025	0.0038	0.0035	0.0034	0.0033	0.0027	0.0019	0.0014	0.0011	0.0008
44	-	-	-	-	0.0015	0.0032	0.0032	0.0033	0.0030	0.0033	0.0021	0.0018	0.0013	0.0012	0.0011
45	-	-	-	-	0.0006	0.0025	0.0032	0.0033	0.0035	0.0033	0.0024	0.0021	0.0014	0.0011	0.0012
46	-	-	-	-	0.0002	0.0020	0.0030	0.0030	0.0035	0.0033	0.0023	0.0022	0.0018	0.0014	0.0010
47	-	-	-	-	0.0001	0.0022	0.0029	0.0029	0.0033	0.0027	0.0026	0.0019	0.0018	0.0012	0.0011
48	-	-	-	-	≅ 0	0.0018	0.0029	0.0033	0.0031	0.0029	0.0026	0.0021	0.0013	0.0012	0.0012
49	-	-	-	-	-	0.0015	0.0028	0.0028	0.0029	0.0029	0.0026	0.0018	0.0016	0.0014	0.0010
50	-	-	-	-	-	0.0013	0.0025	0.0030	0.0029	0.0027	0.0026	0.0024	0.0021	0.0014	0.0012
51	-	-	-	-	-	0.0011	0.0021	0.0031	0.0026	0.0023	0.0023	0.0021	0.0017	0.0015	0.0011
52	-	-	-	-	-	0.0007	0.0019	0.0024	0.0027	0.0026	0.0024	0.0021	0.0019	0.0014	0.0013
53	-	-	-	-	-	0.0004	0.0021	0.0020	0.0024	0.0029	0.0021	0.0021	0.0020	0.0015	0.0011
54	-	-	-	-	-	0.0003	0.0016	0.0025	0.0022	0.0024	0.0027	0.0021	0.0019	0.0013	0.0014
55	-	-	-	-	-	≅ 0	0.0012	0.0019	0.0022	0.0023	0.0021	0.0024	0.0019	0.0017	0.0013
56	-	-	-	-	-	≅ 0	0.0008	0.0021	0.0022	0.0020	0.0021	0.0018	0.0015	0.0017	0.0011
57	-	-	-	-	-	-	0.0010	0.0018	0.0019	0.0018	0.0020	0.0021	0.0015	0.0016	0.0016
58	-	-	-	-	-	-	0.0008	0.0014	0.0020	0.0021	0.0023	0.0019	0.0019	0.0015	0.0013
59	-	-	-	-	-	-	0.0005	0.0016	0.0021	0.0021	0.0020	0.0022	0.0019	0.0018	0.0015
60	-	-	-	-	-	-	0.0002	0.0012	0.0017	0.0018	0.0020	0.0021	0.0020	0.0020	0.0014
61	-	-	-	-	-	-	0.0003	0.0011	0.0016	0.0019	0.0016	0.0018	0.0019	0.0020	0.0014
62	-	-	-	-	-	-	0.0002	0.0009	0.0013	0.0018	0.0019	0.0019	0.0017	0.0018	0.0013
63	-	-	-	-	-	-	≅ 0	0.0009	0.0014	0.0017	0.0014	0.0018	0.0021	0.0015	0.0014
64	-	-	-	-	-	-	≅ 0	0.0008	0.0014	0.0014	0.0016	0.0019	0.0016	0.0016	0.0013

n \ N	16	24	32	40	48	56	64	72	80	88	96	104	112	120	128
65	-	-	-	-	-	-	-	0.0007	0.0014	0.0017	0.0018	0.0014	0.0013	0.0017	0.0013
66	-	-	-	-	-	-	-	0.0004	0.0011	0.0014	0.0016	0.0015	0.0018	0.0017	0.0014
67	-	-	-	-	-	-	-	0.0005	0.0011	0.0018	0.0014	0.0015	0.0018	0.0013	0.0013
68	-	-	-	-	-	-	-	0.0003	0.0006	0.0014	0.0017	0.0014	0.0014	0.0015	0.0014
69	-	-	-	-	-	-	-	0.0003	0.0008	0.0009	0.0014	0.0013	0.0013	0.0014	0.0014
70	-	-	-	-	-	-	-	0.0001	0.0010	0.0012	0.0014	0.0015	0.0014	0.0015	0.0015
71	-	-	-	-	-	-	-	≅ 0	0.0007	0.0011	0.0013	0.0013	0.0017	0.0014	0.0013
72	-	-	-	-	-	-	-	≅ 0	0.0004	0.0009	0.0012	0.0013	0.0014	0.0014	0.0016
73	-	-	-	-	-	-	-	-	0.0005	0.0010	0.0014	0.0013	0.0013	0.0012	0.0011
74	-	-	-	-	-	-	-	-	0.0004	0.0007	0.0008	0.0011	0.0011	0.0012	0.0013
75	-	-	-	-	-	-	-	-	0.0002	0.0006	0.0010	0.0012	0.0013	0.0014	0.0014
76	-	-	-	-	-	-	-	-	0.0003	0.0007	0.0010	0.0012	0.0013	0.0011	0.0011
77	-	-	-	-	-	-	-	-	0.0001	0.0006	0.0009	0.0011	0.0012	0.0012	0.0013
78	-	-	-	-	-	-	-	-	0.0001	0.0004	0.0009	0.0011	0.0013	0.0011	0.0011
79	-	-	-	-	-	-	-	-	≅ 0	0.0004	0.0009	0.0011	0.0011	0.0012	0.0012
80	-	-	-	-	-	-	-	-	≅ 0	0.0005	0.0006	0.0007	0.0010	0.0010	0.0010
81	-	-	-	-	-	-	-	-	-	0.0001	0.0007	0.0007	0.0010	0.0010	0.0012
82	-	-	-	-	-	-	-	-	-	0.0002	0.0006	0.0009	0.0010	0.0009	0.0011
83	-	-	-	-	-	-	-	-	-	0.0002	0.0007	0.0009	0.0011	0.0009	0.0010
84	-	-	-	-	-	-	-	-	-	0.0001	0.0004	0.0009	0.0008	0.0008	0.0012
85	-	-	-	-	-	-	-	-	-	0.0001	0.0006	0.0006	0.0010	0.0007	0.0011
86	-	-	-	-	-	-	-	-	-	≅ 0	0.0004	0.0010	0.0008	0.0010	0.0008
87	-	-	-	-	-	-	-	-	-	≅ 0	0.0004	0.0005	0.0007	0.0009	0.0008
88	-	-	-	-	-	-	-	-	-	≅ 0	0.0002	0.0005	0.0008	0.0007	0.0008
89	-	-	-	-	-	-	-	-	-	-	0.0003	0.0006	0.0010	0.0009	0.0008
90	-	-	-	-	-	-	-	-	-	-	0.0002	0.0006	0.0007	0.0007	0.0008
91	-	-	-	-	-	-	-	-	-	-	0.0002	0.0003	0.0007	0.0008	0.0010
92	-	-	-	-	-	-	-	-	-	-	0.0001	0.0003	0.0007	0.0008	0.0006
93	-	-	-	-	-	-	-	-	-	-	0.0001	0.0003	0.0006	0.0008	0.0007
94	-	-	-	-	-	-	-	-	-	-	0.0001	0.0004	0.0003	0.0010	0.0008
95	-	-	-	-	-	-	-	-	-	-	≅ 0	0.0003	0.0003	0.0007	0.0007
96	-	-	-	-	-	-	-	-	-	-	≅ 0	0.0004	0.0005	0.0007	0.0007
97	-	-	-	-	-	-	-	-	-	-	-	0.0001	0.0004	0.0007	0.0006
98	-	-	-	-	-	-	-	-	-	-	-	0.0001	0.0004	0.0007	0.0006
99	-	-	-	-	-	-	-	-	-	-	-	0.0001	0.0003	0.0006	0.0006
100	-	-	-	-	-	-	-	-	-	-	-	0.0001	0.0003	0.0005	0.0005
101	-	-	-	-	-	-	-	-	-	-	-	≅ 0	0.0003	0.0004	0.0005
102	-	-	-	-	-	-	-	-	-	-	-	≅ 0	0.0003	0.0004	0.0005
103	-	-	-	-	-	-	-	-	-	-	-	≅ 0	0.0001	0.0004	0.0004
104	-	-	-	-	-	-	-	-	-	-	-	≅ 0	0.0002	0.0003	0.0005
105	-	-	-	-	-	-	-	-	-	-	-	-	0.0001	0.0003	0.0004
106	-	-	-	-	-	-	-	-	-	-	-	-	0.0001	0.0002	0.0005
107	-	-	-	-	-	-	-	-	-	-	-	-	0.0001	0.0003	0.0004
108	-	-	-	-	-	-	-	-	-	-	-	-	≅ 0	0.0002	0.0005
109	-	-	-	-	-	-	-	-	-	-	-	-	0.0001	0.0002	0.0004
110	-	-	-	-	-	-	-	-	-	-	-	-	≅ 0	0.0004	0.0003
111	-	-	-	-	-	-	-	-	-	-	-	-	≅ 0	0.0002	0.0002
112	-	-	-	-	-	-	-	-	-	-	-	-	≅ 0	0.0001	0.0003
113	-	-	-	-	-	-	-	-	-	-	-	-	-	0.0001	0.0002
114	-	-	-	-	-	-	-	-	-	-	-	-	-	≅ 0	0.0002
115	-	-	-	-	-	-	-	-	-	-	-	-	-	0.0001	0.0003
116	-	-	-	-	-	-	-	-	-	-	-	-	-	≅ 0	0.0002
117	-	-	-	-	-	-	-	-	-	-	-	-	-	≅ 0	0.0002
118	-	-	-	-	-	-	-	-	-	-	-	-	-	≅ 0	0.0001
119	-	-	-	-	-	-	-	-	-	-	-	-	-	≅ 0	0.0002
120	-	-	-	-	-	-	-	-	-	-	-	-	-	≅ 0	0.0001
121	-	-	-	-	-	-	-	-	-	-	-	-	-	-	0.0001
122	-	-	-	-	-	-	-	-	-	-	-	-	-	-	0.0001
123	-	-	-	-	-	-	-	-	-	-	-	-	-	-	≅ 0
124	-	-	-	-	-	-	-	-	-	-	-	-	-	-	0.0001
125	-	-	-	-	-	-	-	-	-	-	-	-	-	-	≅ 0
126	-	-	-	-	-	-	-	-	-	-	-	-	-	-	≅ 0
127	-	-	-	-	-	-	-	-	-	-	-	-	-	-	≅ 0
128	-	-	-	-	-	-	-	-	-	-	-	-	-	-	≅ 0

Table B.4: Kurtosis values of the real and imaginary parts of the IMD RV in selected sub-channels (n) for OFDM/QPSK signals with 16 to 128 sub-channels (N).

n \ N	16	24	32	40	48	56	64	72	80	88	96	104	112	120	128
1	3.7662	3.5669	3.4442	3.3572	3.3160	3.2724	3.2404	3.2231	3.2089	3.1898	3.1749	3.1609	3.1411	3.1316	3.1236
2	4.0541	3.7296	3.5414	3.4329	3.3649	3.3077	3.2619	3.2318	3.2198	3.2006	3.1835	3.1629	3.1555	3.1420	3.1370
3	4.1828	3.8160	3.6172	3.4779	3.4036	3.3269	3.2883	3.2561	3.2278	3.2224	3.1899	3.1793	3.1645	3.1516	3.1404
4	4.2979	3.9017	3.6616	3.5269	3.4293	3.3677	3.3169	3.2701	3.2427	3.2147	3.1994	3.1799	3.1725	3.1537	3.1402
5	4.3458	3.9512	3.6886	3.5608	3.4577	3.3815	3.3330	3.2913	3.2581	3.2270	3.2156	3.1869	3.1662	3.1661	3.1531
6	4.4063	4.0004	3.7327	3.5809	3.4858	3.4104	3.3420	3.3063	3.2675	3.2501	3.2323	3.2046	3.1850	3.1713	3.1624
7	4.4149	4.0159	3.7678	3.6090	3.4998	3.4180	3.3727	3.3119	3.2851	3.2533	3.2424	3.2126	3.1916	3.1758	3.1636
8	4.4416	4.0329	3.7795	3.6275	3.5082	3.4345	3.3809	3.3231	3.2887	3.2527	3.2272	3.2013	3.1989	3.1797	3.1649
9	4.4416	4.0615	3.8050	3.6473	3.5229	3.4332	3.3781	3.3384	3.3009	3.2649	3.2441	3.2225	3.1918	3.1874	3.1732
10	4.4149	4.0648	3.8139	3.6602	3.5441	3.4661	3.4079	3.3449	3.3059	3.2743	3.2527	3.2354	3.2082	3.1892	3.1778
11	4.4063	4.1010	3.8323	3.6699	3.5549	3.4767	3.4066	3.3555	3.3080	3.2742	3.2560	3.2312	3.2102	3.1954	3.1807
12	4.3458	4.1031	3.8511	3.6765	3.5628	3.4786	3.4207	3.3567	3.3169	3.2951	3.2636	3.2388	3.2192	3.1979	3.1845
13	4.2979	4.1031	3.8725	3.6927	3.5774	3.4940	3.4156	3.3635	3.3358	3.3065	3.2661	3.2409	3.2283	3.2056	3.1883
14	4.1828	4.1010	3.8529	3.6958	3.5817	3.4874	3.4327	3.3770	3.3375	3.2992	3.2702	3.2535	3.2319	3.2008	3.1932
15	4.0541	4.0648	3.8758	3.7329	3.5826	3.4964	3.4490	3.3739	3.3558	3.3037	3.2689	3.2572	3.2362	3.2069	3.1972
16	3.7662	4.0615	3.9034	3.7226	3.5771	3.4979	3.4507	3.3870	3.3478	3.3150	3.2784	3.2594	3.2340	3.2099	3.2074
17	-	4.0329	3.9034	3.7266	3.6115	3.5060	3.4443	3.3858	3.3383	3.3247	3.2878	3.2607	3.2409	3.2210	3.2101
18	-	4.0159	3.8758	3.7329	3.6017	3.5143	3.4674	3.3960	3.3583	3.3198	3.2856	3.2675	3.2382	3.2180	3.2097
19	-	4.0004	3.8529	3.7181	3.6214	3.5212	3.4713	3.4184	3.3541	3.3299	3.2897	3.2760	3.2413	3.2237	3.2105
20	-	3.9512	3.8725	3.7456	3.6095	3.5169	3.4604	3.3984	3.3627	3.3162	3.2992	3.2594	3.2452	3.2262	3.2170
21	-	3.9017	3.8511	3.7456	3.6169	3.5338	3.4505	3.4126	3.3681	3.3223	3.3029	3.2824	3.2575	3.2252	3.2083
22	-	3.8160	3.8323	3.7181	3.6256	3.5347	3.4819	3.4023	3.3581	3.3295	3.2981	3.2769	3.2475	3.2297	3.2147
23	-	3.7296	3.8139	3.7329	3.6392	3.5441	3.4659	3.4159	3.3598	3.3323	3.3044	3.2783	3.2514	3.2412	3.2257
24	-	3.5669	3.8050	3.7266	3.6484	3.5415	3.4653	3.4201	3.3631	3.3365	3.3022	3.2734	3.2578	3.2379	3.2113
25	-	-	3.7795	3.7226	3.6484	3.5436	3.4578	3.4158	3.3743	3.3376	3.2942	3.2795	3.2512	3.2333	3.2216
26	-	-	3.7678	3.7329	3.6392	3.5465	3.4758	3.4231	3.3816	3.3426	3.3051	3.2829	3.2573	3.2413	3.2235
27	-	-	3.7327	3.6958	3.6256	3.5572	3.4772	3.4275	3.3813	3.3424	3.3059	3.2938	3.2624	3.2389	3.2276
28	-	-	3.6886	3.6927	3.6169	3.5520	3.4792	3.4444	3.3808	3.3425	3.3065	3.2958	3.2587	3.2396	3.2319
29	-	-	3.6616	3.6765	3.6095	3.5520	3.4850	3.4285	3.3870	3.3501	3.3145	3.2842	3.2667	3.2409	3.2318
30	-	-	3.6172	3.6699	3.6214	3.5572	3.4872	3.4232	3.3707	3.3489	3.3158	3.2911	3.2685	3.2450	3.2345
31	-	-	3.5414	3.6602	3.6017	3.5465	3.4918	3.4269	3.3966	3.3452	3.3328	3.2843	3.2633	3.2466	3.2287
32	-	-	3.4442	3.6473	3.6115	3.5436	3.4843	3.4322	3.3975	3.3571	3.3227	3.2982	3.2834	3.2519	3.2313
33	-	-	-	3.6275	3.5771	3.5415	3.4843	3.4496	3.3874	3.3683	3.3328	3.3054	3.2795	3.2542	3.2329
34	-	-	-	3.6090	3.5826	3.5441	3.4918	3.4408	3.3865	3.3630	3.3232	3.2883	3.2703	3.2465	3.2311
35	-	-	-	3.5809	3.5817	3.5347	3.4872	3.4414	3.3985	3.3484	3.3209	3.3029	3.2750	3.2638	3.2309
36	-	-	-	3.5608	3.5774	3.5338	3.4850	3.4497	3.3958	3.3642	3.3260	3.2995	3.2776	3.2571	3.2407
37	-	-	-	3.5269	3.5628	3.5169	3.4792	3.4497	3.4003	3.3638	3.3251	3.3056	3.2817	3.2664	3.2422
38	-	-	-	3.4779	3.5549	3.5212	3.4772	3.4414	3.4046	3.3637	3.3322	3.2985	3.2713	3.2554	3.2383
39	-	-	-	3.4329	3.5441	3.5143	3.4758	3.4408	3.3985	3.3638	3.3307	3.2981	3.2924	3.2485	3.2407
40	-	-	-	3.3572	3.5229	3.5060	3.4578	3.4496	3.4057	3.3592	3.3319	3.3122	3.2883	3.2620	3.2437
41	-	-	-	-	3.5082	3.4979	3.4653	3.4322	3.4057	3.3652	3.3248	3.3032	3.2820	3.2601	3.2432
42	-	-	-	-	3.4998	3.4964	3.4659	3.4269	3.3985	3.3715	3.3418	3.3054	3.2827	3.2585	3.2486
43	-	-	-	-	3.4858	3.4874	3.4819	3.4232	3.4046	3.3669	3.3332	3.3087	3.2821	3.2496	3.2532
44	-	-	-	-	3.4577	3.4940	3.4505	3.4285	3.4003	3.3716	3.3488	3.3014	3.2879	3.2623	3.2494
45	-	-	-	-	3.4293	3.4786	3.4604	3.4444	3.3958	3.3716	3.3408	3.3143	3.2815	3.2780	3.2497
46	-	-	-	-	3.4036	3.4767	3.4713	3.4275	3.3985	3.3669	3.3410	3.3087	3.2887	3.2708	3.2459
47	-	-	-	-	3.3649	3.4661	3.4674	3.4231	3.3865	3.3715	3.3481	3.3161	3.2883	3.2699	3.2594
48	-	-	-	-	3.3160	3.4332	3.4443	3.4158	3.3874	3.3652	3.3499	3.3183	3.3090	3.2770	3.2499
49	-	-	-	-	-	3.4345	3.4507	3.4201	3.3975	3.3592	3.3499	3.3157	3.2985	3.2643	3.2568
50	-	-	-	-	-	3.4180	3.4490	3.4159	3.3966	3.3638	3.3481	3.3156	3.2902	3.2674	3.2555
51	-	-	-	-	-	3.4104	3.4327	3.4023	3.3707	3.3637	3.3410	3.3187	3.2904	3.2701	3.2542
52	-	-	-	-	-	3.3815	3.4156	3.4126	3.3870	3.3638	3.3408	3.3131	3.3037	3.2773	3.2521
53	-	-	-	-	-	3.3677	3.4207	3.3984	3.3808	3.3642	3.3488	3.3131	3.2882	3.2724	3.2555
54	-	-	-	-	-	3.3269	3.4066	3.4184	3.3813	3.3484	3.3332	3.3187	3.3017	3.2735	3.2586
55	-	-	-	-	-	3.3077	3.4079	3.3960	3.3816	3.3630	3.3418	3.3156	3.2925	3.2778	3.2619
56	-	-	-	-	-	3.2724	3.3781	3.3858	3.3743	3.3683	3.3248	3.3157	3.3055	3.2823	3.2596
57	-	-	-	-	-	-	3.3809	3.3870	3.3631	3.3571	3.3319	3.3183	3.3055	3.2831	3.2653
58	-	-	-	-	-	-	3.3727	3.3739	3.3598	3.3452	3.3307	3.3161	3.2925	3.2778	3.2569
59	-	-	-	-	-	-	3.3420	3.3770	3.3581	3.3489	3.3322	3.3087	3.3017	3.2797	3.2590
60	-	-	-	-	-	-	3.3330	3.3635	3.3681	3.3501	3.3251	3.3143	3.2882	3.2866	3.2711
61	-	-	-	-	-	-	3.3169	3.3567	3.3627	3.3425	3.3260	3.3014	3.3037	3.2866	3.2675
62	-	-	-	-	-	-	3.2883	3.3555	3.3541	3.3424	3.3209	3.3087	3.2904	3.2797	3.2554
63	-	-	-	-	-	-	3.2619	3.3449	3.3583	3.3426	3.3232	3.3054	3.2902	3.2778	3.2602
64	-	-	-	-	-	-	3.2404	3.3384	3.3383	3.3376	3.3328	3.3032	3.2985	3.2831	3.2635

n \ N	16	24	32	40	48	56	64	72	80	88	96	104	112	120	128
65	-	-	-	-	-	-	-	3.3231	3.3478	3.3365	3.3227	3.3122	3.3090	3.2823	3.2635
66	-	-	-	-	-	-	-	3.3119	3.3558	3.3323	3.3328	3.2981	3.2883	3.2778	3.2602
67	-	-	-	-	-	-	-	3.3063	3.3375	3.3295	3.3158	3.2985	3.2887	3.2735	3.2554
68	-	-	-	-	-	-	-	3.2913	3.3358	3.3223	3.3145	3.3056	3.2815	3.2724	3.2675
69	-	-	-	-	-	-	-	3.2701	3.3169	3.3162	3.3065	3.2995	3.2879	3.2773	3.2711
70	-	-	-	-	-	-	-	3.2561	3.3080	3.3299	3.3059	3.3029	3.2821	3.2701	3.2590
71	-	-	-	-	-	-	-	3.2318	3.3059	3.3198	3.3051	3.2883	3.2827	3.2674	3.2569
72	-	-	-	-	-	-	-	3.2231	3.3009	3.3247	3.2942	3.3054	3.2820	3.2643	3.2653
73	-	-	-	-	-	-	-	-	3.2887	3.3150	3.3022	3.2982	3.2883	3.2770	3.2596
74	-	-	-	-	-	-	-	-	3.2851	3.3037	3.3044	3.2843	3.2924	3.2699	3.2619
75	-	-	-	-	-	-	-	-	3.2675	3.2992	3.2981	3.2911	3.2713	3.2708	3.2586
76	-	-	-	-	-	-	-	-	3.2581	3.3065	3.3029	3.2842	3.2817	3.2780	3.2555
77	-	-	-	-	-	-	-	-	3.2427	3.2951	3.2992	3.2958	3.2776	3.2623	3.2521
78	-	-	-	-	-	-	-	-	3.2278	3.2742	3.2897	3.2938	3.2750	3.2496	3.2542
79	-	-	-	-	-	-	-	-	3.2198	3.2743	3.2856	3.2829	3.2703	3.2585	3.2555
80	-	-	-	-	-	-	-	-	3.2089	3.2649	3.2878	3.2795	3.2795	3.2601	3.2568
81	-	-	-	-	-	-	-	-	-	3.2527	3.2784	3.2734	3.2834	3.2620	3.2499
82	-	-	-	-	-	-	-	-	-	3.2533	3.2689	3.2783	3.2633	3.2485	3.2594
83	-	-	-	-	-	-	-	-	-	3.2501	3.2702	3.2769	3.2685	3.2554	3.2459
84	-	-	-	-	-	-	-	-	-	3.2270	3.2661	3.2824	3.2667	3.2664	3.2497
85	-	-	-	-	-	-	-	-	-	3.2147	3.2636	3.2594	3.2587	3.2571	3.2494
86	-	-	-	-	-	-	-	-	-	3.2224	3.2560	3.2760	3.2624	3.2638	3.2532
87	-	-	-	-	-	-	-	-	-	3.2006	3.2527	3.2675	3.2573	3.2465	3.2486
88	-	-	-	-	-	-	-	-	-	3.1898	3.2441	3.2607	3.2512	3.2542	3.2432
89	-	-	-	-	-	-	-	-	-	-	3.2272	3.2594	3.2578	3.2519	3.2437
90	-	-	-	-	-	-	-	-	-	-	3.2424	3.2572	3.2514	3.2466	3.2407
91	-	-	-	-	-	-	-	-	-	-	3.2323	3.2535	3.2475	3.2450	3.2383
92	-	-	-	-	-	-	-	-	-	-	3.2156	3.2409	3.2575	3.2409	3.2422
93	-	-	-	-	-	-	-	-	-	-	3.1994	3.2388	3.2452	3.2396	3.2407
94	-	-	-	-	-	-	-	-	-	-	3.1899	3.2312	3.2413	3.2389	3.2309
95	-	-	-	-	-	-	-	-	-	-	3.1835	3.2354	3.2382	3.2413	3.2311
96	-	-	-	-	-	-	-	-	-	-	3.1749	3.2225	3.2409	3.2333	3.2329
97	-	-	-	-	-	-	-	-	-	-	-	3.2013	3.2340	3.2379	3.2313
98	-	-	-	-	-	-	-	-	-	-	-	3.2126	3.2362	3.2412	3.2287
99	-	-	-	-	-	-	-	-	-	-	-	3.2046	3.2319	3.2297	3.2345
100	-	-	-	-	-	-	-	-	-	-	-	3.1869	3.2283	3.2252	3.2318
101	-	-	-	-	-	-	-	-	-	-	-	3.1799	3.2192	3.2262	3.2319
102	-	-	-	-	-	-	-	-	-	-	-	3.1793	3.2102	3.2237	3.2276
103	-	-	-	-	-	-	-	-	-	-	-	3.1629	3.2082	3.2180	3.2235
104	-	-	-	-	-	-	-	-	-	-	-	3.1609	3.1918	3.2210	3.2216
105	-	-	-	-	-	-	-	-	-	-	-	-	3.1989	3.2099	3.2113
106	-	-	-	-	-	-	-	-	-	-	-	-	3.1916	3.2069	3.2257
107	-	-	-	-	-	-	-	-	-	-	-	-	3.1850	3.2008	3.2147
108	-	-	-	-	-	-	-	-	-	-	-	-	3.1662	3.2056	3.2083
109	-	-	-	-	-	-	-	-	-	-	-	-	3.1725	3.1979	3.2170
110	-	-	-	-	-	-	-	-	-	-	-	-	3.1645	3.1954	3.2105
111	-	-	-	-	-	-	-	-	-	-	-	-	3.1555	3.1892	3.2097
112	-	-	-	-	-	-	-	-	-	-	-	-	3.1411	3.1874	3.2101
113	-	-	-	-	-	-	-	-	-	-	-	-	-	3.1797	3.2074
114	-	-	-	-	-	-	-	-	-	-	-	-	-	3.1758	3.1972
115	-	-	-	-	-	-	-	-	-	-	-	-	-	3.1713	3.1932
116	-	-	-	-	-	-	-	-	-	-	-	-	-	3.1661	3.1883
117	-	-	-	-	-	-	-	-	-	-	-	-	-	3.1537	3.1845
118	-	-	-	-	-	-	-	-	-	-	-	-	-	3.1516	3.1807
119	-	-	-	-	-	-	-	-	-	-	-	-	-	3.1420	3.1778
120	-	-	-	-	-	-	-	-	-	-	-	-	-	3.1316	3.1732
121	-	-	-	-	-	-	-	-	-	-	-	-	-	-	3.1649
122	-	-	-	-	-	-	-	-	-	-	-	-	-	-	3.1636
123	-	-	-	-	-	-	-	-	-	-	-	-	-	-	3.1624
124	-	-	-	-	-	-	-	-	-	-	-	-	-	-	3.1531
125	-	-	-	-	-	-	-	-	-	-	-	-	-	-	3.1402
126	-	-	-	-	-	-	-	-	-	-	-	-	-	-	3.1404
127	-	-	-	-	-	-	-	-	-	-	-	-	-	-	3.1370
128	-	-	-	-	-	-	-	-	-	-	-	-	-	-	3.1236

References

[1] J. A. C. Bingham, "Multicarrier modulation for data transmission: An idea whose time has come," *IEEE Communications Magazine*, vol. 28, pp. 5-14, May 1990.

[2] W. Y. Zou and Y. Wu, "COFDM: an overview," *IEEE Transactions on Broadcasting*, vol. 41, pp. 1-8, March 1995.

[3] ETSI, "Digital audio broadcasting (DAB); DAB to mobile, portable and fixed receivers," European Telecommunications Standard, ETS 300-401, February 1995.

[4] ETSI, "Digital video broadcasting (DVB); Framing structure, channel coding, and modulation for digital terrestrial television," European Telecommunications Standard, ETS 300-744, March 1997.

[5] ETSI, "Broadband radio access networks (BRAN); HIPERLAN type 2; Physical (PHY) layer," European Telecommunications Standard, TS 101-475, April 2000.

[6] IEEE, "Supplement to standard for telecommunications and information exchange between systems – LAN/MAN specific requirements – Part 11: Wireless LAN medium access control (MAC) and physical layer (PHY) specifications: High speed physical layer in the 5 GHz band," IEEE 802.11a, July 1999.

[7] IEEE, "Further higher-speed physical layer extension in the 2.4 GHz band," IEEE 802.11g, January 2000.

[8] H. Ogawa, D. Polifko and S. Banba, "Millimeter-wave fiber optics systems for personal radio communication," *IEEE Transactions on Microwave Theory and Techniques*, vol. 40, pp. 2285-2292, December 1992.

[9] W. I Way, "Optical fiber-based microcellular systems: An overview," *IEICE Transactions on Communications*, vol. E76-B, pp. 1091-1102, September 1993.

[10] H. Ogawa, "Microwave and millimeter-wave fiber optic technology for sub-carrier transmission systems," *IEICE Transactions on Communications*, vol. E76-B, pp. 1078-1090, September 1993.

[11] J. O'Reilly and P. Lane, "Remote delivery of video services using mm-waves and optics," *Journal of Lightwave Technology*, vol. 12, pp. 369-375, February 1994.

[12] K. Kitayama, "Architectural considerations of fiber-radio millimetre-wave wireless access systems," *Fiber and Integrated Optics*, vol. 19, pp. 167-186, April 2000.

[13] P. Banelli and S. Cacopardi, "Theoretical analysis and performance of OFDM signals in nonlinear AWGN channels," *IEEE Transactions on Communications*, vol. 48, pp. 430-441, March 2000.

[14] P. Banelli, G. Baruffa and S. Cacopardi, "Effects of HPA non linearity on frequency multiplexed OFDM signals," *IEEE Transactions on Broadcasting*, vol. 47, pp. 123-136, June 2001.

[15] A. Barbieri, G. Cariolaro and L. Vangelista, "Nonlinear models of TWT revisited for OFDM systems," *Proceedings of the 38th Midwest Symposium on Circuits and Systems*, vol. 1, pp. 522-525, August 1996.

[16] E. Costa, M. Midrio and S. Pupolin, "Impact of amplifier nonlinearities on OFDM transmission system performance," *IEEE Communications Letters*, vol. 3, pp. 37-39, February 1999.

[17] E. Costa and S. Pupolin, "M-QAM-OFDM system performance in the presence of a nonlinear amplifier and phase noise," *IEEE Transactions on Communications*, vol. 50, pp. 462-472, March 2002.

[18] R. Dinis and A. Gusmão, "On the performance evaluation of OFDM transmission using clipping techniques," *Proceedings of the IEEE Vehicular Technology Conference*, vol. 5, pp. 2923-2928, September 1999.

[19] R. Gross and D. Veeneman, "Clipping distortion in DMT ADSL systems," *Electronics Letters*, vol. 29, pp. 2080-2081, November 1993.

[20] R. Gross and D. Veeneman, "SNR and spectral properties for a clipped DMT ADSL signal," *Proceedings of the IEEE International Conference on Communications*, vol. 2, pp. 843-847, May 1994.

[21] R. O'Neill and L. B. Lopes, "Envelope variations and spectral splatter in clipped multicarrier signals," *Proceedings of the IEEE International Symposium on Personal, Indoor and Mobile Radio Communications*, vol. 1, pp. 71-75, September 1995.

[22] Q. Shi, "OFDM in bandpass nonlinearity," *IEEE Transactions on Consumer Electronics*, vol. 42, pp. 253-258, August 1996.

[23] C. van den Bos, M. H. L. Kouwenhoven and W. A. Serdijn, "Effect of smooth non-linear distortion on OFDM BER," *Proceedings of the IEEE International Symposium on Circuits and Systems*, vol. 4, pp. 469-472, May 2000.

[24] C. van den Bos, M. H. L. Kouwenhoven and W. A. Serdijn, "The influence of non-linear distortion on OFDM bit error rate," *Proceedings of the IEEE International Conference on Communications*, vol. 2, pp. 1125-1129, June 2000.

[25] C. van den Bos, M. H. L. Kouwenhoven and W. A. Serdijn, "Effect of smooth nonlinear distortion on OFDM symbol error rate", *IEEE Transactions on Communications*, vol. 49, pp. 1510-1514, September 2001.

[26] M. L. Doelz, E. T. Helad and D. L. Martin, "Binary data transmission techniques for linear systems," *Proceedings of the IRE*, vol. 45, pp. 656-661, May 1957.

[27] R. R. Mosier and R. G. Clabaugh, "Kineplex, a bandwidth efficient binary transmission system," *AIEE Transactions (Part I: Communications and Electronics)*, vol. 76, pp. 723-728, January 1958.

[28] G. C. Porter, "Error-distribution and diversity performance of a frequency-differential PSK HF modem," *IEEE Transactions on Communication Technology*, vol. 16, pp. 567-575, August 1968.

[29] P. A. Bello, "Selective fading limitations of the Kathryn modem and some system design considerations," *IEEE Transactions on Communication Technology*, vol. 13, pp. 320-333, September 1965.

[30] M. S. Zimmerman and A. L. Kirsch, "The AN/GSC-10 (KATHRYN) variable rate data modem for HF radio," *IEEE Transactions on Communication Technology*, vol. 15, pp. 197-205, April 1967.

[31] A. L. Kirsch, P. R. Gray and D. W. Hanna, Jr., "Field test results of the AN/GSC-10 (KATHRYN) digital data terminal," *IEEE Transactions on Communication Technology*, vol. 17, pp. 118-128, April 1969.

[32] B. Hirosaki, "An analysis of automatic equalizers for orthogonally multiplexed QAM systems," *IEEE Transactions on Communications*, vol. 28, pp. 73-83, January 1980.

[33] B. Hirosaki, "An orthogonally multiplexed QAM system using the discrete Fourier transform," *IEEE Transactions on Communications*, vol. 29, pp. 982-989, July 1981.

[34] B. Hirosaki, S. Hasegawa and A. Sabato, "Advanced groupband data modem using orthogonally multiplexed QAM technique," *IEEE Transactions on Communications*, vol. 34, pp. 587-592, June 1986.

[35] L. Cimini, Jr., "Analysis and simulation of a digital mobile channel using frequency division multiplexing," *IEEE Transactions on Communications*, vol. 33, pp. 665-675, July 1985.

[36] J. S. Chow, J. C. Tu and J. M. Cioffi, "A discrete multitone transceiver system for HDSL applications," *IEEE Journal on Selected Areas in Communications*, vol. 9, pp. 895-908, August 1991.

[37] P. S. Chow, J. C. Tu and J. M. Cioffi, "Performance evaluation of a multichannel transceiver system for ADSL and VHDSL services," *IEEE Journal on Selected Areas in Communications*, vol. 9, pp. 909-918, August 1991.

[38] M. Alard and R. Lassalle, "Principles of modulation and channel coding for digital broadcasting for mobile receivers," *EBU Technical Review*, no. 224, pp. 3-25, August 1987.

[39] B. Le Floch, R. Albert-Lassalle, and D. Castelain, "Digital sound broadcasting to mobile receivers," *IEEE Transactions on Consumer Electronics*, vol. 35, pp. 493-503, August 1989.

[40] J. F. Hélard and B. Le Floch, "Trellis coded orthogonal frequency division multiplexing for digital video transmission," *Proceedings of the IEEE Global Telecommunications Conference*, vol. 2, pp. 785-791, December 1991.

[41] ITU-T, "Asymmetrical digital subscriber line (ADSL) transceivers," ITU-T Recommendation G.992.1, July 1999.

[42] J. G. Proakis. *Digital Communications, 3rd ed.* New York: McGraw-Hill, 1995.

[43] S. Haykin. *Communication Systems, 3rd ed.* New York: Wiley, 1994.

[44] A. R. S. Bahai and B. R. Saltzberg. *Multi-carrier Digital Communications: Theory and Applications of OFDM.* New York: Kluwer Academic/Plenum Publishers, 1999.

[45] R. van Nee and R. Prasad. *OFDM for Wireless Multimedia Communications.* Norwood, MA: Artech House, 2000.

[46] S. B. Weinstein and P. M. Ebert, "Data transmission by frequency-division multiplexing using the discrete Fourier transform," *IEEE Transactions on Communication Technology*, vol. 19, pp. 628-634, October 1971.

[47] A. Peled and A. Ruiz, "Frequency domain data transmission using reduced computational complexity algorithms," *Proceedings of the IEEE International Conference on Acoustics, Speech and Signal Processing*, vol. 2, pp. 964-967, April 1980.

[48] A. Ruiz, J. M. Cioffi and S. Kasturia, "Discrete multiple tone modulation with coset coding for the spectrally shaped channel," *IEEE Transactions on Communications*, vol. 40, pp. 1012-1029, June 1992.

[49] L. E. Franks. *Signal Theory.* Englewood Cliffs, NJ: Prentice-Hall, 1969.

[50] W. A. Gardner. *Introduction to Random Processes with Applications to Signals and Systems.* New York: McGraw-Hill, 1989.

[51] A. Papoulis. *Probability, Random Variables, and Stochastic Processes, 3rd ed.* New York: McGraw-Hill, 1991.

[52] T. Pollet, M. van Bladel and M. Moeneclaey, "BER sensitivity of OFDM systems to carrier frequency offset and Wiener phase noise," *IEEE Transactions on Communications*, vol. 43, pp. 191-193, February/March/April 1995.

[53] T. Pollet and M. Moeneclaey, "Synchronizability of OFDM signals," *Proceedings of the IEEE Global Telecommunications Conference*, vol. 3, pp. 2054-2058, November 1995.

[54] L. Wei and C. Schlegel, "Synchronization requirements for multi-user OFDM on satellite mobile and two-path Rayleigh-fading channels," *IEEE Transactions on Communications*, vol. 43, pp. 887-895, February/March/April 1995.

[55] P. Robertson and S. Kaiser, "Analysis of the effect of phase noise in OFDM systems," *Proceedings of the IEEE International Conference on Communications*, vol. 3, pp. 1652-1657, June 1995.

[56] H. Steendam, M. Moeneclaey and H. Sari, "The effects of carrier phase jitter on the performance of orthogonal frequency division multiple access systems," *IEEE Transactions on Communications*, vol. 46, pp. 456-459, April 1998.

[57] L. Tomba, "On the effects of Wiener phase noise in OFDM systems," *IEEE Transactions on Communications*, vol. 46, pp. 580-583, May 1998.

[58] A. G. Armada and M. Calvo, "Phase noise and sub-carrier spacing effects on the performance of an OFDM communication system," *IEEE Communications Letters*, vol. 2, pp. 11-13, January 1998.

[59] A. G. Armada, "Understanding the effects of phase noise in orthogonal frequency division multiplexing (OFDM)," *IEEE Transactions on Broadcasting*, vol. 47, pp. 153-159, June 2001.

[60] T. Pollet, P. Spruyt and M. Moeneclaey, "The BER performance of OFDM systems using non-synchronized sampling," *Proceedings of the IEEE Global Telecommunications Conference*, vol. 1, pp. 253-257, November 1994.

[61] T. N. Zogakis and J. M. Cioffi, "The effects of timing jitter on the performance of a discrete multitone system," *IEEE Transactions on Communications*, vol. 44, pp. 799-808, July 1996.

[62] R. J. Westcott, "Investigation of multiple f.m./f.d.m. carriers through a satellite t.w.t. operating near saturation," *IEE Proceedings,* vol. 114, pp. 726-740, June 1967.

[63] C. Rapp, "Effects of HPA-nonlinearity on a 4-DPSK/OFDM-signal for a digital sound broadcasting system," *Proceedings of the 2nd European Conference on Satellite Communications*, pp. 179-184, October 1991.

[64] S. Merchán, A. G. Armada and J. L. García, "OFDM performance in amplifier nonlinearity," *IEEE Transactions on Broadcasting*, vol. 44, pp. 106-113, March 1998.

[65] G. Santella and F. Mazzenga, "A model for performance evaluation in M-QAM-OFDM schemes in presence of nonlinear distortions," *Proceedings of the IEEE Vehicular Technology Conference*, vol. 2, pp. 830-834, July 1995.

[66] G. Santella and F. Mazzenga, "A hybrid analytical-simulation procedure for performance evaluation in M-QAM-OFDM schemes in presence of nonlinear distortions," *IEEE Transactions on Vehicular Technology*, vol. 47, pp. 142-151, February 1998.

[67] M. Pauli and H. P. Kuchenbecker, "Minimization of the intermodulation distortion of a non-linearly amplified OFDM signal," *Wireless Personal Communications*, vol. 4, pp. 93-101, January 1997.

[68] X. Li and L. J. Cimini, Jr., "Effects of clipping and filtering on the performance of OFDM," *Proceedings of the IEEE Vehicular Technology Conference*, vol. 3, pp. 1634-1638, May 1997.

[69] X. Li and L. J. Cimini, Jr., "Effects of clipping and filtering on the performance of OFDM," *IEEE Communications Letters*, vol. 2, pp. 131-133, May 1998.

[70] T. May and H. Rohling, "Reducing the peak-to-average power ratio in OFDM radio transmission systems," *Proceedings of the IEEE Vehicular Technology Conference*, vol. 3, pp. 2474-2478, May 1998.

[71] P. Van Eetvelt, G. Wade and M. Tomlinson, "Peak to average power reduction for OFDM schemes by selective scrambling," *Electronics Letters*, vol. 32, pp. 1963-1964, October 1996.

[72] R. W. Baüml, R. F. H. Fischer and J. B. Hüber, "Reducing the peak-to-average power ratio of multicarrier modulation by selective mapping," *Electronics Letters*, vol. 32, pp. 2056-2057, October 1996.

[73] S. H. Müller and J. B. Hüber, "OFDM with reduced peak-to-average power ratio by optimum combination of partial transmit sequences," *Electronics Letters*, vol. 33, pp. 368-369, February 1997.

[74] S. H. Müller and J. B. Hüber, "A novel peak power reduction scheme for OFDM," *Proceedings of the IEEE International Symposium on Personal, Indoor and Mobile Radio Communications*, vol. 3, pp. 1090-1094, September 1997.

[75] L. J. Cimini, Jr., and N. R. Sollenberger, "Peak-to-average power ratio reduction of an OFDM signal using partial transmit sequences," *Proceedings of the IEEE International Conference on Communications*, vol. 1, pp. 511-515, June 1999.

[76] L. J. Cimini, Jr., and N. R. Sollenberger, "Peak-to-average power ratio reduction of an OFDM signal using partial transmit sequences," *IEEE Communications Letters*, vol. 4, pp. 86-88, March 2000.

[77] A. E. Jones, T. A. Wilkinson and S. K. Barton, "Block coding scheme for reduction of peak to mean power ratio of multicarrier transmission schemes," *Electronics Letters*, vol. 30, pp. 2098-2099, December 1994.

[78] T. A. Wilkinson and A. E. Jones, "Minimisation of the peak to mean envelope power ratio of multicarrier transmission schemes by block coding," *Proceedings of the IEEE Vehicular Technology Conference*, vol. 2, pp. 825-829, July 1995.

[79] R. D. J. van Nee, "OFDM codes for peak-to-average power reduction and error correction," *Proceedings of the IEEE Global Telecommunications Conference*, vol. 1, pp. 740-744, November 1996.

[80] J. A. Davis and J. Jedwab, "Peak-to-mean power control and error correction for OFDM transmission using Golay sequences and Reed-Muller codes," *Electronics Letters*, vol. 33, pp. 267-268, February 1997.

[81] J. A. Davis and J. Jedwab, "Peak-to-mean power control in OFDM, Golay complementary sequences, and Reed-Muller codes," *IEEE Transactions on Information Theory*, vol. 45, pp. 2397-2417, November 1999.

[82] A. Brajal and A. Chouly, "Compensation of nonlinear distortions for orthogonal multicarrier schemes using predistortion," *Proceedings of the IEEE Global Telecommunications Conference*, vol. 3, pp. 1909-1914, November 1994.

[83] M. G. Di Benedetto and P. Mandarini, "Application of MMSE predistortion to OFDM systems," *IEEE Transactions on Communications*, vol. 44, pp. 1417-1420, November 1996.

[84] A. N. D'Andrea, V. Lottici and R. Reggiannini, "Nonlinear predistortion of OFDM signals over frequency-selective fading channels," *IEEE Transactions on Communications*, vol. 49, pp. 837-843, May 2001.

[85] H. Rohling, T. May, K. Bruninghaus and R. Grunheid, "Broad-band OFDM radio transmission for multimedia applications," *Proceedings of the IEEE*, vol. 87, pp. 1778-1789, October 1999.

[86] B. Le Floch, M. Alard and C. Berrou, "Coded orthogonal frequency division multiplex," *Proceedings of the IEEE*, vol. 83, pp. 982-996, June 1995.

[87] P. Höher, "TCM on frequency-selective land-mobile fading channels," *Proceedings of the 5th Tirrenia International Workshop on Digital Communications*, Tirrenia, Italy, September 1991.

[88] J.-J. van de Beek, O. Edfors, M. Sandell, S. K. Wilson and P. O. Börjesson, "On channel estimation in OFDM systems," *Proceedings of the IEEE Vehicular Technology Conference*, vol. 2, pp. 815-819, July 1995.

[89] O. Edfors, M. Sandell, J.-J. van de Beek, S. K. Wilson and P. O. Börjesson, "OFDM channel estimation by singular value decomposition," *Proceedings of the IEEE Vehicular Technology Conference*, vol. 2, pp. 923-927, April/May 1996.

[90] F. Daffara and A. Chouly, "Maximum-likelihood frequency detectors for orthogonal multicarrier systems," *Proceedings of the IEEE International Conference on Communications*, vol. 2, pp. 766-771, May 1993.

[91] W. D. Warner and C. Leung, "OFDM/FM frame synchronization for mobile radio data communication," *IEEE Transactions on Vehicular Technology*, vol. 42, pp. 302-313, August 1993.

[92] F. Claβen and H. Meyr, "Frequency synchronization algorithms for OFDM systems suitable for communication over frequency selective fading channels," *Proceedings of the IEEE Vehicular Technology Conference*, vol. 3, pp. 1655-1659, June 1994.

[93] K. W. Kang, J. Ann and H. S. Lee, "Decision-directed maximum-likelihood estimation of OFDM frame synchronisation offset," *Electronics Letters*, vol. 30, pp. 2153-2154, December 1994.

[94] P. H. Moose, "A technique for orthogonal frequency division multiplexing frequency offset correction," *IEEE Transactions on Communications*, vol. 42, pp. 2908-2914, October 1994.

[95] F. Daffara and O. Adami, "A new frequency detector for orthogonal multicarrier transmission techniques," *Proceedings of the IEEE Vehicular Technology Conference*, vol. 2, pp. 804-809, July 1995.

[96] M. Sandell, J.-J. van de Beek and P. O. Börjesson, "Timing and frequency synchronisation in OFDM systems using the cyclic prefix," *Proceedings of the International Symposium on Synchronisation*, pp. 16-19, December 1995.

[97] J.-J. van de Beek, M. Sandell, M. Isaksson and P. O. Börjesson, "Low-complex frame synchronization in OFDM systems," *Proceedings of the IEEE International Conference on Universal Personal Communications*, pp. 982-986, November 1995.

[98] T. M. Schmidl and D. C. Cox, "Robust frequency and timing synchronisation for OFDM," *IEEE Transactions on Communications*, vol. 45, pp. 1613-1621, December 1997.

[99] I. Kalet, "The multitone channel," *IEEE Transactions on Communications*, vol. 37, pp. 119-124, February 1989.

[100] C. E. Shannon, "Communication in the presence of noise," *Proceedings of the IRE*, vol. 37, pp. 10-21, January 1949.

[101] T. Keller and L. Hanzo, "Adaptive multicarrier modulation: A convenient framework for time-frequency processing in wireless communications," *Proceedings of the IEEE*, vol. 88, pp. 611-640, May 2000.

[102] J. Mikkonen, J. Aldis, G. Awater, A. Lunn and D. Hutchison, "The magic WAND – Functional overview," *IEEE Journal on Selected Areas in Communications*, vol. 16, pp. 953-972, August 1998.

[103] R. W. Chang, "Synthesis of band-limited orthogonal signals for multichannel data transmission," *Bell Syst. Tech. J.*, vol. 45, pp. 1775-1796, December 1966.

[104] B. R. Saltzberg, "Performance of an efficient parallel data transmission system," *IEEE Transactions on Communication Technology*, vol. 15, pp. 805-811, December 1967.

[105] R. W. Chang and R. A. Gibbey, "A theoretical study of performance of an orthogonal multiplexing data transmission scheme," *IEEE Transactions on Communication Technology*, vol. 16, pp. 529-540, August 1968.

[106] M. R. D. Rodrigues and I. Darwazeh, "Fast OFDM: A proposal for doubling the data rate of OFDM schemes," *Proceedings of the International Conference on Telecommunications*, vol. 3, pp. 484-487, June 2002.

[107] J. Oh and M. Lim, "The bandwidth efficiency increasing method of multicarrier CDMA and its performance evaluation in comparison with DS-CDMA with rake receivers," *Proceedings of the IEEE Vehicular Technology Conference*, vol. 1, pp. 561-565, May 1999.

[108] M. R. D. Rodrigues and J. J. O'Reilly, "Assessment of the performance of radio-over-fibre based wireless networks employing OFDM signalling," *Proceedings of the London Communications Symposium 1999*, pp. 47-50, July 1999.

[109] M. R. D. Rodrigues and J. J. O'Reilly, "Statistical characterisation of the response of a Volterra non-linearity to a cyclo-stationary zero-mean Gaussian stochastic process," *Proceedings of the IEEE International Symposium on Information Theory*, p. 8, June/July 2002.

[110] M. R. D. Rodrigues, I. Darwazeh and J. J. O'Reilly, "Volterra series assessment of non-linearly distorted OFDM signals: Power density spectrum evaluation," accepted for presentation at the *2nd IMA Conference on Mathematics in Communications*, Lancaster, U.K., December 2002.

[111] M. Schetzen. *The Volterra and Wiener Theories of Nonlinear Systems.* New York: Wiley, 1980.

[112] W. J. Rugh. *Nonlinear Systems – The Volterra/Wiener Approach.* Baltimore, MD: Johns Hopkins University Press, 1981.

[113] S. Narayanan, "Transistor distortion analysis using Volterra series representation," *Bell Syst. Tech. J.*, vol. 46, pp. 991-1023, May/June 1967.

[114] R. E. Maurer and S. Narayanan, "Noise loading analysis of a third-order nonlinear system with memory," *IEEE Transactions on Communication Technology*, vol. 16, pp. 701-712, October 1968.

[115] S. Narayanan, "Intermodulation distortion of cascaded transistors," *IEEE Journal of Solid State Circuits*, vol. 4, pp. 97-106, June 1969.

[116] S. Narayanan, "Application of Volterra series to intermodulation distortion analysis of a transistor feedback amplifier," *IEEE Transactions on Circuit Theory*, vol. 17, pp. 518-527, November 1970.

[117] J. J. Bussgang, L. Ehrman and J. W. Graham, "Analysis of nonlinear systems with multiple inputs," *Proceedings of the IEEE*, vol. 62, pp. 1088-1119, August 1974.

[118] H. M. Salgado and J. J. O'Reilly, "Volterra series analysis of distortion in semiconductor laser diodes," *IEE Proceedings-J*, vol. 138, pp. 379-382, December 1991.

[119] L. Hassine, Z. Toffano, F. Lamnabhi-Lagarrigue, A. Destrez and C. Birocheau, "Volterra functional series expansions for semiconductor lasers under modulation," *IEEE Journal of Quantum Electronics*, vol. 30, pp. 918-928, April 1994.

[120] H. M. Salgado and J. J. O'Reilly, "Experimental validation of Volterra series nonlinear modelling for microwave subcarrier optical systems," *IEE Proceedings-Optoelectronics*, vol. 143, pp. 209-213, August 1996.

[121] E. Bedrosian and S. O. Rice, "The output properties of Volterra systems (nonlinear systems with memory) driven by harmonic and Gaussian inputs," *Proceedings of the IEEE*, vol. 59, pp. 1688-1707, December 1971.

[122] J. Goldman, "A Volterra series description of crosstalk interference in communication systems," *Bell Syst. Tech. J.*, vol. 52, pp. 649-668, May/June 1973.

[123] W. J. Lawless and M. Schwartz, "Binary signaling over channels containing quadratic nonlinearities," *IEEE Transactions on Communications*, vol. 22, pp. 288-297, March 1974.

[124] S. Benedetto, E. Biglieri and R. Daffara, "Performance of multilevel baseband digital systems in a nonlinear environment," *IEEE Transactions on Communications*, vol. 24, pp. 1166-1175, October 1976.

[125] S. Benedetto, E. Biglieri and R. Daffara, "Modelling and performance evaluation of nonlinear satellite links – A Volterra series approach," *IEEE Transactions on Aerospace and Electronic Systems*, vol. 15, pp. 494-506, July 1979.

[126] S. Benedetto and E. Biglieri. *Principles of Digital Transmission: With Wireless Applications.* New York: Kluwer Academic/Plenum Publishers, 1999.

[127] T. L. Lim and J. K. Omura, "Error rate estimates in digital communication over nonlinear channel with memory," *IEEE Transactions on Communications*, vol. 31, pp. 407-412, March 1983.

[128] M. Maqusi, "Performance of baseband digital data transmission in nonlinear channels with memory," *IEEE Transactions on Communications*, vol. 33, pp. 715-719, July 1985.

[129] J. J. O'Reilly and H. M. Salgado, "Performance assessment of optical subcarrier multiplexing systems: Implications of laser distortion," *Proceedings of the IEEE Global Telecommunications Conference*, vol. 3, pp. 1845-1848, December 1991.

[130] H. M. Salgado and J. J. O'Reilly, "Performance assessment of FM broadcast subcarrier-multiplexed optical systems", *IEE Proceedings-J*, vol. 140, pp. 397-403, December 1993.

[131] H. M. Salgado and J. J. O'Reilly, "Accurate performance modeling of subcarrier multiplexed fiber/radio systems: Implications of laser nonlinear distortion and wide dynamic range" *IEEE Transactions on Communications*, vol. 44, pp. 988-996, August 1996.

[132] K. V. Peddanarappagari and M. Brandt-Pearce, "Volterra series transfer function of single-mode fibers," *Journal of Lightwave Technology*, vol. 15, pp. 2232-2241, December 1997.

[133] K. V. Peddanarappagari and M. Brandt-Pearce, "Volterra series approach for optimizing fiber-optic communications system designs," *Journal of Lightwave Technology*, vol. 16, pp. 2046-2055, November 1998.

[134] D. Middleton. *An Introduction to Statistical Communication Theory*. New York: IEEE Press, 1996.

[135] J. Jong and W. E. Stark, "Performance analysis of coded multicarrier spread-spectrum systems in the presence of multipath fading and non-linearities," *IEEE Transactions on Communications*, vol. 49, pp. 168-179, January 2001.

[136] M. C. Jeruchim, P. Balaban and K. S. Shanmugan. *Simulation of Communication Systems: Modeling, Methodology, and Techniques, 2nd ed.* New York: Kluwer Academic/Plenum Publishers, 2000.

[137] M. R. D. Rodrigues and J. J. O'Reilly, "Error probability assessment of radio-over-fibre based wireless networks employing OFDM signalling," *Proceedings of the London Communications Symposium 2000*, pp. 95-99, September 2000.

[138] M. R. D. Rodrigues and J. J. O'Reilly, "An analytic technique to assess the impact of non-linearities on the error probability of OFDM signals in RoF based wireless networks," *Proceedings of the IEEE International Symposium on Information Theory 2001*, p. 316, June 2001.

[139] M. R. D. Rodrigues, I. Darwazeh and J. J. O'Reilly, "Volterra series assessment of non-linearly distorted OFDM signals: Error probability evaluation," accepted for presentation at the *2nd IMA Conference on Mathematics in Communications*, Lancaster, U.K., December 2002.

[140] E. Y. Ho and Y. S. Yeh, "A new approach for evaluating the error probability in the presence of intersymbol interference and additive Gaussian noise," *Bell Syst. Tech. J.*, vol. 49, pp. 2249-2265, November 1970.

[141] O. Shimbo and M. I. Celebiler, "The probability of error due to intersymbol interference and Gaussian noise in digital communication systems," *IEEE Transactions on Communication Technology*, vol. 19, pp. 113-119, April 1971.

[142] S. Benedetto, G. De Vincentiis and A. Luvison, "Error probability in the presence of intersymbol interference and additive noise for multilevel digital signals," *IEEE Transactions on Communication Technology*, vol. 21, pp. 181-188, March 1973.

[143] B. Saltzberg, "Intersymbol interference error bounds with application to ideal bandlimited signalling," *IEEE Transactions on Information Theory*, vol. 14, pp. 563-568, July 1968.

[144] R. Lugannami, "Intersymbol interference and probability of error in digital systems," *IEEE Transactions on Information Theory*, vol. 15, pp. 682-688, November 1969.

[145] V. K. Prabhu, "Modified Chernoff bounds for PAM systems with noise and interference," *IEEE Transactions on Information Theory*, vol. 28, pp. 95-100, January 1982.

[146] J. R. F. da Rocha and J. J. O'Reilly, "Modified Chernoff bound for binary optical communications," *Electronics Letters*, vol. 18, pp. 708-710, January 1982.

[147] J. J. O'Reilly and J. R. F. da Rocha, "Improved error probability evaluation methods for direct detection optical communication systems," *IEEE Transactions on Information Theory*, vol. 33, pp. 839-848, November 1987.

[148] C. W. Helstrom, "Calculating error probabilities for intersymbol and cochannel interference," *IEEE Transactions on Communications*, vol. 34, pp. 430-435, May 1986.

[149] S. Benedetto, E. Biglieri, A. Luvinson and V. Zingarelli, "Moment-based performance evaluation of digital transmission systems," *IEE Proceedings-I*, vol. 139, pp. 258-266, June 1992.

[150] M. R. D. Rodrigues and J. J. O'Reilly, "An analytic technique to assess the impact of frequency dependent non-linearities on the error probability of OFDM/M-PSK and OFDM/M-QAM signals," *Proceedings of the 35th Annual Conference on Information Sciences and Systems*, vol. 2, pp. 748-752, March 2001.

[151] M. R. D. Rodrigues and J. J. O'Reilly, "On the distribution of the intermodulation distortion in OFDM communication systems," *Proceedings of the London Communications Symposium 2001*, pp. 87-90, September 2001.

[152] M. R. D. Rodrigues, I. Darwazeh and J. J. O'Reilly, "On the distribution of the intermodulation distortion and the error probability of non-linearly distorted OFDM signals," *Proceedings of the 36th Annual Conference on Information Sciences and Systems*, pp. 636-641, March 2002.

[153] M. R. D. Rodrigues and I. Darwazeh, "On the behaviour of non-linearly distorted OFDM signals," *Proceedings of the London Communications Symposium 2002*, pp. 113-116, September 2002.

[154] M. Kendall and A. Stuart. *The Advanced Theory of Statistics: Distribution Theory, 4th ed.* London: Charles Griffin & Company Limited, 1977.

[155] W. Feller. *An Introduction to Probability Theory and Its Applications, 3rd ed.* New York: Wiley, 1968.

[156] J. H. Miller and J. B. Thomas, "Detectors for discrete-time signals in non-Gaussian noise," *IEEE Transactions on Information Theory*, vol. 18, pp. 241-250, March 1972.

[157] A. Akinniyi and J. Long, "Statistical characterization of intermodulation products in a multicarrier LPA design," *Proceedings of the IEEE Vehicular Technology Conference*, pp. 688-691, May 1993.

[158] M. Kavehrad and M. Joseph, "Maximum entropy and the method of moments in performance evaluation of digital communications systems," *IEEE Transactions on Communications*, vol. 34, pp. 1183-1189, December 1986.

[159] F. Solms, P.G.W. van Rooyen and J. S. Kunicki, "Maximum entropy and minimum relative entropy in performance evaluation of digital communication systems," *IEE Proceedings – Communications*, vol. 142, pp. 250-254, August 1995.

[160] R. Weinstock. *Calculus of Variations with Applications to Physics and Engineering.* New York: Dover, 1974.

[161] M. R. D. Rodrigues and J. J. O'Reilly, "An analytic technique to determine the impact of non-linearities on the PDS of OFDM signals in RoF based wireless networks," *Proceedings of the International Symposium on Information Theory and Its Applications*, vol. 2, pp. 769-773, November 2000.

[162] M. R. D. Rodrigues, I. Darwazeh and J. J. O'Reilly, "Assessment of the impact of optical non-linearities on the performance of OFDM signals in optical fibre supported wireless networks," accepted for presentation at the *International Symposium on Information Theory and its Applications*, Xi'an, China, October 2002.

[163] W. I. Way. *Broadband Hybrid Fiber/Coax Access System Technologies.* New York: Academic Press, 1999.

[164] R. Sabella, "Performance analysis of wireless broadband systems employing optical fiber links," *IEEE Transactions on Communications*, vol. 47, pp. 715-721, May 1999.

[165] J. M. Senior. *Optical Fiber Communications: Principles and Practice, 2nd ed.* Englewood Cliffs, NJ: Prentice Hall, 1992.

[166] G. Keiser. *Optical Fiber Communications, 2nd ed.* New York: McGraw-Hill, 1991.

[167] R. Syms and J. Cozens. *Optical Guided Waves and Devices.* New York: McGraw-Hill, 1992.

[168] A. Yariv. *Optical Electronics in Modern Communications.* New York: Oxford University Press, 1997.

[169] G. P. Agrawal and N. K. Dutta. *Long-Wavelength Semiconductor Lasers.* New York: Van Nostrand Reinhold Company, 1986.

[170] H. Kressel and J. K. Butler. *Semiconductor Lasers and Heterojunction LEDs.* New York: Academic Press, 1977.

[171] R. S. Tucker and I. P. Kaminow, "High-frequency characteristics of directly modulated InGaAsP ridge waveguide and buried heterostructure lasers," *Journal of Lightwave Technology*, vol. 2, pp. 385-393, August 1984.

[172] R. S. Tucker, "High-speed modulation of semiconductor lasers," *Journal of Lightwave Technology*, vol. 3, pp. 1180-1192, December 1985.

[173] H. M. Salgado. *Performance Assessment of Subcarrier Multiplexed Optical Systems: Implications of Laser Non-linearities.* PhD Thesis, School of Electronic Engineering and Computer Systems, University of Wales, Bangor, United Kingdom, 1993.

[174] H. M. Salgado, J. M. Ferreira and J. J. O'Reilly, "Extraction of semiconductor intrinsic laser parameters by intermodulation distortion analysis," *IEEE Photonics Technology Letters*, vol. 9, pp. 1331-1333, October 1997.

[175] F. Koyama and K. Iga, "Frequency chirping in external modulators," *Journal of Lightwave Technology*, vol. 6, pp. 87-93, January 1988.

[176] A. J. Redfern and G. T. Zhou, "Nonlinear channel identification and equalization for OFDM systems," *Proceedings of the IEEE International Conference on Acoustics, Speech and Signal Processing*, vol. 6, pp. 3521-3524, May 1998.

[177] D. Karampatsis, M. R. D. Rodrigues and I. Darwazeh, "Implications of linear phase dispersion on OFDM and Fast-OFDM systems," *Proceedings of the London Communications Symposium 2002*, pp. 117-120, September 2002.